

**The Development of Analytical
Procedures for Analysis of Trace
Metals in Pharmaceutical
Formulations and the Speciation of
Arsenic in Antacids**

Samar Hosam Thiab

A thesis submitted in fulfilment of the requirements of
Liverpool John Moores University for the degree of
Doctor of Philosophy

February 2018

Abstract

The reliability of data obtained from the existing United States Pharmacopeia (USP) method, USP <231> for elemental impurities (EI) have been questioned in the literature(1). New regulations regarding EI in pharmaceutical products were recently implemented on the 1st January 2018. The new regulations are USP <232>/<233> and the International Council for Harmonisation equivalent guidelines (ICH Q3D). The new regulations include the use of instrumentation such as inductively coupled plasma optical emission spectroscopy (ICP-OES) and inductively coupled plasma mass spectrometry (ICP-MS).

The aim of this work was to develop, optimise and validate analytical methods for the determination of Class 1 and Class 2A elements, arsenic (As), cadmium (Cd), mercury (Hg), lead (Pb), cobalt (Co), nickel (Ni) and vanadium (V) simultaneously in pharmaceutical products in compliance with the new guidelines. The developed ICP-OES and ICP-MS methods were validated using the only available solid standard reference material (SRM) *NIST 3280 Multivitamin/Multielement tablets*. It was found that relying solely on spiked addition technique as suggested by USP<233> is inefficient as it may not reflect clearly the method's accuracy particularly when the sample preparation involves the use of microwave (MW)-assisted acid digestion step, which is very common for pharmaceutical samples.

Sample preparation was performed using a developed MW-assisted acid digestion method with reverse aqua regia. It was found that reaching a temperature of 210°C for sample's digestion is necessary to get EI recoveries of greater than 95% and pre-digestion grinding was found to be beneficial to minimise variation in data and get relative standard deviation (RSD) of less than 5%. The validation results showed good linearity ($R^2 > 0.995$) over a wide range with low limits of detection (LoDs) and limits of quantification (LoQs). The calculated LoQs in ng/mL are As (5.86, 1.149), Cd (0.87, 0.037), Hg (2.23, 1.701) Pd (4.73, 0.041), Co (1.58, 0.299),

Ni (1.74, 0.159) and V (7.64, 0.485) for ICP-OES and ICP-MS incorporated with collision reaction cell (CCT) respectively.

Twenty-four commercially available pharmaceutical products including analgesic tablets, cough remedies, flu powders and antacids were analysed. Four products contained Cd in concentrations exceeding the permitted daily exposure limit (PDE) of 5µg/day when the maximum dose is taken, and nine products exceeded the 5µg/day PDE of Pb. This is especially concerning for the paediatric products because children are more susceptible to EI adverse effects as for example, they can absorb up to 40-70% of ingested Pb.

The antacids were found to contain As and although the levels quantified were below the PDE (15µg/day), a speciation method using an ion-pair reversed phase high performance liquid chromatography (HPLC)-ICP-MS was optimised and validated according to ICH Q2B guidelines as no information regarding what species are present in such products is available in the literature. Four arsenic species were selected, arsenite (As^{III}), arsenate (As^V), monomethyl arsonate (MMA) and dimethyl arsonate (DMA). Calibrations with R²>0.995 for all four species in the range of 1 to 50 ng/L and % recoveries>95% with RSD<5% were obtained. Arsenic was extracted from the samples using MW assisted extraction with 0.3M phosphoric acid at 55°C for 10 minutes, 75°C for 10 minutes and 95°C for 1 hour. The species were stable after being exposed to the extraction procedure (spiked recoveries >95%). This method was able to extract 95% or more of arsenic for all products. The ion-pair reversed phase chromatography was performed using a mobile phase: 10mmol/L tetrabutylammonium, 20mmol/L potassium dihydrogen orthophosphate and 2% methanol at pH 6 with a C₁₈ column. The speciation analysis results for all the antacids showed that approximately 50% of the extracted As was present as the most toxic As^{III} form.

The work demonstrates some of the potential issues with the new regulations and the availability of suitable solid SRM and seeks to provide workable solutions for the analysis.

Acknowledgement

The work presented in this thesis would not have been possible without my close association with many people. I take this opportunity to extend my sincere gratitude and appreciation to all those who made this PhD thesis possible.

First, I would like to express my deep gratitude to my supervisor Dr Philip Riby for the continuous support, countless advice, patience and motivation throughout my PhD study. His guidance helped me in all the time of research and writing of this thesis. I would also like to thank my co-supervisor Prof Mark Wainwright for his feedback during my study.

I am grateful to Dr Simon Nelms (Thermo Fisher Scientific) for analysing TAC tablets and to CEM for their kind donation of the microwaves.

I am thankful for all the technicians in LJMU School of Pharmacy and Biomolecular Sciences, especially Dr Nicola Dempster and Phil Salmon for their support.

Special thanks goes to Applied Science Private University in Amman, Jordan for financing the scholarship.

It has been a great pleasure to share labs and office with my fellow PhD students and Postdocs, with whom I have shared moments of deep anxiety but also of big excitement.

Some special words of gratitude go to my friends who have always been a major source of support when things would get a bit discouraging: Ruba, Ruqayah, Hend, Shaymaa, Hiba, Rana, Nashwa and Rugaya. Thanks for always being there for me.

Last but not the least, a very special word of thanks goes to my father Hosam, mother Maryam, my brothers Ahmad and Saeed and my sister Sarah for supporting me spiritually throughout my study. Thanks for the encouragement, cheerfulness and enthusiasm to help me chase my dreams.

List of Contents

Abstract.....	i
Acknowledgement	iii
List of Contents	iv
List of Tables	vii
List of Figures	x
List of Abbreviations and Symbols	xv
Chapter 1.....	
1. Introduction	1
1.1 Elemental impurities in pharmaceutical products and excipients.....	1
1.1.1 Active pharmaceutical ingredient (API)	3
1.1.2 Excipients	5
1.1.3 Utilities and environmental factors	8
1.1.4 Manufacturing equipment.....	9
1.1.5 Container closure system (CCS)	10
1.2 Elemental impurities guidelines.....	12
1.2.1 USP <231> <i>Heavy metals</i> test limitations	12
1.2.2 USP <232> elemental impurities-limits, USP <233> elemental impurities- procedures, and ICH Q3D guidelines	15
1.3 Human toxicity of Class 1 and Class 2A elements.....	18
1.3.1 Toxicity of Class 1 elements	18
1.3.2 Toxicity of Class 2A elements.....	24
1.4 Validation Issues	27
1.5 Principles of instruments used in this work.....	28
1.5.1 Microwave assisted extraction of elements form pharmaceuticals for ICP-OES and ICP-MS determination.....	28
1.6 Inductively coupled plasma (ICP) for elemental impurities analysis in pharmaceuticals	37
1.6.1 ICP advantages	42
1.6.2 ICP-Sample Introduction	42
1.6.3 Inductively coupled plasma optical emission spectroscopy (ICP-OES).....	44
1.6.4 Inductively coupled plasma mass spectrometry (ICP-MS).....	53
1.7 Metals speciation	61
1.7.1 Arsenic speciation using high performance liquid chromatography (HPLC)-ICP-MS	64
1.8 Aims and objectives	70
Chapter 2.....	

2. The Optimisation, Validation and Analysis of Analgesics, cold and cough remedies by ICP-OES in Compliance ICH-Q3D Guidelines	71
2.1 Introduction	71
2.2 Experimental	74
2.2.1 Reagents and Materials	74
2.2.2 Samples	75
2.2.3 Instrumentation	77
2.2.4 ICP-OES Optimisation.....	78
2.2.5 Analytical figures of merit and method validation	79
2.2.6 Optimisation of microwave assisted acid digestion procedure	80
2.2.7 Analysis of analgesic tablets, cold and cough remedies	83
2.3 Results and discussion	84
2.3.1 ICP-OES Optimisation.....	84
2.3.2 Analytical figures of merit and method validation	104
2.3.3 Optimisation of microwave assisted acid digestion procedure	106
2.3.4 Analysis of analgesic tablets, cold and cough remedies	120
2.4 Conclusion.....	124
Chapter 3.....	
3. The Optimisation, Validation and Analysis of analgesics, cough remedies, cold and flu products and antacids by ICP-MS in Compliance ICH-Q3D Guidelines.....	126
3.1 Introduction	126
3.2 Experimental	128
3.2.1 Reagents and Materials	128
3.2.2 Samples	128
3.2.3 Instrumentation	131
3.2.4 ICP-MS Optimisation.....	132
3.2.5 Analytical figures of merit and method validation	135
3.2.6 Sample preparation and revalidation of the microwave assisted acid digestion procedure.....	136
3.2.7 Analysis of pharmaceutical samples	136
3.3 Results and discussion	136
3.3.1 ICP-MS Optimisation.....	136
3.3.2 Method validation and analytical figures of merit	171
3.3.3 Revalidation of the microwave assisted acid digestion procedure	174
3.4 Analysis of pharmaceutical samples	177
3.4 Conclusion.....	184

Chapter 4.....	
4. Speciation of Arsenic in Antacids Using Reversed Phase HPLC-ICP-MS.....	185
4.1 Introduction	185
4.2 Experimental	188
4.2.1 Reagents and Materials	188
4.2.2 Samples	189
4.2.3 Instrumentation	189
4.2.4 HPLC analytical figures of merit and validation	190
4.2.5 Sample preparation	191
4.3 Results and discussion	192
4.3.1 Testing the separation efficiency of mobile phase-1.....	192
4.3.2 Testing the separation efficiency of mobile phase-2.....	201
4.3.3 HPLC method validation.....	213
4.3.4 Samples preparation and analysis	217
4.4.4. Speciation of arsenic in antacids.....	222
4.4 Conclusion.....	226
Chapter 5.....	
5.1 General Conclusion	227
5.2 Future work.....	229
References	230
Meetings, Conferences and Publications.....	246
Funding	248

List of Tables

Table 1.1 PDEs ($\mu\text{g}/\text{day}$) for Elemental Impurities(10)	16
Table 1.2 Elements to be considered in risk assessment(10)	17
Table 1.3 Arsenic species chemical formula and structure*.....	65
Table 2.1 Analgesic tablets and cold and cough remedies product information	75
Table 2.2 CEM-SP-D microwave programme used to digest the samples.....	77
Table 2.3 Overview of ICP-OES, iCAP 6500 series optimised parameters for.....	77
Table 2.4 Class 1 and Class 2A LoDs and LoQs (ng/mL) calculated using different RF powers	101
Table 2.5 ICP-OES limits of detection and Limits of quantification for Class 1 and Class 2A elements	104
Table 2.6 Linearity data for Class 1 and Class 2A elements using ICP-OES.....	105
Table 2.7 The concentration of elements (ng/mL) in NIST 2380 after dilution	106
Table 2.8 Obtained concentrations using the developed and optimised ICP-OES method for reverse aqua regia following microwave digestion, $n=3$	107
Table 2.9 One-stage microwave-assisted acid digestion procedure for NIST 3280, at different temperatures, using ICP-OES for analysis. $n=3$	107
Table 2.10 Optimisation of digestion time using three-stages digestion procedure, $n=3$..	110
Table 2.11 Percentage recoveries for NIST 3280 using 9 HNO_3 : 1 HCl , $n=3$	112
Table 2.12 NIST 3280 percentage recoveries using different temperatures for the microwave assisted acid digestion methods, $n=3$	113
Table 2.13 Validation for Class 1 elements using two different techniques (mean $\pm \sigma$, $n=3$)	115
Table 2.14 Analysis results of three TAC formulas containing different levels of Class 1 and Class 2A elements using ICP-OES, $n=3$	116
Table 2.15 Digestion repeatability when two different techniques were used to grind NIST 3280 tablets prior to digestion, $n=3$	118
Table 2.16 Concentrations ($\mu\text{g}/\text{g}$) obtained with and without the use of Sc 225.2nm and Y 371nm as internal standards, $n=3$	120
Table 2.17 Elemental impurities ($\mu\text{g}/\text{day}$) in analgesic tablets analysed using ICP-OES (mean $\pm \sigma$, $n=3$)	121
Table 2.18 Elemental impurities ($\mu\text{g}/\text{day}$) in cold and cough remedies analysed using ICP-OES mode (mean $\pm \sigma$, $n=3$)	122
Table 2.19 Daily exposure ($\mu\text{g}/\text{day}$) for Tixylix when given in different dosages based on patient's age.....	123
Table 3.1 Cold and flu powders and antacids product information	129
Table 3.2 Overview of ICP-MS Thermo XSeries optimised parameters in CCT operation mode	131
Table 3.3 Passed tune test conditions, ICP-MS Thermo XSeries	132
Table 3.4 Class 1 and Class 2A elements atomic masses optimised for elemental analysis using ICP-MS and their relative abundance.....	134
Table 3.5 CEM-SPD microwave programme used to digest the samples	136
Table 3.6 Class 1 and Class 2A LoDs and LoQs (ng/mL) calculated using ICP-MS-standard mode at different RF powers	165
Table 3.7 Class 1 and Class 2A LoDs and LoQs (ng/mL) calculated using ICP-MS-CCT mode at different RF powers	166

Table 3.8 NIST 3280 Multivitamin/Multielement tablets elemental recoveries (mean and RSD, (n=3)) using different helium gas flow rates with ICP-MS-CCT.	168
Table 3.9 NIST 3280 elements' isotopes recoveries and RSDs using different internal standards	169
Table 3.10 Concentrations of Hg in TAC-formulas and RSDs using different internal standards, n=3	170
Table 3.11 ICP-MS limits of detection and Limits of quantification for Class 1 and Class 2A elements	171
Table 3.12 Linearity data for Class 1 and Class 2A elements using ICP-MS-CCT.....	172
Table 3.13 Accuracy and repeatability results of the optimised ICP-MS-CCT method obtained using NIST 3280 expressed as % recoveries and RSDs respectively, n=3	173
Table 3.14 Analysis results of three TAC formulas containing different levels of Class 1 and Class 2A, n=3	173
Table 3.15 Obtained concentrations using the developed and optimised ICP-MS-CCT method for reverse aqua regia following microwave digestion, n=3.....	174
Table 3.16 Percentage recoveries for NIST 3280 using 9 HNO ₃ : 1 HCl and reverse aqua regia for digestion, n=3	175
Table 3.17 NIST 3280 percentage recoveries using different temperatures for the microwave assisted acid digestion methods, n=3	176
Table 3.18 Elemental impurities (µg/day) in analgesic tablets analysed using ICP-MS-CCT mode (mean ± σ, n=3).....	178
Table 3.19 Elemental impurities (µg/day) in cold and cough remedies analysed using ICP-MS-CCT mode (mean ± σ, n=3)	179
Table 3.20 Elemental impurities (µg/day) in cold and flu powders analysed using ICP-MS-CCT mode (mean ± σ, n=3).....	180
Table 3.21 Elemental impurities (µg/day) in antacids analysed using ICP-MS-CCT mode (mean ± σ, n=3).....	182
Table 4.1 Tested chromatographic conditions using mobile phase-1	193
Table 4.2 The structure and pKa of As ^{III} , As ^V , MMA and DMA.....	194
Table 4.3 The resolution of the four arsenic species using mobile phase-2 with Phenomenex Kinetex C ₁₈ column and Phenomenex Gemini C ₁₈ column	203
Table 4.4 Tested chromatographic conditions using mobile phase-2	203
Table 4.5 The resolution of the four arsenic species using Phenomenex Gemini C ₁₈ column and mobile phase-2 with and without malonic acid at pH=6.....	210
Table 4.6 Linearity results for the developed HPLC-ICP-MS method	213
Table 4.7 Accuracy and Precision results, n=3	213
Table 4.8 Total arsenic concentration ± σ (ng/g) in commercially available antacids, n=3.	217
Table 4.9 Concentration of arsenic species ± σ (ng/g) using microwave assisted extraction with 0.3M H ₃ PO ₄ at 55°C for 10 minutes, 75°C for 10 minutes and 95°C for 30 minutes, n=3	220
Table 4.10 Concentration of arsenic species ± σ (ng/g) in antacids containing alginate using microwave assisted extraction with 0.3 M H ₃ PO ₄ at 55°C for 10 minutes, 75°C for 10 minutes and 95°C for 60 minutes, n=3	220
Table 4.11 % Recovery of spiked samples prepared in water and H ₃ PO ₄ subjected to the microwave extraction procedure; 55°C for 10 minutes, 75°C for 10 minutes and 95°C for 60 minutes, n=3	221
Table 4.12 Arsenic content in the dried mass obtained from Gaviscon suspension.....	223

Table 4.13 Concentration of arsenic species $\pm \sigma$ (ng/g) in antacids without alginates using microwave assisted extraction with 0.3 M H_3PO_4 at 55°C for 10 minutes, 75°C for 10 minutes and 95°C for 1 hours, n=3	223
Table 4.14 Percentage of As^{III} in the analysed antacid products	226

List of Figures

Figure 1.1 Source of elemental impurities in the final pharmaceutical product. (Adopted from ICH Q3D guidelines(10)).	2
Figure 1.2 Different sources of excipients used in the pharmaceutical formulations (Adopted from Teasdale et al, 2015(15)).	6
Figure 1.3 Illustration of risk factors associated with CCS (Adapted from Teasdale et al, 2015(15)).	11
Figure 1.4 Electromagnetic radiation spectrum(106)	31
Figure 1.5 Schematic representation of the water molecules alternating alignment under the oscillating electric field induced by MW. A) Water molecules without the influence of MW. B) Water molecules under the influence of MW. (Adapted from Flores EM,2014(112))	33
Figure 1.6 Schematic representation of the ionic conduction under the oscillating MW electric field. (Adapted from Flores EM,2014(112))	34
Figure 1.7 Graphical illustration of monomode and multimode microwaves. (Adapted from Nüchter et al, 2003(118)).	36
Figure 1.8 Graphical illustration of ICP torch	38
Figure 1.9 Plasma regions and temperatures ($^{\circ}\text{K} \pm 10\%$) and the different plasma zones....	40
Figure 1.10 Different processes that occur when an aerosol droplet is injected into the ICP discharge (Adopted from Boss CB and Fredeen KJ, 1999(134))	41
Figure 1.11 Basic components of ICP-OES instrument (Adopted from Boss CB and Fredeen KJ, 1999(134))	44
Figure 1.12 Rutherford-Bohr model of an atom showing its excitation to a higher energy state followed by its decay to a lower energy state by releasing the gained energy (Adapted from Boss CB and Fredeen KJ, 1999(134))	46
Figure 1.13 Spectral interferences: A) Background shift, B) wing overlap and C) direct spectral overlap	49
Figure 1.14 Basic components of ICP-MS instrument (Adopted from Thomas R, 2004 (145))	53
Figure 1.15 Thermo XSeries ICP-MS cones	55
Figure 1.16 Graphical illustration of the position of CRC in ICP-MS instrument (Adopted from Thomas R, 2004 (145))	59
Figure 1.17 Graphical illustration of a typical HPLC-ICP-MS	69
Figure 2.1 The signal and signal/blank ratios for arsenic (300 ng/mL) at three different wavelengths using different ICP-OES nebuliser gas flow rates.	84
Figure 2.2 The signal and signal/blank ratios for cadmium (300 ng/mL) at three different wavelengths using different ICP-OES nebuliser gas flow rates.	85
Figure 2.3 The signal and signal/blank ratios for mercury (300 ng/mL) at three different wavelengths using different ICP-OES nebuliser gas flow rates.	85
Figure 2.4 The signal and signal/blank ratios for lead (300 ng/mL) at four different wavelengths using different ICP-OES nebuliser gas flow rates.	85
Figure 2.5 The signal and signal/blank ratios for cobalt (300 ng/mL) at four different wavelengths using different ICP-OES nebuliser gas flow rates.	86
Figure 2.6 The signal and signal/blank ratios for nickel (300 ng/mL) at four different wavelengths using different ICP-OES nebuliser gas flow rates.	86
Figure 2.7 The signal and signal/blank ratios for vanadium (300 ng/mL) at four different wavelengths using different ICP-OES nebuliser gas flow rates.	86

Figure 2.8 The signal and signal/blank ratios for arsenic (300 ng/mL) at three different wavelengths using different ICP-OES pump rates	88
Figure 2.9 The signal and signal/blank ratios for cadmium (300 ng/mL) at three different wavelengths using different ICP-OES pump rates	88
Figure 2.10 The signal and signal/blank ratios for mercury (300 ng/mL) at three different wavelengths using different ICP-OES pump rates	89
Figure 2.11 The signal and signal/blank ratios for lead (300 ng/mL) at four different wavelengths using different ICP-OES pump rates	89
Figure 2.12 The signal and signal/blank ratios for cobalt (300 ng/mL) at four different wavelengths using different ICP-OES pump rates	89
Figure 2.13 The signal and signal/blank ratios for nickel (300 ng/mL) at four different wavelengths using different ICP-OES pump rates	90
Figure 2.14 The signal and signal/blank ratios for vanadium (300 ng/mL) at four different wavelengths using different ICP-OES pump rates	90
Figure 2.15 The signal and signal/blank ratios for arsenic (300 ng/mL) at three different wavelengths using different ICP-OES auxiliary gas flow rates	91
Figure 2.16 The signal and signal/blank ratios for cadmium (300 ng/mL) at three different wavelengths using different ICP-OES auxiliary gas flow rates	91
Figure 2.17 The signal and signal/blank ratios for mercury (300 ng/mL) at three different wavelengths using different ICP-OES auxiliary gas flow rates	92
Figure 2.18 The signal and signal/blank ratios for lead (300 ng/mL) at four different wavelengths using different ICP-OES auxiliary gas flow rates	92
Figure 2.19 The signal and signal/blank ratios for cobalt (300 ng/mL) at four different wavelengths using different ICP-OES auxiliary gas flow rates	92
Figure 2.20 The signal and signal/blank ratios for nickel (300 ng/mL) at four different wavelengths using different ICP-OES auxiliary gas flow rates	93
Figure 2.21 The signal and signal/blank ratios for vanadium (300 ng/mL) at four different wavelengths using different ICP-OES auxiliary gas flow rates	93
Figure 2.22 The signal and signal/blank ratios for arsenic (300 ng/mL) at three different wavelengths using different ICP-OES coolant gas flow rates	94
Figure 2.23 The signal and signal/blank ratios for cadmium (300 ng/mL) at three different wavelengths using different ICP-OES coolant gas flow rates	94
Figure 2.24 The signal and signal/blank ratios for mercury (300 ng/mL) at three different wavelengths using different ICP-OES coolant gas flow rates	95
Figure 2.25 The signal and signal/blank ratios for lead (300 ng/mL) at four different wavelengths using different ICP-OES coolant gas flow rates	95
Figure 2.26 The signal and signal/blank ratios for cobalt (300 ng/mL) at four different wavelengths using different ICP-OES coolant gas flow rates	95
Figure 2.27 The signal and signal/blank ratios for nickel (300 ng/mL) at four different wavelengths using different ICP-OES coolant gas flow rates	96
Figure 2.28 The signal and signal/blank ratios for vanadium (300 ng/mL) at four different wavelengths using different ICP-OES coolant gas flow rates	96
Figure 2.29 The signal and signal/blank ratios for arsenic (300 ng/mL) at three different wavelengths using different ICP-OES radio frequency powers	97
Figure 2.30 The signal and signal/blank ratios for cadmium (300 ng/mL) at three different wavelengths using different ICP-OES radio frequency powers	97
Figure 2.31 The signal and signal/blank ratios for mercury (300 ng/mL) at three different wavelengths using different ICP-OES radio frequency powers	97

Figure 2.32 The signal and signal/blank ratios for lead (300 ng/mL) at four different wavelengths using different ICP-OES radio frequency powers	98
Figure 2.33 The signal and signal/blank ratios for cobalt (300 ng/mL) at four different wavelengths using different ICP-OES radio frequency powers	98
Figure 2.34 The signal and signal/blank ratios for nickel (300 ng/mL) at four different wavelengths using different ICP-OES radio frequency powers	98
Figure 2.35 The signal and signal/blank ratios for vanadium (300 ng/mL) at four different wavelengths using different ICP-OES radio frequency powers	99
Figure 2.36 V 292.4nm Calibration line obtained using RF power of 1300W.....	100
Figure 2.37 Calibration curve with poor correlation coefficient when using As 449.4nm due to the poor signal at this wavelength.	102
Figure 2.38 Wavelength interferences determined using iTEVA software.....	103
Figure 2.39 Thermal degradation of caps when holding at 220°C for 20 minutes	108
Figure 2.40 Sample loss due to caps damage during digestion procedure when holding at 220°C for 20 minutes	108
Figure 2.41 NIST 3280 digest using: A) One-stage procedure, B) Three-stages procedure.	109
Figure 2.42 The pressure profile for microwave digestion procedure of NIST 3280. A) One-stage digestion procedure at 210 °C with a hold for 20 minutes and B) Three-stages digestion procedure at 120°C, 180°C and 210°C with a hold for 5 minutes at each temperature.....	109
Figure 2.43 NIST 3280 powder, ground using: A) Glass mortar and pestle, B) Mixer mill... ..	118
Figure 3.1 The signal and signal/blank ratios for arsenic (30 ng/mL) using ICP-MS standard and CCT modes at different nebuliser gas flow rates (L/min)	137
Figure 3.2 The signal and signal/blank ratios for cadmium (30 ng/mL) using ICP-MS standard and CCT modes at different nebuliser gas flow rates (L/min)	138
Figure 3.3 The signal and signal/blank ratios for mercury (30 ng/mL) using ICP-MS standard and CCT modes at different nebuliser gas flow rates (L/min)	139
Figure 3.4 The signal and signal/blank ratios for lead (30 ng/mL) using ICP-MS standard and CCT modes at different nebuliser gas flow rates (L/min)	140
Figure 3.5 The signal and signal/blank ratios for cobalt (30 ng/mL) using ICP-MS standard and CCT modes at different nebuliser gas flow rates (L/min)	140
Figure 3.6 The signal and signal/blank ratios for nickel (30 ng/mL) using ICP-MS standard and CCT modes at different nebuliser gas flow rates (L/min)	141
Figure 3.7 The signal and signal/blank ratios for vanadium (30 ng/mL) using ICP-MS standard and CCT modes at different nebuliser gas flow rates (L/min).....	142
Figure 3.8 The signal and signal/blank ratios for arsenic (30 ng/mL) using ICP-MS standard and CCT modes at different pump rates (rpm).....	143
Figure 3.9 The signal and signal/blank ratios for cadmium (30 ng/mL) using ICP-MS standard and CCT modes at different pump rates (rpm).....	143
Figure 3.10 The signal and signal/blank ratios for mercury (30 ng/mL) using ICP-MS standard and CCT modes at different pump rates (rpm)	144
Figure 3.11 The signal and signal/blank ratios for lead (30 ng/mL) using ICP-MS standard and CCT modes at different pump rates (rpm).....	145
Figure 3.12 The signal and signal/blank ratios for cobalt (30 ng/mL) using ICP-MS standard and CCT modes at different pump rates (rpm).....	146
Figure 3.13 The signal and signal/blank ratios for nickel (30 ng/mL) using ICP-MS standard and CCT modes at different pump rates (rpm).....	147

Figure 3.14 The signal and signal/blank ratios for vanadium (30 ng/mL) using ICP-MS standard and CCT modes at different pump rates (rpm)	148
Figure 3.15 The signal and signal/blank ratios for arsenic (30 ng/mL) using ICP-MS standard and CCT modes at different auxiliary gas flow rates (L/min).....	149
Figure 3.16 The signal and signal/blank ratios for cadmium (30 ng/mL) using ICP-MS standard and CCT modes at different auxiliary gas flow rates (L/min)	149
Figure 3.17 The signal and signal/blank ratios for cadmium (30 ng/mL) using ICP-MS standard and CCT modes at different auxiliary gas flow rates (L/min)	150
Figure 3.18 The signal and signal/blank ratios for lead (30 ng/mL) using ICP-MS standard and CCT modes at different auxiliary gas flow rates (L/min).....	151
Figure 3.19 The signal and signal/blank ratios for cobalt (30 ng/mL) using ICP-MS standard and CCT modes at different auxiliary gas flow rates (L/min).....	151
Figure 3.20 The signal and signal/blank ratios for nickel (30 ng/mL) using ICP-MS standard and CCT modes at different auxiliary gas flow rates (L/min).....	152
Figure 3.21 The signal and signal/blank ratios for vanadium (30 ng/mL) using ICP-MS standard and CCT modes at different auxiliary gas flow rates (L/min)	153
Figure 3.22 The signal and signal/blank ratios for arsenic (30 ng/mL) using ICP-MS standard and CCT modes at different coolant gas flow rates (L/min)	154
Figure 3.23 The signal and signal/blank ratios for cadmium (30 ng/mL) using ICP-MS standard and CCT modes at different coolant gas flow rates (L/min).....	155
Figure 3.24 The signal and signal/blank ratios for mercury (30 ng/mL) using ICP-MS standard and CCT modes at different coolant gas flow rates (L/min).....	156
Figure 3.25 The signal and signal/blank ratios for lead (30 ng/mL) using ICP-MS standard and CCT modes at different coolant gas flow rates (L/min)	157
Figure 3.26 The signal and signal/blank ratios for cobalt (30 ng/mL) using ICP-MS standard and CCT modes at different coolant gas flow rates (L/min)	158
Figure 3.27 The signal and signal/blank ratios for nickel (30 ng/mL) using ICP-MS standard and CCT modes at different coolant gas flow rates (L/min)	158
Figure 3.28 The signal and signal/blank ratios for vanadium (30 ng/mL) using ICP-MS standard and CCT modes at different coolant gas flow rates (L/min).....	159
Figure 3.29 The signal and signal/blank ratios for arsenic (30 ng/mL) using ICP-MS standard and CCT modes at different RF powers (W)	160
Figure 3.30 The signal and signal/blank ratios for cadmium (30 ng/mL) using ICP-MS standard and CCT modes at different RF powers (W)	160
Figure 3.31 The signal and signal/blank ratios for mercury (30 ng/mL) using ICP-MS standard and CCT modes at different RF powers (W)	161
Figure 3.32 The signal and signal/blank ratios for lead (30 ng/mL) using ICP-MS standard and CCT modes at different RF powers (W)	162
Figure 3.33 The signal and signal/blank ratios for cobalt (30 ng/mL) using ICP-MS standard and CCT modes at different RF powers (W)	162
Figure 3.34 The signal and signal/blank ratios for nickel (30 ng/mL) using ICP-MS standard and CCT modes at different RF powers (W)	163
Figure 3.35 The signal and signal/blank ratios for vanadium (30 ng/mL) using ICP-MS standard and CCT modes at different RF powers (W)	164
Figure 4.1 Obtained chromatogram for a mixture of AsV, AsIII, MMA and DMA using mobile phase-1 pH =2.7 with Kinetex C18 column	193
Figure 4.2 Obtained chromatogram for a mixture of AsV, AsIII, MMA and DMA using mobile phase-1 at pH =2.7 with Gemini C18 column	193

Figure 4.3 Ionisation of 1. As ^{III} , 2. As ^V , 3. MMA and 4. DMA at different pH.....	195
Figure 4.4 A general illustration of the interaction between the positively charged arsenic species and butanesulfonate as an ion pairing agent used with reversed phase chromatography	196
Figure 4.5 A general illustration of the interaction between the negatively charged arsenic species and tetramethylammonium as an ion pairing agent used with reversed phase chromatography	197
Figure 4.6 Chromatograms obtained using mobile phase-1 with Kinetex C18 column at pH A)2, B)2.7, C)3, D)4 and E)4.5 respectively	198
Figure 4.7 Order of elution of As ^V , As ^{III} , MMA and DMA using mobile phase-1 at pH=3 with Kinetex C18 column	199
Figure 4.8 Chromatograms obtained using mobile phase-1 with Gemini C18 column at pH A)2, B)2.7, C)3, D)4 and E)4.5 respectively	200
Figure 4.9 Chromatograms obtained using mobile phase-2 at pH=6 with A) Phenomenex Kinetex C18 column and B) Phenomenex Gemini C18 column	202
Figure 4.10 a general illustration of the interaction between the negatively charged arsenic species and TBA	204
Figure 4.11 Chromatograms using mobile phase-2 with Phenomenex Gemini C18 column at pH A)3, B)4, C)5, D)6 and E)7 respectively.	205
Figure 4.12 Chromatogram obtained using Phenomenex Gemini C18 column + mobile phase-2 containing A) 0 mmol/L TBA, B) 5 mmol/L TBA, C) 10 mmol/L TBA and D) 20 mmol/L TBA	207
Figure 4.13 Chromatogram obtained using Phenomenex Gemini C18 column + mobile phase-2 at pH=6. A) 10 mmol/L TBA, 1 mmol/L malonic acid, 20 mmol/L KH ₂ PO ₄ and 2% methanol, B)10 mmol/L TBA, 1 mmol/L malonic acid and 2% methanol	208
Figure 4.14 Chromatograms obtained using Phenomenex Gemini C18 column + mobile phase-2 at pH=6. A) 10 mmol/L TBA, 1 mmol/L malonic acid, 20 mmol/L KH ₂ PO ₄ and 2% methanol, B) 10 mmol/L TBA, 20 mmol/L KH ₂ PO ₄ and 2% methanol.....	209
Figure 4.15 Ionisation of malonic acid at different pH	210
Figure 4.16 Chromatogram obtained using Phenomenex Gemini C18 column + mobile phase-2 at pH=6. A) 10 mmol/L TBA, 20 mmol/L KH ₂ PO ₄ and 2% methanol, B) 10 mmol/L TBA and 2% methanol.....	211
Figure 4.17 Illustration of As-species elution order; obtained by injecting a standard of each species separately as well as a mixture of the four selected As-species.....	212
Figure 4.18 Obtained chromatogram for Gaviscon chewable tablets using microwave assisted extraction with water for 30 minutes at 80°C.....	218
Figure 4.19 Obtained chromatogram for Gaviscon chewable tablets using microwave assisted extraction with water for 30 minutes at 95°C.....	219
Figure 4.20 Obtained chromatogram for Gaviscon chewable tablets using microwave assisted extraction with H ₃ PO ₄ for 30 minutes at 95°C.....	219
Figure 4.21 The interconversion of As ^{III} to As ^V after exposing a standard in water and H ₃ PO ₄ to microwaves for more than 80 minutes	222
Figure 4.22 Obtained chromatograms for Rennie Extra with alginate & Rennie without alginate using microwave assisted extraction with 0.3 M H ₃ PO ₄ at 55°C for 10 minutes, 75°C for 10 minutes and 95°C for 60 minutes	224

List of Abbreviations and Symbols

%	Percent
°C	Degrees Celsius
µg	microgram
µm	micrometres
¹H NMR	Proton nuclear magnetic resonance
A/D	Analog-to-digital
AAS	Atomic absorption spectrometry
AC	Alternating current
AFS	Atomic fluorescence spectrometry
Ag	Silver
a.k.a.	Also known as
Al	Aluminium
amu	Atomic mass unit
API	Active pharmaceutical ingredient
Ar	Argon
As	Arsenic
AsA	Para-arsanilic acid
AsB	Arsenobetaine
AsC	Arsenocholine
As-Gly	Arsenosugar-glycerol
As^{III}	Arsenite
As^V	Arsenate
Au	Gold
B	Boron
Ba	Barium
BBB	Blood brain barrier
c	The speed of light
Ca	Calcium
CCD	Charge-coupled device
CCS	Container closure system
CCT	Collision cell technology
CRC	Collision/reaction cell
Cd	Cadmium
CID	Charge-injection device
CNS	Central nervous system
Co	Cobalt
Cr	Chromium
CT	Cryotrapping
Cts/S	Counts/second
Cu	Copper
DC	Direct current
DMA	Dimethylarsenic acid
DNA	Deoxyribonucleic acid
DRC	Dynamic reaction cell
EDTA	Ethylenediaminetetraacetic acid

EI	Elemental impurities
ETV	Electrothermal vaporization
<i>f</i>	Frequency
FCC	Federal Communications Commission
FDA	Food and Drug Administration
Fe	Iron
g	Gram
Ga	Gallium
GC	Gas chromatographic
GF-AAS	Graphite furnace atomic absorption spectroscopy
GI	Gastrointestinal
GMP	Good Manufacturing Practice
GU	Genitourinary
h	Planck's constant
H₂O₂	Hydrogen peroxide
H₂SO₄	sulfuric acid
HCl	Hydrochloric acid
HDPE	High-density polyethylene
He	Helium
HEPA	High-efficiency particulate air
HF	Hydrofluoric acid
Hg	Mercury
HG	Hydride generation
HNO₃	Nitric acid
HPLC	High performance liquid chromatography
Hz	Hertz
IARC	The International Agency for Research on Cancer
IC	Integrated circuit
ICH	International Council for Harmonisation
ICP	Inductively coupled plasma
ICP-MS	Inductively coupled plasma mass spectrometry
ICP-OES	Inductively coupled plasma optical emission spectroscopy
IEC	Interelement correction
In	Indium
IOM	Institute of Medicine
Ir	Iridium
JP	Japanese Pharmacopoeia
K	Potassium
KED	Kinetic energy discrimination
Kg	Kilogram
KH₂PO₄	Potassium dihydrogen orthophosphate
L	Litre
La	Lanthanum
LC	Liquid chromatographic
LDPE	Low-density polyethylene
Li	Lithium
LoD	Limit of detection

LoQ	Limit of quantification
m	Meter
m/z	Mass-to-charge ratio
Mg	Magnesium
MHz	Megahertz
MIC	Microwave induced combustion
min	minute
mL	millilitre
mm	Millimetre
MMA	Monomethylarsonic acid
mmol	Milli mole
Mn	Manganese
Mo	Molybdenum
ms	millisecond
MW	Microwave
Na	Sodium
Na₂HPO₄	Disodium phosphate
NaCl	Sodium chloride
NF	National Formulary
ng	Nanogram
Ni	Nickel
NIST	National Institute of Standards and Technology
Os	Osmium
P	Phosphorus
Pb	Lead
Pd	Palladium
PDA	Photodiode array
PDEs	Permitted daily exposures
PEEK	Polyetheretherketone
PET	Polyethylene terephthalate
PF	Pharmacopeia Forum
pH	Potential hydrogen
Ph. Eur.	European Pharmacopoeia
pK_a	The negative base-10 logarithm of the acid dissociation constant (K _a) of a solution
PMT	Photomultiplier tube
Pt	Platinum
PTFE	Polytetrafluoroethylene
PW	Purified water
QA/QC	Quality Assurance/Quality Control
RF	Radio frequency
Rh	Rhodium
ROX	Roxarsone
RSD	Relative standard deviation
Ru	Ruthenium
Sb	Antimony
Sc	Scandium

Se	Selenium
SF	Sector field
Si	Silicon
Sn	Tin
SPE	solid phase extraction
Sr	Strontium
TAC	Technical and analytical challenges sub-committee of the Coalition for Rational Implementation of the USP Elemental Impurities Requirements
Tb	Terbium
TBA	Tetrabutylammonium
Tl	Thallium
TMAO	Trimethylarsine oxide
TXRF	Reflection X-ray fluorescence
UK	United Kingdom
USA	United States of America
USP	United States Pharmacopeia
UV	Ultraviolet
V	Vanadium
W	Watts
WFI	Water-for injection
WHO	World Health Organisation
Y	Yttrium
Zn	Zinc
ΔE	Energy difference
ϵ'	Dielectric constant
ϵ''	Dielectric loss factor
λ	Wavelength

Chapter 1

Introduction

1. Introduction

The toxicity of various elements has been well-documented for many years. Early recorded cases including the poisoning of the Chinese emperor, *Qin-Shi-Huang* from his attempt to become immortal by taking pills containing mercury (Hg), which resulted in his death(2). Another common example is arsenic (As) which is historically known for its toxicity. It was used for centuries as a poison and during the Middle Ages, the acutely toxic tasteless powder; arseneous oxide was used for homicides particularly by impatient heirs(3). During the First World War, an organoarsenic compound with high toxicity known as Lewisite was used as a chemical weapon(4, 5). Lead (Pb) is another famous element for its toxicity, especially on the blood, renal tubules and motor neurons. Children who lived in old houses where leaded paints were used developed symptoms of lead poisoning including weight loss, irritability, abdominal pain, renal failure as well as behaviour and learning difficulties(6, 7).

Recently, elemental impurities (EI) in pharmaceutical products and excipients have been gaining more interest, especially with the new guidelines being implemented on the 1st January 2018. These guidelines are the United States Pharmacopeia (USP) <232>/<233>(8, 9) and the International Conference on Harmonisation (ICH) Q3D guidelines(10). The purpose of the guidelines is to help produce more reliable EI data, to minimise the unwanted effects of EI and to reduce the potential toxicity of such elements(11).

1.1 Elemental impurities in pharmaceutical products and excipients

Elemental impurities in pharmaceutical products may arise from many different sources(12). They may be intentionally added during synthesis, such as catalysts, or

from the reagents used such as raw materials, solvents and formulation agents(12). They also may just be present as contaminants introduced during the manufacturing process from the transferring pipelines or reaction vessels for example, or by leaching from the packaging materials(12). Figure 1.1 illustrates the different sources that contribute to elemental impurities in pharmaceutical products.

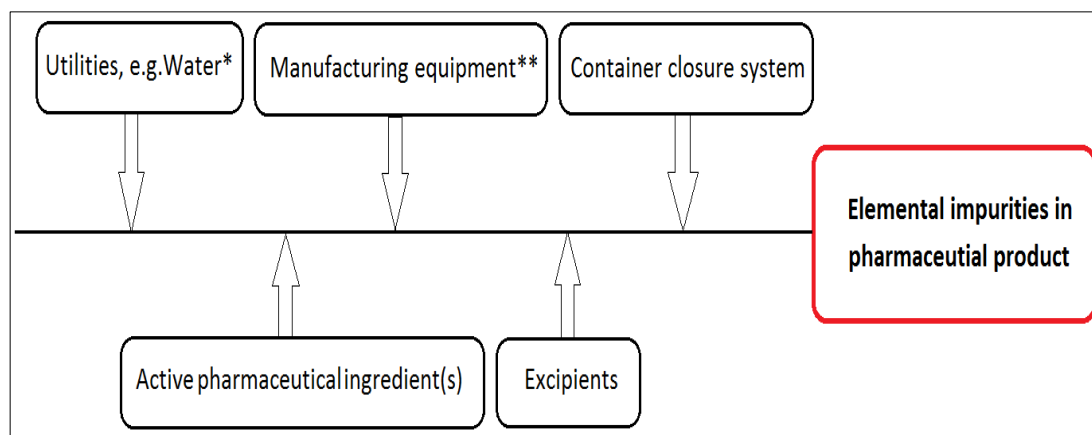


Figure 1.1 Source of elemental impurities in the final pharmaceutical product.
(Adopted from ICH Q3D guidelines(10)).

**Fulfilling the water quality requirements as stated in the various pharmacopoeias reduces elemental impurities introduced from water.*

***Maintaining Good Manufacturing Practice (GMP) processes in the selection and qualification of equipment reduces the risk of introducing elemental impurities to the product.*

These impurities are of great concern, since they do not have a therapeutic benefit and some contaminants have inherent toxicity(13). In addition, these elements may have adverse effects on the active pharmaceutical ingredient(s)-(APIs) stability and shelf-life by catalysing the degradation of drug substances(13).

This necessitates the monitoring of impurities throughout the manufacturing process from raw materials to the final pharmaceutical product and the control of elemental impurities levels within acceptable limits(14).

1.1.1 Active pharmaceutical ingredient (API)

APIs are an important contributor to the total EI in a final pharmaceutical product. Their impurity profile depends on their synthetic route as EI can be from the solvents, organic and/or inorganic reagents, water or catalysts used during their synthesis in addition to the metals that can be introduced from the manufacturing equipment and the primary containers(15, 16). Although there are only a few papers published in the literature showing EI profile in APIs, from those a study where four APIs, (dicyclomin hydrochloride, ethambutol, pyrazinamide and furazolidone) were analysed using inductively coupled plasma mass spectrometry (ICP-MS) found that all four APIs contain iron (Fe)(17). In addition, dicyclomin hydrochloride contains titanium, manganese and zinc. Ethambutol and pyrazinamide contain chromium (Cr) and copper (Cu), while furazolidone contains lead (Pb), Cr, manganese (Mn), copper (Cu) and zinc (Zn)(17). The method used was validated using a standard reference water ; NIST 1643b, rather than a solid pharmaceutical reference material, which is more representative of the solid APIs(17).

In another study, atenolol, captopril, levodopa, primaquine diphosphate, propranolol hydrochloride and sulfamethoxazole were analysed by ICP-MS validated using the spike addition technique recommended by the regulations. A single reaction chamber digestion was used and As, cadmium (Cd),mercury (Hg), Pb, nickel (Ni), vanadium (V), Cr and molybdenum (Mo) were quantified in levels less than 5.44 µg/g(18). Additionally, calcium folinate, enalapril maleate and levodopa were analysed using ICP-MS and found to contain different concentrations of Pd, V, Cu, Zn,

Mo and tin (Sn) in concentrations ranging from 0.13 to 8.2 $\mu\text{g/g}$ (19). Again, in this study the spike addition technique was used to validate the method.

Since the analysed medications in both studies are not taken in concentrations higher than 300 mg daily, the EI levels are not posing a great risk, especially considering the more toxic metals like Cd and Pb were found in concentrations not exceeding 0.2 $\mu\text{g/g}$ (18, 19).

Many APIs are synthesised with the aid of metal catalysts to accelerate the rate of the chemical reaction, such as platinum group catalysts, so they are a source of trace metal contamination(20). However if Good Manufacturing Practices (GMPs) are maintained, catalysts are usually considered a low risk of contamination as they are usually efficiently removed after completion of the API synthesis(21). Catalysts may be classified as either homogeneous or heterogeneous depending on whether their molecules are dispersed in the same reactant phase or not. Recovering the catalyst after completion of the chemical reaction is necessary to keep the commercial applications affordable. Most catalysts are more expensive than the products(22). Heterogeneous catalysts like platinum-bismuth-carbon or palladium-carbon can be filtered and removed easily from the reaction mixture(21).

There are some published studies where analysts looked for catalysts in pharmaceuticals, for example palladium (Pd) was found in a concentration of 0.077 $\mu\text{g/g}$ in enalapril maleate and platinum (Pt) was found in a concentration of 2.36 $\mu\text{g/g}$ in calcium folinate(19). Techniques other than ICP-MS were also used to measure metal catalysts in APIs such as total reflection X-ray fluorescence (TXRF) spectrometry that was used to determine rhodium (Rh), Pd, iridium (Ir) and Pt in an

antifungal medication and a pyridinyl bisphosphonate(23). The precision of the TXRF method ranged between 9% to 20% probably due to the deposition of the dissolved API sample on the reflector as noted by the researchers(23). Pd, Pt and Rh were also determined using high resolution continuum source graphite furnace atomic absorption spectrometry and direct solid sample analysis(24). Pd was found in concentrations ranging from 4.9-24.1 µg/g and it was mentioned that having a solid matrix-matched standard for calibration was challenging(24).

Other factors that contribute to elemental impurities found in the API include the processing aids, inorganic reagents, solvents and manufacturing equipment used during their synthesis. For example, processing aids like silica and charcoal as well as inorganic reagents like magnesium stearate, sodium chloride and potassium sulphate are commonly used in the manufacturing of APIs. In general, using pure compounds as required by regulators minimise the risk of metal contamination(15). In the case of solvents, if they are used in compliance with the corresponding guidelines such as ICH Q3C; guideline for residual solvents, the risk of introducing metals to the API is insignificant(25). For manufacturing equipment, they are usually made of compatible materials that ensure minimal leaching of metals such as stainless steel, hastelloy steel and glass that are resistant to corrosions. Steels are known to contain chromium, nickel, copper, cobalt, vanadium and molybdenum that may leach under harsh reaction conditions like high or low pH and high temperature(15).

1.1.2 Excipients

One of the major sources of EI in pharmaceutical products are the excipients that play an important role in delivering the API to the patient(26, 27). They are added as bulking agents to make small doses physically large enough to be handled easily,

binders to help hold a tablet together, coating to protect the formulation from moisture or light, colouring and flavouring agents to enhance patient compliance, as well as lubricants to facilitate the dosage form handling in the manufacturing facility(26, 27). These excipients usually constitute a considerable amount of the final pharmaceutical product consumed by patients(28).

Factors that contribute to the final EI profile of the excipients are similar to those contributing to the APIs elemental impurities. In addition, the source of excipients used in the formulation of pharmaceuticals plays an important role in the overall of EI in the final product, because the metal content in excipients is often inherent, so reducing, removing or controlling the metals content in them is not easy(28).

Excipients used in pharmaceuticals industry have different origins as illustrated in Figure 1.2.

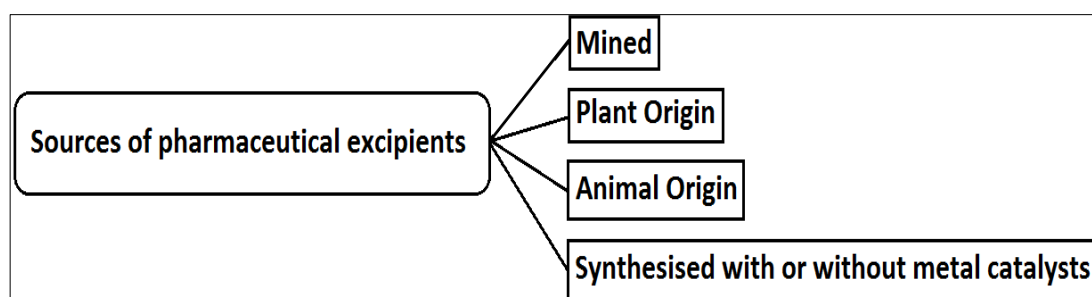


Figure 1.2 Different sources of excipients used in the pharmaceutical formulations (Adopted from Teasdale et al, 2015(15))

Mined excipients, such as talc are more challenging when assessing the risk of EI contributed from their use, because of the natural variations resulting from the geographical and geological location of the mine(15). For example, a kaolin mine near Kaznejov, Czech Republic was found from periodic testing to contain 12 to 55 µg/g of Pb, while Trimouns talc mine in Midi-Pyrenees, France is tested once a year and

found to contain less than 10 µg/g of Pb. Some of these excipients are mineral based and obtained by the conversion of mined ores like titanium dioxide that is widely used in sunscreens to protect from ultraviolet light and is also used in capsule shells(29).

Excipients obtained from plant or animal origin, such as cellulose derivatives, alginate, carrageenan, lactose, gelatine, etc. also have variable levels of metals depending on their uptake by the living organism(28). Factors contributing to that are for example the soil composition and its metal content that can be absorbed by the plant in the case of plant derived excipients(30). For marine plants, a factor that contributes to their metal content is what oceans they were harvested from(30).

The control of trace metals levels in synthetic excipients, such as silicones and povidone is easier when GMPs similar to those of the APIs are adhered to(27).

Many excipients contain metal impurities at the 1 to 10 µg/g level and most of them have not been routinely tested, so the variability in metals concentration is often unknown(29). In addition, because the pharmaceutical business for many excipient companies is minor, they may not be willing to comply with the new regulations or may not be able to. This may require buying expensive instrumentation and provide highly skilled operators to minimise the EI content, which may not be feasible for the manufacturers or may result in increasing the pricing to cover for these additional costs(28, 29).

As a result, pharmaceutical companies may find it necessary to perform the EI analysis on the excipients to determine their contribution to the final pharmaceutical

product EI level. The EI in the final product should not exceed the permitted daily exposure (PDE) limits stated in the new guidelines.

Li et al(31) used ICP-MS to analyse 190 samples prepared using microwave-assisted digestion from 31 different excipients. The highest concentration of arsenic was found in ferric oxide yellow (0.80 µg/g). For cadmium the highest concentration was 0.84 µg/g in magnesium hydroxide granular, while for lead, about 2.15 µg/g were determined in titanium dioxide. Metals with lower toxicity were also quantified and the highest concentrations were 123.5 µg/g of cobalt in talc, 154.4 µg/g of nickel in ferrous oxide (black) and 436 µg/g of vanadium in ferric oxide (red). Other metals mentioned in the new guidelines were also analysed and found in concentrations ranging between 0.01 to 59.4 µg/g(31).

The data obtained above clearly indicates that some pharmaceutical products containing these excipients may require changes in excipient sourcing and/or reformulation in order to meet the new PDE requirements.

1.1.3 Utilities and environmental factors

1. Water

The water used in the manufacturing of APIs and the final pharmaceutical product must meet the pharmacopeial requirements, that is to meet the World Health Organisation (WHO) requirements for drinking water, which is then further purified to produce purified water (PW) and water-for injection (WFI)(32). The water quality is monitored routinely as part of standard GMP. As a result the potential of water or water purification systems introducing elemental impurities to the pharmaceutical product is highly unlikely even in large-volume parenterals that contain high volumes of water within their aqueous formulations(15).

2. Air

As part of appropriate GMPs, high-efficiency particulate air (HEPA) filters, which are a type of mechanical air filters that force the air through a fine mesh of about 0.3 micrometres (μm) in diameter, are used in pharmaceutical manufacturing facilities. The fine mesh is capable of trapping fine particle like dust mites and even tobacco smoke. As a result, the risk of air introducing EI to the pharmaceutical products is negligible(33).

1.1.4 Manufacturing equipment

The manufacturing of solid products require many processes like blending, particle size reduction, granulation, tableting, coating, etc. which require various types of equipment. In the case of liquid dosage forms, solid components are dissolved or suspended using metallic equipment(15). As described in Section 1.1.1, this equipment is made of materials like for example stainless steel, that are known to contain Ni and other metals(15). Harsh conditions like the use of corrosive liquids and high or low pH may cause the transfer of metals present within the equipment to the pharmaceutical product(34). However again, maintaining standard GMP reduces the risk of metal contamination from the equipment, but more considerations are required when assessing the risk of metals known to be present in the alloys used in the equipment, as they are usually more likely to be transferred to the product under drastic conditions.

An example of metal transfer from manufacturing equipment to a product is the transfer of iron during high-pressure homogenisation, a process in which the crystalline drug particles are forced with high-pressure to pass through a narrow

homogenisation gap to produce nanosuspensions. The nanosuspensions were analysed by atomic absorption spectroscopy (AAS) and it was found that the erosion of metal is below 1 µg/g(35). AAS sensitivity is inferior to ICP techniques(36), and in the mentioned study the limit of detection (LoD) and limit of quantification (LoQ) were not provided(35).

1.1.5 Container closure system (CCS)

Packaging provides a barrier that protect from biological and physical contamination in addition to facilitating the consumer access to the product by improving its handling(37).

There are guidelines for the CCS to be used for pharmaceutical products. An example is the Food and Drug Administration (FDA) *Guidance for Industry, Container Closure Systems for Packaging Human Drugs and Biologics*(38). Solid-to solid contact is considered low risk when it comes to leachable or extractable metals form CCS. For semi-solid and liquid dosage forms, the risk is higher.

Figure 1.3 represent the risk factors associated with CCS.

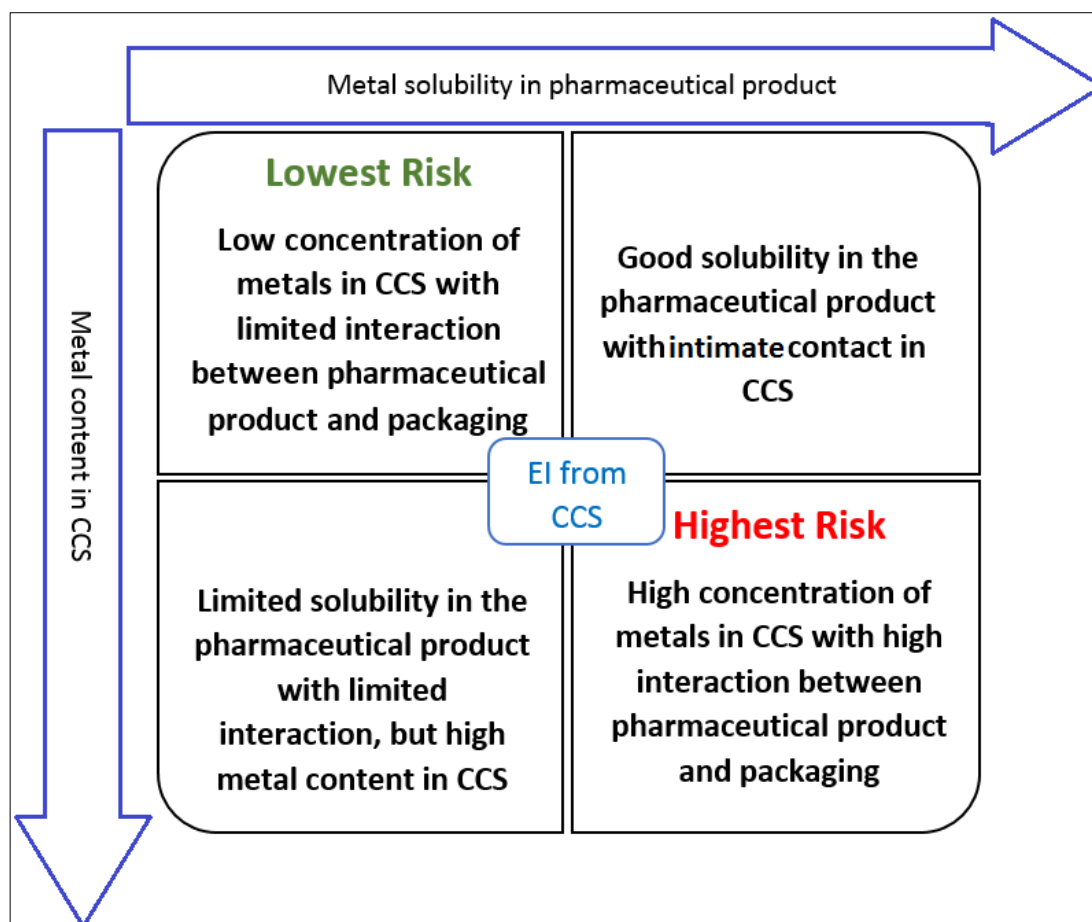


Figure 1.3 Illustration of risk factors associated with CCS (Adapted from Teasdale et al, 2015(15))

Polymers have been used in CCS for decades and a large number of catalysts used during their synthesis are organometallic or inorganic compounds(39). Common examples include the use of antimony-based catalysts in the production of polyethylene terephthalate (PET) and chromium-based catalysts for the polymerisation of polyolefins. Jenke et al(39) published a review about the elemental impurities that can be introduced from CCS to the pharmaceutical products by looking to common packaging materials metal content.

Fliszar et al(40) profiled the metal ions leached from pharmaceutical packaging material using ICP-OES. They tested three types of glass, type 1 clear, type 1 amber and type 1 with silicon dioxide inert coating and found the levels of Pb, Cd and Mg

not exceeding 0.2 µg/g. On the other hand, the level of aluminium (Al) was affected by the presence or absence of ethylenediaminetetraacetic acid (EDTA) as an extracting agent in the tested solution, as 4.7 µg/g were measured with EDTA and 500 ng/g without it. This is because Al has been shown to precipitate in the presence of phosphate solutions. In the same study three plastic CCS were also profiled, those include low-density polyethylene (LDPE), high-density polyethylene (HDPE), and PET bottles. HDPE and PET had metal concentrations not exceeding 0.15 µg/g, while LDPE was found to contain 1.5 µg/g of Al, 0.43 µg/g of Zn, 0.28 µg/g of Mg and 0.26µg/g of calcium(Ca)(40).

It was reported that tungsten microparticles that may be introduced into some pre-filled syringes used with monoclonal antibodies were found to induce protein precipitation and coagulation especially when these protein products are formulated at pH below 6(41).

1.2 Elemental impurities guidelines

1.2.1 USP <231> *Heavy metals* test limitations

The traditional method for determining heavy metals was introduced over hundred years ago in the United States Pharmacopeia's National Formulary (NF) and described as "Heavy Metal Test, USP <231>"(42). Similar tests were provided in the European Pharmacopoeia (Ph. Eur.) and the Japanese Pharmacopoeia (JP).

The method is a wet chemical screening classic colourimetric test and involves the precipitation of insoluble metal sulphides after ignition and combustion of the samples in a high temperature furnace. This is required as a preliminary step to consume the carbon followed by pH adjustment and the addition of freshly prepared

hydrogen sulphide or thioacetamide solution. The results are obtained from visually comparing the obtained colour with a standard solution of Pb. The method assumes that all potential elements behave similarly to the Pb standard(1, 14).

Industry criticism of this method began around fifteen years ago, because it has many limitations, Firstly, high temperatures between two-hundred and six-hundred degrees Celsius (°C) leads to sample loss and can also remove volatile elements such as arsenic (As), cadmium (Cd), mercury (Hg) and lead (Pb) and gave falsely low results(43, 44). In fact, some studies have shown that the use of a furnace may lead to up to fifty percent loss of volatile elements like mercury (Hg) and selenium (Se)(45). The loss is also matrix dependent and recoveries can vary significantly among different analysts because the procedures are labour intensive and time consuming(46).

Secondly, the method lacks sensitivity and specificity, there is no information about the identities of the metals that caused the positive result and the method does not provide any information about the identity of inorganic impurities in the samples. It also assumes that the test is not affected significantly by the sample matrix(1). However, since many metals sulphides may form colloids, and those behave differently to solutions, the traditional method requires that the visual comparison is done in a relatively short time after the formation of the precipitate but before the sample starts to become unstable. Thirdly, the colours of the different metal sulphides range from white to yellow, orange, brown, and black, which makes the visual comparison with the dark brown–coloured lead sulphide difficult and the

interpretation of a result differs between analysts as they differ in how they perform the visual comparison, especially when the analysts are inexperienced(17).

Another disadvantage of the test is that it consumes about two grams (g) of sample in order to achieve appropriate detection (the tests limit is around 10 µg/mL) and such large quantities are usually difficult to obtain at the early stages of drug development, or when the amount of the drug substances to be tested are limited(1).

Fourthly, the procedure involves the use of potentially hazardous solvents like thioacetamide and the fact that the limits specified by the test are based on the ability to observe the precipitate, rather than on the analysis of toxicological data is an important drawback to the traditional method(12, 47).

Finally, the test does not necessarily detect all potential forms and/or valences of elements of concern and it is not applicable to drug substances that are inorganic in nature(48).

In 2008, a panel of experts in a workshop organised by the Institute of Medicine (IOM) agreed to the fact that that USP <231> was inadequate and needed replacement, but finding a suitable analytical method that can be combined with toxicological risk assessment studies was challenging(49).

Attempts have been made to improve these pharmacopeial methods in order to alleviate some of the limitations and shortcomings by introducing instrumental analytical procedures that provide greater selectivity, sensitivity, better precision and yield higher recoveries for a wide range of metals of interest(12, 50).

Based on that, techniques such as inductively coupled plasma optical emission spectroscopy (ICP-OES) and inductively coupled plasma mass spectrometry (ICP-MS) were introduced in the new USP chapters <232>/<233> and (ICH) Q3D guidelines.

1.2.2 USP <232> elemental impurities-limits, USP <233> elemental impurities-procedures, and ICH Q3D guidelines

The limits of elemental impurities in pharmaceutical products are expressed as permitted daily exposure limits (PDEs) in µg (of element)/day. The PDEs are set for each element based on their toxicity evaluation that is related to the extent of exposure and it takes into consideration different route of administrations, oral, parenteral and inhalational as well as the daily dose of the medication.

The limits in ICH Q3D are also expressed as maximum limits when the drug product intake are 10 g/day in addition to the PDEs based on the actual medication daily intake, which can provide higher limits if the maximum daily intake is less than 10 g.

The elements in ICH Q3D are categorised to three different classes those are:

Class 1: arsenic (As), cadmium (Cd), mercury (Hg) and lead (Pb). Inherently toxic elements that require risk assessment for all routes of administration.

Class 2: This class is further subdivided to sub-class 2A, which include elements with high likelihood of occurrence; those are cobalt (Co), nickel (Ni) and vanadium (V), so they require risk assessment for all routes of administration. On the contrary, sub-class 2B includes silver (Ag), gold (Au), iridium (Ir), osmium (Os), palladium (Pd), platinum (Pt), rhodium (Rh), ruthenium (Ru), selenium (Se) and thallium (Tl) that require risk assessment only if they were intentionally added.

Class 3: barium (Ba), chromium (Cr), copper (Cu), lithium (Li), molybdenum (Mo), antimony (Sb), and tin (Sn), these elements are considered to have low toxicity and require risk assessment for oral route only if they were intentionally added, however may require assessment for parenteral and inhalational routes.

The PDEs for all the classified elements are represented in Table 1.1.

Table 1.1 PDEs ($\mu\text{g}/\text{day}$) for Elemental Impurities(10)

Element	Class	Oral	Parenteral	Inhalation
Cd	1	5	2	2
Pb	1	5	5	5
As	1	15	15	2
Hg	1	30	3	1
Co	2A	50	5	3
V	2A	100	10	1
Ni	2A	200	20	5
Tl	2B	8	8	8
Au	2B	100	100	1
Pd	2B	100	10	1
Ir	2B	100	10	1
Os	2B	100	10	1
Rh	2B	100	10	1
Ru	2B	100	10	1
Se	2B	150	80	130
Ag	2B	150	10	7
Pt	2B	100	10	1
Li	3	550	250	25
Sb	3	1200	90	20
Ba	3	1400	700	300
Mo	3	3000	1500	10
Cu	3	3000	300	30
Sn	3	6000	600	60
Cr	3	11000	1100	3

PDEs have not been established for elements that have low inherent toxicity, such as aluminium (Al), boron (B), calcium (Ca), iron (Fe), potassium (K), magnesium (Mg), manganese (Mn), sodium (Na), tungsten (W) and zinc (Zn).

There two options to calculate the level of EI and compare the results with the guidelines. The first is to analyse the final finished product. The second is to analyse the individual ingredients from which the product is manufactured, and by knowing the mass of each ingredient, calculate the contribution of the EIs from each component and hence the total exposure.

The guidelines require evaluation of the elemental impurities in the pharmaceutical products by performing a risk assessment procedure to predict the EI introduced from all possible sources and comparing that to the established PDEs. Table 1.2 shows the elements to be considered in risk assessment.

Table 1.2 Elements to be considered in risk assessment(10)

Element	Class	If intentionally added (all routes)	If not intentionally added		
			Oral	Parenteral	Inhalation
Cd	1	yes	yes	yes	yes
Pb	1	yes	yes	yes	yes
As	1	yes	yes	yes	yes
Hg	1	yes	yes	yes	yes
Co	2A	yes	yes	yes	yes
V	2A	yes	yes	yes	yes
Ni	2A	yes	yes	yes	yes
Tl	2B	yes	no	no	no
Au	2B	yes	no	no	no
Pd	2B	yes	no	no	no
Ir	2B	yes	no	no	no
Os	2B	yes	no	no	no
Rh	2B	yes	no	no	no
Ru	2B	yes	no	no	no
Se	2B	yes	no	no	no
Ag	2B	yes	no	no	no
Pt	2B	yes	no	no	no
Li	3	yes	no	yes	yes
Sb	3	yes	no	yes	yes
Ba	3	yes	no	no	yes
Mo	3	yes	no	no	yes
Cu	3	yes	no	yes	yes
Sn	3	yes	no	no	yes
Cr	3	yes	no	no	yes

If the total EI level is consistently less than 30% of the PDE, then there is no need for additional controls. However, if that is not the case, then establishment of controls is required to ensure that the EI level does not exceed the PDE in the pharmaceutical product.

The USP <232> chapter specifies the elements and the limits. The revised <232> chapter that was published in the Pharmacopeial Forum (PF) 42(2) [Mar-Apr 2016](51) has identical PDEs as the ICH Q3D(10). The alignment of the guidelines helped resolving the confusion caused by the different limits and requirements that the USP and ICH guidelines used to have(8). On the other hand, chapter <233> deals with the analytical procedure including sample preparation and instrumental methods for analysing the elements. It describes two ICP techniques, ICP-OES and ICP-MS as well as the validation requirements(9).

1.3 Human toxicity of Class 1 and Class 2A elements

1.3.1 Toxicity of Class 1 elements

1.3.1.1 Arsenic toxicity

Many As poisoning incidents have been reported over the years. For example, in 1943, As-tainted sausage poisoned around 150 people and caused the death of two consumers in St. Andrews, Scotland. In 1955, As-contaminated infant formula poisoned 12,000 Japanese infants and resulted in the death of 130 infants(52). Moreover, in 1972, 11 cases of poisoning occurred in western Minnesota after well water and soil As levels were elevated due to contamination from grasshopper bait placed on the ground in the 1930s(52).

Arsenic is predominantly absorbed from the small intestine. Minimal absorption occurs via inhalation and skin contact. The major pathway for elimination of As compounds from the body is urinary excretion(53).

The toxic effects result from the ability of arsenic to activate up to two hundred enzymes particularly those required for the synthesis and repair of deoxyribonucleic acid (DNA) and those required for cellular energy pathways(54).

Exposure to high doses of As may result in a life threatening acute poisoning characterised initially by abdominal pain, nausea, vomiting, severe diarrhoea, diffuse skin rash, cardiac abnormalities, acute psychosis and seizures(54). In addition, peripheral neuropathy and encephalopathy may occur and were reported with acute As poisoning. On the other hand, chronic As poisoning results in multisystem diseases(5, 54). Residual amounts of As stay in highly keratinised tissues like hair and nails. Finally, the carcinogenicity of arsenic is also proven and it can affect several organs such as skin, liver, bladder, kidneys, prostate and lungs(55, 56).

1.3.1.2 Cadmium toxicity

Cadmium is highly absorbed from the lungs, while only about 5% of it is absorbed from the GI tract(57). Once absorbed, it is rapidly cleared from the blood and accumulated in various tissues particularly those rich in metallothionin like the liver and kidneys(57). Metallothionin is a low molecular weight metal binding protein and when Cd binds to it its residence time in the body is prolonged due to its very slow clearance and that enhances the probability of neoplastic transformation induced by Cd(57). The internalised Cd- metallothionin is degraded in endosomes and lysosomes

releasing free Cd into the cytosol generating reactive oxygen species that activate cell death pathways(58).

Both the IARC and the US National Toxicology Program concluded that there is enough evidence of Cd human carcinogenicity as it is linked to cancers of the respiratory system, liver, kidneys, prostate, hematopoietic system and stomach(57, 59).

Acute Cd poisoning caused by oral ingestion of large doses of the metal is characterised by severe salivation, nausea, vomiting, abdominal pain, bloody diarrhoea, painful spasm of the anal sphincter, vertigo and loss of consciousness(58). If the acute poisoning is caused as a result of inhaling Cd, the symptoms include in addition to vomiting, metallic taste, dry throat or cough, headache with flu-like symptoms, muscle weakness, chest pain, asthma-like bronchospasm, pneumonitis and even fatal acute pulmonary oedema(58, 60, 61). Damage to the liver and kidneys can also occur in case of acute Cd poisoning(61). Chronic exposure to cadmium affects the kidneys, lungs and the skeleton causing chronic bronchitis, emphysema, pulmonary fibrosis and renal dysfunction characterized by tubular proteinuria(58). The nephrotoxicity is also partially responsible for the skeletal manifestations like bone defects due to osteomalacia, osteoporosis and spontaneous fractures(60). Chronic Cd exposure also increases blood pressure and causes myocardial dysfunctions(58, 59).

1.3.1.3 Mercury toxicity

Mercury toxicity is long known and it is reported as an inducer for public health disasters in Minamata Bay, Japan when methylmercury chloride effluent from a

factory that used Hg as a catalyst in the production of vinyl chloride and acetaldehyde was released into Minamata Bay(62, 63). In Iraq, bread made from methylmercury-treated grain was consumed by people in two different occasions, 1959-1960 and 1971-1972 poisoning many and causing foetal deformities when pregnant women consumed that bread during those periods(62, 63).

Inhalation of Hg vapour is very hazardous because it is almost completely absorbed and about 75% of it is retained(62). The systems that are affected the most are the nervous, pulmonary, genitourinary (GU), GI and haemopoietic systems. Hg induces mitochondrial dysfunction and oxidative stress(64).

Elemental mercury is poorly absorbed in the GI tract and is readily eliminated in faeces(62). Inorganic salts of mercury are corrosive to gastric mucosa and accumulate in the proximal convoluted tubules of the kidneys(62). Organic mercury compounds are more toxic and the poisoning symptoms can be delayed for weeks with methyl and ethyl mercury being the most toxic because of their complete absorption from the GI tract and slow excretion(62, 63).

In addition to the elimination of mercury in faeces, it is also eliminated in urine and significant amounts are shed in sweat, tears, saliva and milk in case of breast-feeding women(63). It also crosses the placental and is teratogenic(62). Prenatal exposure have been associated with neurodevelopmental delays and cognitive deficits and larger doses induce a form of cerebral palsy(63).

Acute Hg poisoning by inhalation causes symptoms that include cough, chest tightness, dyspnea, fever, chills, general weakness and GI upset. In addition to peripheral neuropathy and even renal failure(62).

Chronic exposure to organic Hg affects the central nervous system (CNS) because compounds like methylmercury can cross the blood brain barrier (BBB)(62) causing irritability, insomnia, headache, hearing loss, constricted visual fields, decreased cognitive function, tremors, seizures, ataxia, slurred speech, hallucinations, paralysis, coma, and eventually death(63). Chronic mercury poisoning also causes pneumonitis, necrotizing bronchiolitis, pulmonary oedema, nephrotic syndrome, hypertension, myocardial infarction, arrhythmia, reduction in heart rate variability, generalized atherosclerosis and overall increase in total cardiovascular mortality(64).

Skin contact results in gray or blue-black pigmentation, cutaneous burns, contact dermatitis, and exfoliation. Chronic exposure also result in mercurialentis, which is gray or brown discoloration of the lens of the eye(62).

1.3.1.4 Lead toxicity

In 1678, Vernatti probably made the earliest record of Pb poisoning among white-lead workers in England(65). In 1892, Pb poisoning of children exposed to white leaded paint was reported in Brisbane, Australia(66).

In 1900s, Hamilton, who was a pathologist that pioneered industrial control of occupational Pb exposure, recognized occupational Pb exposure by inhalation of dust and fumes. Additionally, in 1904, Gibson concluded that lead paint in houses was responsible for poisoning children(67). Children exposed to lead showed signs of learning difficulties, school failure and behavioral disorders(66).

Human exposure to Pb could occur via inhalation and ingestion. Lead's absorption is affected by many factors with pregnant women and children being more vulnerable as they may absorb 40% to 70% of ingested Pb. Pb is excreted with urine and faeces. The unexcreted portion is distributed and exchanged among haematologic, renal, neurologic and mineralised tissues like teeth and bones.

Lead's toxicity results from its ability to bind strongly to sulfhydryl groups on proteins leading to distortion of structural proteins and enzymes. In addition to its ability to interfere with the development of the endogenous opiate system. It can also mimic or compete with calcium hindering its physiological functions. Due to that, lead poisoning affects many systems in the human, but the one most affected is the CNS(66, 68, 69).

Acute Pb poisoning causes limb and joint pains, haemolysis, renal tubular damage with glycosuria and aminoaciduria, acute hepatorenal failure, convulsions, coma and eventually death. Surviving severe lead poisoning in children left them with permanent neurological disorders including deafness and mental retardation(65, 70).

Chronic Pb poisoning affect the central and peripheral nervous systems, haemopoietic system, GU system, musculoskeletal system and GI tract(65-67). CNS Pb toxicity symptoms include headaches, irritability, agitation, ataxia, drowsiness confusion and convulsions. Peripheral neuropathy is associated with wrist or foot drop(65, 66). Haemopoietic toxicity symptoms are characterised by anaemia, hemolysis and hypertension(66, 67). Regarding the GU system, Pb poisoning reduces glomerular filtration rate, causes interstitial nephritis and nonspecific proximal tubular dysfunction(66, 67). Because Pb is deposited in mineralised tissues, bones

formation is altered(65). Additionally, GI symptoms like nausea, vomiting, abdominal pain, metallic taste, anorexia, constipation or diarrhoea appear with Pb poisoning(67). Because of lead's ability to cross the placenta, it was associated with preterm delivery and low birth weights. It is also secreted with breast milk increasing infants' exposure to the toxic metal(69). Finally, inorganic lead is classified as a Group 2A carcinogen by IARC, which means it is likely to cause human cancer(71).

1.3.2 Toxicity of Class 2A elements

1.3.2.1 Cobalt toxicity

Cobalt is an essential element required for human and animals metabolism. It is necessary for the formation of cobalamin, also known as vitamin B₁₂, which catalyses the production of genetic material. Co also plays a role in the formation of red blood cells(72). Traditionally, Co was used in medicine as a treatment for anaemia, however, in the 1940s it was found that it blocks iodine uptake by the thyroid gland and thus reduces its activity and causing goiter(73, 74).

Cobalt poisoning has been reported over a number of years. In the 1960s, some breweries in Quebec City; Canada, Omaha; Nebraska and in Minneapolis; Minnesota used 1–1.5 mg cobalt chloride/L beer to reduce the foaming of soap residues from electric dishwashers causing what was known as beer drinker's cardiomyopathy. However, co-factors like inadequate protein and vitamin intake as well as Zn depletion contributed to the development of the cardiomyopathy in those who consumed that beer(75).

In the 1970s high-speed grinding disks coated with abrasive microdiamonds embedded in binding cobalt powder were introduced to the diamond industry in Belgium. This was accompanied by progressive increase in respiratory disease among

workers due to inhaling the metal's dust and it was referred to as hard-metal pneumoconiosis. Acute exposure causes cough, wheezing and malaise, while chronic exposure led to pulmonary fibrosis(76). Several other cases of Co poisoning in patients who had undergone metal-on-metal hip replacement or other procedures involving similar prostheses were reported as well(77-79).

Cobalt is absorbed from both the GI and respiratory tracts. Following absorption, it is distributed to the liver, kidneys, pancreas, and heart, with the relative content in skeleton and skeletal muscle increasing with time. Co is mainly eliminated with urine(73, 80).

Cobalt poisoning symptoms are nausea, vomiting, chronic thyroiditis, goiter, myxoedema, blindness, deafness and peripheral neuropathy(81). In addition to cognitive decline characterised by memory loss and poor concentration, disorientation as well as muscle weakness, numbness and tremor(74, 80, 82). In case of acute inhalational exposure, hypersensitivity pneumonitis usually occurs that evolves to chronic fibrosis after long-term exposure. Skin contact with Co is reported to cause allergic contact dermatitis(74, 80, 82).

1.3.2.2 Nickel toxicity

In 1890, Mond and co-workers(83) discovered one of the most toxic chemicals encountered industrially; nickel carbonyl. Nickel carbonyl is a highly volatilised compound produced as an intermediate in the separation of nickel from its ores, the fabrication of nickel and nickel alloy components, the manufacturing of high purity nickel powders and catalysts(83). Inhalation of nickel carbonyl produces initial and delayed symptoms. The initial symptoms include cough, tightness in the chest,

nausea, vomiting and frontal headache, while chronic exposure for several years can induce carcinoma of the respiratory tract(84, 85).

Nickel is normally present in human tissues. It helps maintaining proper functioning of the body, increasing hormonal activity and is involved in lipid metabolism. It is absorbed via the skin, respiratory and GI tracts(86). Toxicity of Ni results from its interference with the metabolism of essential elements like Fe, Mn, Ca, Zn, Cu and/or Mg(85).

Skin contact causes dermatitis and produces erythema, eczema and lichenification of the skin. Dermatitis and eczema can be aggravated when Ni is ingested. Other symptoms resulting from exposure to high concentrations of Ni are asthma, conjunctivitis, high blood pressure, dizziness, difficulty sleeping, neurological deficit and developmental deficits in children. In addition, it increases the risk of lung cancer and cardiovascular diseases(87). Finally, when Ni is introduced into the body, it generates reactive oxygen species and free radicals that may also damage the kidneys and the liver(88).

1.3.2.3 Vanadium toxicity

Vanadium compounds like sodium metavanadate were traditionally used to treat tuberculosis, syphilis, diabetes and anaemia(89).

Vanadium has oxidising abilities and can inhibit oxidative phosphorylation in the body(89). It is absorbed from the lungs and accumulates there with age. Limited amounts are absorbed via GI tract following ingestion and skin absorption is minor in humans. It is mainly excreted in the urine and a fraction is eliminated in the faeces(90). Exposure to toxic amounts of V causes headache, dizziness, skin rash, digestive problems like nausea, vomiting, stomach pain, diarrhoea, inflammation to

the GI tract, and loss of appetite. Respiratory symptoms include rhinitis, wheezing, cough, sore throat, nasal haemorrhage, irritation to nose, throat and the upper respiratory tract mucosa, chest pain, bronchitis and pneumonia(89, 90).

1.4 Validation Issues

The validation of any optimised analytical procedure is important to make sure that the method is accurate and precise.

In USP <233>(9), the recommended validation procedure is to spike the samples at concentrations ranging from 50% to 150% of the indicated limit value for each target element. The method is considered accurate if the spike recovery was between 70% to 150% for the mean of three replicate preparations at each concentration. For precision, six spiked samples are required to be analysed and the acceptance criteria for the repeatability is a relative standard deviation (RSD) not more than 20% for each target element and for intermediate precision, RSD of not more than 25% for each target element is acceptable(9).

Many methods published in the literature regarding the determination of EI in pharmaceuticals were validated as described in USP <233> (13, 17, 47, 123-129).

However, using a standard reference material (SRM) ensures the highest level of accuracy and precision in routine analytical measurements(91).

SRM is a well characterised material that is sufficiently homogenous, stable and is certified for one or more chemical and physical properties. It is used to validate analytical measurements by ensuring the accuracy and precision of an analytical method as well as its long-term adequacy(92).

For EI in pharmaceutical products only one solid SRM is available and that is from the National Institute of Research and Technology, *NIST 3280 multivitamin/multielement* tablets. Each tablet weighs approximately 1.5 g and consists of vitamins, carotenoids, and minerals. It is usually used to validate analytical methods developed for the analysis of vitamins and carotenoids. However, it also has certified levels of elements. The elements included in the *NIST 3280* tablets are B, Ca, Cl, Cu, I, Fe, Mg, K, Zn, As, Cr, Pb, Mo, Ni, Se, Cd, Co, Na, Ti, V, Sb, Sn, silicon (Si), phosphorus (P) lanthanum (La) and strontium (Sr). It is produced by blending vitamin and mineral pre-mixes with the remaining excipients. Fat-soluble vitamins and carotenoids were added as gelatine beadlets and then the tablets were coated with yellow aluminium lake, triethyl citrate, polysorbate 80, hypromellose, and titanium dioxide(93).

However, this reference material has Class 1 elements in levels unrepresentative of the guidelines. Arsenic for example is present in a concentration of 0.132 ± 0.044 $\mu\text{g/g}$ (93) in comparison with the guidelines limit of 6 $\mu\text{g/g}$ in the finished drug product with daily intake of 2.5 g(10). In addition, it does not include Hg.

1.5 Principles of instruments used in this work

The following sections discuss the principles of the instruments used in this work for the determination of Class 1 and Class 2A elements in pharmaceutical products.

1.5.1 Microwave assisted extraction of elements form pharmaceuticals for ICP-OES and ICP-MS determination

One of the challenges facing pharmaceutical industry now regarding the implementation of the new EI guidelines is preparing the different samples for analysis using appropriate procedures. Most analytical procedures require samples

to be prepared as solutions. This include ICP-OES and ICP-MS, the two techniques suggested as an alternative to USP <231> in addition to other techniques useful for this purpose such as AAS(94). The use of microwave (MW) assisted wet digestion to prepare samples was first described in 1975 by Abu-Samra et al(95) to prepare biological samples for metals analysis using flame atomic absorption and since that time it has become widely used in many fields.

In the USP <233> chapter, the proposed sample preparation method for materials that are not directly soluble in organic or aqueous solvents is closed vessel digestion using concentrated acid(s)(96). The closed vessel digestion is chosen in order to minimise the loss of volatile impurities like Hg which was shown to be completely lost when the samples are digested using techniques that require ignition and combustion at high temperatures(8, 97). It also minimises contamination from the surrounding laboratory environment. Using closed vessel digestion method allows the use of temperatures higher than the boiling point of the acids involved in the digestion due to the elevated pressure of the system. The pressure builds up in the vessel from the gases obtained as a result of heating the liquid mixture. Vapour will also be produced from the heated acids themselves, but it lacks the ability of absorbing MW energy, so will have a lower temperature than the liquid mixture. Eventually the vapour will condense on the cool vessel wall(98).

MW assisted digestion provides a suitable way for digesting samples in pressurised closed vessels with minimum loss of elements when appropriate acids are used.

The method gives efficient digestion in a reasonable amount of time and was found to be superior to the dry ashing method in recovering elements like Pb and Hg when analysing EI in medicinal plants(99, 100). In one of the mentioned studies, up to 0.5

g of *Peumus boldus*, *Paulinia cupana*, *Passiflora incarnata L.*, and *Maytenus ilicifolia* were digested in closed vessels using nitric acid (HNO_3) and gave recoveries ranging between 96 and 103% for Class 1 elements; As, Cd, Hg and Pb(99).

In general for MW assisted digestion, HNO_3 is used as oxidizing agent alone or combined with other acids such as hydrochloric acid (HCl), sulfuric acid (H_2SO_4) or even hydrofluoric acid (HF) to get complete digestion of silica containing matrices(101). Sometimes it also used in combination with hydrogen peroxide (H_2O_2) and many others including alkaline reagents(102, 103). HNO_3 is used widely due to its suitability to most instrumental techniques.

Accordingly, the use of MW assisted acid digestion followed by analysis using ICP-OES or ICP-MS became very popular to fulfil the new pharmacopeial requirement. In a study to determine elemental impurities in pharmaceutical excipients, the samples were prepared using closed-vessel MW assisted digestion with a “vent-and-reseal” design to control the pressure and avoid over-pressurising the system which may lead to sample loss(31).

Even though MW assisted acid digestion was successfully applied to many samples, it has some limitations with certain type of applications due to the nature of the samples used. It was reported that the used of MW assisted digestion using HNO_3 for tricyclic APIs including carbamazepine, imipramine hydrochloride and amitriptyline hydrochloride was not effective as a yellow-orange solid residue was formed and it was identified as stable nitro compounds using proton nuclear magnetic resonance (^1H NMR)(97). To overcome the problem MW induced combustion (MIC) that integrates the combustion and acid digestion into an oxygen-pressurised thick-wall closed-vessel was used. It was very efficient and gave recoveries for As, Cd, Hg and

Pb of 94-103%(97). Combustion techniques convert carbon and hydrogen to their corresponding oxidation products allowing organic matrices to be completely decomposed and thus minimise analysis interferences(100).

1.5.1.1 Microwave Fundamentals

The interaction between the sample during digestion and the MW electromagnetic radiation is similar to that between energy and matter in general. MW have frequencies ranging from 300 up to 300,000 megahertz (MHz) and wavelengths (λ) ranging from one meter (m) to one millimetre (mm)(104). They are between infrared radiation and radio frequencies in the electromagnetic radiation spectrum(104). Frequencies between 915 and 22,125 MHz can be used for scientific, medical and industrial purposes according to the US Federal Communications Commission (FCC)(105).

Figure 1.4 illustrates the position of MW in regards to the electromagnetic radiation spectrum.

The Figure originally presented here cannot be made freely available via LJMU E-Theses Collection because of copyright. The Figure was sourced at <https://www.autodesk.com/products/eagle/blog/electromagnetic-wireless-electronic-basics/>

Figure 1.4 Electromagnetic radiation spectrum(106)

Material may transmit, absorb and/or reflect MW depending on their nature, such as structure and composition. Transparent materials allow MW to pass through them easily. Absorptive and conductive materials will increase in temperature when they

are exposed to MW because of energy transfer. Unlike conventional heating, MW heating does not result from direct heat transfer, but it is due to the energy conversion from electromagnetic energy to thermal energy(107). MW heating is usually referred to as dielectric heating because of the electric field resulting from the electromagnetic radiation(108).

For liquids, energy transfer occurs via two mechanisms when they are subjected to MW. Those are dipolar rotation and ionic conduction, and this depends on the dipoles and ions present in them which affect the type of interaction occurring. Both interactions increase the molecular movement throughout the volume of the material and thus produce volumetric heating(107, 109). In homogeneous liquids, the MW energy will redistribute between molecules giving uniform heating, while for heterogeneous systems the heating may become selective. This non-uniformity heating results from the different components ability to interact with MW energy(110).

1.5.1.2 Dipole Rotation

This process occurs when polar molecules, e.g. water, are subjected to the oscillated electric field from the MW and align with it, followed by returning to the disordered state and vice versa in a relatively very short time, see Figure 1.5 This result in a very rapid heating(107, 110, 111).

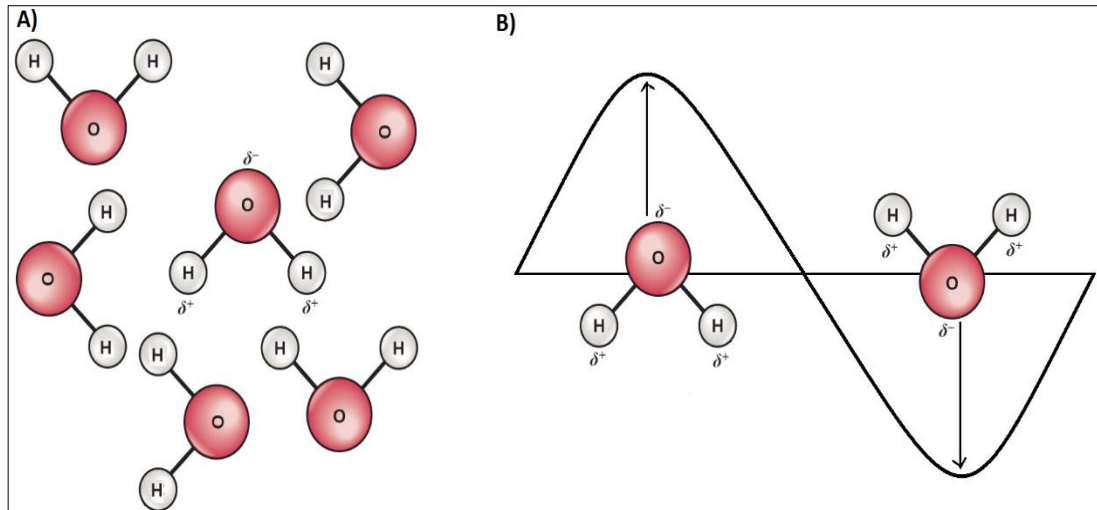


Figure 1.5 Schematic representation of the water molecules alternating alignment under the oscillating electric field induced by MW. A) Water molecules without the influence of MW. B) Water molecules under the influence of MW. (Adapted from Flores EM,2014(112))

1.5.1.3 Ionic conduction

This occurs when the liquid's charges flow as a result of the interaction with the oscillating MW electric field, causing the ions to be in motion and thus suffers from resistance to its movement from the other species present. This process generates heat around the ions and as the temperature increases the ion flow will increase as well and the cycle continues(109, 111, 113). Anions and cations must be present in the solution to contribute to the heating process and so, their concentration and mobility are directly related to the heating resulting from MW.

Solutions heating degrees with MW can vary due to many factors including ion mobility, which depends on the ions size, charge, conductivity and temperature(109, 111, 113). Figure 1.6 illustrates the ionic conduction under the oscillating MW electric field.

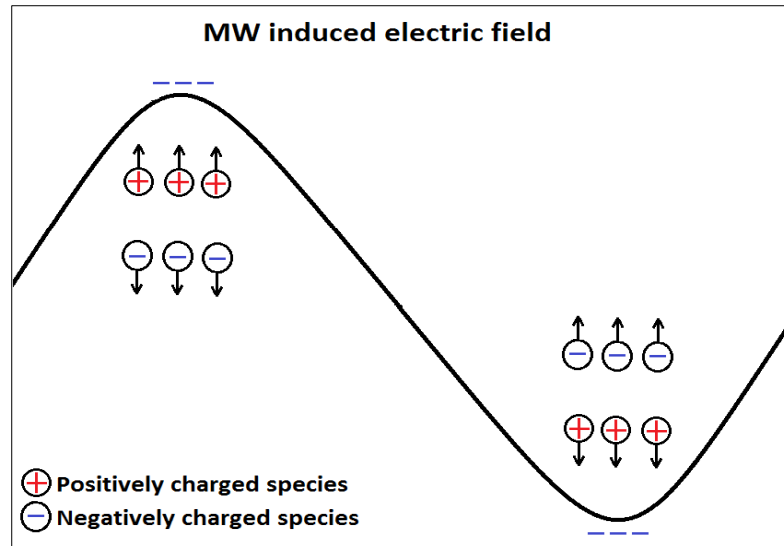


Figure 1.6 Schematic representation of the ionic conduction under the oscillating MW electric field. (Adapted from Flores EM,2014(112))

1.5.1.4 Dielectric Heating

The dielectric properties of materials play an important role in their interaction with MW. It represents the different materials abilities to convert electromagnetic energy into heat(111, 114).

The materials capacity of absorbing MW is directly related to the MW penetration degree into the material. Reflective materials are not penetrated by MW, while transparent materials will be easily penetrated. For absorptive materials, electromagnetic energy will convert to heat according to their dissipation factors, or loss tangent ($\tan \delta$) which depends on the relation between the dielectric loss factor (ϵ'') and the dielectric constant, also known as relative permittivity (ϵ') of the material(19, 115), as presented in Equation 1.1:

$$\tan \delta = \epsilon'' / \epsilon' \dots \text{Equation 1.1}$$

ϵ'' expresses the ability of a material to convert the absorbed electromagnetic energy to heat by dissipating it, while ϵ' measures the ability of a material to polarise under the influence of external electric field(19, 115).

Polar liquids that have permanent dipole moments within their molecules have comparatively higher ϵ' than nonpolar liquids that become polarised when an external electric field is applied to them(113).

Regarding the microwave equipment components, the walls are made of reflective materials and the accessories inside are made of transparent materials(116).

1.5.1.5 Monomode and multimode microwave equipment

Microwave digestion systems can be categorised according to the delivery method of the MW energy to monomode and multimode systems. These are constructed differently to meet research applications(117). Magnetrons are commonly used as the radiation source in microwaves(118).

Monomode microwaves have small cavities that allow the MW to be directly focused on the liquid mixture, resulting in a well defined MW field with high density that enhance heating rates, yet only one sample can be digested each run(119). As heating and digestion proceed, the internal pressure of the vessel usually increases due to the vaporisation of part the digested material. To prevent damage to the vessel because of the excessive pressure developed during digestion, the cap is displaced from a sealing position into a non-sealing position when internal pressure exceeds a predetermined value(120).

Because the vessels used with monomode microwaves are smaller, the likelihood of high pressure build up is more probable. The high pressure activates the cap-

releasing mechanism causing sometimes significant losses of elements like Hg or those that form volatile compounds like As, Sb and Sn(98).

On the other hand, multimode microwaves have large cavities that distribute the MW in a chaotic manner, causing non-uniform distribution of heat. However, they can take more than one sample in the same run, but the time required for heating and cooling the system is much longer with the bigger cavity(110, 117). Homogenizing the MW field for multimode microwaves can be obtained by using two magnetrons facing each other, to help irradiating the samples from all directions(118). Figure 1.7 represents graphical illustration of monomode and multimode microwaves.

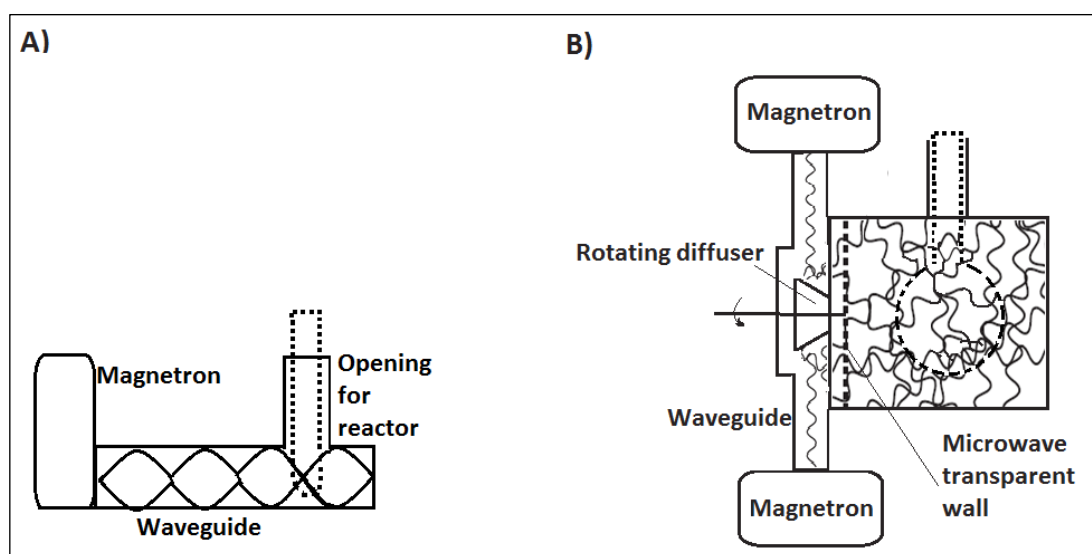


Figure 1.7 Graphical illustration of monomode and multimode microwaves.
(Adapted from Nüchter et al, 2003(118))

Recently microwaves that have direct multimode cavities to provide efficient heating like monomode microwaves and at the same time can take more than one sample in the same run as multimode microwaves have become available to provide the advantages of both types(121).

1.6 Inductively coupled plasma (ICP) for elemental impurities analysis in pharmaceuticals

ICP based instruments have been used in the pharmaceutical applications discussed in the previous sections(13, 17, 47, 122-128).

Plasma is a state of matter that consist of positively and negatively charged particles with approximately equal charge density in addition to neutral atoms, molecules and radicals, so its overall charge is roughly zero(129). It is formed by heating a gas enough to cause the atoms to collide and ionise as the random kinetic energy of the molecules exceeds the ionisation energy. That is why sometimes it is simply referred to as an ionised gas and it is considered the fourth state of matter(130). Plasma was given its name which means 'moldable substance' in Greek by Irving Langmuir in the 1920s who pioneered this type of work(131).

The plasma has distinctive characteristics because it is electrically conductive, so its behavior can be dominated by electric and magnetic fields(132).

Argon (Ar) is usually the gas used to produce plasma for ICP-OES and ICP-MS. Once generated, the plasma is then used to dissociate the sample as well as exciting and ionising atoms for atomic and ionic emission. In addition, Ar-ICP is able to efficiently generate singly charged ions from the elements in the sample making the metals detection with OES and MS very suitable(133, 134).

ICP development started In 1940s by Babat, who published a paper about the characteristics of 'electrodless discharges' produced at atmospheric pressure during World War II(19, 135). The next step in the evolution of ICP was in 1960s when Reed

described the formation, stabilisation and thermal isolation Ar-ICP(136). In 1970s, Velmer Fassel in the United States of America (USA) made breakthrough developments of the ICP, which is now used today(136). He_(g) demonstrated its use as ion source for mass spectrometry(137). In the same period, Greenfield in the United Kingdom (UK) also recognised the use of ICP as a spectroscopic source(135, 138, 139).

For modern ICP, a pure gas, usually argon is directed through a torch. Other gases that are used including helium (He) and nitrogen, the gas purity is important as contaminants might quench the torch(130-132). Conventional torches consist of three accurately aligned concentric tubes made of silica, quartz or any other suitable material for argon flow and sample aerosol injection(134-136, 140). The spacing between the outer and middle tubes is narrow to allow high velocity emerging of gas introduced in between. The outside chamber design makes the gas spiral tangentially around it as it proceeds upward. See Figure 1.8.

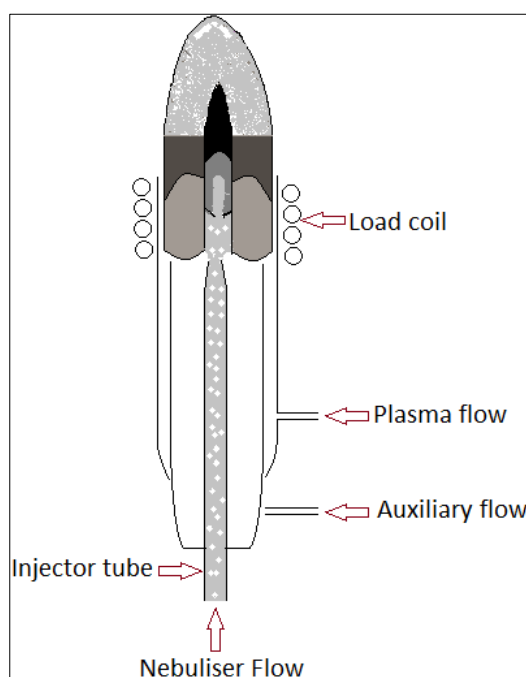


Figure 1.8 Graphical illustration of ICP torch

The outermost, longest tube at the top end of the torch is surrounded by a water or gas cooled induction coil, usually made of copper and known as the load coil that is connected to a radio frequency (RF) generator. When RF power (700 -1500 watts (W)) is applied to the load coil, a rapidly oscillating current that moves back and forth within the coil at a rate corresponding to generator's frequency (27-40 MHz) generates magnetic and electric fields(134-136). As the gas is swirled in a controlled flow rate through the two annular spaces between the tubes in the torch, a spark is applied to it from a Tesla coil initiating the gas ionisation by stripping some electrons from the gas atoms. The resulting electrons then interact with the magnetic field and are accelerated by it(135, 136). This process is called inductive coupling(134). The electrons produced with high energy will then ionise more gas atoms by collision excitation and this chain reaction continues forming the ICP discharge that consists of the gas atoms, ions and electrons and is sustained by the continuous supply of RF energy that is transferred to it through inductive coupling between the coil and the ionised gas within the torch(137, 141, 142).

The ICP discharge has a very intense white colour, sometimes called the argon continuum, when $\text{Ar}_{(g)}$ is used. The ICP temperature ranges from 6000 to 10000 °K, so one of the controlled high gas flow rate (10-20 Liter/minute (L/min)) between the outer and middle tubes functions is to protect the wall and the tip of the torch from the intense heat by cooling it, so it is referred to as the coolant flow. This gas is also called the plasma flow or the "outer" gas flow and is normally about 7-15 L/min(134-136). It is worth mentioning that different plasma regions differ in their temperature. In addition, the plasma can be divided to zones where different processes occur,

Koirtyohann et al. suggested names for each zone(134, 140, 143). Figure 1.9 represents the ICP torch, plasma regions temperature and the different plasma zones.

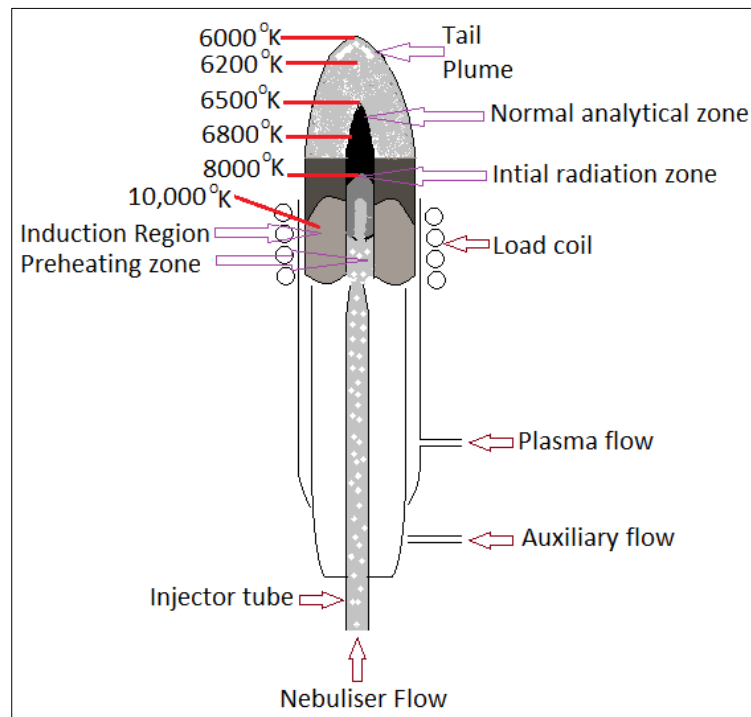


Figure 1.9 Plasma regions and temperatures ($^{\circ}\text{K} \pm 10\%$) and the different plasma zones

ICP's resemble a toroidal or annular shape in the energy input region. The base of the discharge is doughnut-shaped as the sample aerosol injected from the nebuliser via the inner gas flow forms a hole through the center of the discharge.

The sample aerosol introduction into the plasma is made easier by the auxiliary flow, a.k.a intermediate flow that runs directly under the plasma toroid and keeps the plasma discharge off the intermediate and injector tubes in the torch. It is usually about 1-3 L/min and when organic samples are analysed, the auxiliary flow helps reducing carbon formation on the tip of the injector tube(134, 136).

The doughnut itself is where the induction energy transfers from the coil to the plasma, so it is called the induction zone(134-136, 138). As mentioned before, the

aerosol, which is a very fine mist of droplets produced from the liquid samples is carried into the center of the plasma by the inner gas flow; the nebuliser, and is produced as a result of the high plasma temperature desolvating the samples by removing the solvents in which its dissolved leaving small salt particles(134-136, 138). Then, these particles are vaporised into individual molecules of gas, which then dissociate into atoms in a process known as atomization, these processes occur in the preheating zone. Finally, the ICP excites and ionises the formed atoms in the initial radiation zone and the normal analytical zone(134-136). The exact mechanisms of excitation and ionisation are not very clear, but it is believed to be as a result of the analytes atoms collisions with the high-energy electrons(134, 140). See Figure 1.10

The Figure originally presented here cannot be made freely available via LJMU E-Theses Collection because of copyright. The Figure was sourced at *Boss CB, Fredeen KJ. Concepts, instrumentation and techniques in inductively coupled plasma optical emission spectrometry. Chapter 2: General Characteristics of ICP-OES. Norwalk: Perkin Elmer; 1999.*

Figure 1.10 Different processes that occur when an aerosol droplet is injected into the ICP discharge (Adopted from Boss CB and Fredeen KJ, 1999(134))

1.6.1 ICP advantages

Compared to flames, furnaces and electrothermal methods, ICP provides many advantages due to its superiority in vaporizing, atomizing, exciting and ionising multielements in different samples reproducibly. This is due to the higher temperature provided by ICP in comparison to the mentioned techniques, where the temperature maximally reaches 3300 °K. The elevated ICP temperature also reduces chemical interferences as the analyte particles reside for about two milliseconds in the high temperature and that is considerably longer time compared to flames and furnaces that helps reducing matrix interferences(134, 136). Furthermore, the sample's aerosol is directed into the center of the ICP discharge, which prevent it from interfering with the energy transfer from the load coil to the discharge unlike non-ICP discharges and this leads to minimised matrix effects and higher stability. Finally, ICP is capable of analysing large number of samples in a relatively short period with very good detection limits over a wide range for most elements(135, 140).

1.6.2 ICP-Sample Introduction

The samples are introduced to the ICP using nebulisers that generally use gas flow to deliver the aerosol after converting liquids into a fine mist in a spray chamber and thence the torch. The samples introduced to ICP can be liquids in nature or solids dissolved in suitable solvents. The nebulisation process is critical to deliver the sample in a suitable form; that is small droplets, so that the plasma can then desolvate, vaporise, atomise, ionise, and excite(134, 135).

Two forces are successfully able to break up the liquid sample into aerosols to be delivered for ICP; those are ultrasonic mechanical forces and pneumatic forces. The

latter is the most commonly used for commercial ICP nebulisers(125, 144). The different types of nebulisers used with ICP instruments are concentric, micro-concentric, cross-flow, Babington and ultrasonic nebulisers(136, 145-148).

The produced sample aerosol is then transported to the torch in order to be injected into the plasma. A spray chamber is placed between the nebuliser and the torch, to ensure that only small droplets reach the plasma(148, 149). The main function of the spray chamber is to eliminate large droplets (>10 μm in diameter) produced by the nebuliser. Another function is to smooth out pulses during nebulisation that result from pumping the sample solution(134).

In addition, some ICP-MS spray chambers are externally cooled to 2–5°C to minimize the amount of solvent going into the plasma, enhance the sample's thermal stability, reduce oxide species and allow the aspiration of organic solvents more easily(145).

The drainage characteristics have an impact on the performance of ICP instrument and it is important to be continuous and smooth(148). In addition to the drainage system carrying away excess sample from the spray chamber to a waste container, it provides the backpressure required to force the nebuliser gas carrying the sample aerosol to flow through the torch and into the plasma discharge(134, 148, 150). The drainage systems can be blocks, loops, U-tubes or tubing connected to a peristaltic pump(134).

1.6.3 Inductively coupled plasma optical emission spectroscopy (ICP-OES)

Figure 1.11 illustrates the layout and major components of ICP-OES instrument

The Figure originally presented here cannot be made freely available via LJMU E-Theses Collection because of copyright. The Figure was sourced at *Boss CB, Fredeen KJ. Concepts, instrumentation and techniques in inductively coupled plasma optical emission spectrometry. Chapter 3: ICP-OES Instrumentation. Norwalk: Perkin Elmer; 1999.*

Figure 1.11 Basic components of ICP-OES instrument (Adopted from Boss CB and Fredeen KJ, 1999(134))

ICP-OES is one of the most common methods for elemental analysis. It can analyse various types of dissolved samples with good detection limits and low interference for most elements. After the sample is introduced as an aerosol and became excited and ionised by the plasma, the emitted radiation in the ultraviolet (UV)/visible range from the excited elements decaying back to lower energy states is sampled for measurement using optical spectrometer(134, 135, 151). Each excited element has a typical emission spectrum and emits specific λ . Furthermore, the element concentration in the sample is proportional to the radiation intensity(151).

Understanding the nature of atomic and ionic spectra is useful to better understand these processes.

1.6.3.1 Nature of atomic and ionic spectra

In 1913, Ernest Rutherford and Niels Bohr introduced the Rutherford–Bohr model of atoms. The model describes the atom as a positively charged nucleus surrounded by negatively charged electrons that travel in circular, discrete orbitals around the

nucleus. These orbitals have distinct energy levels that increase as it gets far from the nucleus. Each atom has a certain number of orbitals(152-154).

Normally, electrons are in their ground state that is the lowest energy state available. The atoms energy can be increased by collision with other atoms, ions, electrons or molecules, or by absorbing electromagnetic radiation. When this happens, many possible phenomena can take place, but mostly the absorbed energy will excite the atom, or will increase its kinetic energy(152, 154).

When the atom is in the excited state, an electron from the ground state orbital promotes to an orbital with higher energy level. This state is less stable, so the atom will lose energy by collision with other particles or emission of a photon i.e. electromagnetic radiation to decay back to a more stable, less energy state, thus the excited electron returns to its original orbital. The energy required for electron transitions between orbitals must be equal to the energy difference between two levels regardless whether it was radiational or thermal, i.e. collisions(152, 154).

Sometimes, when absorbed energy is high, electrons may completely dissociate from the atom in a process called ionisation, because it leads to the formation of ions with a net positive charge. For many atoms, more than one electron can be completely removed when applying suitable energies known as ionisation potentials that differ for each element. Ions also have ground and excited states and behave similarly to atoms regarding excitation and decay processes(134, 155).

For radiative transitions, a photon's energy can be derived through Planck's equation:

$$\Delta E = hf = hc/\lambda \dots \text{Equation 1.2}$$

Where the energy (ΔE) equals Planck's constant (h) times its frequency (f) and thus is proportional to its f , or inversely to its wavelength (λ), since c is the speed of light and equals $f\lambda$.

Each element has characteristic energy levels and consequently unique absorption and emission wavelengths(134, 154). Figure 1.12 represents the excitation of atom followed by its decay to a more stable state.

The Figure originally presented here cannot be made freely available via LJMU E-Theses Collection because of copyright. The Figure was sourced at *Boss CB, Fredeen KJ. Concepts, instrumentation and techniques in inductively coupled plasma optical emission spectrometry. Chapter 1: An Overview of Elemental Analysis via Atomic Spectroscopy Techniques. Norwalk: Perkin Elmer; 1999.*

Figure 1.12 Rutherford-Bohr model of an atom showing its excitation to a higher energy state followed by its decay to a lower energy state by releasing the gained energy (Adapted from Boss CB and Fredeen KJ, 1999(134))

The ICP in the instrument can populate a wide number of different energy levels for various elements simultaneously all the time, which gives flexibility to the technique by allowing the measurement of several emission λ for the same element and the emission obtained for various different elements concurrently. This characteristic provide advantages as explained, but is also disadvantageous, because the interferences increases with increasing the number of emission λ (134, 151).

The torch can be operated in vertical position, so the analytical zone is viewed radially; i.e. side-on viewing, or it can be put horizontally, so the analytical zone is viewed axially; i.e. end-on viewing. In addition, a combination of both can be used called dual viewing. Radial ICPs are more robust and more resistant to matrix effects, but less

sensitive. On the other hand, axial ICPs are more sensitive to analytes but also more prone to matrix effects. This is because of the longer bath length which allows the production of higher analyte emission and thus improved the sensitivity that is reflected in five to ten fold improvement in detection limits(156, 157). Regardless of the ICP viewing configuration, a focusing optic like a concave mirror or convex lens is usually needed to collect the radiation and focus the plasma image onto the spectrometer or the wavelength dispersion device(134, 151).

Wavelength dispersion devices discriminate emissions from an element as well as from other elements or molecules. Diffraction grating are the most common physical wavelength dispersion devices. Other devices like interferometers, filters and prisms are used, but are less common(134, 158). After the emission line is isolated by the spectrometer, a detector is used to measure the emission intensity. For ICP-OES, photomultiplier tube (PMT) used to be very common(134).

More advanced detectors referred to as array detectors were developed and used in ICP-OES. These include photodiode array (PDA)(159, 160) and solid-state or semiconductor radiation detectors like the charge-injection device (CID) and the charge-coupled device (CCD)(161-163). CID and CCD provide greater flexibility and greater choice of analyte λ compared to PMT-ICP-OES in addition to the simultaneous measurements and faster analysis time. Both CID and CCD contain a two dimensional array of light sensitive elements called pixels that are capable of storing a number of electrons. The stored electrons liberate when the light reaches the surface of the detector(164).

Finally, the electrical current measured by the detector is converted into voltage signal, which in turn is converted into digital information via an analog-to-digital (A/D) converter. The digital information is then processed by a computer to be used by the analyst with the aid of a computer software(134).

1.6.3.2 ICP-OES interferences

When a spectral line produced by one element is very close to a line produced by another element, interference between them occurs and the measured intensity in this case is a combination of the intensities of the two emission lines that does not give a true indication of the abundance of either element(165).

By analysing calibration standards of known concentrations, quantitative measurement of the sample becomes possible. However, interferences can cause the signals coming from the sample different than those from the calibration solution of the same concentration of the analytes and thus affects the method accuracy(166). The level of interference is dependent upon the composition of the sample, the gases used in the instrument, and the resolution of the spectrometer.

The biggest problems in ICP-OES is spectral interferences, so selecting suitable lines for trace element analysis is a prerequisite(165).

The matrix of the sample to be analysed also plays a role in increasing or decreasing interferences. Simple matrices like for example deionised water are easier to analyse with minimum interferences, while matrices containing elements that emit line-rich spectra like Na, K, Ca, Mg, Fe and Al are more problematic(166).

1.6.3.2.1 Spectral interferences

Spectral interferences are categorised into three different types based on their cause(134, 165).

Figure 1.13 represents the spectral interferences discussed in this section.

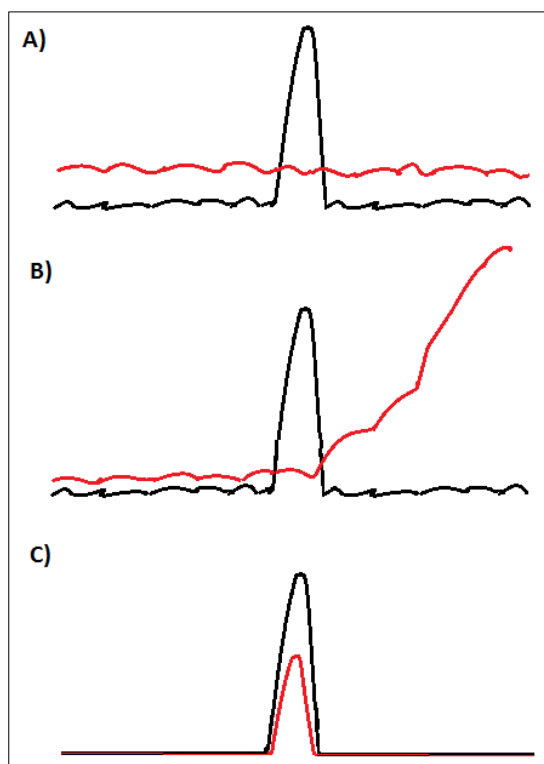


Figure 1.13 Spectral interferences: A) Background shift, B) wing overlap and C) direct spectral overlap

Background Continuum: It is radiation distributed continuously over the wavelength range of the spectrometer and increases with decreasing wavelength, particularly below 200 nm(167).

It originates from stray light within the spectrometer, the presence of molecular species, line-broadening or recombination which is the capture of electrons by ions. About 200 argon lines have been observed predominantly between 350 and 450nm when Ar_(g) is for ICP-OES, making it inapplicable to be used for the analysis of halides and other non-metals(166).

Additional worsening of this type of interference occurs when the samples are dissolved in organic solvents due to the intense carbon lines(167).

Line-Broadening and Wing Interference: Broadening of spectral lines can occur due to several different reasons. These can be due to Doppler effects, foreign gas, or resonance effects(167).

Atoms motion is random and in many directions with slightly different speeds. This leads to single atoms emitting the light at slightly different wavelengths according to their individual movement away from or toward the detector. This phenomenon causes Doppler broadening and produces a Gaussian profile as the wing intensities diminish rapidly contributing with not more than 0.01 nm to the background.

Foreign gas broadening is usually ignored, because it is even less than Doppler broadening. It results from collisions between unlike atoms. A similar phenomenon called Stark broadening is caused by collisions between excited atoms and ions and/or electrons(166, 167).

The collisions between atoms and other particles changes atoms' energy and thus the required excitation energy will also change slightly(166, 167).

The presence of an element in a very high concentration in the sample also causes very intense emission and broadened spectral line resulting in sloping background shift. This occurs due to the collisions between similar atoms and is referred to as resonance broadening(134).

Direct Spectral Overlap: It is the appearance of two lines to be directly overlapped when both are within the spectral bandpass of the spectrometer. Usually in detectors, observing only one wavelength is impossible due to the finite widths of the exit slits, so the light reaching the detector is of small range of wavelengths and this limitation is responsible for direct spectral overlap(166, 167)

Techniques for correcting ICP-OES spectral interferences

i. Line selection

Selecting λ with highest emission for the analyte is useful to get the best sensitivity, however, if this spectral line suffers from severe interferences, alternative λ can be selected for the same analyte(166, 167).

ii. Background correction

This is used to compensate for continuum interferences. A one-point background correction method can be used when the background is static across the spectral wavelengths of interest and is performed by measuring a single point at the background and subtracting the intensity from the gross signal to derive the analyte concentration(134, 167).

Practically the background is much more complicated and using the one-point correction leads to erroneous results, so mathematical procedures have been developed to automatically extract the analyte line from a structured background comprising continuum, line interferences and instrument drift such as interelement correction (IEC). Convolution techniques, Fourier deconvolution give two to three fold improvements in resolution, but multivariate statistical methods such as Kalman filtering, multiple linear regression (MLR), partial least squares (PLS) analysis and the generalized standard additions method (GSAM) give greater resolutions(167).

1.6.3.2.2 Non-spectral matrix effects

These effects are produced because of the physical or chemical properties of the sample's matrix when they are different than the standards used for quantitative analysis(168, 169).

Matrix-induced effects can depress or enhance the analyte signal intensity and they can also affect the resolution of the observed signals. They are highly dependent on the experimental conditions such as the applied power, the pump speed, the gas flow rate, etc.(170)

For example, the matrix influences the nebulisation efficiency, which is proportional to the signal intensity. Nebulisation efficiency is the percent of sample aerosol that reaches the plasma. As mentioned before, only droplets that have a diameter of 10 μ m or less can reach the plasma(168, 170).

The aerosol droplet size is governed by the physical properties of the sample matrix such as viscosity, surface tension and density. The flow rate of the sample solution also plays a role and is influenced by the peristaltic pump speed and the tubing diameter, in addition to the sample gas flow rate(168, 170).

The acid content of samples is the most common influencer of the matrix physical properties. High acid concentrations increase the viscosity, which in turn reduces the nebulisation efficiency(168, 170).

Other differences such as the dissolved solid content and the presence of trace organics also contribute to the matrix-induced effects(169, 170).

Matrix matching between samples and standards is difficult. This is due to the fact that one can never matrix match standards to samples exactly all the time and attempts to do so are time consuming. However, matrix interferences can be reduced by preparing samples and all standards in the same acid matrix and by using

an internal standard to compensate for physical interferences such as scandium (Sc) and yttrium (Y)(168).

1.6.4 Inductively coupled plasma mass spectrometry (ICP-MS)

Figure 1.14 illustrates the layout and major components of ICP-MS instrument

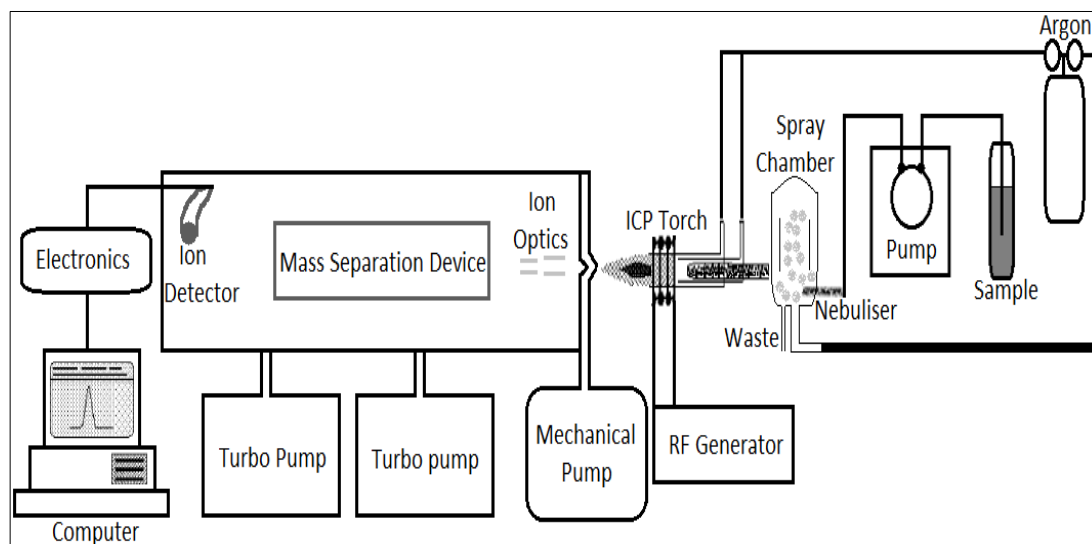
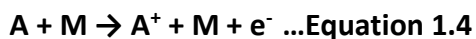


Figure 1.14 Basic components of ICP-MS instrument (Adopted from Thomas R, 2004 (145))

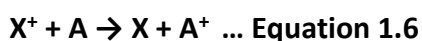
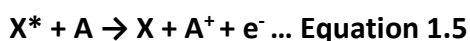
In this technique, the number of singly charged ions from the elemental species within a sample is measured instead of the emitted radiation. A mass spectrometer is used to separate the ions of various elements according to their mass-to-charge (m/z) ratio. ICP-MS has high sample throughput rates similar to ICP-OES, but with higher linear dynamic range and sensitivity(168, 171). This is because, in ICP-MS, the plasma torch is used to generate positively charged ions, not photons. These positive ions are detected in large quantities giving ICP-MS its low detection capability(145, 172).

As mentioned before, the high temperature of ICP atomises the analyte, which is then ionised by a number of processes. These include thermal ionisation, which is

induced by the collision of atoms, ions and free electrons in the plasma(173) as illustrated in equations 1.3 and 1.4:



Other processes are penning ionisation, which is caused by charge exchange between analyte atoms and plasma gas metastable species (Equation 1.5), in addition to charge transfer resulting from the transfer of energy from an ion to an analyte (Equation 1.6).



Both penning ionisation and charge transfer are effective when the energy of the colliding species is similar to the ionisation energy of the analyte atom(173).

The point at which the ions produced from the ICP are introduced to the mass spectrometer is generally referred to as the interface. It is the most critical region of ICP-MS, because the produced ions must be consistently transported efficiently and with the electrical integrity from the plasma, which is at atmospheric pressure of 760 Torr, to the mass spectrometer analyser at approximately 10^{-6} Torr. This is achieved through the intermediate vacuum region created by the two interface cones(171, 172). The interface region is maintained at a pressure of about 1 to 2 Torr using a mechanical roughing pump. The interface consists of two metallic cones, usually made of nickel, but could also be made of platinum to improve tolerance to corrosive acids(145, 166). They have very small orifices to allow the ions to pass through to the ion optics, where they are guided into the mass separation device(145, 171).

The first cone is called the sampler cone and it is the one closer to the plasma with an orifice of about 0.8 to 1.2 mm. The second cone is called the skimmer cone and it is located shortly after the sampler cone. It is more pointed and smaller with an orifice of about 0.4 to 0.8 mm(171). Figure 1.5 represents Thermo XSeries ICP-MS cones.



Figure 1.15 Thermo XSeries ICP-MS cones

Because of the small cones orifices, it is recommended to keep the dissolved solids below 0.2%. Otherwise, the matrix components will deposit rapidly around the cones orifices leading to a decrease in the sensitivity and signal stability if the instrument is used for extended time. Dissolved solid materials can also be deposited on the ion optics of the mass spectrometer(166).

The load coil in ICP-MS is grounded to keep the interface region as close to zero potential as possible, by eliminating the secondary discharge or pinch effect resulting from the capacitive coupling between the load coil and the plasma that causes a potential difference of a few hundred volts (100 – 200 volts). This secondary discharge increases interferences by increasing the number of the doubly charged species, spreading the kinetic energy of sampled ions widely making the optimisation of the ion optics erratic and decrease orifices lifetime(145, 172).

The ions are separated according to their m/z using a mass separation device that is kept at an operating vacuum of about 10^{-6} Torr with a second turbomolecular pump. The classical mass analysers are the quadrupole mass analysers that consist of four parallel cylindrical rods. The rods have the same diameter and length and serve as electrodes. They are made of metals like molybdenum or stainless steel and are sometimes coated with ceramic to resist corrosion. Opposite rods are connected electrically by placing a direct current (DC) field and a time dependent radiofrequency alternating current (AC) to each pair of rods. Ions of a selected mass are then allowed to pass through the rods to the detector by selecting optimum AC/DC ratio on each pair of rods. Ions that are not of the correct m/z are pumped out of the system by colliding with the rods or exiting the path between them(174, 175). The ions emerging from the mass analysers are converted into electrical signals that have magnitudes proportional to analyte concentrations using a detector(176). Several detectors are available such as channel electron multiplier, discrete dynode electron multiplier and Faraday cup(177-180). The obtained signal is then processed using computers and sophisticated software(166).

1.6.4.1 ICP-MS Interferences

Most elements have more than one isotope, which is the same chemical element with the same number of protons, but with a different number of neutrons, so they have different mass numbers. ICP-MS can be used to measure individual isotopes of an element or the ratio between two isotopes. As in ICP-OES, the interferences in ICP-MS can be classified as spectral and non-spectral interferences(145).

1.6.4.1.1 Spectral interferences

There are three main types of spectral interferences, isobaric, polyatomic and doubly charged ion interferences(181).

Isobaric interferences: Isobaric interferences refer to different elements whose isotopes share the same mass(182). An example is Fe and Ni as both have isotopes at mass 58, so any measurement at m/z 58 will have contribution from both elements. Similar interferences occur at m/z 40 when Ca is measured, because argon's most abundant isotope is at mass 40.

Polyatomic interferences: Polyatomic interferences result from the combination of two or more isotopes from different elements that usually occur in the plasma(183). Various factors contribute to this type of interferences, these include the used plasma/nebuliser gas, other elements in the sample, matrix components and the used solvents. In addition, oxygen and nitrogen from the surroundings air can cause polyatomic interferences. Spectral overlaps caused by argon ions alone or in contribution with other species are very common(184). Examples include $^{40}\text{Ar}^{16}\text{O}^+$, which is formed when argon and oxygen are co-present and interferes with Fe major isotope at mass 56. $^{40}\text{Ar}^{35}\text{Cl}^+$ which is formed when HCl is used as part of the sample matrix interferes with the only arsenic isotope at mass 75. Another example is $^{40}\text{Ar}^{12}\text{C}^+$ which is formed when organic solvents are used and it interferes with the most abundant isotope of Cr at mass 52. In addition, matrix and solvent species combine and form interferences of their own like $^{32}\text{S}^{32}\text{O}_2^+$ that forms when sulfuric acid is used and interferes with the major isotope of Zn at mass 64(183).

Doubly charged interferences: Doubly charged interferences occur when an ion is generated with a double positive charge producing an isotopic peak at half its

mass(185). An example is barium (Ba) that can form $^{138}\text{Ba}^{2+}$, m/z 69, which interferes with gallium (Ga) most abundant isotope at mass 69. Alkaline and rare earth elements form doubly charged ions to a greater extent than other elements(186).

These spectral interferences can create challenges to measuring certain elements like for example V, which has two isotopes at 50 and 51 atomic mass unit (amu). ^{51}V is the most abundant isotope, but cannot be used with chloride matrices due to the great contribution from $^{16}\text{O}^{35}\text{Cl}^+$ at mass 51, leaving ^{50}V that have an abundance of 0.25% as the only practical isotope to use(187).

Tables with the most common ICP-MS spectral interferences are available online and in literature(183).

Techniques for correcting ICP-MS spectral interferences

i. Mathematical correction equations

The principle is similar to IEC in ICP-OES, where the intensity of interfering ions or species is measured at another mass free from interference and a correction is applied taking into consideration the ratio of the intensity of the interfering ion/species at the analyte mass to its intensity at the alternate mass. However, if analyte intensity is extremely low and the intensity of the interference is high, mathematical equations are not ideally suited for correcting interferences(145).

ii. Cool/cold plasma use

Using lower RF powers (650-800 W) produce plasma with lower temperature and this reduces interferences resulting from the ionisation of argon and it also minimises the formation of doubly charged species. Cool plasma was proved to benefit elements

with low ionisation potential like Na and Li, however, maintaining the plasma stability at such low temperature is difficult and the majority of other elements are hard to ionise at these temperatures, thus require hotter plasma(145).

Attempts to minimise Ar-based interferences include using different gases such as nitrogen, or Ar-N₂-H₂ mixed gas, but careful optimisation is required, and other interferences appear such as ArNH⁺ and ArN⁺(181).

iii. Collision/reaction cells (CRC)

In this technique a collision or reaction gas such as helium, hydrogen or xenon, is introduced into a cell under vacuum positioned prior to the analyser. This gas will collide with both the interfering polyatomic species and the analytes. However, polyatomic species will lose kinetic energy more readily than the analytes, because they are usually larger in size. As a result, the interfering polyatomic species get expelled in the mass analyse without being detected. In other word, this technique depends on kinetic energy discrimination (KED) to minimise polyatomic interferences(181, 188). See Figure 1.16.

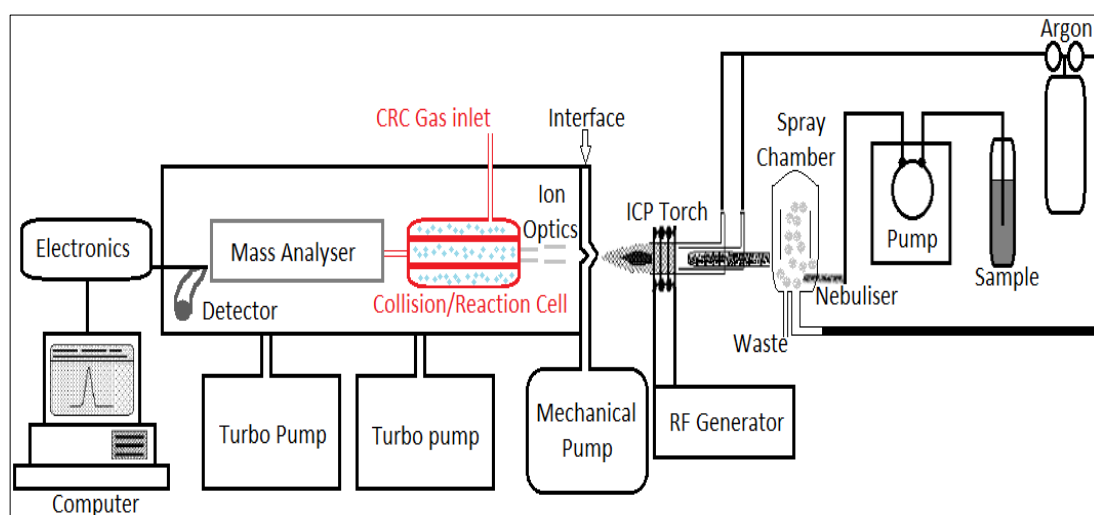


Figure 1.16 Graphical illustration of the position of CRC in ICP-MS instrument
(Adopted from Thomas R, 2004 (145))

Another approach is to use a dynamic reaction cell (DCR) in which a reaction gas such as oxygen, hydrogen, methane or ammonia are introduced in the pressurised cell positioned prior to the analyser. The gas reacts with the interfering species and convert them to other species that have different masses and do not overlap with the analyte of interest to form interference-free species(181, 182, 189).

An example is the reduction of $^{38}\text{Ar}^1\text{H}^+$ to the harmless H_3^+ ion to minimise the interference with $^{39}\text{K}^+$.

The limitation of DRC is that it cannot correct for doubly charged interfering species(181, 190).

iv. High-resolution mass analysers or sector field (SF) analysers

A disadvantage to quadrupole-base ICP-MS is the limited resolving power of $300 \text{ m}/\Delta\text{m}$; (has a resolution of 0.7–1.0 atomic mass unit (amu)) of ions interfering with the analyte(191). Although collision cell technology (CCT) reduces polyatomic interferences, high resolution mass analysers ICP-MS have more powerful resolving capability than quadrupole-based instruments(179, 181). Their resolving power amounts to $10,000 \text{ m}/\Delta\text{m}$ (191).

This approach, particularly using double focusing magnetic sector mass analysers, has proved to be able to separate many of the problematic polyatomic and molecular interferences, without the need to use cool plasma conditions or collision/reaction cells(192).

1.6.4.1.2 Matrix effects

In addition to the matrix effects described for ICP-OES in Section 1.4.5.4, ICP-MS suffers from salt buildup on the orifice of the interface sampler cone and space discharge affects(193).

Space charge effects occur at the interface between the skimmer cone and the ion optics and result in suppressing the signal with high concentrations of a matrix element(194). This can be particularly severe when the matrix ions are of a heavier mass than the analyte ions due to the fact that heavier masses have higher kinetic energy than lighter masses. Space charge effect may lead to poor sensitivity and detection limits when trace levels of low-mass analytes are being measured in the presence of high-mass matrices that dominate the ion beam by pushing the lighter ions out of the way(195).

The most common method to compensate for matrix effects is the use of suitable internal standard(s)(196). Furthermore, diluting samples with high level of dissolved solids reduces the clogging of the sampler cone(195).

1.7 Metals speciation

A chemical species is a specific form of an element defined regarding its electronic or oxidation state or isotopic composition and molecular structure. Speciation analysis can be defined as analytical analysis in which individual chemical species of an element are quantified in a sample. The use of hyphenated techniques which are developed by the coupling of a separation technique and an on-line spectrometric detection technology became very popular for this purpose to exploit the advantages of both(197).

Several techniques have been used throughout the years for the speciation of metals, such as soft X-ray spectromicroscopy, electrophoretic separations with suitable detection devices(198-200). In addition to the combination of GC separation with an element-specific detectors, the combination of chromatography systems

with atomic fluorescence spectrometry (AFS) instrumentation(201), electrospray ionization mass spectrometry, chemical vapour generation (CVG)-AAS(202), hydride generation (HG) coupled with infrared spectroscopy or spectrophotometry(203, 204) and most commonly the combination of chromatographic techniques with ICP-OES and ICP-MS(205, 206).

One of the advantages of ICP-OES and ICP-MS is that they can be easily interfaced to gas chromatographic gas chromatographic (GC) or liquid chromatographic (LC) separation techniques as part of the sample introduction system, which would allow speciation of elements. Identification of individual chemical forms gives an in depth understanding of the toxicity of elements(207).

According to ICH Q3D guidelines, the total concentration of elemental impurities in pharmaceuticals is what is needed to assess compliance with PDEs. However, providing speciation information could be used to justify higher levels for less toxic species(10). In the USP <232>, As and Hg speciation are required in certain cases. For As, speciation is needed when the As limit is exceeded using a total procedure. For Hg, only specific monographs for articles that have the potential to contain methylmercury requires speciation. Other than that if the total Hg is not exceeding the limit, speciation is not necessary(8).

Speciation of trace metals in pharmaceutical products is a complex task and require proper extraction and separation techniques. This research area still need more development and one of the challenges is the lack of suitable pharmaceutical reference material for speciation of metals in pharmaceuticals(16, 201).

Very limited applications are available in the literature regarding the speciation of metals as impurities in pharmaceutical products. In one application, hydride generation-cryotrapping-gas chromatography-atomic absorption spectrometry (HG-CTAAS) was applied for the analysis of arsenites and arsenates as well as their mono-, di-, and trimethyl substituted species in the injectable medication, N-methylglucamine antimonite, which is used for the treatment of visceral leishmaniasis(202). Five commercial samples were analysed and As was found in concentrations ranging from 0.9 to 2.3 mg/L with 7% to 10% of the content present as the trivalent form. This method was selected because of its cheaper cost, however, Moraes et al(202) acknowledged the superior sensitivity of ICP-MS as a detector for this purpose.

Another study published by Narin et al(208), stated that a solid phase extraction (SPE) procedure for the speciation of chromium (Cr^{III} and Cr^{VI}) in environmental and pharmaceutical samples was developed, however, the pharmaceutical sample used was Solgar chromium picolinate vegetable capsules, which are better described as nutritional supplements. In addition, only the total concentration of Cr was provided in the results section and compared with the manufacturer's stated Cr concentration(208).

Other than the mentioned studies the rest of speciation analysis of metals in the pharmaceutical field is for metal-based pharmaceuticals(48). An example is the speciation of Sb^{III} and Sb^{V} in Sb-based medication(209-214).

1.7.1 Arsenic speciation using high performance liquid chromatography (HPLC)-ICP-MS

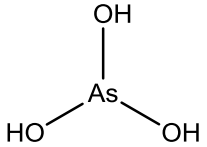
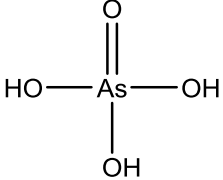
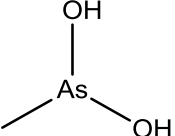
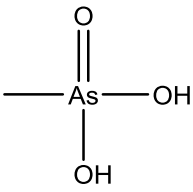
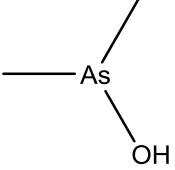
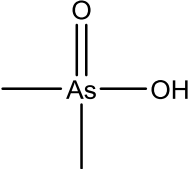
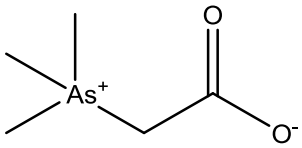
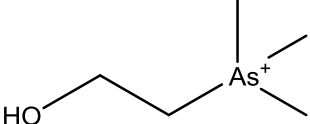
1.7.1.1 Toxicity of arsenic species

According to the WHO, chronic exposure to arsenic may cause many health issues including neurotoxicity, cardiovascular diseases, skin lesions and cancer(56, 215).

Studies conducted for many years focused on analysing total arsenic levels rather than its species. Although ensuring low levels of total arsenic in commercial products will guarantee toxic forms to be low as well; however, it was demonstrated that the determination of total arsenic levels only is insufficient for risk assessment regarding the hazard it poses to humans, because different arsenic species differ in their bioavailability, biotransformation and toxicity. In general, inorganic arsenic compounds are more toxic than organic arsenics(4, 55, 216-221).

Arsenite (As^{III}) is more toxic than arsenate (As^V) which in turn is more toxic than monomethyl arsonic acid (MMA) while the least toxic is dimethylarsinic acid (DMA), also known as cacodylic acid. Trivalent arsenicals are more toxic than pentavalent forms and this includes organic compounds(222). On the contrary, arsenobetaine (AsB) and arsenocholine (AsC) are considered nontoxic due to their excretion and elimination in urine(55, 217, 223-226). The structures of the mentioned arsenic compounds are illustrated in Table 1.3.

Table 1.3 Arsenic species chemical formula and structure*

Abb.**	Name	Chemical Formula	Structure
As ^{III}	Arsenite (arsenous acid)	As(OH) ₃	
As ^V	Arsenate (arsenic acid)	AsO(OH) ₃	
MMA ^{III}	Monomethylarsonous acid	CH ₃ As(OH) ₂	
MMA ^V	Monomethylarsonic acid	CH ₃ AsO(OH) ₂	
DMA ^{III}	Dimethylarsinous acid	(CH ₃) ₂ AsOH	
DMA ^V	Dimethylarsinic acid	(CH ₃) ₂ AsOOH	
AsB	Arsenobetaine	(CH ₃) ₃ As ⁺ CH ₂ COO ⁻	
AsC	Arsenocholine	(CH ₃) ₃ As ⁺ +CH ₂ CH ₂ OH	

*Structures are generated using ChemDraw 16.0.1

** Abbreviation

Arsenic was speciated in biological samples like blood, serum, plasma, urine, faeces, hair, nail, hepatocytes and bladder using various techniques(206, 227).

The IARC, which is part of the WHO, classifies inorganic arsenic compounds as “carcinogenic to humans” (Group 1), because there is evidence for their human carcinogenicity. Monomethylarsonic acid and dimethylarsinic acid are classified as “possibly carcinogenic to humans” (Group 2B), based on experimental animals studies. The other organic compounds are not classifiable as to their carcinogenicity in humans(216, 228-231).

With the increasing awareness of the fact that arsenic toxicity depends on its chemical form and oxidation state, speciation of arsenic for quantitative determination of individual species is gaining more importance (215, 217, 228, 230).

In addition, the knowledge of different species stability under different conditions such as temperature, pH, redox potential and salinity is important and determines the type of procedures used for extracting arsenic species from solid samples as well as the suitable storage condition(215, 221, 232, 233).

1.7.1.2 Sources of arsenic

Arsenic is found in many environmental systems and is introduced naturally and from various human activities like agriculture and industry. It is well known as a contaminant for water systems as result of leaching from arsenic containing sediments and rocks; an example is the famous Bangladesh arsenic crisis that started in 1970s(224, 230, 234). The release of As from gold mine wastes in Northwest of Minas Gerais, Brazil was studied by collecting mine samples and windblown dust samples from that area. As was mainly found in the pentavalent form and all air particulate (filter) samples contained As-rich particles up to 313 mg As/kg. Both samples exhibited solid-phase As species and thus not easily available(235).

Seafood is another common source that exposes humans to arsenic, as marine organisms are capable of absorbing and bioaccumulating arsenic in high levels from sea water(236). Various arsenic species were found in fish, shellfish, crustaceans, algae and seaweeds due to biotransformation processes. This includes As^{III}, As^V, MMA, DMA, AsB, AsC and trimethylarsine oxide (TMAO). *Hizikia fusiformis*, which is a type of brown algae widely used in Japanese diet, was found to contain high concentrations of inorganic arsenic(206). Arsenic was measured and speciated in three deep sea hydrothermal vent worms (*Ridgeia piscesae*, *Paralvinella sulfincola* and *Paralvinella palmiformis*) obtained from the Juan de Fuca Ridge in the Northwest Pacific. *P. sulfincola* and *P. palmiformis* were found to have significantly higher arsenic concentrations than *R. piscesae*. The arsenic species found in one worm species, *R. piscesae* were 36 µg/g ±14% inorganic arsenic, 2 µg/g ±2% monomethyl arsenic, 34 µg/g ±21% dimethyl arsenic, 7 µg/g ±16% unknown methyl arsenical, 5 µg/g ±9% OSO₃-arsenosugar, and about 17 µg/g of thio-arsenicals(237). Total arsenic and its species were determined in marine biota like clams, pearl oyster, cuttlefish and shrimps from seven offshore sites in the western Arabian Gulf. AsB, DMA, TMAO, AsC, arsenosugar-glycerol (As-Gly) and inorganic arsenic were speciated using HPLC-ICP-MS. 58-81% of the total As was in the form of AsB and only 0.03-0.8% were found in the more toxic inorganic forms(238). Arsenic and mercury were determined and speciated in the muscles and livers of 26 fishes obtained from seven freshwater fish species caught in the River Elbe, Germany. The median concentrations of As in fish liver were 162 µg/kg and in fish muscles were 92 µg/kg. AsB was dominant and arsenolipids were speciated from methanolic extracts of the fish using HPLC-ICP-MS(239).

Supplements derived from marine organisms like cod liver oil and capelin oil were also noted to contain arsenic in them. In addition, cases of arsenic intoxication were also reported in South Asian Countries after the consumption of a bird's nest(216, 219, 240-245).

The use of arsenic compounds as pesticides and herbicides also contribute to human exposure to arsenic. Aryloarsenicals are widely used as food additives for animals. This includes 4-hydroxy-3-nitrophenylarsonic acid (Roxarsone, ROX) and para-arsanilic acid (AsA) (4-aminophenylarsonic acid) both are commonly used in the poultry industry to prevent diseases and promote growth. Arsenic was also detected in measurable concentrations in dog food. Although only a small amount of arsenic is absorbed by animals and the rest is excreted unchanged, the use of animal litter as organic fertilisers contributes to increasing arsenic levels in fruit, vegetables(246, 247) and rice as all are capable of accumulating it(218, 246-251). Rice is well known for accumulating As^{III} and As^V and it is a main source of food in many countries(252-254). Fruit juices including apple and grape juices were found to contain high levels of arsenic and in some cases more than WHO 10 µg/L arsenic levels stated for drinking water quality guideline and these juices are important beverages consumed worldwide(206). Freeze-dried apples themselves were found to contain quantifiable levels of As^{III}, As^V, DMA and MMA with the first two species being predominant(55, 226, 242, 255-258).

The use of arsenic containing compounds as wood preservative, and in manufacturing semiconductors as well as the other industrial uses like the

production of glass and alloys are also responsible for polluting the environment with arsenic(232, 241).

1.7.1.3 HPLC-ICP-MS

This is the most widely used technique for multielement speciation analysis. Coupling of liquid chromatography with ICP-MS is straightforward because the nebulizer can be connected to the column outlet via a transfer tubing and can accept the effluent from HPLC using different chromatographic separation techniques like ion exchange, ion-pairing, reversed-phase, size-exclusion, etc.(259, 260). Figure 1.17 represents a typical HPLC-ICP-MS instrument.

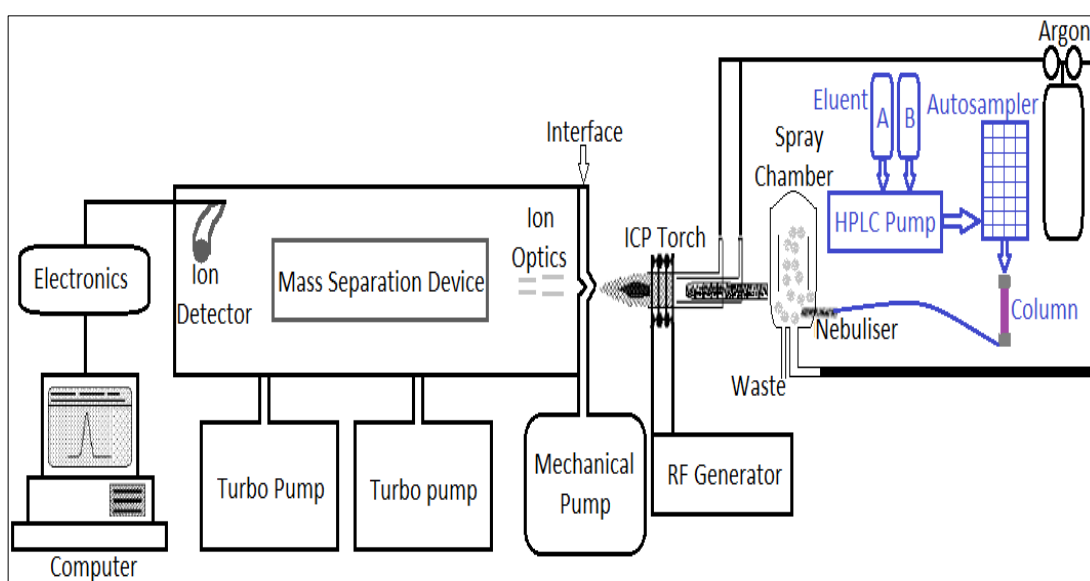


Figure 1.17 Graphical illustration of a typical HPLC-ICP-MS

However, the selected mobile phase composition which depends on the relative polarity, solubility and the molecular weight of separated species should also be tolerable by ICP. In addition, its flow rate must be compatible with that of the nebuliser which might limit the technique(259).

1.8 Aims and objectives

The aim of this work is to determine Class 1 and Class 2A EI in pharmaceutical products and since the new guidelines suggest analytical techniques for this purpose, but without providing standard analytical procedures and methods, this work objectives are:

1. Development of microwave assisted acid digestion for efficient extraction of EI from pharmaceutical samples.
2. Optimisation of ICP-OES method for the determination of EI in pharmaceutical products.
3. Optimisation of ICP-MS method for the determination of EI in pharmaceutical products.
4. Validation of the optimised ICP-OES and ICP-MS analytical techniques using a solid reference material unlike the majority of the available work relying solely on spiked addition technique to validate the analytical method.
5. Development and validation of HPLC-ICP-MS method for the speciation of arsenic in antacids as there is not any published data about what arsenic forms are present in oral pharmaceutical products.

Chapter 2

**The Optimisation, Validation and
Analysis of Analgesics, cold and
cough remedies by ICP-OES in
Compliance with ICH-Q3D
Guidelines**

2. The Optimisation, Validation and Analysis of Analgesics, cold and cough remedies by ICP-OES in Compliance ICH-Q3D Guidelines

2.1 Introduction

Inductively coupled plasma optical emission spectroscopy and inductively coupled plasma mass spectrometry have both been suggested as potential analytical solutions for the assessment of EI in pharmaceutical products. The following two chapters will consider the application of both techniques to analyse analgesic tablets, cold and cough syrups, cold and flu powders and antacids. The work will attempt to produce optimised and validated methods and assess the applicability of the techniques.

In this chapter, ICP-OES will be considered. Published work in the literature where instrumental techniques were applied to commercially available pharmaceutical products is limited(1, 13, 45, 46, 125, 127, 128, 261-265). However, ICP-OES was used in previous studies to measure EI in some antitussive products(47). In the mentioned study, the samples were prepared in two different ways. The first method was to directly introduce the syrups after proper dilution, while the second method was to digest 2-3 ml of the syrups in PTFE vessels placed into a steel pressurised bomb. The vessels were then heated on a hot plate up to 130°C, only calcium, magnesium and iron were quantified, while the rest of the elements were below the detection limits(47). Although interesting, the work only studies a limited number of elements and not those in the Class 1 and Class 2A impurities required under the regulations.

In another study, Pb and Cd were analysed in paediatric syrups manufactured in different countries including England, Ireland, France, India, Pakistan, Egypt and Nigeria using AAS. The samples were prepared using dry ashing method on a hot plate and then using a furnace at 500°C. After that reverse aqua regia was added to digest the samples that were again heated to dryness before the addition of deionised water and finally analysed using AAS. Cd were present in detectable limits in almost all the products while Pb was detected in twenty-five products out of the fifty that were tested(263). This work was carried out before the introduction of the new regulations where the limits have had been significantly lowered and accordingly AAS would now lack the sensitivity required as it has a lower dynamic range and short-term precision in comparison with ICP based instruments(266).

Støving et al(45) used an ICP-OES method for quantitation of As, Cd, Cu, Cr, Fe, Hg, Ir, Mn, Mo, Ni, Os, Pb, Pd, Pt, Rh, Ru, V and Zn in iron oxide coated tablets manufactured by H. Lundbeck, Denmark, according to USP guidelines. The work was completed in 2013 before the final version of the guidelines was released. Reverse aqua regia was used to digest the samples and spiked recoveries were between 85.3–103.8% except for Os, which had a spiked recovery of 161.5% due to memory effect. Fe and Pt were quantified in concentration of $182.8 \pm 18.1 \mu\text{g/g}$ and $2.8 \pm 0.2 \mu\text{g/g}$, respectively. However, the method does not include Co and was validated using the spike addition technique only. In addition, the precision and accuracy of the method regarding the quantification of Os is poor (RSD 13.7%) and needs further development, which was even noted by the researchers(45).

ICP-OES was also used to measure EI in tricyclic antidepressants, which are hard to decompose with acids. Solid sampling electrothermal vaporization (ETV) was used to introduce the samples(127). Ten samples of pharmaceuticals, including amitriptyline hydrochloride, carbamazepine, clozapine, cyclobenzaprine hydrochloride, imipramine hydrochloride, ketotifen fumarate, loratadine, nortriptyline hydrochloride, promethazine hydrochloride and tetracycline hydrochloride, were analysed using ETV-ICP-OES to measure As, Cd, Cr, Cu, Mn, Mo, Ni, Pb, Pd, Pt, Rh, Ru and V. It was found that all elements were below the limit of detection (LoD), except for Cr that was measured in a concentration of $5.7 \pm 0.4 \mu\text{g/g}$ in cyclobenzaprine hydrochloride only(127). The elements determined in this study are from different classes, however, the more toxic elements such as Hg from Class 1 and Co from Class 2A were not included. The method was validated by comparing the obtained results with those obtained using ICP-MS for samples prepared using MIC. Recoveries were in the range of 91 to 103%. Hg was not included because of its high volatility, so this method is not suitable for it due to low sensitivity and/or losses in the pyrolysis step as noted in the paper. In addition, the method does not achieve the limits established by USP for As, Pb, V, Mo, Pd and Pt(127).

ICP-OES was also used in a market surveillance study to determine Fe, Cu and Zn in 113 pharmaceutical samples; those include captopril, enalapril, benazepril, lisinopril, ramipril, quinapril, valsartan, losartan, olmesartan, candesartan, hydrochlorothiazide, carbamazepine, diclofenac, paracetamol, tilidine and naloxone(265). Fe was found in some samples in concentrations ranging from 6 to 7115 $\mu\text{g/g}$, Cu was found in concentrations lower than the quantification limits and Zn was quantified in two samples only (ramipril and candesartan) in a concentration less than 20 $\mu\text{g/g}$. Other

techniques were used to quantify the remaining elements; those are ICP-MS and atomic absorption spectrometry technologies (GFAAS, CVAAS, HGAAS). All the mentioned techniques were validated using spike addition technique(265).

As mentioned before in the introduction, relying solely on spiked addition technique to validate the analytical method is insufficient, because usually an acid digestion method is employed in pharmaceutical samples. As a result, there is some question as to the validity of the results since the digestion process is not fully tested in the procedure involved. Using a solid SRM is important to validate not only the analysis procedure, but also the efficiency of the samples preparation method.

ICP-OES would present a convenient tool for use in the pharmaceutical industry, as it is commonly available as a routine quality assurance/quality control (QA/QC) tool. Hence, it was decided to investigate its application in the analysis of elemental impurities.

This work focuses on the development of an ICP-OES method to analyse the Class 1 elements As, Cd, Hg and Pb and Class 2A Co, Ni and V and then applying it to commercial analgesic tablets and cold and cough syrups. The method validation and current issues related to the availability of an appropriate standard will be discussed.

2.2 Experimental

2.2.1 Reagents and Materials

Trace metal grade acids, nitric acid (67-69% HNO₃) and hydrochloric acid (34-37% HCl) were used for all experiments (Fisher Scientific, UK). Elements standards for ICP-OES and ICP-MS 1000 µg/mL each (SCP Science, QMX UK) were used for calibration. Eight

standard solutions were prepared by dilution with 4% reverse aqua regia (3 HNO₃ : 1 HCl v/v) to get concentrations ranging from 30 to 300 ng/mL as well as a blank. 100 ng/mL of Sc and Y were added as internal standards to the calibration and samples.

Ultrapure water with a resistivity of 18 MΩ cm was obtained using TripleRed water purification system (TripleRed laboratory technology, UK). To filter the samples; 0.45µm polytetrafluoroethylene (PTFE) membrane filter (Agilent Technologies, China, supplied by Crawford Scientific, UK) were used.

Standard reference material; *NIST 3280 Multivitamin/Multielement tablets* (National Institute of Standards and Technology, USA; supplied by Laboratory of the Government Chemist (LGC), UK) was used to validate the method.

2.2.2 Samples

Six samples of analgesic tablets and six cold and cough remedies were acquired from local retailers in the Liverpool area. Some of the cold and cough remedies contain API like paracetamol or herbal extracts in them, while others were just for soothing the throat. See Table 2.1

Table 2.1 Analgesic tablets and cold and cough remedies product information

Product	Ingredients	Maximum daily dose for patients 12 years old and over (g/day)
Analgesic tablets		
Paracetamol value health	API: paracetamol Excipients: potato starch, pregelatinised maize starch, magnesium stearate, talc and colloidal silica	4.64
Hedex Extra	API: paracetamol and caffeine Excipients: starch pregelatinised, maize starch, polyvinyl pyrrolidone, potassium sorbate, talc, stearic acid, croscarmellose sodium, hypromellose and triacetin	5.52

Product	Ingredients	Maximum daily dose for patients 12 years old and over (g/day)
Anadin Extra	API: paracetamol Excipients: maize starch, pregelatinised maize starch, magnesium stearate, povidone and sodium starch glycolate	4.56
Paracetamol Bell's Healthcare	API: paracetamol, aspirin and caffeine Excipients: maize starch, microcrystalline cellulose, hydrogenated vegetable oil, hydroxypropyl methylcellulose, polyethylene glycol, pregelatinised starch and povidone	5.04
Anadin Original	API: aspirin and caffeine Excipients: microcrystalline cellulose, maize starch, hydroxypropyl methylcellulose, polyethylene glycol, calcium stearate and quinine sulphate	4.80
Boots-Aspirin	API: aspirin Excipients: potato starch, talc, calcium carbonate, lactose, citric acid, sodium lauryl sulphate and sodium saccharin	4.20
Cold and cough remedies		
Tixylix	Glycerol, honey, sucrose, citric acid, benzoic acid, lemon oil, distilled lime oil, terpeneless lemon oil and purified water	48.20
Calpol SixPlus	API: paracetamol Excipients: maltitol, sorbitol liquid, glycerol, dispersible cellulose, xanthan gum, polysorbate 80, methyl parahydroxybenzoate, propyl parahydroxybenzoate, acesulfame potassium, saccharin sodium and purified water.	96.96
Nelsons Sootha	Byronia dioica, honey, sorbitol, lemon juice, methylparaben and water	19.01
Calcough	Glycerine, sucrose, citric acid monohydrate, sodium benzoate, anthocyanin, blackcurrant flavour, blackcurrant juice, glucose and purified water	52.50
Lemsip	Guaifenesin, sucrose, sodium, glycerol and water	57.04
Superdrug bronchial Balsam	Menthol, aniseed oil, capsicum tincture, ginger oleoresin, clove oil, peppermint oil, glycerine, glucose, sucrose, tragacanth, benzoic acid, caramel, benzoin tincture, tolu tincture, ethanol and purified water	89.00

All products were processed and analysed within ten days of their purchase, which was before the expiry date.

2.2.3 Instrumentation

For samples preparation Mixer Mill MM200 (Retsch, Germany) with 10 mL zirconium oxide grinding jars with push-fit lid and zirconium oxide grinding balls was used to grind the tablets at 20 Hz for 2 minutes. Microwave assisted acid digestion SP-D Microwave (CEM, Discover software) was used with 35 mL Pyrex vessels. The digestion programme is provided in Table 2.2.

Table 2.2 CEM-SP-D microwave programme used to digest the samples

Stage 1: Ramp Time= 5 min, Temperature= 120°C, Hold time= 5 min
Stage 2: Ramp Time= 5 min, Temperature= 180°C, Hold time= 5 min
Stage 3: Ramp Time= 5 min, Temperature= 210°C, Hold time= 5 min

Elemental analysis was performed using ICP-OES (Thermo iCAP 6500 Duo, Thermo UK) with standard nebuliser, spray chamber and fittings. The instrument is equipped with a CETAC ASX 520 series (Thermo UK) autosampler and data was collected using Thermo Scientific iTEVA Software. The optimised ICP-OES conditions used to analyse the samples are provided in Table 2.3.

Table 2.3 Overview of ICP-OES, iCAP 6500 series optimised parameters

RF Power	1300 W
Nebuliser Gas Flow	0.7 L/min
Pump Speed	60 rpm
Auxiliary Gas Flow	2.0 L/min
Coolant Gas Flow	20 L/min
Selected wavelengths	As (189.0 nm), Cd (214.4 nm), Hg (184.9 nm), Pb (220.3 nm), Co (228.6 nm), Ni (231.6 nm) and V (292.4 nm)

2.2.4 ICP-OES Optimisation

Nebuliser gas flow, pump rate, auxiliary gas flow, coolant gas flow, and radio frequency (RF) power were optimised starting from the lowest possible value that generated a signal to the highest possible value. Signals were assessed by measuring a stock solution containing a known concentration (300 ng/mL) of the seven elements (As, Cd, Hg, Pb, Co, Ni and V) at different settings for each parameter within its operational range. The data obtained was assessed by comparing the signals and signal to blank ratios to obtain a setting with the best sensitivity for the elements.

The signal to blank ratio was calculated by dividing the average signal obtained using a multielement standard with a concentration of 300 ng/mL by the average signal obtained using a blank (2% reverse aqua regia).

2.2.4.1 Optimisation of nebuliser gas flow rate

The procedure described in Section 2.2.4 was followed using a nebuliser gas flow rate range of 0.3-1.2 L/min.

2.2.4.2 Optimisation of pump rate

The procedure described in Section 2.2.4 was followed using a pump rate range of 30-120 rpm.

2.2.4.3 Optimisation of auxiliary gas flow rate

The procedure described in Section 2.2.4 was followed using an auxiliary gas flow rate range of 0.2-2.0 L/min.

2.2.4.4 Optimisation of coolant gas flow rate

The procedure described in Section 2.2.4 was followed using a coolant gas flow rate range of 10-20 L/min.

2.2.4.5 Optimisation of RF power

The procedure described in Section 2.2.4 was followed using RF power range of 750-1350 W.

2.2.4.6 Wavelengths selection

Twenty-five different wavelengths for the seven elements in total were tested to determine the optimal analytical wavelength for each element that gave the lowest limit of detection (LoD) and limit of quantification (LoQ) with minimum interferences.

The tested wavelengths were as the following: As (189.0, 193.7 and 449.4 nm), Cd (214.4, 226.5 and 326.1 nm), Hg (184.9, 194.2 and 253.6 nm), Pb (182.2, 216.9, 220.3 and 261.4 nm), Co (228.6, 230.7, 237.8 and 238.8 nm), Ni (216.5, 221.6, 231.6 and 341.4) and V (292.4, 309.3, 310.2 and 311.0 nm).

2.2.5 Analytical figures of merit and method validation

Linearity, range, precision, accuracy and specificity of the developed analytical method were evaluated using ICH Q2B guidelines(267).

2.2.5.1 Limits of detection and limits of quantification

Limits of detection (LoD) and Limits of quantification (LoQ) were calculated as described by Miller and Miller(268). Ten blanks (2% reverse aqua regia) were measured in triplicate along with a series of standards (10 to 300 ng/ml) and then the LoDs and LoQs were calculated using three times the standard deviation (3σ) and ten times the standard deviation (10σ) criteria respectively.

2.2.5.2 Linearity and range

Linearity was studied in the range of 5 to 50,000 ng/ml for Cd and Hg, 5 to 100,000 ng/mL for Pb, Co and Ni and in the range of 10 to 100,000 ng/ml for As and V.

Eight concentration points were assayed in triplicate.

2.2.5.3 Accuracy and precision

The accuracy and precision were evaluated using *NIST 3280 multivitamin/multielement* tablets. The samples were also spiked with 50 ng/mL with respect to As, Cd, Hg, Pb, Co, V and Ni to complete a recovery analysis. The experiment was performed in triplicate.

The precision of the method was evaluated as the repeatability, i.e. relative standard deviation (RSD).

2.2.6 Optimisation of microwave assisted acid digestion procedure

Microwave assisted acid digestion method was developed using *NIST 3280* tablets.

The exact preparation procedure as stated in *NIST 3280* certificate was not followed.

Six *NIST 3280* tablets instead of fifteen were ground and 0.5g were digested instead of 0.4g. The digestion medium was reverse aqua regia not nitric, perchloric, and hydrofluoric (HF) acids(93). The use of HF was avoided because of the safety issues(269, 270) and the lower number of tablets was used to avoid moisture gain by a large mass of powder.

Hydrofluoric acid is an extremely corrosive inorganic acid that is usually added to the digestion medium in order to completely digest materials like silicone dioxide.

Exposure to hydrofluoric acid causes skin and eye burns and irritation, cough and

swelling of throat if inhaled, and in severe exposure pulmonary oedema(269, 270). Systemic effects include hypokalemia, hypocalcemia, hypomagnesemia and cardiac arrhythmias. Additionally, death was reported due to adverse effect of hydrofluoric acid exposure(269).

Eight ml of reverse aqua (6 mL HNO₃ and 2 mL HCl) were added to 0.5 g of ground tablets and the vessels were allowed to stand in a fume hood for 20 min. Cylindrical (6x3 mm) PTFE covered stirring bars (VWR, Europe) were added to the vessels to ensure continuous mixing and heat distribution within the samples. Finally, the samples were then vortex mixed using a rota mixer (Hook and Tucker Zenyx, UK) and placed in the microwave.

Following digestion, samples were filtered. 4% reverse aqua regia was used to rinse the digestion vessels and the used filters three times (approximately 4 to 6 mL were used each time) to ensure complete transfer of the extracted elements. Then the filtered samples were diluted with deionised water to a final volume of 25 mL (Stock-1).

A further ten-fold dilution was performed by transferring 1 mL from Stock-1 to a 10 mL volumetric flask and completing the volume with deionised water after the addition of internal standards. Gold (Au) was also added to the final samples and the calibration standards in a concentration of 1 µg/mL to overcome the memory effect of Hg(271-273).

2.2.6.1 Optimisation of the of microwave assisted acid digestion procedure temperature

Maximum temperatures of 140, 160, 180, 200 and 210°C were used during the digestion method development.

3.2.6.2 Optimisation of the microwave assisted acid digestion procedure time

Holding times of 5, 10, 15 and 20 min were also tried to determine the optimum time for digestion.

2.2.6.3 Optimisation of different acid ratios

In addition to using reverse aqua regia to digest *NIST 3280*, an acid ratio of 9 HNO₃: 1 HCl v/v (7.2 mL HNO₃ and 0.8 mL HCl) was also tested to compare microwave extraction efficiency using different acid ratios.

Reverse aqua regia is used for environmental samples when the use of more corrosive and toxic acids is to be avoided(274, 275). It was also used for pharmaceutical APIs(18). The HNO₃: 1 HCl v/v acid ratio was tested as well because it was also used before to digest samples prior to ICP-based analysis(276). It was also used sometimes in combination with other reagents like hydrogen peroxide(277).

With each tested condition, three samples of *NIST 3280* were digested and assayed in triplicate.

2.2.6.4 Microwave assisted acid digestion procedure validation

The developed digestion procedure was validated by calculating the percentage recoveries for the elements of interest; using the certified values of *NIST 3280* and

spike recoveries. Spiked samples were prepared using the exact procedure as stated in Section 2.2.6, but with the addition of a spike of 50 ng/mL of the elements.

The optimum method was chosen based on obtaining accepted recoveries that is 70%–150% according to USP <233> with repeatability expressed as the relative standard deviation (RSD) to be <20%(9). However, because a standard reference material was used, recoveries between 95-105% with RSD of <5% were regarded as acceptable.

2.2.6.5 Tablets grinding and sample homogeneity

The effect of different grinding techniques on the method's precision and sample homogeneity was tested by grinding six tablets using a glass mortar and pestle and another six tablets using the mixer mill as described in Section 2.2.3.

2.2.6.6 Selection of suitable internal standard(s)

Scandium (Sc) and yttrium (Y) (100 ng/ml) were added to both samples and standards prior to analysis. The corrected results for the internal standard were obtained using Thermo iTEVA software and compared with those without the internal standards.

2.2.7 Analysis of analgesic tablets, cold and cough remedies

For the analysis of the analgesic tablets, cold and cough remedies the samples were analysed using the optimised and validated ICP-OES method describe in Table 2.3. Solid samples were prepared as described in Section 2.2.6, using only one dilution step. For syrups, 0.5 g were directly weighed into the vessels after shaking the products' containers to make sure that all the components are mixed before sampling.

2.3 Results and discussion

2.3.1 ICP-OES Optimisation

A comparison of signals and signal to blank ratios was performed. This allowed the assessment of the maximum signal but by using signal/blank ratio, it was also possible to assess the maximum sensitivity.

2.3.1.1 Optimisation of nebuliser gas flow rate

The nebuliser gas flow rate affects the analyte atomisation level by controlling the sample's droplet size and its transit time through the plasma. Higher rates decrease the residence time, so the analyte will have shorter time to acquire the energy needed for transition and vice versa(278).

Figures 2.1-2.7 show the signal and signal/blank ratios for Class 1 and Class 2A elements at different λ across the tested nebuliser gas flow rate of 0.3-1.2 L/min.

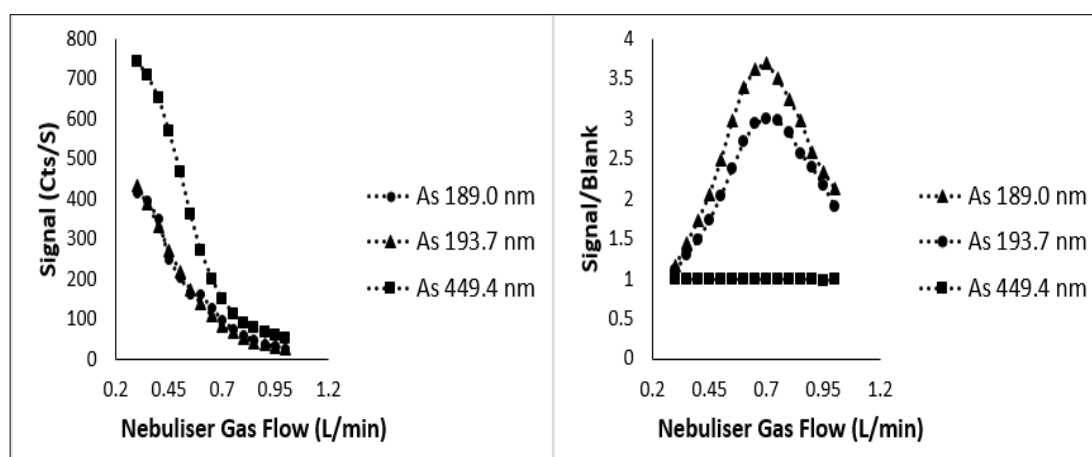


Figure 2.1 The signal and signal/blank ratios for arsenic (300 ng/mL) at three different wavelengths using different ICP-OES nebuliser gas flow rates

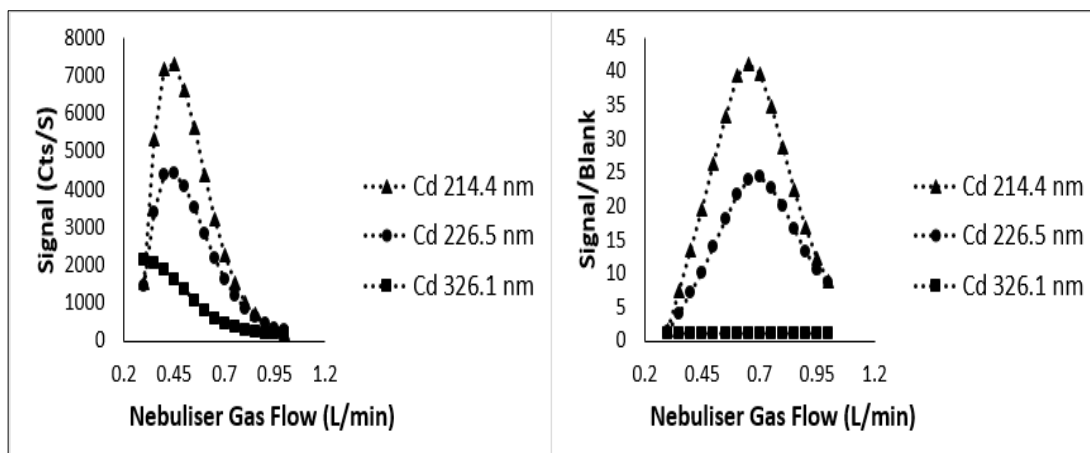


Figure 2.2 The signal and signal/blank ratios for cadmium (300 ng/mL) at three different wavelengths using different ICP-OES nebuliser gas flow rates

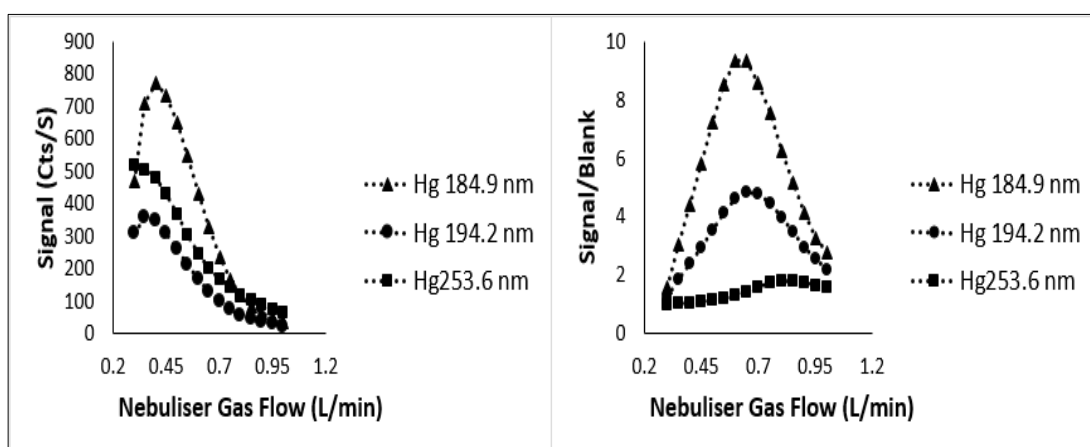


Figure 2.3 The signal and signal/blank ratios for mercury (300 ng/mL) at three different wavelengths using different ICP-OES nebuliser gas flow rates

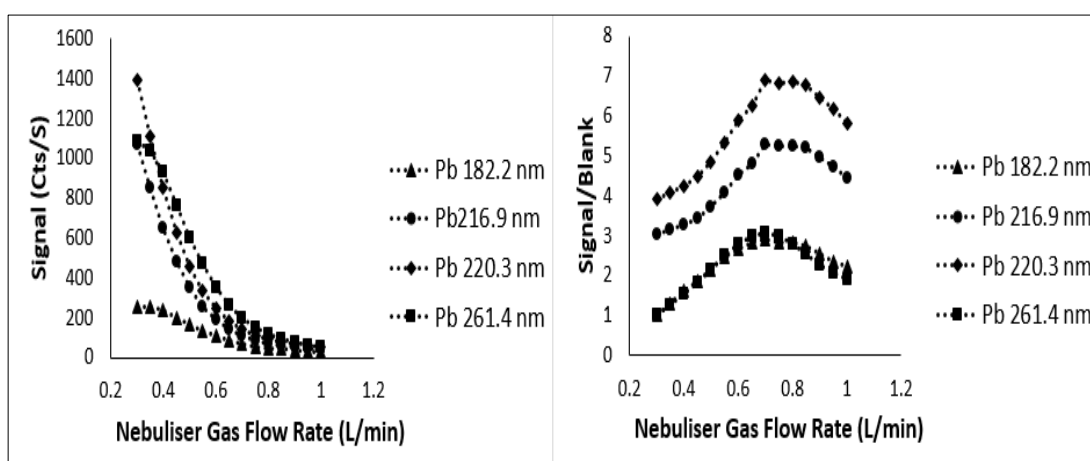


Figure 2.4 The signal and signal/blank ratios for lead (300 ng/mL) at four different wavelengths using different ICP-OES nebuliser gas flow rates

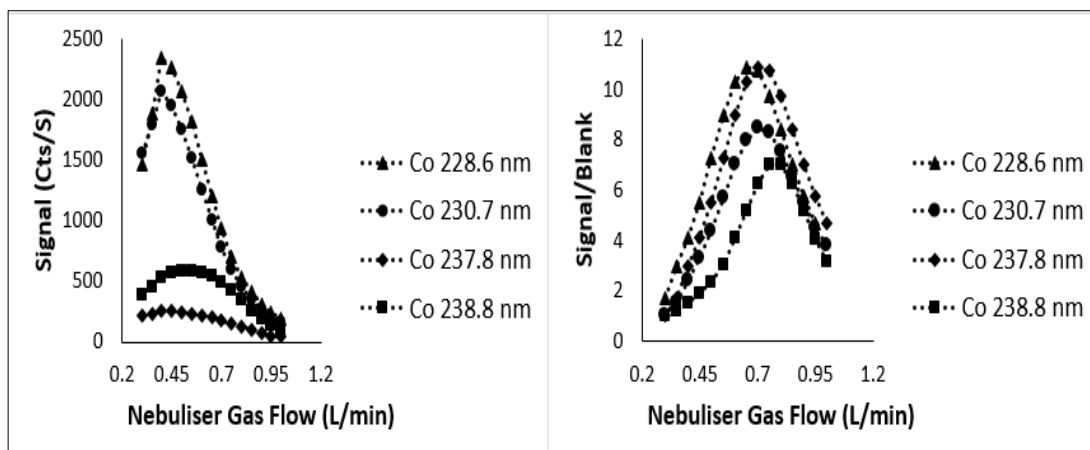


Figure 2.5 The signal and signal/blank ratios for cobalt (300 ng/mL) at four different wavelengths using different ICP-OES nebuliser gas flow rates

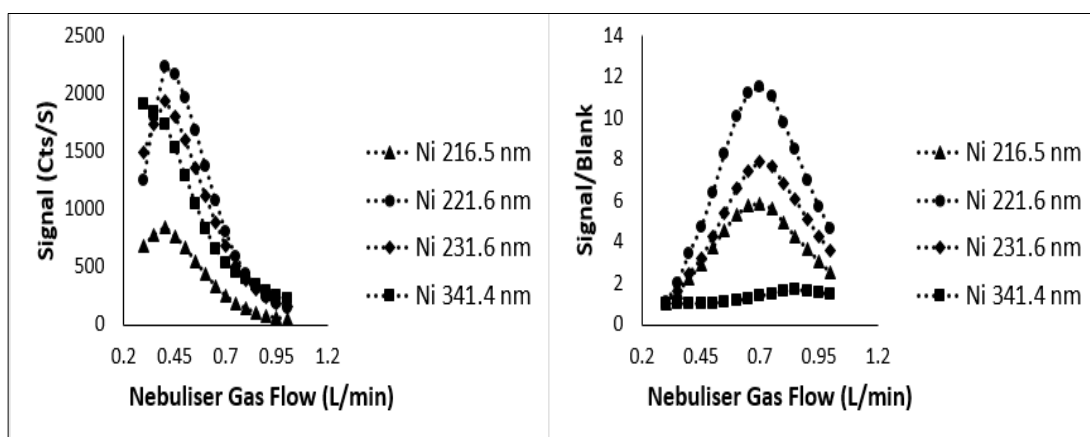


Figure 2.6 The signal and signal/blank ratios for nickel (300 ng/mL) at four different wavelengths using different ICP-OES nebuliser gas flow rates

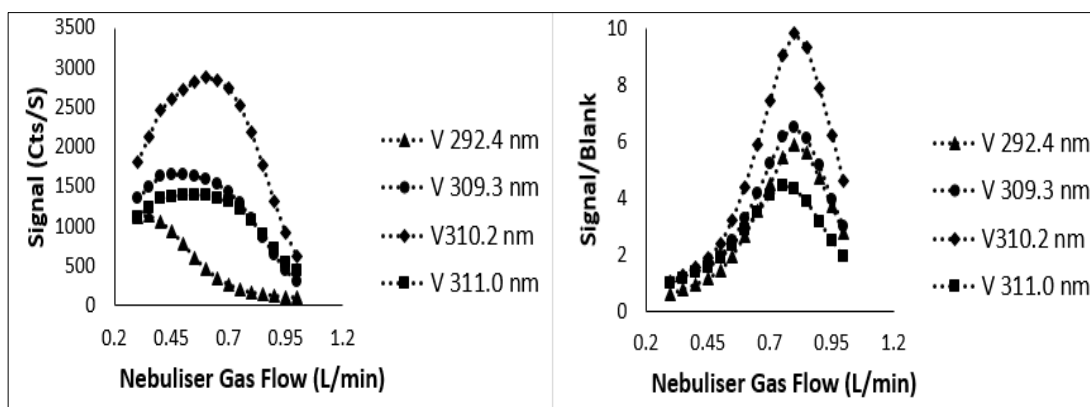


Figure 2.7 The signal and signal/blank ratios for vanadium (300 ng/mL) at four different wavelengths using different ICP-OES nebuliser gas flow rates

From the previous Figure 2.1-2.7, it is clear that relying on the analyte signal only does not ensure best sensitivity. As sensitivity is indicated by the signal to blank ratio, it is important for the signal to be high but also the blank to be low to obtain the maximum ratio. In cases where a high signal is obtained if the corresponding blank is high the ratio will be low. Here by looking at Figures 2.1 to 2.7 the signal can be seen as well as the ratio. If the signal for one condition is high but the ratio is low the difference is caused by a high blank level. The optimum point for each condition was based on the signal/blank ratio to maximise sensitivity.

At higher nebuliser flow rates bigger droplets are formed and when this is combined with lower residence time in the plasma leading to a drop in all elements signals (Figures 2.1-2.7). By observing the corresponding ratio plots, a maximum sensitivity is clearly seen at 0.7 L/min for all elements.

For some elements, the difference in signals and signal/blank ratios is obvious, like for example As (Figure 2.1). Looking at the signal only gives an indication that the best nebuliser gas flow rate is 0.2 L/min unlike signal/blank were the highest ratio; that is the highest analyte signal with the lowest blank signal was achieved at a nebuliser flow rate of 0.7 L/min. Another example from Class 2A elements is Co (Figure 2.5), where the highest signal appears to be at 0.4 L/min, while the highest signal/blank ratio is at 0.7 L/min.

The same goes for the rest of the elements where the nebuliser gas flow rate that gave the highest sensitivity was 0.7 L/min. An exception is V, as a higher signal/blank ratio was achieved at a nebuliser gas flow rate of 0.8 L/min. However, for the sake of

time efficiency and analysing all the elements at the same conditions, a small drop in sensitivity (approximately 13%) can be tolerated due to its high PDE of 100 µg/day.

2.3.1.2 Optimisation of pump rate

The pump rate affects the volume of the aerosol droplets and thus the efficiency of nebulisation. Proper nebulisation is important for optimum sensitivity and precision. High pump speed leads to high sample delivery rate, which may increase the formation of large droplets in the spray chamber(278).

Figures 2.8-2.14 show the signal and signal/blank ratios for Class 1 and Class 2A elements at different λ across the tested pump speed range of 30-120 rpm.

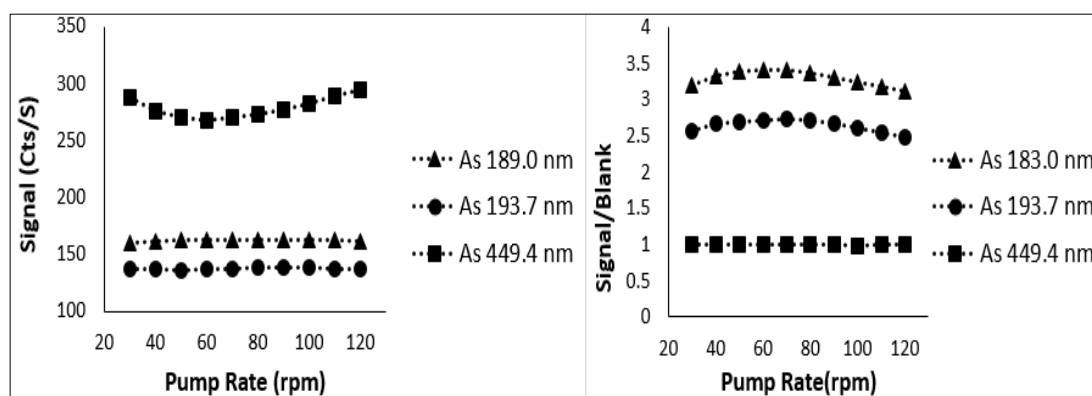


Figure 2.8 The signal and signal/blank ratios for arsenic (300 ng/mL) at three different wavelengths using different ICP-OES pump rates

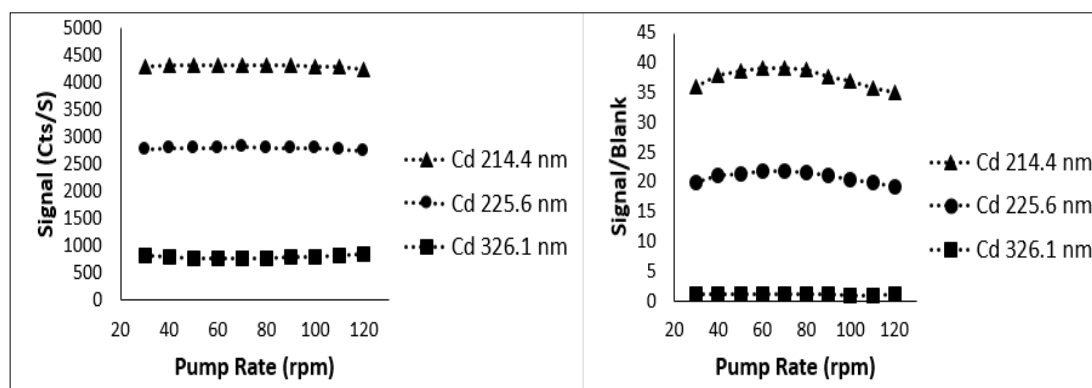


Figure 2.9 The signal and signal/blank ratios for cadmium (300 ng/mL) at three different wavelengths using different ICP-OES pump rates

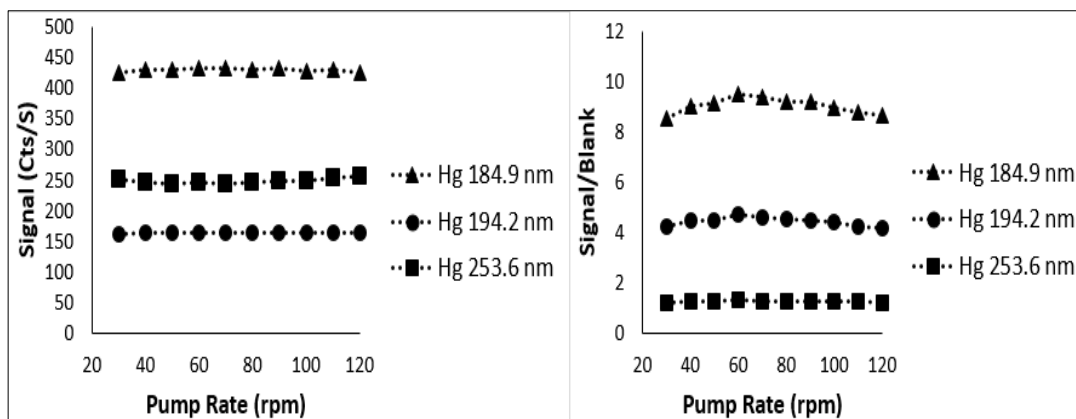


Figure 2.10 The signal and signal/blank ratios for mercury (300 ng/mL) at three different wavelengths using different ICP-OES pump rates

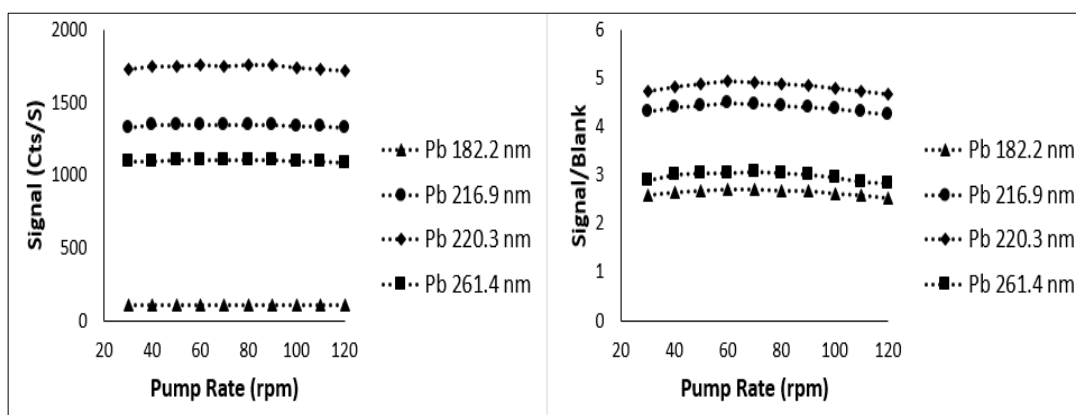


Figure 2.11 The signal and signal/blank ratios for lead (300 ng/mL) at four different wavelengths using different ICP-OES pump rates

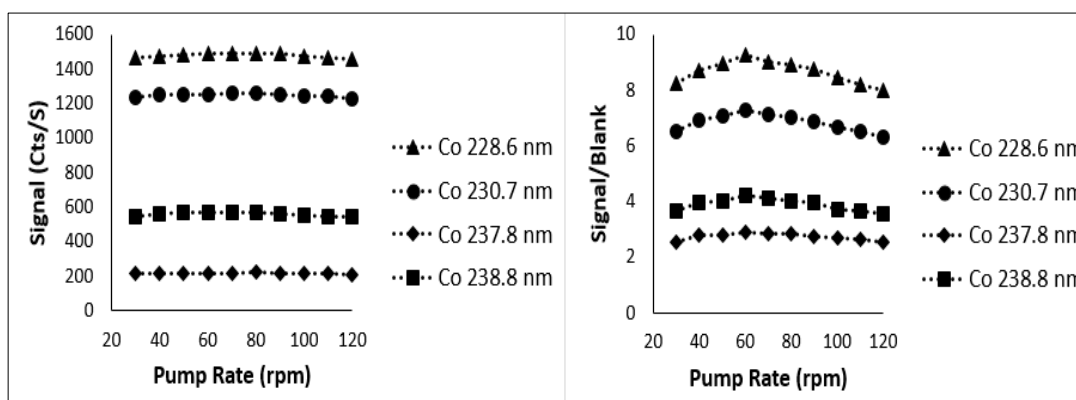


Figure 2.12 The signal and signal/blank ratios for cobalt (300 ng/mL) at four different wavelengths using different ICP-OES pump rates

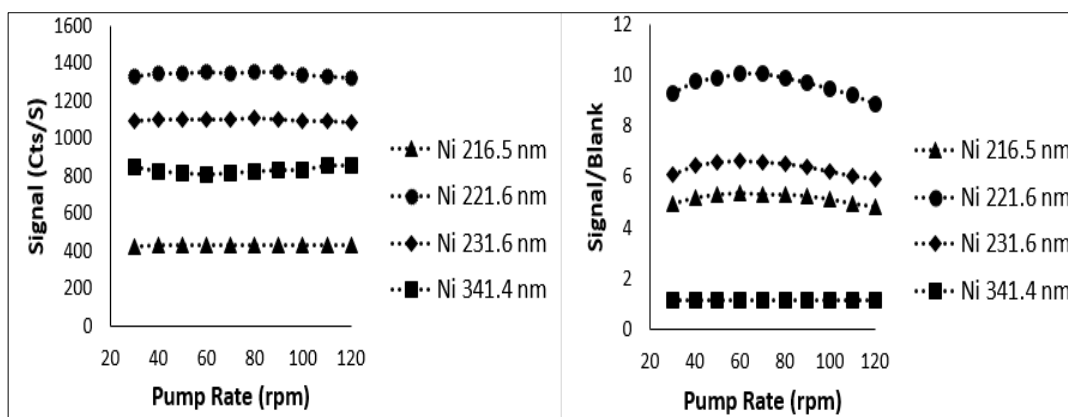


Figure 2.13 The signal and signal/blank ratios for nickel (300 ng/mL) at four different wavelengths using different ICP-OES pump rates

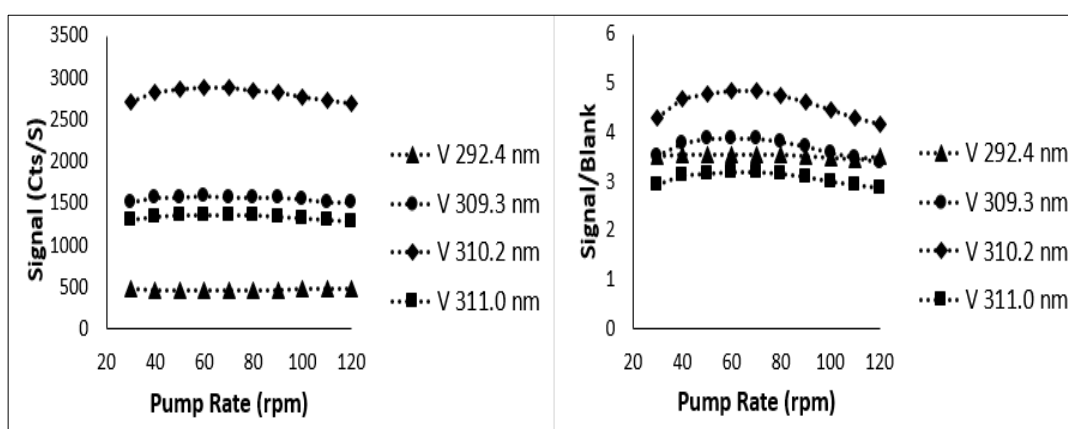


Figure 2.14 The signal and signal/blank ratios for vanadium (300 ng/mL) at four different wavelengths using different ICP-OES pump rates

From the above figures 2.8-2.14, the pump rate in this case has minimal effect on the analytical sensitivity. Both the standard signal and the signal/blank ratio did not show significant change across the tested pump rate range, so it was maintained at 60 rpm.

2.3.1.3 Optimisation of auxiliary gas flow rate

Auxiliary gas flow rate can affect the plasma position with high flow rates moving the plasma forward in the horizontal position. This can affect the signal at the detector by altering the focus of the emission as it changes position. It has a more profound effect with organic samples rather than aqueous samples. It was found that changing

the auxiliary gas flow rate with organic samples could change the distribution of solvent and thus the plasma excitation conditions(279). This is because organics will be consumed resulting in the formation of carbon which can plate onto the torch. Auxiliary gas flows rates can be increase to move the plasma and minimise plating effects as carbon can cause conduction with the RF coil and reduce the applied power to the plasma.

The effect of changing the auxiliary gas flow rate on Class 1 and Class 2A elements dissolved in 2% reverse aqua regia is shown in Figures 2.15 – 2.21.

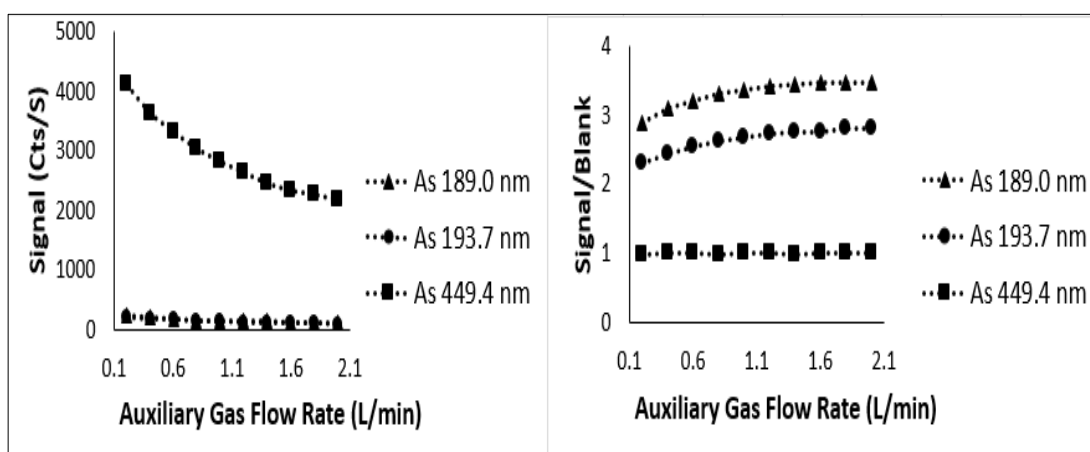


Figure 2.15 The signal and signal/blank ratios for arsenic (300 ng/mL) at three different wavelengths using different ICP-OES auxiliary gas flow rates

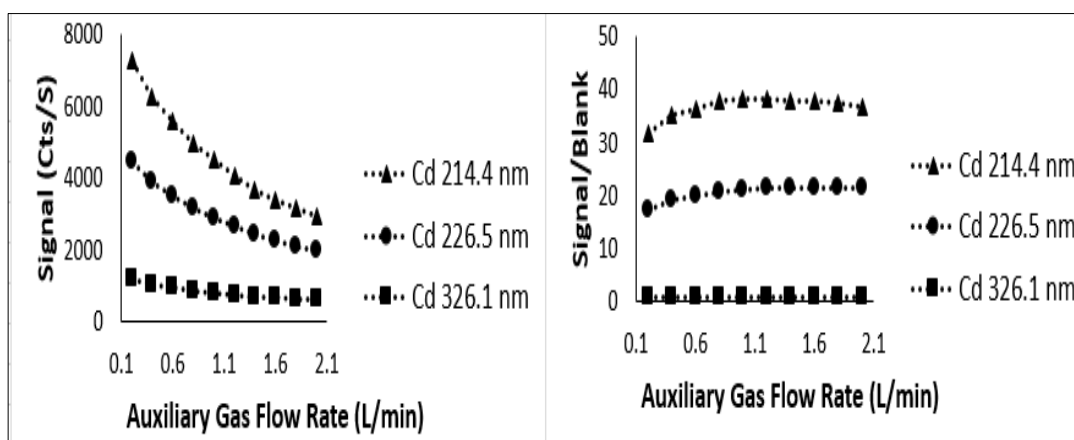


Figure 2.16 The signal and signal/blank ratios for cadmium (300 ng/mL) at three different wavelengths using different ICP-OES auxiliary gas flow rates

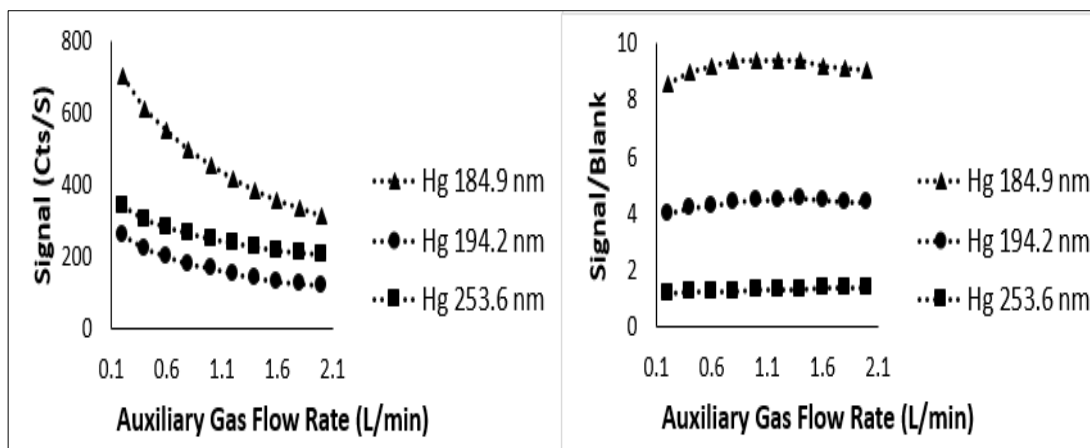


Figure 2.17 The signal and signal/blank ratios for mercury (300 ng/mL) at three different wavelengths using different ICP-OES auxiliary gas flow rates

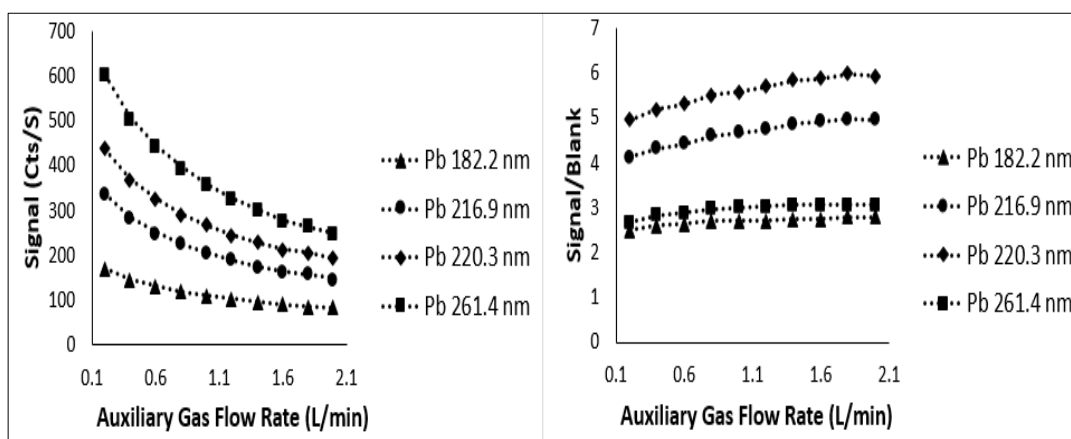


Figure 2.18 The signal and signal/blank ratios for lead (300 ng/mL) at four different wavelengths using different ICP-OES auxiliary gas flow rates

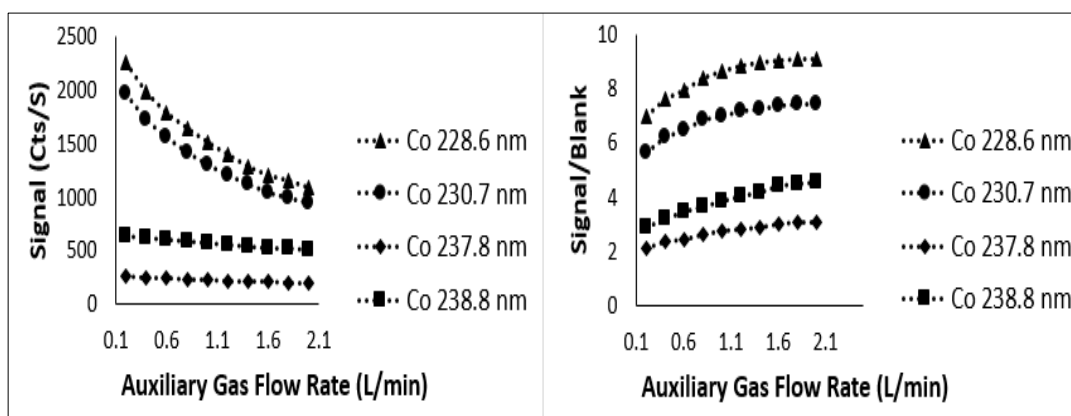


Figure 2.19 The signal and signal/blank ratios for cobalt (300 ng/mL) at four different wavelengths using different ICP-OES auxiliary gas flow rates

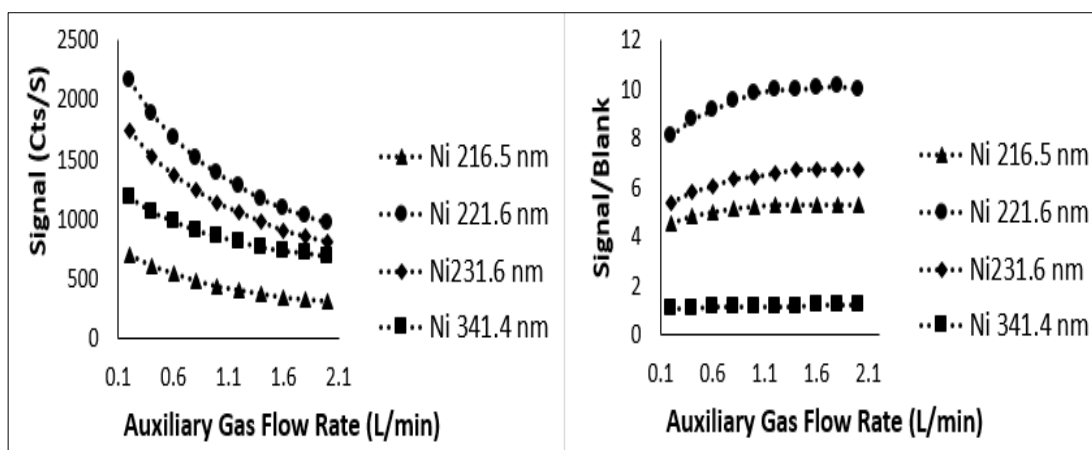


Figure 2.20 The signal and signal/blank ratios for nickel (300 ng/mL) at four different wavelengths using different ICP-OES auxiliary gas flow rates

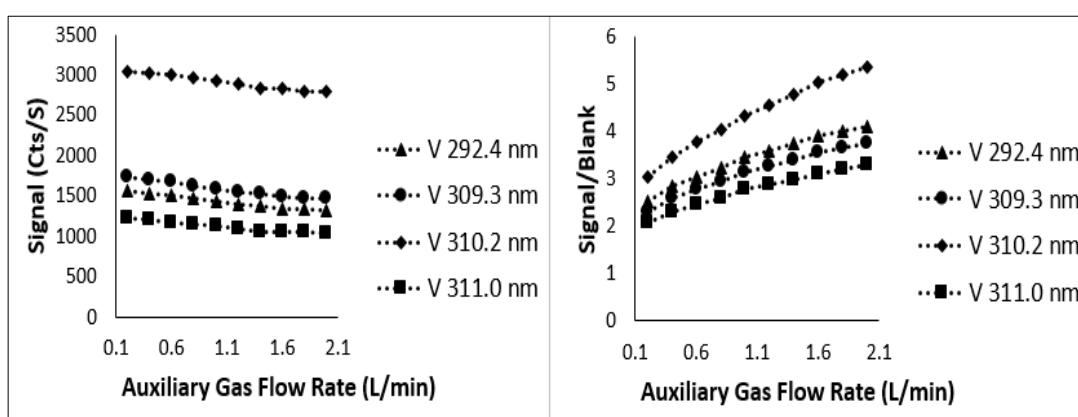


Figure 2.21 The signal and signal/blank ratios for vanadium (300 ng/mL) at four different wavelengths using different ICP-OES auxiliary gas flow rates

From figures 2.15-2.21, the standard signal for all elements dropped at higher auxiliary gas flow rate; however, this was accompanied with similar drops in the blank signal causing the signal/blank ratios to increase with increasing the auxiliary gas flow rate. As a result, an auxiliary gas flow rate of 2 L/min was selected as the optimum because the highest signal/blank ratio for Pb, Co, Ni and V was achieved at that rate. The remaining elements signal/blank ratios seemed not to be significantly affected with changes in the auxiliary gas flow rate. This may be because no organic containing matrix was present. Once a pharmaceutical matrix is present, this may cause an issue

with carbon plating onto the torch. The figures clearly demonstrate however that if adjustment was needed it would have a minimal effect on the sensitivity.

2.3.1.4 Optimisation of coolant gas flow rate

The coolant gas helps maintaining a stable plasma discharge(280), but it has limited effect on the analytical sensitivity(281). This was supported from the signals and signal/blank ratios obtained for Class 1 and Class 2A elements at different coolant gas flow rates. See Figures 2.22-2.28.

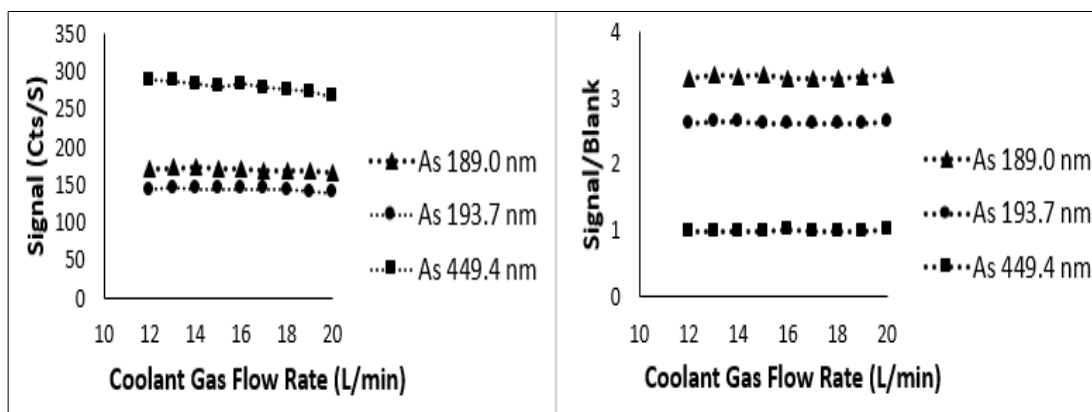


Figure 2.22 The signal and signal/blank ratios for arsenic (300 ng/mL) at three different wavelengths using different ICP-OES coolant gas flow rates

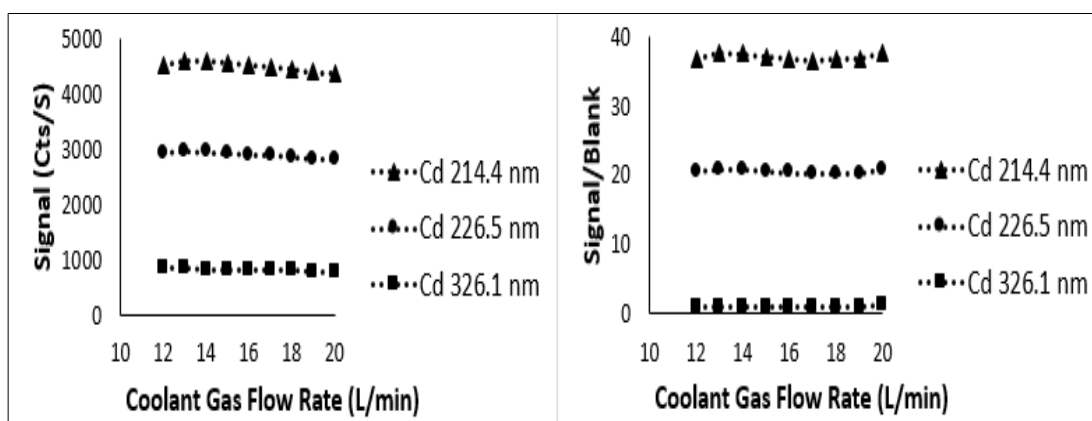


Figure 2.23 The signal and signal/blank ratios for cadmium (300 ng/mL) at three different wavelengths using different ICP-OES coolant gas flow rates

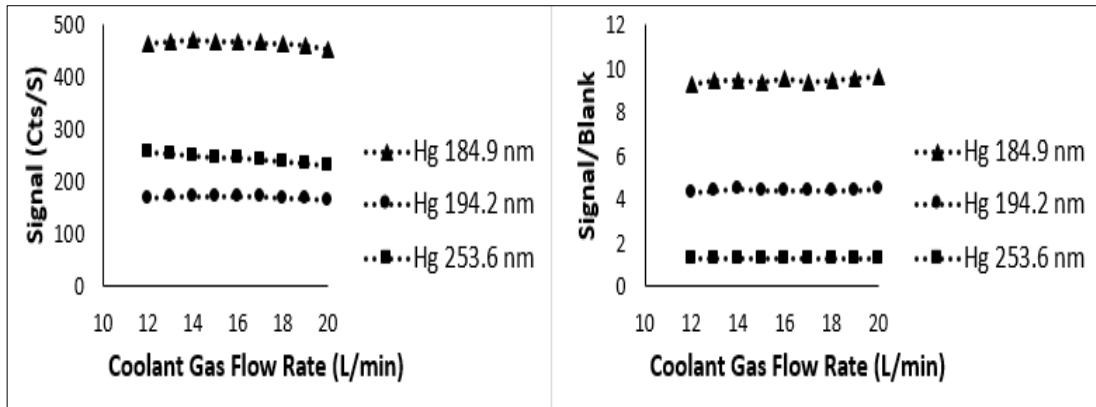


Figure 2.24 The signal and signal/blank ratios for mercury (300 ng/mL) at three different wavelengths using different ICP-OES coolant gas flow rates

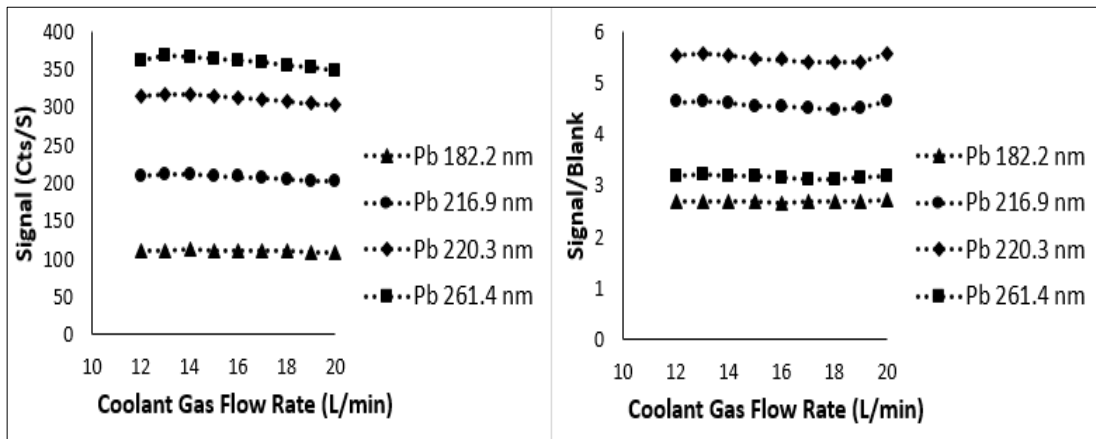


Figure 2.25 The signal and signal/blank ratios for lead (300 ng/mL) at four different wavelengths using different ICP-OES coolant gas flow rates

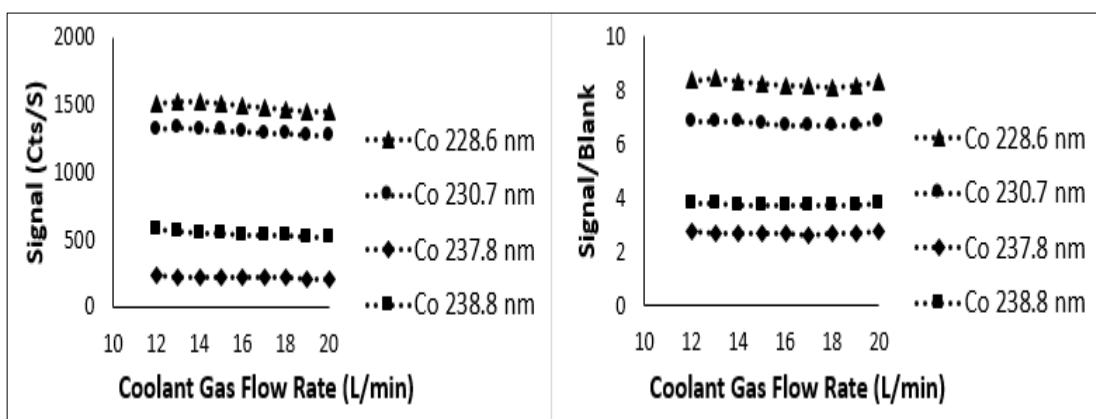


Figure 2.26 The signal and signal/blank ratios for cobalt (300 ng/mL) at four different wavelengths using different ICP-OES coolant gas flow rates

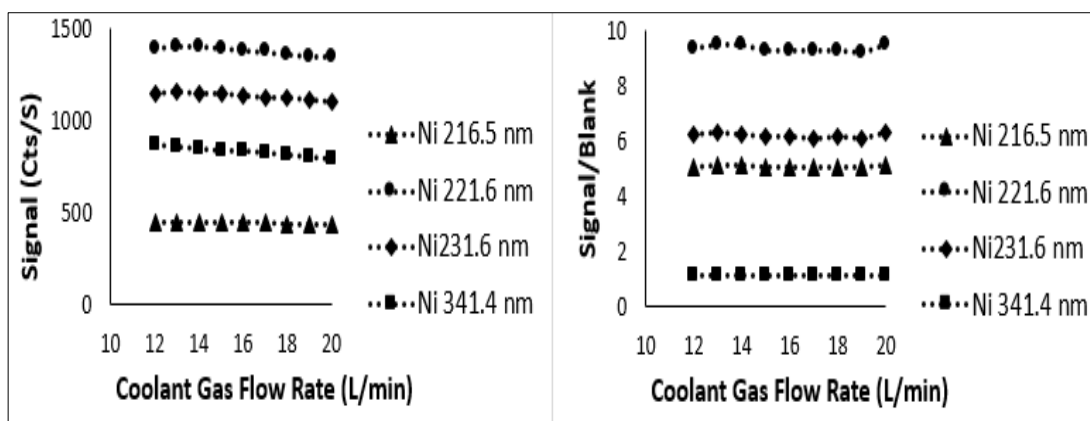


Figure 2.27 The signal and signal/blank ratios for nickel (300 ng/mL) at four different wavelengths using different ICP-OES coolant gas flow rates

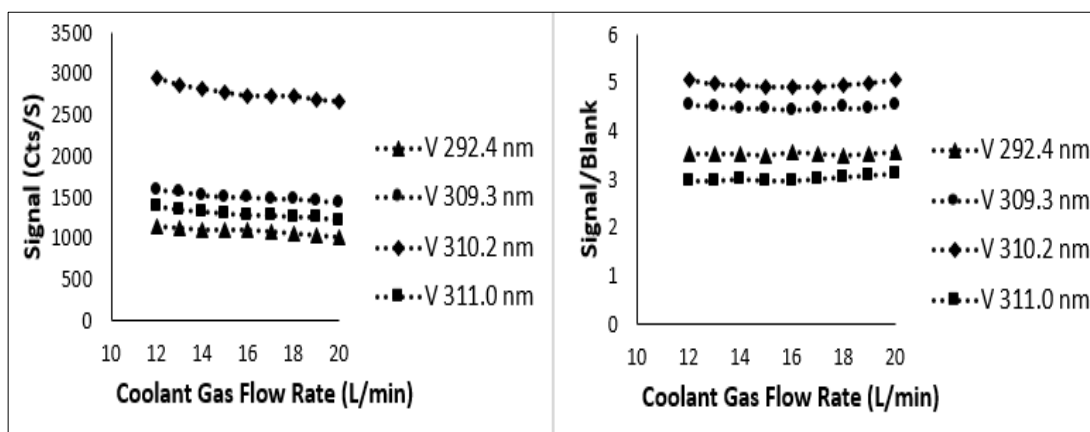


Figure 2.28 The signal and signal/blank ratios for vanadium (300 ng/mL) at four different wavelengths using different ICP-OES coolant gas flow rates

Minimal changes were obtained in signals and signal/blank ratios for most elements at the tested wavelengths when changing the coolant gas flow rate. However, there was a small improvement (about 2%) in signal/blank ratio at a coolant gas flow rate of 20 L/min for As 189.0nm, Cd 214.4nm, Pb 220.3nm and Ni 221.6nm, so it selected as the optimum setting.

2.3.1.5 Optimisation of RF power

One of the most critical settings for achieving optimum conditions and highest sensitivity is the radio frequency power(278).

Figures 2.29-2.35 represent the obtained signals and signal blank ratios using different RF powers over a range of 750-1350 W.

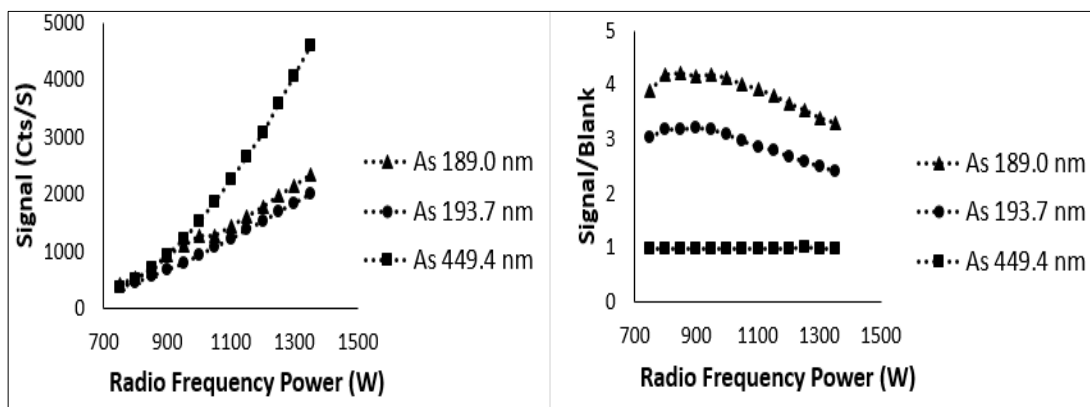


Figure 2.29 The signal and signal/blank ratios for arsenic (300 ng/mL) at three different wavelengths using different ICP-OES radio frequency powers

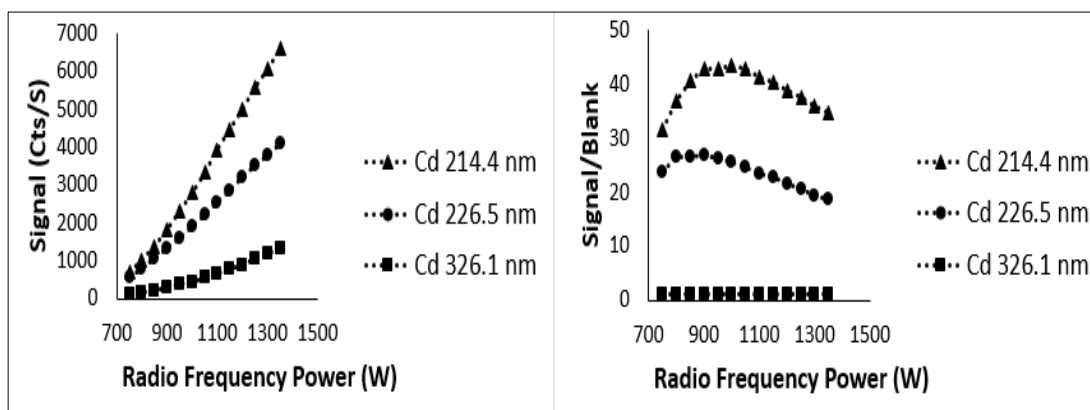


Figure 2.30 The signal and signal/blank ratios for cadmium (300 ng/mL) at three different wavelengths using different ICP-OES radio frequency powers

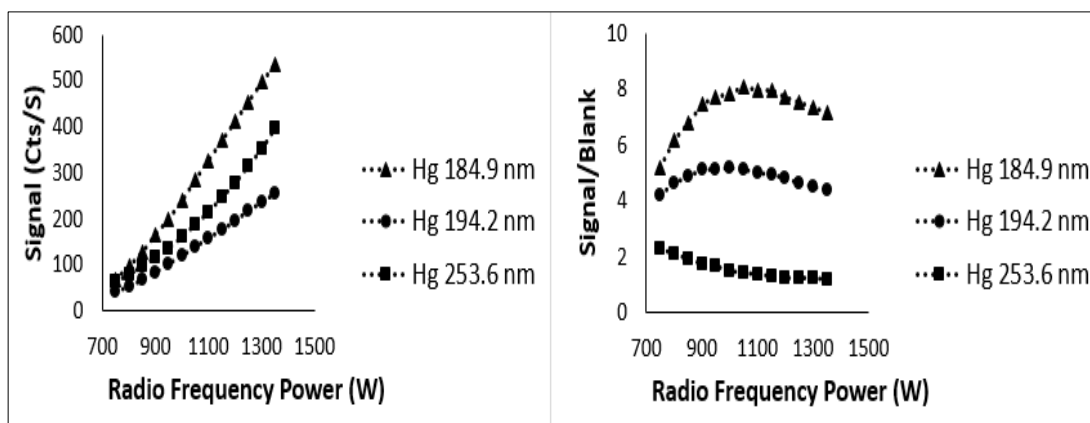


Figure 2.31 The signal and signal/blank ratios for mercury (300 ng/mL) at three different wavelengths using different ICP-OES radio frequency powers

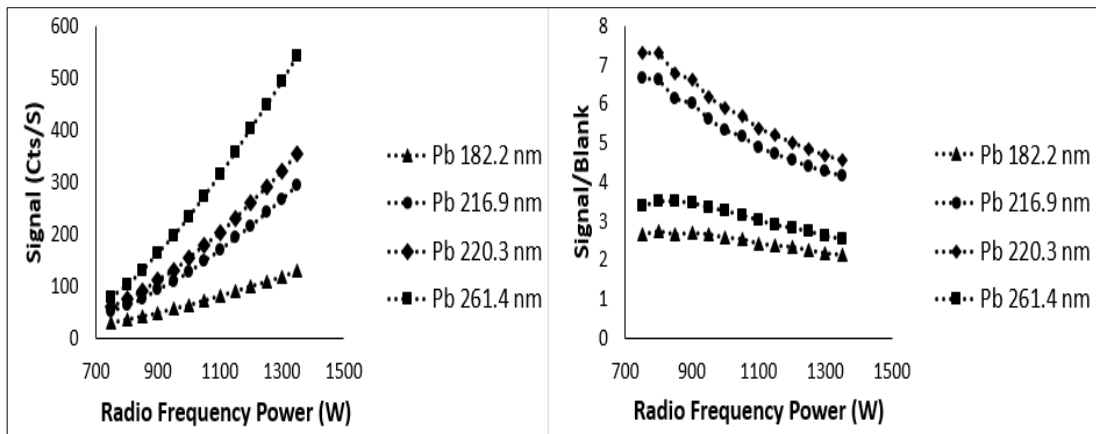


Figure 2.32 The signal and signal/blank ratios for lead (300 ng/mL) at four different wavelengths using different ICP-OES radio frequency powers

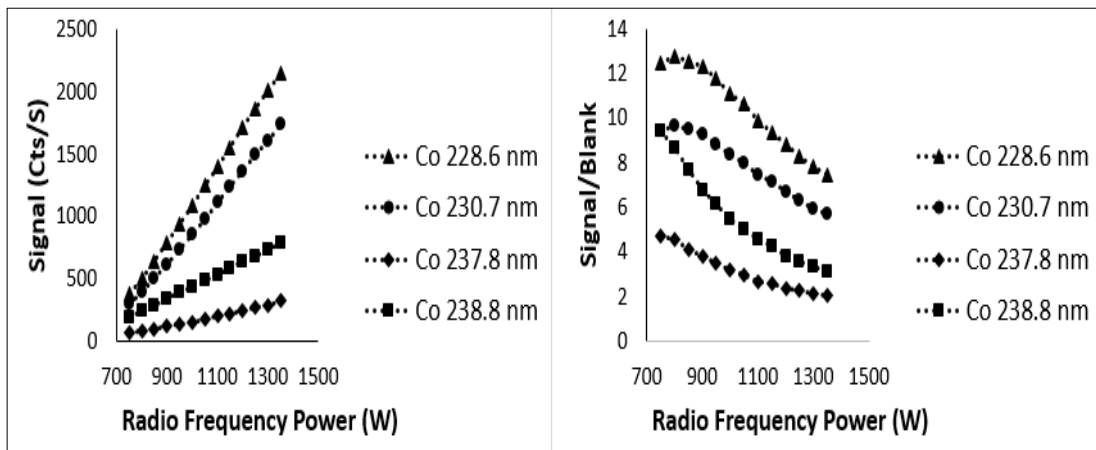


Figure 2.33 The signal and signal/blank ratios for cobalt (300 ng/mL) at four different wavelengths using different ICP-OES radio frequency powers

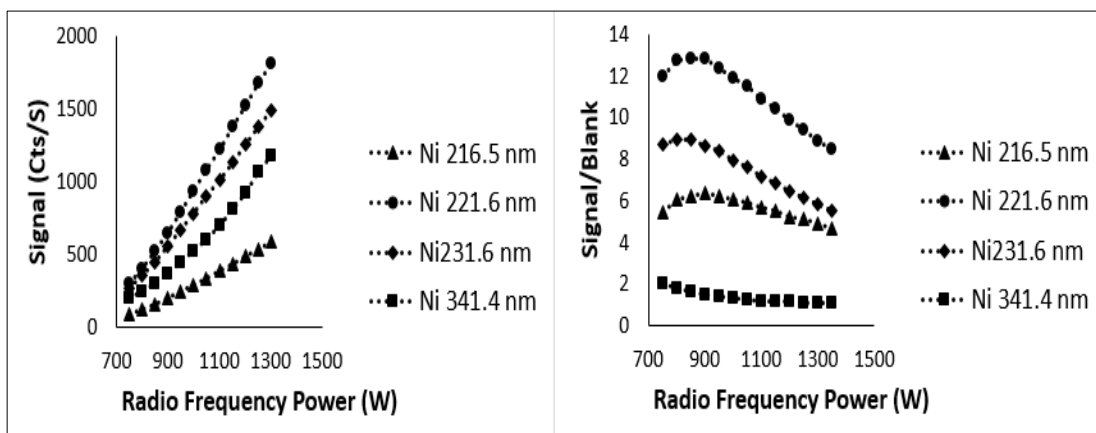


Figure 2.34 The signal and signal/blank ratios for nickel (300 ng/mL) at four different wavelengths using different ICP-OES radio frequency powers

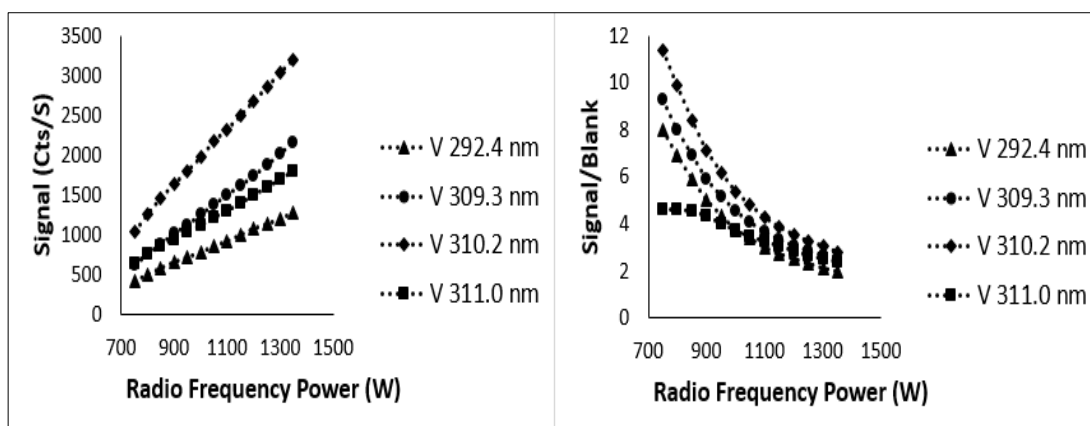


Figure 2.35 The signal and signal/blank ratios for vanadium (300 ng/mL) at four different wavelengths using different ICP-OES radio frequency powers

From the illustrated results in the Figures 2.29-2.35, the standard signal increases with the increase of RF power. Higher plasma powers causes an increase in plasma temperature(133) and as emission intensity is directly proportional to temperature this can be seen in the linear graphs produced for the signal. The issue here is that not only does signal increase linearly but blank signal may also increase linearly which results in the signal/blank ratio plots shown in Figures 2.29-2.35.

The signal/ blank ratio shows the best sensitivity at 800 W. The ratio at this low RF power is high because the blank signal has dropped significantly more than the signal for the standard. This finding is consistent with the fact that the cool plasma is sometimes used to minimise interferences(145). However, the stability of the signal is an issue at these low powers due to the practical limits dictated by the plasma stability. As a result, there is a need to assess the LoD and LoQ at different RF powers. Five RF powers were used to calculated LoD and LoQ for Class 1 and Class 2A elements. Those are 750W, 900W, 1050W, 1150W and 1300W.

LoD and LoQ is the lowest amount of analyte in a sample, which can be detected or quantitatively determined, respectively, with suitable precision and accuracy(267).

An example of how the calculations were performed is the following:

Figure 2.36 represents the calibration line equation and R² value for V 292.4nm at 1300W.

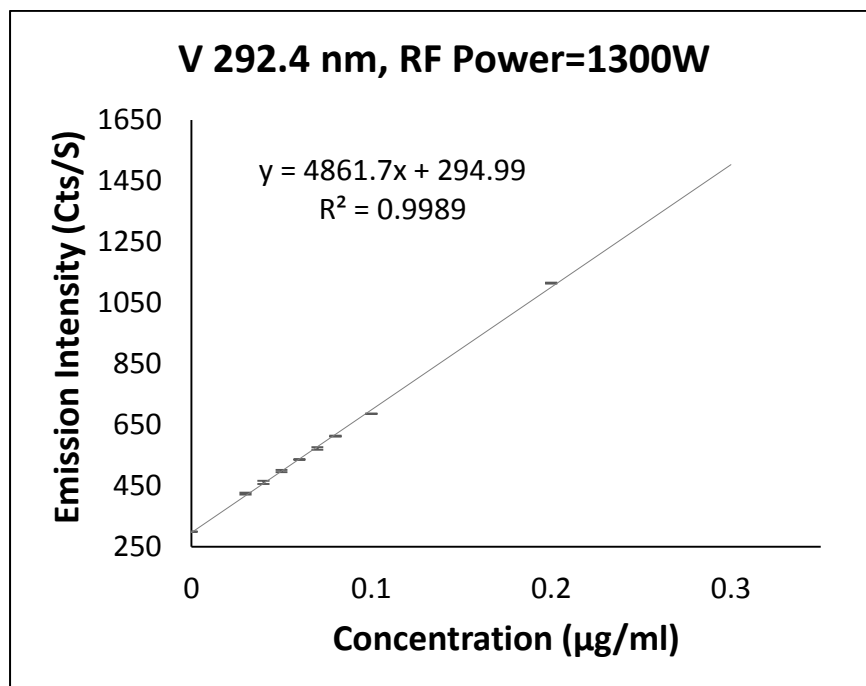


Figure 2.36 V 292.4nm Calibration line obtained using RF power of 1300W

The average of the 10 blanks reading is 296.63 counts/second (Cts/S) with σ of 3.55

From the obtained calibration linear line equation, the slope=4861.7 and the intercept= 294.99

LoD and LoQ are calculated using equation 2.1 and 2.2 respectively.

$$LoD = \frac{(average\ blanks\ reading + 3\sigma) - Intercept}{Slope} \dots \text{Equation 2.1}$$

$$LoQ = \frac{(average\ blanks\ reading + 10\sigma) - Intercept}{Slope} \dots \text{Equation 2.2}$$

$$\text{LoD} = \frac{(296.63 + (3 \times 3.55)) - 294.99}{4861.7} = \frac{(296.63 + 10.65) - 294.99}{4861.7} = \frac{12.29}{4861.7}$$

$$= 0.00253 \text{ } \mu\text{g/mL} = 2.53 \text{ ng/mL}$$

$$\text{LoQ} = \frac{(296.63 + (10 \times 3.55)) - 294.99}{4861.7} = \frac{(296.63 + 35.5) - 294.99}{4861.7} = \frac{37.14}{4861.7}$$

$$= 0.00764 \text{ } \mu\text{g/mL} = 7.64 \text{ ng/mL}$$

Table 2.4 demonstrates the calculated LoDs and LoQs (ng/mL) using different RF powers.

Table 2.4 Class 1 and Class 2A LoDs and LoQs (ng/mL) calculated using different RF powers

RF Power	750W		900W		1050W		1150W		1300W	
	LoD	LoQ								
As189.0	10.62	32.25	4.89	14.72	5.01	14.89	4.09	11.95	1.85	5.86
As193.7	11.31	33.93	7.52	22.23	2.59	7.89	4.28	13.04	2.48	7.28
Cd214.4	2.87	8.75	0.67	2.07	0.71	2.14	0.99	3.01	0.29	0.87
Cd226.5	1.90	5.80	0.79	2.36	0.81	2.43	1.01	3.03	1.05	3.09
Hg184.9	14.18	42.31	3.62	11.22	3.16	9.54	2.62	8.13	0.69	2.23
Hg194.2	9.32	27.97	4.85	14.41	3.51	11.57	2.32	7.09	1.47	4.43
Pb182.2	9.80	30.38	5.89	18.25	4.50	13.49	4.10	12.29	1.76	5.56
Pb216.9	7.91	23.65	4.53	13.59	6.53	19.46	6.14	18.73	1.54	4.88
Pb220.3	9.05	27.26	3.08	9.50	3.35	10.00	3.51	10.29	1.52	4.73
Co228.6	2.86	8.57	1.04	3.08	1.23	3.76	1.27	3.88	0.52	1.58
Co230.7	4.53	13.53	1.52	4.55	1.49	4.45	1.60	4.79	1.10	3.65
Co237.8	32.69	98.07	12.52	40.05	10.71	32.27	6.49	20.11	7.71	25.91
Co238.8	9.49	28.47	3.78	11.52	3.18	9.71	3.65	10.96	3.77	11.18
Ni216.5	4.56	13.91	2.48	7.43	2.08	6.23	1.97	6.01	4.25	12.61
Ni221.6	2.84	8.49	1.07	3.21	0.85	2.58	1.12	3.36	0.97	3.20
Ni231.6	2.35	7.06	1.39	4.16	1.34	4.12	1.28	3.98	0.59	1.74
V292.4	4.89	14.72	2.59	7.85	1.46	4.45	2.05	6.30	2.53	7.64
V309.3	2.65	7.95	2.07	6.41	1.27	4.12	1.45	4.41	4.05	13.18
V310.2	6.86	21.28	4.48	13.67	3.32	10.12	3.02	9.20	3.34	9.99
V311.0	3.31	10.11	2.51	7.53	2.52	7.57	3.45	10.69	4.66	15.09

From Table 2.4, RF power of 1300 W gave the lowest LoD and LoQ for Class 1 and Class 2A elements, so it was chosen as the optimum setting to perform the analysis using ICP-OES.

2.3.1.6 Wavelengths selection

It is worth mentioning that sensitivity was found to be poor for As 449.4 nm, Cd 326.1 nm, Hg 253.6 nm, Ni 341.4 nm, and Pb 261.4 nm, so all these lines were excluded from any further work due to the unreliable results obtained using them. An example is Figure 2.37, which demonstrates clearly the poor correlation obtained for the calibration curve using As 449.4nm.

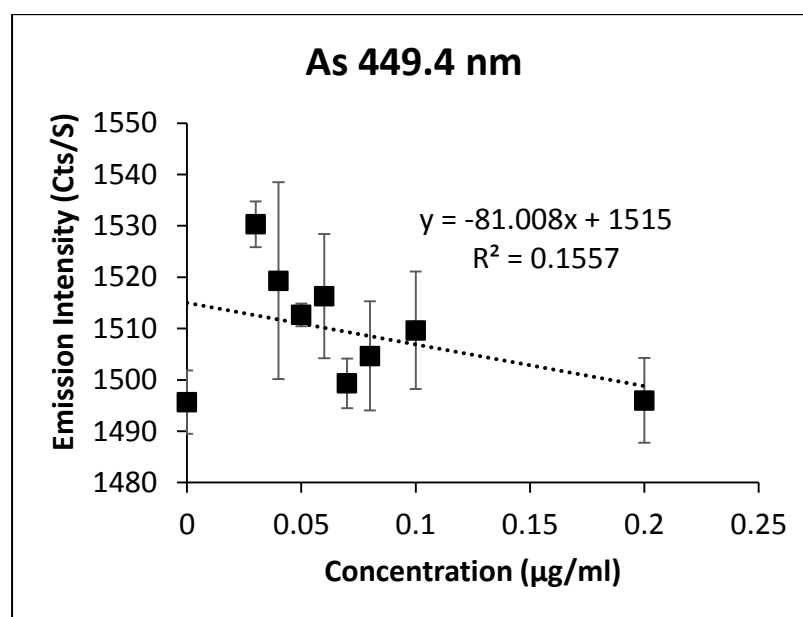


Figure 2.37 Calibration curve with poor correlation coefficient when using As 449.4nm due to the poor signal at this wavelength.

Based on the optimisation results one wavelength was chosen for each element taking into consideration the possible interferences for each line by visual evaluation of the spectra for any potential overlapping peaks. For example, there is a spectral overlap between As 228.8 nm and Cd 228.8 nm. In addition, certain interferences

were found using Thermo iTEVA[®] software such as Mg with V 309.3 nm and Ca with V 310.2 nm (Figure 2.38).

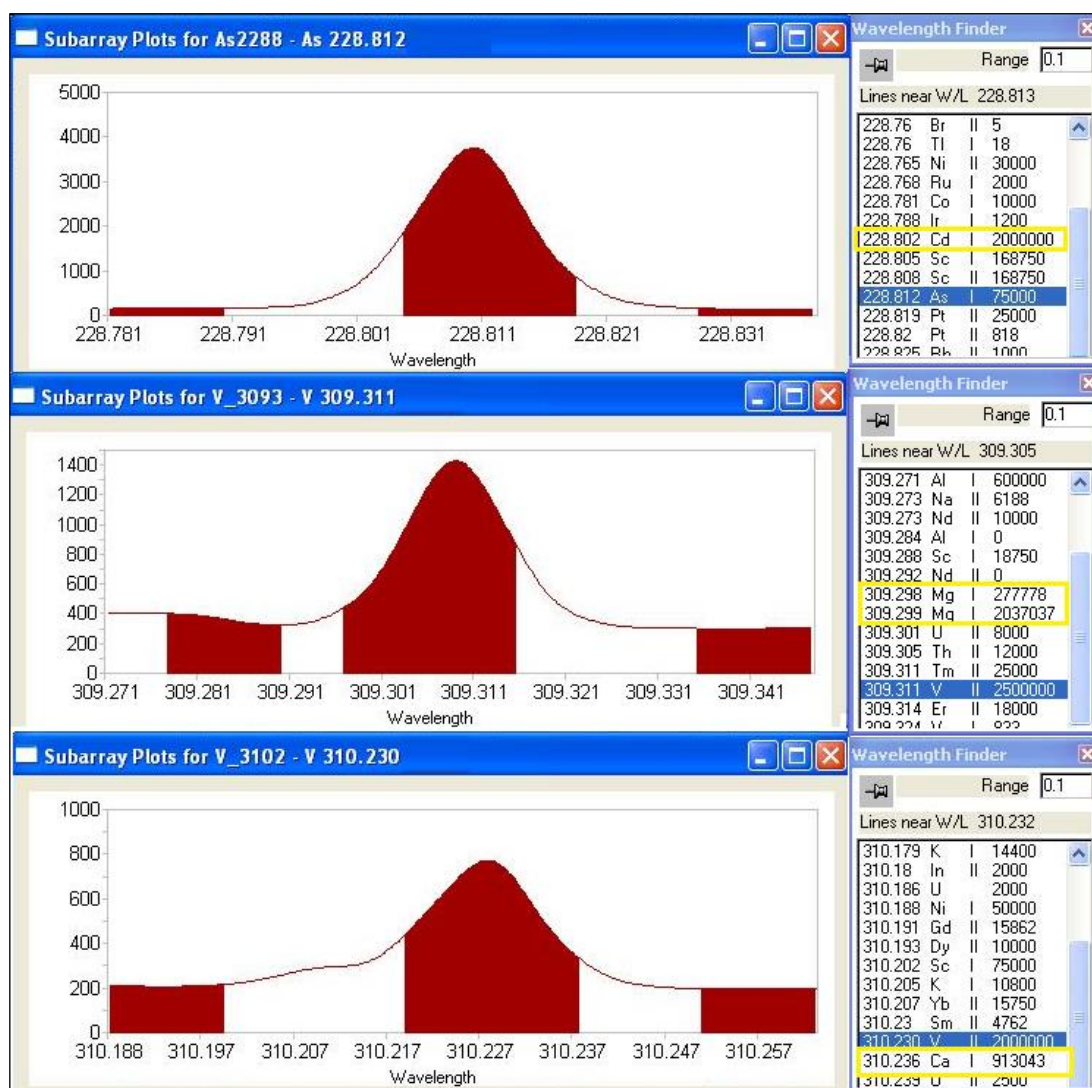


Figure 2.38 Wavelength interferences determined using iTEVA software

The selected wavelengths were as follows: As (189.0 nm), Cd (214.4 nm), Hg (184.9 nm), Pb (220.3 nm), Co (228.6 nm), Ni (231.6 nm) and V (292.4 nm). Other lines were optimised in case a later interference in a sample was observed to allow an alternative line to be adopted.

The optimum conditioned ICP-OES optimum conditions were summarised in Table 2.3.

2.3.2 Analytical figures of merit and method validation

2.3.2.1 Limits of detection and limits of quantification

LoD and LoQ were calculated for Class 1 and Class 2A elements at the selected wavelengths using the optimised ICP-OES conditions as described in Sections 2.3.1.1 - 2.3.1.6

The results are summarised in Table 2.5.

Table 2.5 ICP-OES limits of detection and Limits of quantification for Class 1 and Class 2A elements

Element (λ -nm)	Blanks Av.*	σ	Slope	Intercept	Av.+3 σ	Av.+10 σ	LoD $\mu\text{g/mL}$	LoQ $\mu\text{g/mL}$	LoD ng/mL	LoQ ng/mL
As189.0	41.59	2.78	4857.38	40.93	49.93	69.40	0.0019	0.0059	1.85	5.86
Cd214.4	81.52	3.06	36540.67	79.81	90.69	112.10	0.0003	0.0009	0.30	0.88
Hg184.9	42.34	1.85	8455.48	42.00	47.88	60.83	0.0007	0.0022	0.70	2.23
Pb220.3	103.06	3.50	7634.47	101.93	113.55	138.04	0.0015	0.0047	1.52	4.73
Co228.6	132.70	2.05	13535.48	131.83	138.85	153.21	0.0005	0.0016	0.52	1.58
Ni231.6	137.99	7.51	45238.98	134.02	160.51	213.06	0.0006	0.0017	0.59	1.75
V292.4	296.63	3.55	4861.70	294.99	307.28	332.14	0.0025	0.0076	2.53	7.64

*Av. = Average

2.3.2.1 Linearity and range

According to ICH guidelines, the linearity of an analytical procedure is defined as 'its ability (within a given range) to obtain test results that are directly proportional to the concentration (amount) of analyte in the sample'(267).

Judging the linearity is often done by examining the correlation coefficient (R^2) of the linear regression line for the obtained emission intensity (Cts/S) versus standard analyte concentrations.

Eight concentration points were assayed in triplicate and showed good linearity in the tested range, with a correlation coefficient (R^2) value of above 0.995. The linear

regression equation and its R², for each of the calibration curves are summarised in Table 2.6.

Table 2.6 Linearity data for Class 1 and Class 2A elements using ICP-OES

Element	Range (ng/ml)*	Calibration equation	R ² Value
As 189.0 nm	10 - 100,000	y= 431.51x + 35.96	0.9975
Cd 214.4 nm	5 - 50,000	y= 10599x + 127.1	0.9978
Hg 184.9 nm	5 - 50,000	y= 921.39x + 49.06	0.9997
Pb 220.3 nm	5 - 100,000	y= 871.84x + 59.67	0.9990
Co 228.6 nm	5-100,000	y= 5403.8x + 118.7	0.9978
Ni 231.6 nm	5-100,000	y= 3644x + 192.7	0.9979
V 292.4 nm	10-100,000	y= 3502.9x + 92.84	0.9998

* The lower concentration in the range was chosen by taking into consideration the results obtained from the LoQs calculation.

2.3.2.2 Accuracy and precision

According to ICH guidelines, accuracy is expressed as ‘the closeness of agreement between true value of analyte in samples and test result obtained by the method’, while precision is defined as ‘the closeness of agreement (degree of scatter) between a series of measurements obtained from multiple sampling of the same homogeneous sample under the prescribed conditions’(267).

The precision is expressed as the relative standard deviation (RSD) of replicate measurement and is divided into three categories: repeatability (intra-day precision), intermediate precision (inter-day precision) and reproducibility (between laboratories precision)(267).

The accuracy and precision were evaluated using *NIST 3280*, where % recoveries between 95-105% indicate the method’s accuracy and RSD less than 5% were targeted for acceptable precision. A microwave assisted acid digestion procedure

was developed for this purpose and the results will be discussed in the following sections.

2.3.3 Optimisation of microwave assisted acid digestion procedure

NIST 3280 samples were prepared for digestion as described in Section 2.2.6.

The first challenge of using the only available solid standard reference material; *NIST 3280*, was the low concentration of Class 1 elements (As, Cd Hg and Pd) that becomes below the optimised ICP-OES method's LoQs (Table 2.7). The second challenge as mentioned before is the absence of Hg. As a result validating the ICP-OES method for Class 1 elements is impractical using *NIST 3280*.

Table 2.7 The concentration of elements (ng/mL) in *NIST 2380* after dilution

Element	ICP-OES-LoQs	NIST 3280 ⁽⁹³⁾	After 50X Dilution	After 500X Dilution
As	5.86	132	2.64	0.264
Cd	0.87	80.15	1.603	0.1603
Hg	2.23	N/A	N/A	N/A
Pb	4.73*	272.7	5.454	0.5454
Co	1.58	810	16.2	1.62
Ni	1.74	8430	168.6	16.86
V	7.64	8000	160	16

*Although Pb LoQ is lower than the nominal concentration after 50X dilution, the variation and error in the sample preparation as well as the inherent variation of Pb concentration within *NIST 3280* made the measurement of Pb using ICP-OES unreliable.

In the initial development steps, reverse aqua regia was used as the digestion medium, since it contains more hydrochloric acid than the 9 HNO₃ : 1HCl (v/v), which helps digesting organic matrices more efficiently.

A blank (8 ml reverse aqua regia) subjected to the exact same procedure as *NIST 3280*, filtered and finally diluted, was analysed in triplicate using ICP-OES to check if it adds any elements to the samples and thus gives false high results. All elements

concentrations were below LoDs and thus there is no risk of contaminating the samples during preparation (See Table 2.8).

Table 2.8 Obtained concentrations using the developed and optimised ICP-OES method for reverse aqua regia following microwave digestion, $n=3$

Element	Concentration (ng/ml)	RSD
As 189.0 nm	<LoD (1.85)	37.78
Cd 214.4 nm	<LoD (0.30)	78.25
Hg 184.9 nm	<LoD (0.70)	35.93
Pb 220.3 nm	0.59	68.15
Co 228.6 nm	0.47	25.36
Ni 231.6 nm	<LoD (0.59)	31.84
V 292.4 nm	0.54	51.20

2.3.1.1 Optimisation of the of microwave assisted acid digestion procedure temperature

2.3.1.1.1 One stage vs three stages of digestion method

The first parameter to be optimised for the digestion procedure was the temperature. So, ramping for ten minutes followed by holding for twenty minutes at 160°C, 180°C, 200°C and 210°C was performed. The obtained recoveries and RSDs were calculated and represented in Table 2.9.

Table 2.9 One-stage microwave-assisted acid digestion procedure for *NIST 3280*, at different temperatures, using ICP-OES for analysis. $n=3$

Element λ -nm	160°C		180°C		200°C		210°C	
	%Recovery*	RSD	%Recovery	RSD	%Recovery	RSD	%Recovery	RSD
As189.0	<LoQ (5.86)	-						
Cd214.4	<LoQ (0.88)	-						
Hg184.9	N/A	-	N/A	-	N/A	-	N/A	-
Pb220.3	<LoQ (4.73)	-						
Co228.6	49.65	11.07	70.09	22.84	58.67	10.66	79.49	12.67
Ni231.6	54.95	71.23	78.93	16.63	63.68	22.36	72.71	15.62
V292.4	72.28	12.05	55.69	18.99	86.57	36.76	88.62	19.42

* Concentration (ng/g)

Going beyond 210°C caused practical problems represented as occasional damaged caps (Figure 2.39) and thus sample loss (Figure 2.40) due to the rapid pressure build-up and the continuous venting and release of hot vapour to reduce the pressure.



Figure 2.39 Thermal degradation of caps when holding at 220°C for 20 minutes

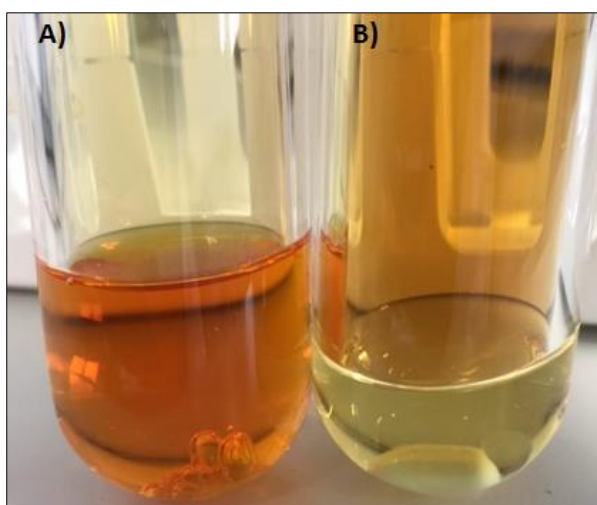


Figure 2.40 Sample loss due to caps damage during digestion procedure when holding at 220°C for 20 minutes

In addition, increasing the temperature to 200°C and beyond using a one-stage digestion procedure caused charring of some of the powder at the vessel's wall, which led to poor repeatability and inconsistent results. To overcome this problem a three-stages procedure was tried where the temperature is increased gradually to

allow the different samples components to digest at different stages and that was successful in preventing charring as well as in reducing the pressure build up. Figure 2.41 shows the digested samples using one and three stages procedure.

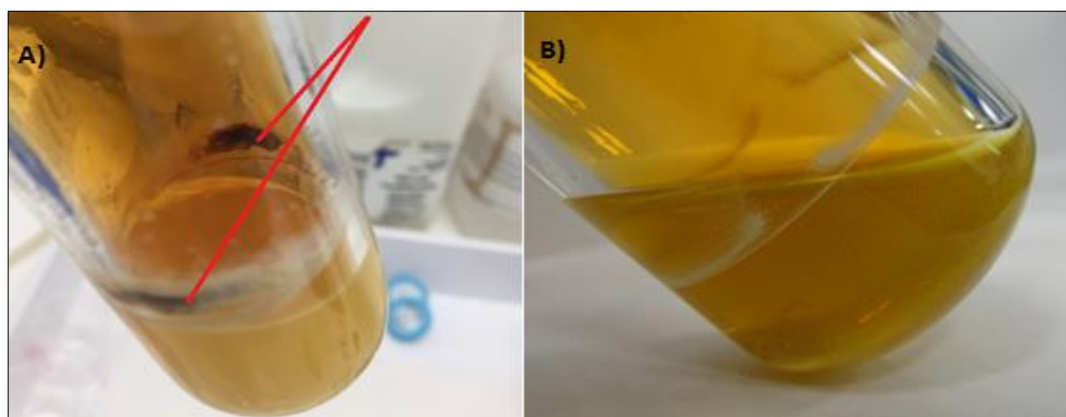


Figure 2.41 *NIST 3280* digest using: A) One-stage procedure, B) Three-stages procedure

To reduce caps deformation, custom venting at low temperatures were included in the three-stages digestion procedure to minimise the hot vapour contact with the caps. The results obtained were found to be acceptable while keeping the caps physically intact. Figure 2.42 shows the pressure build up and vent using one-stage and three-stages digestion procedure.

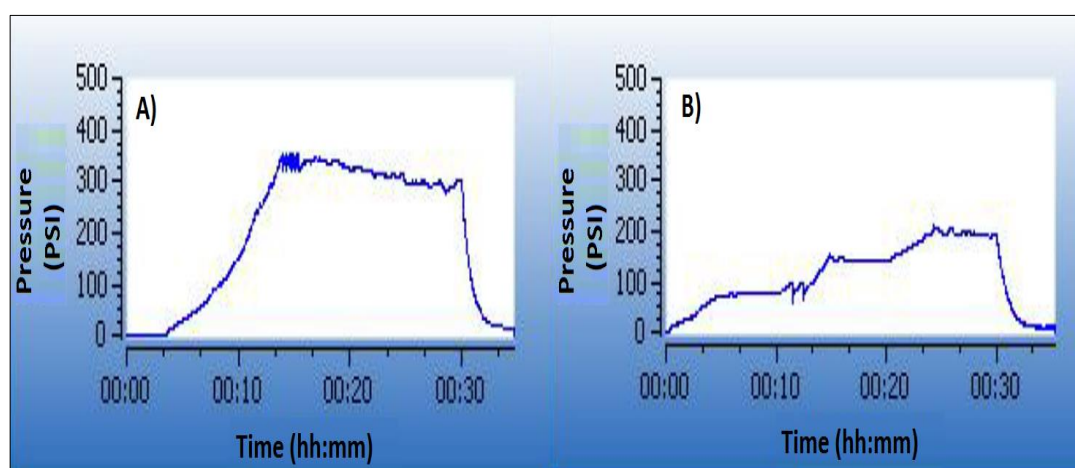


Figure 2.42 The pressure profile for microwave digestion procedure of *NIST 3280*. A) One-stage digestion procedure at 210 °C with a hold for 20 minutes and B) Three-stages digestion procedure at 120°C, 180°C and 210°C with a hold for 5 minutes at each temperature.

2.3.1.2 Optimisation of the three-stages digestion procedure time

From Table 2.9, 210°C gave recoveries of more than 70% for Class 2A elements, but with poor repeatability, so this temperature was used in the third stage of the digestion procedure. 120°C and 180°C were used for the first and second stages respectively.

The effect of hold time on the percentage recoveries for the elements was studied by holding for 5, 10 and 15 minutes at the same temperature, which is 210°C. The obtained results showed satisfactory recoveries with good precision by holding for 5 minutes only, so for the sake of time efficiency holding for 5 minutes was chosen to study the effect of different temperatures. Table 2.10 illustrates the obtained results.

Table 2.10 Optimisation of digestion time using three-stages digestion procedure, *n*=3

Method 1-Total time = 40 minutes		
Stage 1: Ramp Time= 5 min, Temperature= 120°C, Hold time= 5 min		
Stage 2: Ramp Time= 5 min, Temperature= 180°C, Hold time= 5 min		
Stage 3: Ramp Time= 5 min, Temperature= 210°C, Hold time= 15 min		
Element	% Recovery	RSD
As 189.0 nm	<LoQ (5.86 ng/g)	-
Cd 214.4 nm	<LoQ (0.88 ng/g)	-
Hg 184.9 nm	N/A	-
Pb 220.3 nm	<LoQ (4.73 ng/g)	-
Co 228.6 nm	99.96	1.45
Ni 231.6 nm	104.03	1.58
V 292.4 nm	104.28	1.4

Table 2.10, continued

Method 2-Total time = 35 minutes		
Stage 1: Ramp Time= 5 min, Temperature= 120°C, Hold time= 5 min		
Stage 2: Ramp Time= 5 min, Temperature= 180°C, Hold time= 5 min		
Stage 3: Ramp Time= 5 min, Temperature= 210°C, Hold time= 10 min		
Element	% Recovery	RSD
As 189.0 nm	<LoQ (5.86 ng/g)	-
Cd 214.4 nm	<LoQ (0.88 ng/g)	-
Hg 184.9 nm	N/A	-
Pb 220.3 nm	<LoQ (4.73 ng/g)	-
Co 228.6 nm	98.4	5.74
Ni 231.6 nm	103.92	4.83
V 292.4 nm	103.18	4.72
Method 3-Total time = 30 minutes		
Stage 1: Ramp Time= 5 min, Temperature= 120°C, Hold time= 5 min		
Stage 2: Ramp Time= 5 min, Temperature= 180°C, Hold time= 5 min		
Stage 3: Ramp Time= 5 min, Temperature= 210°C, Hold time= 5 min		
Element	% Recovery	RSD
As 189.0 nm	<LoQ (5.86 ng/g)	-
Cd 214.4 nm	<LoQ (0.88 ng/g)	-
Hg 184.9 nm	N/A	-
Pb 220.3 nm	<LoQ (4.73 ng/g)	-
Co 228.6 nm	99.82	3.88
Ni 231.6 nm	100.11	4.25
V 292.4 nm	96.88	3.02

At this point, a solid residue was still present in the mixture after digesting *NIST 3280*. This is due to the presence of ingredients like silicon dioxide that will not be fully digested using reverse aqua regia. The use of more corrosive and toxic acids like hydrofluoric acid is not necessary, because all the elements of interest are extracted and dissolved in the liquid phase, which is supported by the good recoveries and RSDs obtained (Table 2.10- Method 3).

2.3.1.3 Testing the elements extraction efficiency of different acid ratios

Nitric acid alone is commonly used to extract elements and digest samples(282-287), so the next step in the procedure development was to try a higher ratio of nitric acid

as the digestion medium. In this case, a ratio of 9 HNO₃: 1 HCl. The obtained results are illustrated in Table 2.11.

Table 2.11 Percentage recoveries for NIST 3280 using 9 HNO₃: 1 HCl, n=3

Stage 1: Ramp Time= 5 min, Temperature= 120°C, Hold time= 5 min

Stage 2: Ramp Time= 5 min, Temperature= 180°C, Hold time= 5 min

Stage 3: Ramp Time= 5 min, Temperature= 210°C, Hold time= 5 min

Element	NIST 3280 certificate		Spike addition	
	% Recovery	RSD	Spiked Recovery	RSD
As 189.0 nm	<LoQ (5.86 ng/g)	-	102.03	1.58
Cd 214.4 nm	<LoQ (0.88 ng/g)	-	99.52	2.17
Hg 184.9 nm	N/A	-	98.17	3.82
Pb 220.3 nm	<LoQ (4.73 ng/g)	-	97.64	2.25
Co 228.6 nm	95.67	6.22	99.10	1.65
Ni 231.6 nm	76.47	4.73	95.24	2.84
V 292.4 nm	99.50	3.21	101.78	1.23

Reverse aqua regia was more efficient in extracting Ni than the 9 HNO₃ : 1 HCl (v/v) acid ratio, which is consistent with previous findings. Ni recoveries were about 70-80% using SRM 1573 (certified tomato leaves), BCR 146 (certified sewage sludge)(288), SRM 1575 (certified pine needles), RM 8433 (certified corn bran) and RM 8436 (certified durum wheat flour)(284).

Based on that, reverse aqua regia was the acid mixture used to digest pharmaceutical samples in this work.

2.3.1.4 Microwave assisted acid digestion procedure validation

2.3.1.4.1 Digestion efficiency assessment using spike addition vs. NIST 3280 certified levels

The reliability of the spike recoveries recommended for validation by USP <233>(96) was tested using the three-stages optimised method at different maximum temperatures (140, 160, 180 and 210°C). The % recoveries based on the certified elements levels were also calculated.

As demonstrated in Table 2.12 spike recoveries were between 95-105% even at low temperatures where actually only a fraction of the elements was extracted which is reflected clearly in the recoveries calculated based on *NIST 3280* certificate as they were in some cases below USP <233> accepted recovery of 70%.

That suggest the need for validating any developed procedure using a solid reference material that represents the whole process rather than relying solely on spiked recoveries.

Table 2.12 *NIST 3280* percentage recoveries using different temperatures for the microwave assisted acid digestion methods, *n*=3

Method 1				
Stage 1: Ramp Time= 5 min, Temperature= 50°C, Hold time= 5 min				
Stage 2: Ramp Time= 5 min, Temperature= 110°C, Hold time= 5 min				
Stage 3: Ramp Time= 5 min, Temperature= 140°C , Hold time= 5 min				
<i>NIST 3280</i> certified levels			Spike addition	
Element	% Recovery	RSD	Spiked Recovery	RSD
As 189.0 nm	<LoQ (5.86 ng/g)	-	99.30	1.18
Cd 214.4 nm	<LoQ (0.88 ng/g)	-	98.73	4.77
Hg 184.9 nm	N/A	-	97.59	4.68
Pb 220.3 nm	<LoQ (4.73 ng/g)	-	100.27	3.94
Co 228.6 nm	60.07	7.71	95.23	2.68
Ni 231.6 nm	55.69	16.63	104.69	2.09
V 292.4 nm	63.26	8.249	101.18	2.48
Method 2				
Stage 1: Ramp Time= 5 min, Temperature= 70°C, Hold time= 5 min				
Stage 2: Ramp Time= 5 min, Temperature= 130°C, Hold time= 5 min				
Stage 3: Ramp Time= 5 min, Temperature= 160°C , Hold time= 5 min				
<i>NIST 3280</i> certified levels			Spike addition	
Element	% Recovery	RSD	Spiked Recovery	RSD
As 189.0 nm	<LoQ (5.86 ng/g)	-	102.19	1.05
Cd 214.4 nm	<LoQ (0.88 ng/g)	-	97.69	2.33
Hg 184.9 nm	N/A	-	100.80	2.54
Pb 220.3 nm	<LoQ (4.73 ng/g)	-	95.43	4.95
Co 228.6 nm	52.44	7.53	103.76	2.33
Ni 231.6 nm	61.83	9.53	99.88	3.86
V 292.4 nm	68.95	5.99	96.07	2.27

Table 2.12, continued

Method 3				
Stage 1: Ramp Time= 5 min, Temperature= 90°C, Hold time= 5 min				
Stage 2: Ramp Time= 5 min, Temperature= 150°C, Hold time= 5 min				
Stage 3: Ramp Time= 5 min, Temperature= 180°C , Hold time= 5 min				
<i>NIST 3280 certified levels</i>			Spike addition	
Element	% Recovery	RSD	Spiked Recovery	RSD
As 189.0 nm	<LoQ (5.86 ng/g)	-	98.18	1.41
Cd 214.4 nm	<LoQ (0.88 ng/g)	-	99.81	4.15
Hg 184.9 nm	N/A	-	102.44	2.17
Pb 220.3 nm	<LoQ (4.73 ng/g)	-	96.81	4.95
Co 228.6 nm	76.07	6.78	95.47	5.04
Ni 231.6 nm	72.27	10.05	95.54	3.78
V 292.4 nm	80.88	4.18	101.76	3.16
Method 4				
Stage 1: Ramp Time= 5 min, Temperature= 110°C, Hold time= 5 min				
Stage 2: Ramp Time= 5 min, Temperature= 170°C, Hold time= 5 min				
Stage 3: Ramp Time= 5 min, Temperature= 200°C , Hold time= 5 min				
<i>NIST 3280 certified levels</i>			Spike addition	
Element	% Recovery	RSD	Spiked Recovery	RSD
As 189.0 nm	<LoQ (5.86 ng/g)	-	95.85	5.01
Cd 214.4 nm	<LoQ (0.88 ng/g)	-	103.19	2.44
Hg 184.9 nm	N/A	-	102.42	3.53
Pb 220.3 nm	<LoQ (4.73 ng/g)	-	96.68	2.64
Co 228.6 nm	62.71	3.36	97.83	4.77
Ni 231.6 nm	63.97	7.40	101.11	2.52
V 292.4 nm	88.57	4.91	104.60	2.27
Method 5				
Stage 1: Ramp Time= 5 min, Temperature= 120°C, Hold time= 5 min				
Stage 2: Ramp Time= 5 min, Temperature= 180°C, Hold time= 5 min				
Stage 3: Ramp Time= 5 min, Temperature= 210°C , Hold time= 5 min				
<i>NIST 3280 certified levels</i>			Spike addition	
Element	% Recovery	RSD	Spiked Recovery	RSD
As 189.0 nm	<LoQ (5.86 ng/g)	-	95.62	4.85
Cd 214.4 nm	<LoQ (0.88 ng/g)	-	97.98	2.52
Hg 184.9 nm	N/A	-	97.88	3.78
Pb 220.3 nm	<LoQ (4.73 ng/g)	-	102.41	3.17
Co 228.6 nm	99.82	3.88	103.49	2.75
Ni 231.6 nm	100.11	4.25	97.76	3.70
V 292.4 nm	96.88	3.02	95.02	3.53

2.3.1.4.2 Validating the optimised digestion procedure for Class 1 elements

For As, Cd, Hg and Pb the method was validated by comparing the results obtained for the analysis of an experimental formulation of certified tablets that are still under development with those obtained from ICP-MS using kinetic energy discrimination (KED). This gave results from an identical sample via two different analysis techniques.

Those tablets were prepared in cooperation with the Coalition for Rational Implementation of the USP Elemental Impurities Requirements/Technical and Analytical Challenges (TAC) sub-committee, by spraying standard solutions of elements over pharmaceutical grade lactose. The next step was granulation of the lactose and other powdered excipients and then compressing it as tablets, each weighing approximately 0.25 g. Gold standard was also added in a similar way to retain Hg within the tablets(289).

The results showed good agreement as illustrated in Table 2.13.

Table 2.13 Validation for Class 1 elements using two different techniques (mean \pm σ , n=3)

Optimised ICP-OES method	ICP-MS using (KED)
As 189.0 nm=2.37 \pm 0.006 μ g/g, RSD=1.70	⁷⁵ As = 2.45 \pm 0.06 μ g/g, RSD=2.40
Cd 214.4 nm =0.85 \pm 0.005 μ g/g, RSD=0.60	¹¹¹ Cd =0.87 \pm 0.02 μ g/g, RSD=2.21
Hg 184.9 nm=3.47 \pm 0.019 μ g/g, RSD=0.55	²⁰² Hg =3.80 \pm 0.08 μ g/g, RSD=2.05
Pb 220.3 nm=1.71 \pm 0.048 μ g/g, RSD=2.78	²⁰⁸ Pb =1.89 \pm 0.02 μ g/g, RSD=1.13

To make reference tablets that are more representative of real pharmaceutical samples and thus provide better reflection of the digestion procedure efficiency, test tablets formulated from excipient containing EI such as iron oxide and silicon dioxide were produced by TAC sub-committee. The excipients were added in amounts that would theoretically provide three different concentrations of Class 1 and Class 2A elements.

Those tablets were digested in 10 mL reverse aqua regia instead of 8 mL because they contain considerably higher amounts of silicon dioxide that is hard to digest. Following preparation. The samples were analysed using the optimised ICP-OES method.

Table 2.14 illustrate the obtained results.

Table 2.14 Analysis results of three TAC formulas containing different levels of Class 1 and Class 2A elements using ICP-OES, $n=3$

Element	Formula-1 (30% PDE)	ICP-OES		
	Theoretical($\mu\text{g/g}$)*	Concentration($\mu\text{g/g}$)	RSD	%Recovery
As 189.0 nm	6.65	3.83	2.74	57.59
Cd 214.4 nm	1.58	1.36	3.09	86.08
Hg 184.9 nm	6.48	3.92	2.34	60.49
Pb 220.3 nm	2.27	2.28	2.44	100.44
Co 228.6 nm	8.68	7.96	5.51	91.71
Ni 231.6 nm	6.58	5.79	4.53	87.99
V 292.4 nm	22.25	19.64	3.64	88.27

Element	Formula-2 (100% PDE)	ICP-OES		
	Theoretical($\mu\text{g/g}$)*	Concentration($\mu\text{g/g}$)	RSD	%Recovery
As 189.0 nm	19.8	15.17	4.61	76.62
Cd 214.4 nm	5.26	4.94	3.75	93.92
Hg 184.9 nm	19.45	18.89	5.14	97.12
Pb 220.3 nm	6.67	6.41	3.94	96.10
Co 228.6 nm	22.08	19.61	5.01	88.81
Ni 231.6 nm	10.55	10.24	2.24	97.06
V 292.4 nm	22.7	18.28	3.31	80.53

Element	Formula-3 (300% PDE)	ICP-OES		
	Theoretical($\mu\text{g/g}$)*	Concentration($\mu\text{g/g}$)	RSD	%Recovery
As 189.0 nm	49.2	45.55	3.42	92.58
Cd 214.4 nm	15.76	12.63	2.15	80.14
Hg 184.9 nm	48.61	51.09	2.84	105.10
Pb 220.3 nm	17.35	14.59	3.47	84.09
Co 228.6 nm	50.12	37.67	2.76	75.16
Ni 231.6 nm	16.75	13.43	3.94	80.18
V 292.4 nm	0.9	<LoD (2.53×10^{-3})	-	-

*The theoretical concentrations were calculated based on available EI data for each excipient(31) and from the certified values in case of silicon dioxide, where an XRF reference material was used in the formulation

The calculated elements % recoveries for the three formulations were more than 70% except for As and Hg in formula 1. This low recovery (about 60%) is due to more than one factor. Firstly, as the amount of excipients containing the elements was reduced, the homogenisation and distribution of the excipients in the formula becomes more challenging. With the fact that only three tablets were used for digestion, the homogenisation issue becomes more significant. Secondly and more importantly, the recoveries were based on EI concentrations taken from work by Li et al(31). However different batches of excipients were used from the original paper and hence because of varying concentrations the theoretical levels maybe inaccurate. With higher amounts of the excipients being used in formulas 2 and 3, the excipients distribution throughout the formulas improved and higher recoveries were obtained.

2.3.1.5 Tablets grinding and sample homogeneity

Another challenge arose during the development of the microwave assisted acid digestion procedure was the variation of the results which suggested a problem in the homogeneity of the samples.

Before digesting the tablets, it was necessary to grind a suitable number of them to get a homogenized mixture to be used to get the 0.5g of the powder for digestion.

Two techniques were used to grind the tablets and homogenise the powder, the first one was using glass mortar and pestle and the second one was using a mixer mill.

A comparison of RSDs using the two grinding techniques are shown in Table 2.15. It was clear that using the mixer mill enhanced the homogeneity of the samples as the RSD dropped from 6-10 to less than 5% for all elements. The difference in

homogeneity was obvious by naked eye as flakes of the tablets' coating material were seen in the powder's mixture when the glass mortar and pestle were used to grind them. Figure 2.43 illustrates the difference in homogeneity represented by the powder appearance when both techniques were used for grinding the tablets.

Table 2.15 Digestion repeatability when two different techniques were used to grind *NIST 3280* tablets prior to digestion, $n=3$

Element	Using Glass Mortar and pestle		Using Mixer Mill MM200	
	%Recovery	RSD	%Recovery	RSD
Co 228.6 nm	102.82	7.56	99.82	3.88
Ni 231.6 nm	97.52	7.96	99.10	4.82
V 292.4 nm	97.02	7.27	96.88	3.02



Figure 2.43 *NIST 3280* powder, ground using: A) Glass mortar and pestle, B) Mixer mill

This suggests that for coated tablets such as *NIST 3280* using an instrumental method for grinding might be necessary especially when the tablets are coated with materials that could include trace elements to get reproducible results.

Some coating materials such as ferric oxide (red, yellow and black) were found to contain 0.03-0.037 $\mu\text{g/g}$ of Pb, 0.04-0.080 $\mu\text{g/g}$ of As, 37.8-123.5 $\mu\text{g/g}$ of Co, 57.7-96.0 $\mu\text{g/g}$ of Ni and 43.9-436 $\mu\text{g/g}$ of V. Another example for a coating material is

titanium dioxide, which is used to coat *NIST 3280*. It was found to contain 0.08 µg/mL of As, 0.04 µg/g of Cd, 0.01 µg/g of Hg, 2.15 µg/g of Pb, 3.31 µg/g of Co, 12.90 µg/g of Ni, 5.30 µg/g of V(31). The inability of the grinding method to evenly distribute the elemental impurities from the coating would cause the variation seen in the mortar and pestle technique.

2.3.1.6 Selection of suitable internal standard(s)

Internal standardisation is effective in maintaining long-term stability, improving accuracy and precision for ICP-OES by reducing errors caused by uncontrolled variation in noise response and the different composition of samples matrices(290, 291).

Two internal standards were used to improve accuracy and precision of the optimised ICP-OES method, Sc 225.2 nm and Y 371 nm. The corrected results obtained using iTEVA software after analysing the reference tablets were compared with those obtained without internal standard correction for the same samples. The results illustrated in Table 2.16 shows that both Sc and Y were effective in improving the method's precision, however, Sc was more efficient in improving the results accuracy as Y generated lower concentration in comparison with the certified levels. As a result, Sc 225.2nm was selected as the internal standard to be used for all the analysed samples using ICP-OES.

Table 2.16 Concentrations ($\mu\text{g/g}$) obtained with and without the use of Sc 225.2nm and Y 371nm as internal standards, $n=3$

Element-nm	With Sc 225.5	With Y 371	Without IS*	Reference
		TAC-Tablets		ICP-MS (KED)
As 189.0	2.37 \pm 0.006	1.67 \pm 0.004	2.70 \pm 1.35	2.45 \pm 0.06
Cd 214.4	0.85 \pm 0.005	0.72 \pm 0.05	0.78 \pm 0.15	0.87 \pm 0.02
Hg 184.9	3.47 \pm 0.019	3.28 \pm 0.02	3.66 \pm 1.95	3.80 \pm 0.08
Pb 220.3	1.71 \pm 0.048	1.65 \pm 0.042	2.57 \pm 1.82	1.89 \pm 0.02
		NIST 3280-Tablets		Certified levels
Co 228.6	0.80 \pm 0.040	0.70 \pm 0.045	0.81 \pm 0.15	0.81 \pm 0.01
Ni 231.6	8.45 \pm 0.041	8.34 \pm 0.042	8.35 \pm 3.64	8.34 \pm 0.30
V 292.4	7.69 \pm 0.027	7.58 \pm 0.028	7.85 \pm 2.11	8.00 \pm 2.00

*IS= internal standard

2.3.4 Analysis of analgesic tablets, cold and cough remedies

The concentration of elemental impurities in each product was calculated based on the maximum allowed dose as stated by the products' manufacturers to generate numbers that are comparable to the ICH Q3D guidelines where the limits are set as PDEs as described before. The maximum daily doses for cough remedies formulated as syrups were determined by weighing the corresponding volumes using analytical balance.

All product samples were spiked to calculate the spiked recoveries and *NIST 3280* samples were also digested with each product to make sure that the method is accurate each time it was used for product's analysis. The percentage recoveries for quantifiable elements in the reference tablets were always between 95-105% as well as the spiked recoveries.

Table 2.17 and 2.18 summarise the elemental impurities determined in each product.

Table 2.17 Elemental impurities ($\mu\text{g}/\text{day}$) in analgesic tablets analysed using ICP-OES (mean $\pm \sigma$, $n=3$)

Products*	Elements (nm)	ICH Q3D oral PDEs ($\mu\text{g}/\text{day}$)	Concentration ($\mu\text{g}/\text{day}$)	Spiked Recovery	RSD
Paracetamol value health	As 189.0	15	<LoD (1.85×10^{-3})	95.97	3.25
	Cd 214.4	5	0.45 ± 0.009	97.77	2.54
	Hg 184.9	30	<LoD (7.00×10^{-4})	101.91	4.32
	Pb 220.3	5	1.07 ± 0.001	100.03	3.62
	Co 228.6	50	1.07 ± 0.059	98.89	4.51
	Ni 231.6	200	50.71 ± 0.028	99.37	2.64
	V 292.2	100	<LoD (2.53×10^{-3})	101.04	3.41
Hedex Extra	As 189.0	15	<LoD (1.85×10^{-3})	97.79	2.94
	Cd 214.4	5	0.55 ± 0.089	99.03	1.19
	Hg 184.9	30	<LoD (7.00×10^{-4})	96.71	1.42
	Pb 220.3	5	4.14 ± 0.052	99.15	2.74
	Co 228.6	50	2.87 ± 1.10	104.77	3.51
	Ni 231.6	200	<LoD (5.90×10^{-4})	100.18	3.42
	V 292.2	100	<LoD (2.53×10^{-3})	98.24	2.14
Anadin Extra	As 189.0	15	<LoD (1.85×10^{-3})	95.20	3.21
	Cd 214.4	5	0.41 ± 0.009	101.96	2.61
	Hg 184.9	30	<LoD (7.00×10^{-4})	96.64	4.01
	Pb 220.3	5	3.51 ± 0.05	99.63	2.03
	Co 228.6	50	<LoD (5.20×10^{-4})	98.82	2.29
	Ni 231.6	200	<LoQ (1.75×10^{-3})	100.42	2.55
	V 292.2	100	<LoD (2.53×10^{-3})	100.61	3.26
Paracetamol Bell's Healthcare	As 189.0	15	<LoD (1.85×10^{-3})	97.31	2.00
	Cd 214.4	5	0.62 ± 0.054	95.23	3.77
	Hg 184.9	30	<LoD (7.00×10^{-4})	97.75	4.51
	Pb 220.3	5	3.91 ± 0.087	96.41	3.32
	Co 228.6	50	<LoD (5.20×10^{-4})	98.45	2.61
	Ni 231.6	200	<LoQ (1.75×10^{-3})	103.96	3.21
	V 292.2	100	<LoD (2.53×10^{-3})	103.02	2.28

*The remaining two products have all elements levels <LoD.

Table 2.18 Elemental impurities ($\mu\text{g}/\text{day}$) in cold and cough remedies analysed using ICP-OES mode (mean \pm σ , $n=3$)

Products	Elements	ICH Q3D oral PDEs ($\mu\text{g}/\text{day}$)	Concentration ($\mu\text{g}/\text{day}$)	Spiked Recovery	RSD
Tixylix	As 189.0	15	<LoD (1.85×10^{-3})	100.73	4.01
	Cd 214.4	5	6.19 \pm 0.023	97.86	3.17
	Hg 184.9	30	<LoD (7.00×10^{-4})	97.66	3.99
	Pb 220.3	5	22.68 \pm 0.043	95.13	2.11
	Co 228.6	50	<LoQ (1.58×10^{-3})	100.53	2.59
	Ni 231.6	200	<LoQ (1.75×10^{-3})	98.46	2.65
	V 292.2	100	<LoD (2.53×10^{-3})	103.66	3.77
Calpol SixPlus	As 189.0	15	<LoD (1.85×10^{-3})	97.06	2.51
	Cd 214.4	5	<LoD (3.00×10^{-4})	102.01	1.38
	Hg 184.9	30	16.87 \pm 0.031	96.13	1.61
	Pb 220.3	5	55.27 \pm 0.028	98.73	2.81
	Co 228.6	50	11.44 \pm 0.047	95.03	1.45
	Ni 231.6	200	<LoD (5.90×10^{-4})	97.06	1.66
	V 292.2	100	<LoD (2.53×10^{-3})	102.89	3.07
Nelsons Sootha	As 189.0	15	<LoD (1.85×10^{-3})	95.73	1.07
	Cd 226.5	5	2.22 \pm 0.048	97.93	2.05
	Hg 184.9	30	<LoD (7.00×10^{-4})	95.133	4.41
	Pb 220.3	5	7.79 \pm 0.05	97.46	2.15
	Co 228.6	50	<LoQ (1.58×10^{-3})	100.41	3.51
	Ni 231.6	200	<LoQ (1.75×10^{-3})	99.82	3.08
	V 292.2	100	<LoD (2.53×10^{-3})	98.67	2.16
Calcough	As 189.0	15	<LoD (1.85×10^{-3})	100.79	2.98
	Cd 214.4	5	7.23 \pm 0.04	97.13	2.59
	Hg 184.9	30	9.01 \pm 0.027	97.68	1.71
	Pb 220.3	5	20.24 \pm 0.05	95.66	3.52
	Co 228.6	50	6.02 \pm 0.021	102.86	2.08
	Ni 231.6	200	<LoQ (1.75×10^{-3})	100.53	2.29
	V 292.2	100	<LoD (2.53×10^{-3})	104.06	1.79
Lemsip	As 189.0	15	<LoD (1.85×10^{-3})	98.26	1.86
	Cd 214.4	5	9.69 \pm 0.22	97.39	2.17
	Hg 184.9	30	<LoD (7.00×10^{-4})	102.32	2.17
	Pb 220.3	5	25.84 \pm 0.10	98.53	3.89
	Co 228.6	50	9.13 \pm 0.048	96.66	3.56
	Ni 231.6	200	<LoQ (1.75×10^{-3})	99.78	2.35
	V 292.2	100	<LoD (2.53×10^{-3})	96.93	3.14

Products	Elements	ICH Q3D oral PDEs (µg/day)	Concentration (µg/day)	Spiked Recovery	RSD
Superdrug bronchial Balsam	As 189.0	15	<LoD (1.85X10 ⁻³)	95.73	2.98
	Cd 214.4	5	9.21± 0.043	100.33	2.77
	Hg 184.9	30	<LoD (7.00X10 ⁻⁴)	96.26	3.07
	Pb 220.3	5	41.95± 0.26	104.67	2.96
	Co 228.6	50	42.10± 0.059	95.67	1.78
	Ni 231.6	200	<LoQ (1.75X10 ⁻³)	103.33	2.37
	V 292.2	100	<LoD (2.53X10 ⁻³)	99.61	3.86

From the results, it is noted that four products exceed the regulations' PDE for Cd and six products exceed the PDE for Pb.

Hg, Co and Ni were also quantified in some products, but the concentrations present are within the PDEs stated in ICH Q3D guidelines

The daily dosage of medications has an effect on the elemental impurity limits that can be tolerated. For example, Tixylix can be taken in three different daily dosages according to the patient's age. As a result, three different EI concentrations of Cd and Pb will be introduced to the patients based on their age as illustrated in Table 2.19.

Table 2.19 Daily exposure (µg/day) for Tixylix when given in different dosages based on patient's age

Medication maximum daily dosage	Daily Exposure (µg/day)	
	Cd 214.4 nm	Pb 220.3 nm
1-5 years: 12.05 g/day	1.54	5.67
5-12 years: 24.1 g/day	3.09	11.34
>12 years: 48.20 g/day	6.19	22.68

From Table 2.19 , it is clear that the medication dosage plays a role in whether the pharmaceutical product exceeds the permitted limits or not. Taking Cd as an example, if the product is to be given for children under twelve years old, the Cd concentration is less than 5 µg/day; it exceeds the limits once the product is given for children twelve years and older.

2.4 Conclusion

The developed ICP-OES method and microwave assisted acid digestion for pharmaceutical products was successfully validated using *NIST 3280* as well as from supporting results obtained using ICP-MS/KED. The method showed excellent recoveries between 95-105% with good repeatability expressed as RSD of less than 5% for all elements. Those limits met the regulations requirements. The method is also specific as any spectra with major interferences were excluded and only those with minimal interferences were chosen for analysis. LODs and LoQs were below the target limits, which supports the suitability of the ICP-OES for EI determination.

The obtained results for commercial pharmaceutical products that were analysed emphasise the need for a validated method for elemental impurities analysis as many of them exceed the PDEs for both Cd and Pb. This needs high attention as the new regulation was applied to all pharmaceutical products in January 2018 and any products that fail the new requirement will be withdrawn from the market.

This work also highlights the fact that even products with no API may also contain significant amount of trace elements, which emphasises the fact that one of the major sources for elemental impurities is the excipients used for the formulation of pharmaceutical products.

From the previous results, ICP-OES can be successfully used for the determination of EI in pharmaceuticals. However, ICP-OES lacks the sensitivity required to analyse products with high daily intake, that is more than 1 L/day like in the case of large volume parenteral, because the limits will drop below the method's LoQs.

An example is Pb (LoQ= 0.00473 µg/mL) that has a PDE of 5 µg/day, which means it will have a limit of 0.00455 µg/mL for a product with daily dosage of 1,100 mL.

Due to that, a method using ICP-MS that offers higher sensitivity than ICP-OES will be discussed in the next chapter as an alternative for EI determination in pharmaceuticals.

Chapter 3

**The Optimisation, Validation and
Analysis of Commercial
Pharmaceutical Products by ICP-
MS in Compliance with ICH-Q3D
Guidelines**

3. The Optimisation, Validation and Analysis of analgesics, cough remedies, cold and flu products and antacids by ICP-MS in Compliance ICH-Q3D Guidelines

3.1 Introduction

ICP-MS was successfully used by Kauffman et al(262) to measure the concentration of Pb in forty-five pharmaceutical products including some analgesics and nonsteroidal anti-inflammatory drugs (NSAIDs). The highest Pb concentration among ten ibuprofen samples manufactured in India and England was 12 ng/g. It is important to control the concentration of Pb and keep it as low as possible due to its known toxicity that affects various physiological systems including the CNS which could have severe health effects especially on children(6, 7).

In addition, a calcium-based product that is used as antacid was estimated to deliver a maximum daily mass of 2.7µg of Pb per day to consumers(262). However, this study focuses on Pb only and the rest of Class 1 and Class 2A elements were not included.

In another study conducted using microwave induced combustion (MIC)-ICP-MS to assay over the counter enteric coated aspirins of different brands, traces of Class 1 and Class 2 elements were found in different concentrations ranging from 0.002-0.88 µg/g(46). For example, one aspirin brand was found to contain 0.71 µg/g of As, 0.014 µg/g of Pb, 0.57 µg/g of Ni and 0.88 µg/g of V(46). However, the method was validated using spike addition technique only, which is as discussed in Chapter 2 may give false indication of the method's accuracy especially when microwave-assisted techniques are used for sample preparation as in this case where MIC was used. In addition, Co from Class 2A was not included in the analysis.

As mentioned in Section 1.1.1, the instrument was also used to analyse active pharmaceutical ingredients including furazolidone, ethambutol, pyrazinamide and dicyclomine-HCl were traces of Ti, Cr, Mn, Cu, Cd and Pb were found in concentrations ranging from 0.1 to 38.2 ng/g(17). In this study, As and Hg form Class 1 as well as Ni and V from Class 2A were not included in the analysis. Additionally, the samples were digested prior to analysis however; the method was validated using NIST 1643b, which is a water reference sample and the maximum temperature reached was 60-80°C, which was found to be inefficient as discussed in Section 2.3.1.1.

In addition, tablets containing captopril showed As contents of 0.1 µg/g. Another captopril API sample contained 0.3 µg/g of As. The method was validated using spiked addition technique(265).

All the previously mentioned studies emphasise the need for a reliable validated method to analyse elemental impurities in pharmaceuticals and thus control their levels to be within the allowed PDEs, because it is clear that some API(18, 97, 265) and/or excipients(31) used in the production of pharmaceutical products may contain high levels of EI.

However, just like with ICP-OES methods, most of the developed ICP-MS techniques for the analysis of pharmaceutical impurities were validated using spiked recoveries as suggested in USP<233> chapter(1, 18, 265, 292, 293).

This chapter focuses on the development of an ICP-MS method to analyse the Class 1 elements As, Cd, Hg and Pb and Class 2A Co, Ni and V and then applying it to commercial analgesic tablets, cold and cough syrups, cold and flu powders and

antacids. The optimised ICP-MS method was validated using *NIST 3280 Multivitamin/Multielement tablets*.

3.2 Experimental

3.2.1 Reagents and Materials

For the reagents, materials and standard references - see Section 2.2.1.

Eight standard solutions were prepared by dilution with 2% reverse aqua regia (3 HNO₃ : 1 HCl v/v) to get concentrations ranging from 5 to 200 ng/mL as well as a blank. 10 ng/mL of ⁴⁵Sc, ⁹⁸Y, ¹⁰³Rh and ¹⁵⁹Tb were added as internal standards to the calibration and samples in addition to 1 µg/mL of Au.

Argon gas (purity > 99.995%) was supplied by AirProducts, UK and He gas (purity 99.995%) was supplied by BOC, UK.

3.2.2 Samples

The twelve samples analysed using the validated ICP-OES method were reanalysed. In addition, six cold and flu powders provided in sachets and six antacid products were acquired from local retailers in the Liverpool area (Table 3.1).

All products were processed and analysed within ten days of their purchase, before the expiry date.

Table 3.1 Cold and flu powders and antacids product information

Product	Ingredients	Maximum daily dose for patients 12 years old and over (g/day)
Cold and flu powders		
Value Health-with vitamin C	API: paracetamol Excipients: sucrose, sodium citrate, citric acid, tartaric acid, sodium cyclamate, ascorbic acid, starch, natural colour (E 100), spray dried lemon juice and lemon aroma	19.68
Boots-with vitamin C	API: paracetamol Excipients: sucrose, sodium citrate, citric acid, tartaric acid, sodium cyclamate, ascorbic acid, starch, natural colour (E 100), spray dried lemon juice and lemon aroma	19.98
Beechams Honey and Lemon	API: paracetamol and phenylephrine hydrochloride Excipients: ascorbic acid, sucrose, sodium citrate, citric acid, maize starch, sodium cyclamate, saccharin sodium, lemon, lemon, flavour, honey flav-o-lok, honey flavour and caramel (E1 50)	20.58
Beechams Blackcurrant	API: paracetamol and phenylephrine hydrochloride Excipients: Ascorbic acid, sucrose, sodium citrate, citric acid, sodium cyclamate, saccharin sodium, blackcurrant juice, blackcurrant polvaromas, blackcurrant flavour, natural grapeskin (E 163) (contains sulphur dioxide).	20.58
Lemsip-Breath Easy	API: paracetamol and phenylephrine hydrochloride Excipients: ascorbic acid, citric acid, sucrose, aspartame, sodium citrate, saccharin sodium, curcumin WD, lemon and menthol flavours	18.10
Lemsip Max-Lemon	API: paracetamol and phenylephrine hydrochloride Excipients: ascorbic acid, citric acid, sucrose, aspartame, sodium citrate, saccharin sodium, curcumin WD, lemon flavour	19.05

Table 3.1, continued

Product	Ingredients	Maximum daily dose for patients 12 years old and over (g/day)
Antacids		
Gaviscon suspension	API: sodium alginate, sodium bicarbonate and calcium carbonate Excipients: carbomer, methyl (E 218) and propyl (E 216) parahydroxybenzoate, sachharin sodium, fennel flavour, erythrosine, sodium hydroxide and water	84.73
Gaviscon chewable tablets	API: sodium alginate, sodium bicarbonate and calcium carbonate Excipients: xylitol, carmellose sodium, magnesium stearate, macrogol 20000, mannitol (E 421), copovidone, acesulfame-K, aspartame (E 951), mint flavour and carmoisine lake (E 122)	21.42
Rennie Extra	API: calcium bicarbonate, magnesium carbonate and alginic acid Excipients: sodium hydrogen carbonate, sucrose, glucose monohydrate, povidone, talc, magnesium stearate, dextrates, saccharin sodium, lemon cream flavour (contains lemon oil, lime oil, orange oil, l-menthol, vanillin, maltodextrin, gum Arabic, ascorbic acid, butylhydroxyanisol) and peppermint flavour (contains peppermint oil, maltodextrin, gum Arabic, silicon dioxide)	28.10
Superdrug	API: calcium bicarbonate and light magnesium carbonate and sodium bicarbonate Excipients: saccharine sodium maize starch, sucrose, calcium stearate and peppermint oil flavour	18.86
Rennie	API: calcium bicarbonate and heavy magnesium carbonate Excipients: sucrose, glucose, spearmint flavour, talc, povidone, saccharine sodium and magnesium stearate	13.00
Bisodol	API: calcium bicarbonate Excipients: sucrose, maize starch, calcium stearate, spearmint favour and sodium saccharin	7.26

3.2.3 Instrumentation

For sample preparation instrumentation - see Section 2.2.3.

A Thermo XSeries quadrupole-based ICP-MS instrument (Thermo, UK), equipped with a collision reaction cell (CCT) incorporating kinetic energy discrimination was used for the analysis of Class 1 and Class 2A elements. The ICP-MS instrument is equipped with a CETAC ASX 520 series (Thermo, UK) autosampler and data was collected using Thermo Scientific PlasmaLab Software.

Solutions were pumped to the nebuliser using a multi-channel peristaltic pump. The sample introduction unit consisted of a Meinhard concentric nebulizer and conical, impact bead spray chamber cooled to 1 °C in a Peltier cooling mould.

The instrument was optimised based on signal and signal to blank ratios. The ICP-MS optimum conditions used throughout this experiment are listed in Table 3.2.

Table 3.2 Overview of ICP-MS Thermo XSeries optimised parameters in CCT operation mode

Minor	
Lens 2	-36.9
Lens 3	-136.5
Forward power (W)	1400
Horizontal	90
Vertical	370
D2 (V)	-100
DA (V)	-37.6
Coolant gas flow (L/min)	14
Auxiliary gas flow (L/min)	0.9
Major	
Extraction (V)	-130
Lens 1 (V)	-1.5
Focus (V)	0
D1 (V)	-34.5
Pole bias (V)	-7
Hexapole bias (V)	-10

Table 3.2 continued

Nebuliser gas flow (L/min)	0.98
Sampling Depth (mm)	140
Global	
Standard resolution	125
High resolution	125
Analogue detector	1900
PC detector	3850
Add. Gases	
He gas flow rate (mL/min)	3.5
Others	
Pump speed (rpm)	30
Sampling cone and type	Nickel
Skimmer cone and type	Nickel, Xt

3.2.4 ICP-MS Optimisation

Five key parameters were selected for optimisation using signal and signal/blank ratio for both standard and CCT mode. The rest of the parameters were adjusted to pass the tune test were a solution containing 10 ng/mL of a mixture of elements (^7Li , ^9Be , ^{48}Ti , ^{59}Co , ^{115}In , ^{137}Ba , ^{140}Ce , ^{207}Pb , ^{209}Bi , ^{238}U) covering a wide range of atomic masses is used to provide information about peak widths, sensitivity and oxide species. The tune test was performed each time the instrument is to be used on both standard and CCT modes and only after passing the test the analyses were completed. The test is considered successful if the conditions represented in Table 3.3 were met.

Table 3.3 Passed tune test conditions, ICP-MS Thermo XSeries

	Acquisition Parameters	Ratio Results
Standard Mode	$^7\text{Li}>1000$	$^{156}\text{Ce O}/^{140}\text{Ce}<0.03$
	$^{115}\text{In}>250000$	$^{115}\text{In}/^{101}\text{Bkg}>100000$
	$^{238}\text{U}>500000$	$^{238}\text{U}/^{220}\text{Bkg}>100000$
CCT Mode	$^{59}\text{Co}>10000$	$^{156}\text{Ce O}/^{140}\text{Ce}<0.02$
	$^{78}\text{Ar}_2<20$	
	$^{115}\text{In}>50000$	
	$^{238}\text{U}>10000$	

Nebuliser gas flow, pump rate, auxiliary gas flow, coolant gas flow, and radio frequency (RF) power were optimised starting from the lowest practically possible value to the highest possible one, using both standard and CCT mode. That was performed by measuring a stock solution containing a known concentration (30 ng/mL) of the seven elements at different settings for each parameter within the mentioned range, followed by comparing the obtained signals and signal to blank ratios to get a setting with the best sensitivity for the elements.

The signal to blank ratio was calculated by dividing the average signal obtained using a multielement standard with a concentration of 30 ng/mL by the average signal obtained using a blank (2% reverse aqua regia).

3.2.4.1 Optimisation of nebuliser gas flow rate

The procedure described in Section 3.2.4 was followed using a nebuliser gas flow rate range of 0.5-1.3 L/min.

3.2.4.2 Optimisation of pump rate

The procedure described in Section 3.2.4 was followed using a pump rate range of 10-60 rpm.

3.2.4.3 Optimisation of auxiliary gas rate

The procedure described in Section 3.2.4 was followed using an auxiliary gas rate range of 0.5-1.5 L/min.

3.2.4.4 Optimisation of coolant gas rate

The procedure described in Section 3.2.4 was followed using a coolant gas rate range of 10-20 L/min.

3.2.4.5 Optimisation of RF power

The procedure described in Section 3.2.4 was followed using RF power range of 800-1500W.

3.2.4.6 Optimisation of helium gas flow rate for operating CCT

For CCT mode, the helium gas flow rate was also optimised (2.5-4.5 L/min) by analysing *NIST 3280* samples and the best flow rate was decided based on the obtained elements recoveries with minimal interferences and good reproducibility.

3.2.4.7 Selection of suitable internal standards and analytical atomic mass units

Scandium (^{45}Sc), yttrium (^{89}Y), rhodium (^{103}Rh), indium (^{115}In) and terbium (^{159}Tb) (10 ng/ml), were added to both samples and standards prior to analysis. The corrected results for the internal standard was obtained using PlasmaLab software (Thermo UK).

Eighteen different atomic masses for the seven elements in total were tested to determine the optimal analytical atomic mass unit (amu) for each element that gave the lowest LoD and LoQ with minimum interferences. The tested m/z are listed in Table 3.4.

Table 3.4 Class 1 and Class 2A elements atomic masses optimised for elemental analysis using ICP-MS and their relative abundance

Element	% Abundance(294)
^{75}As	100.0000
^{111}Cd	12.8000
^{112}Cd	24.1300
^{113}Cd	12.2200
^{206}Pb	24.1000
^{207}Pb	22.1000
^{208}Pb	52.4000
^{198}Hg	9.9700

Table 3.4, continued

Element	% Abundance(294)
²⁰¹ Hg	13.1800
²⁰² Hg	29.8600
²⁰⁴ Hg	6.8700
⁵⁹ Co	100.0000
⁵⁸ Ni	68.0769
⁶⁰ Ni	26.2231
⁶¹ Ni	1.1399
⁶² Ni	3.6345
⁵⁰ V	0.2500
⁵¹ V	99.7500

4.2.5 Analytical figures of merit and method validation

3.2.5.1 Limits of detection and limits of quantification

LoD and LoQ were calculated as described in Section 2.2.5.1, using 10 blanks and a series of standards ranging from 1 to 30 ng/ml according to the method of Miller and Miller(268)

3.2.5.2 Linearity and range

Linearity was obtained as described in Section 2.2.5.2 and studied in the range of 5-1000 ng/mL ng/ml were eight concentration points were assayed in triplicate.

3.2.5.3 Accuracy and Precision

The accuracy and precision were evaluated using *NIST 3280*. The samples were also spiked with 10 ng/mL with respect to As, Cd, Hg, Pb, Co, V and Ni. The experiment was performed in triplicate.

3.2.6 Sample preparation and revalidation of the microwave assisted acid digestion procedure

The procedure used was identical to that used in Section 2.2.6. However, for microwave assisted acid digestion, SP-D Microwave (CEM) with 80 mL quartz vessels were used instead of the 35 mL vessels and the program used is illustrated in Table 3.5.

Table 3.5 CEM-SPD microwave programme used to digest the samples

Stage 1: Ramp Time= 5 min, Temperature= 120°C, Hold time= 5 min
Stage 2: Ramp Time= 5 min, Temperature= 180°C, Hold time= 5 min
Stage 3: Ramp Time= 5 min, Temperature= 210°C, Hold time= 5 min

3.2.7 Analysis of pharmaceutical samples

Pharmaceutical samples were prepared as described in Section 2.2.7. Following preparation, the samples were analysed using the optimised and validated ICP-MS-CCT method.

3.3 Results and discussion

3.3.1 ICP-MS Optimisation

A comparison of signals and signal to blank ratios was performed as described in Section 2.3.1

3.3.1.1 Optimisation of nebuliser gas flow rate

The standard signal increased with increasing the nebuliser gas flow rate until reaching the optimum value as more droplets with suitable size were produced. However, after the optimum setting big droplets with shorter plasma residence time started from leading to a decrease in sensitivity.

As illustrated in Figure 3.1, the optimum nebuliser gas flow rate for As using ICP-MS standard mode is 0.98 L/min. At this setting, the signal/blank ratio is the highest, which means that at a nebuliser gas flow rate of 0.98 L/min the standard signal is the highest, which is also consistent with the signal graph and the blank signal is the lowest. Using CCT gave the same optimum setting of 0.98 L/min. The signal/blank ratio increased significantly from approximately 7 to 700 when CCT mode was activated due to its capability of reducing polyatomic interference such as $^{40}\text{Ar}^{35}\text{Cl}^+$, $^{59}\text{Co}^{16}\text{O}^+$, and $^{38}\text{Ar}^{37}\text{Cl}^+(183)$.

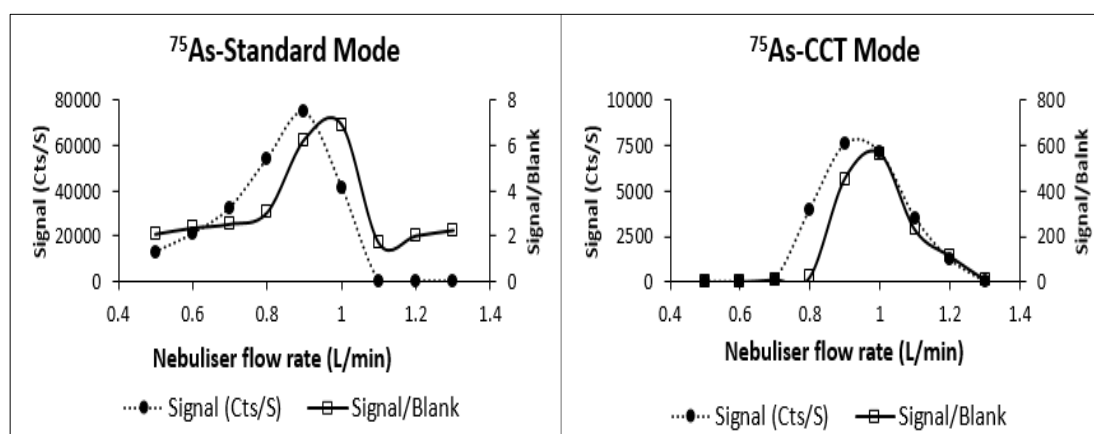


Figure 3.1 The signal and signal/blank ratios for arsenic (30 ng/mL) using ICP-MS standard and CCT modes at different nebuliser gas flow rates (L/min)

For Cd (Figure 3.2), the optimum nebuliser gas flow rate using ICP-MS standard mode is also 0.98 L/min at both standard and CCT modes. However, the highest standard signal was obtained at a flow rate of 1 L/min. This can be explained as a higher drop in the blank signal occurred at a 0.98 L/min nebuliser gas flow rate giving a higher ratio and thus better sensitivity. This emphasises the need to optimise the instrument based on signal/blank ratio to obtain the highest sensitivity, not the standard signal alone.

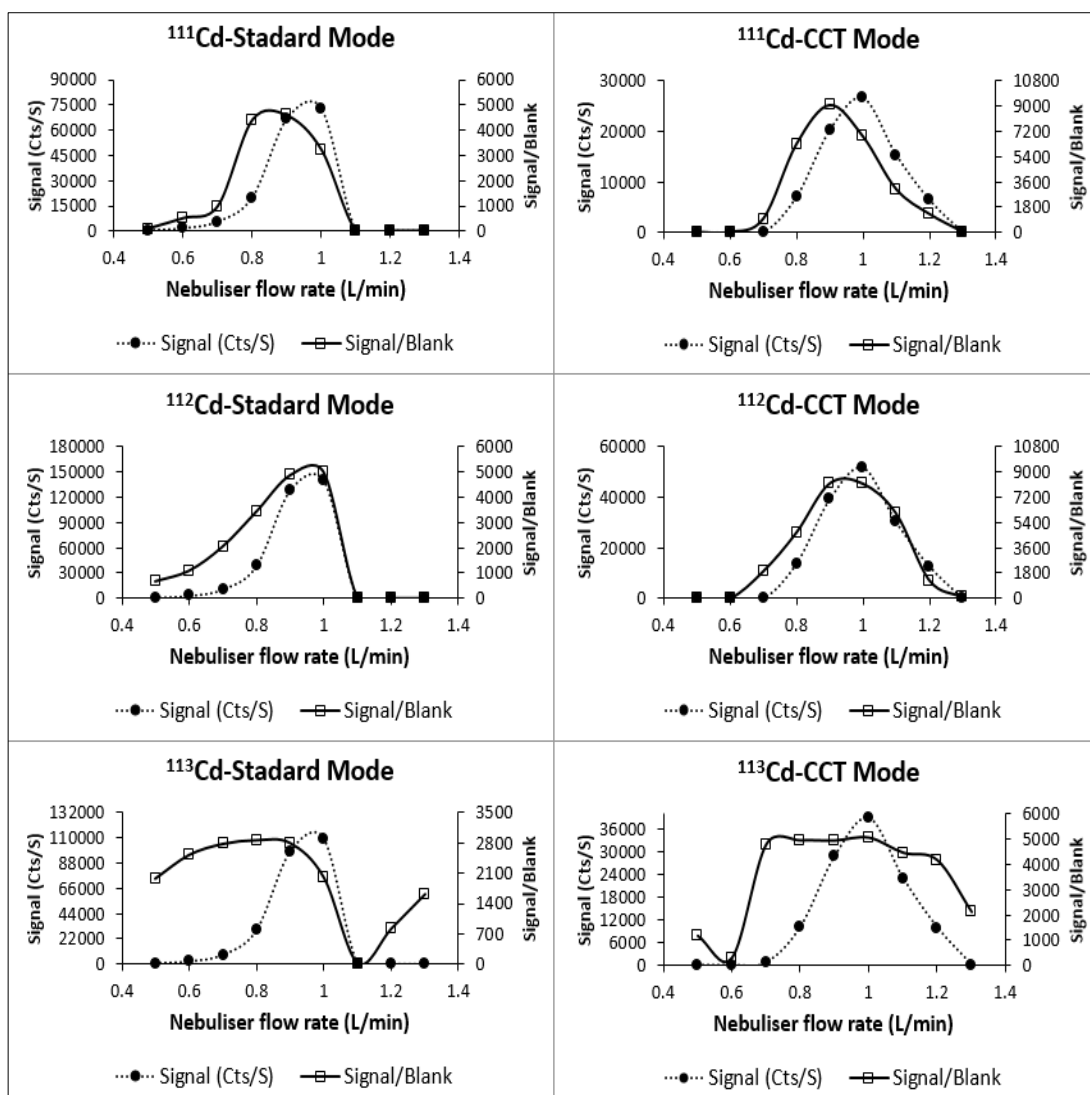


Figure 3.2 The signal and signal/blank ratios for cadmium (30 ng/mL) using ICP-MS standard and CCT modes at different nebuliser gas flow rates (L/min)

On the other hand, Hg showed the highest sensitivity (signal/blank) at a nebuliser gas flow rate of 0.4 L/min on standard mode, and 0.7 L/min on CCT mode. The standard signal was the highest on both cases at a nebuliser gas flow rate of 1-1.1 L/min. Figure 3.3.

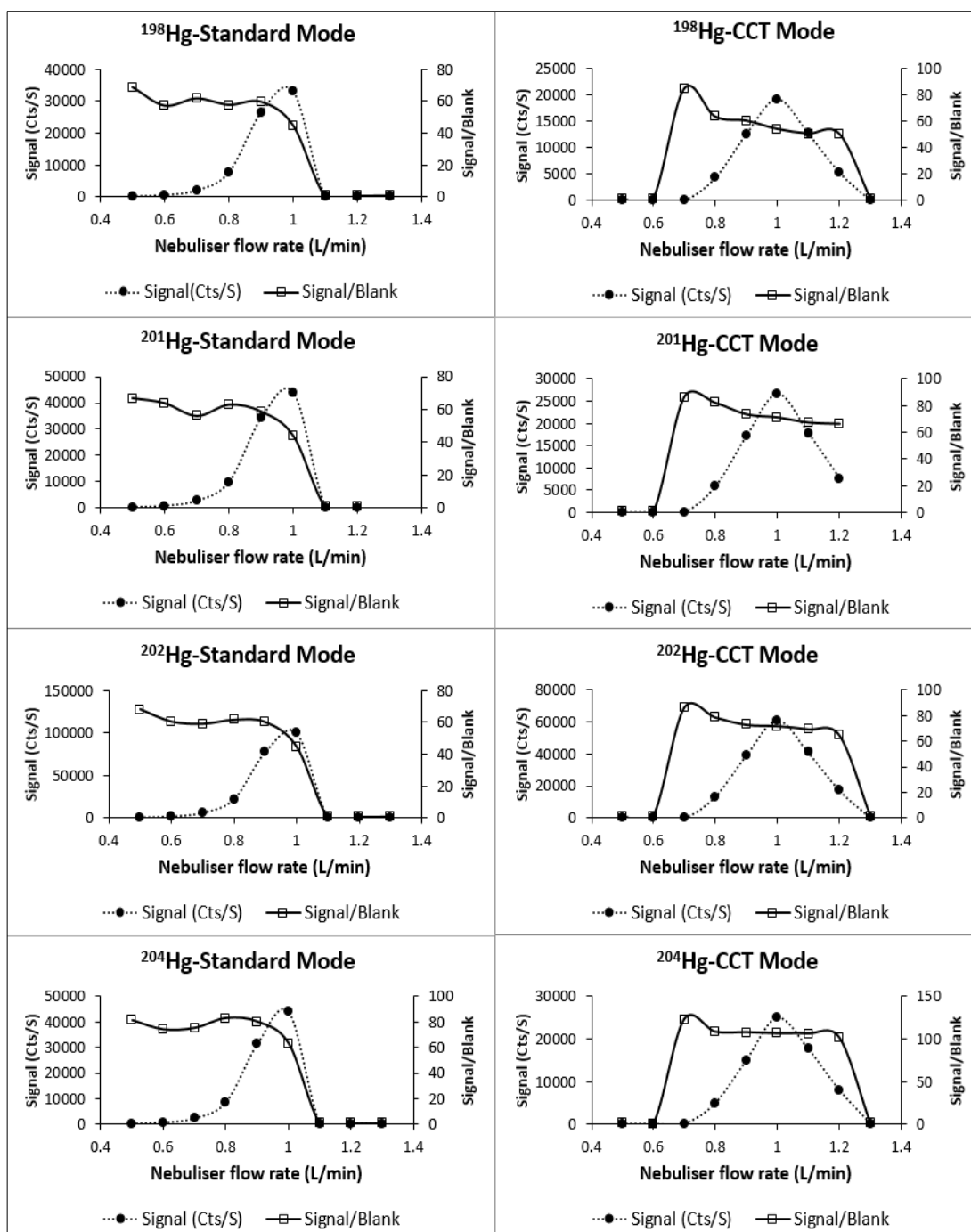


Figure 3.3 The signal and signal/blank ratios for mercury (30 ng/mL) using ICP-MS standard and CCT modes at different nebuliser gas flow rates (L/min)

In the case of Pb (Figure 3.4), the highest signal/blank ratio and best sensitivity was obtained at a nebuliser gas flow rate of 0.98 L/min using both standard and CCT modes. The standard signal was the highest at a nebuliser gas flow rate between 0.9

and 1 L/min on both modes. The high standard signal and the low blank signal at the same settings made signal/blank ratio to be the highest at 0.98 L/min.

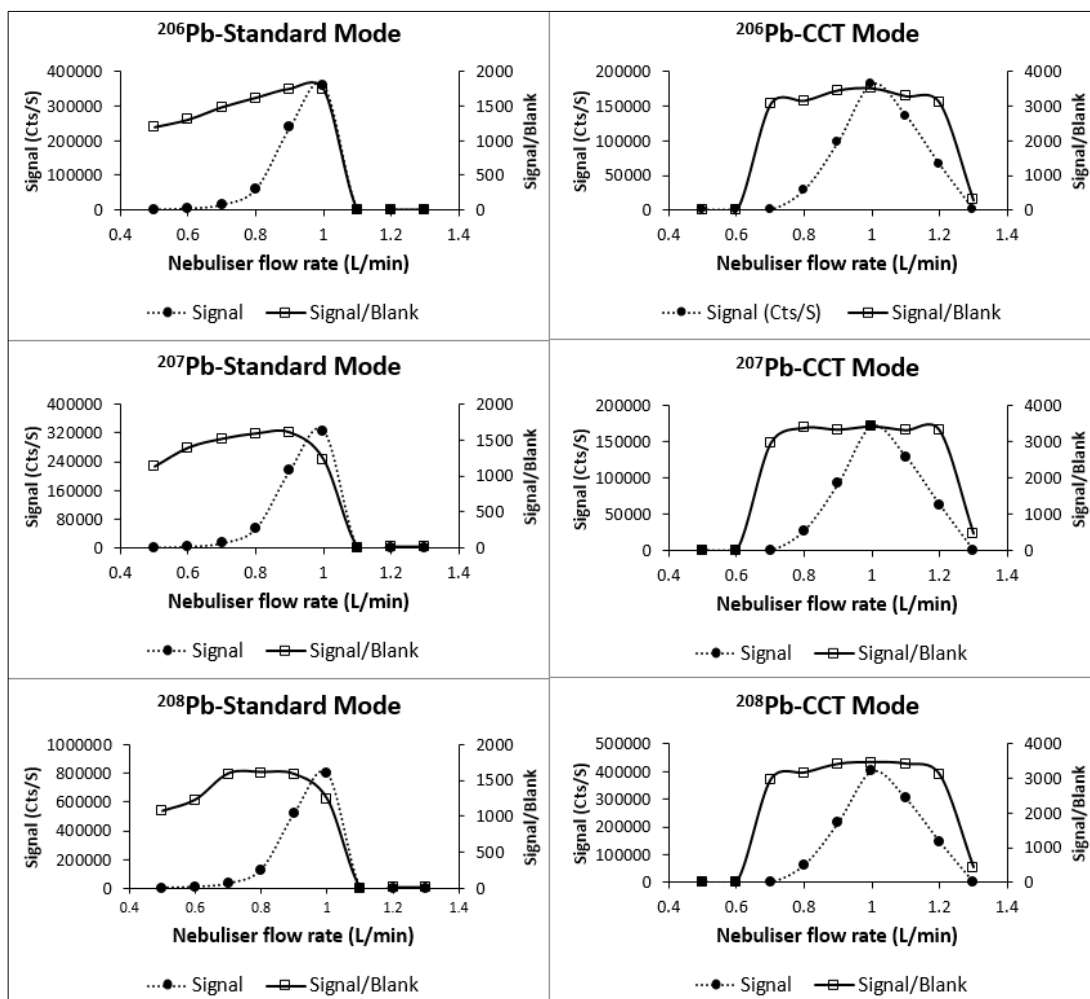


Figure 3.4 The signal and signal/blank ratios for lead (30 ng/mL) using ICP-MS standard and CCT modes at different nebuliser gas flow rates (L/min)

A behaviour similar to Pb was also observed for Co (Figure 3.5)

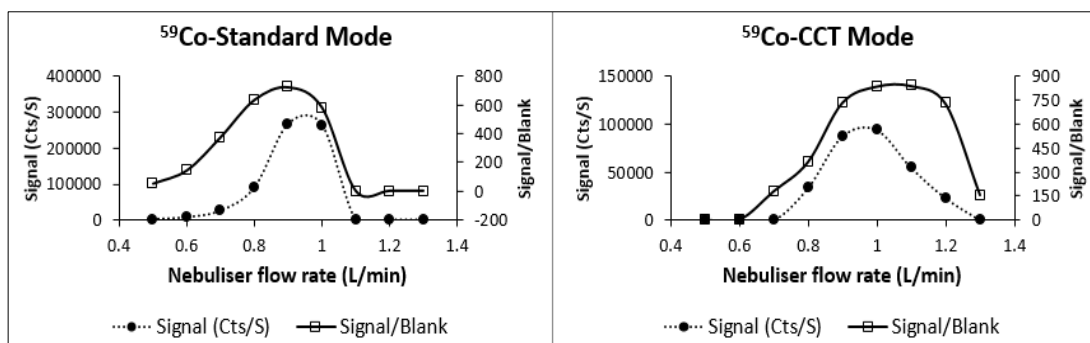


Figure 3.5 The signal and signal/blank ratios for cobalt (30 ng/mL) using ICP-MS standard and CCT modes at different nebuliser gas flow rates (L/min)

Ni and V show similarity in having the highest standard signal accompanied with the highest signal/blank ratio at a nebuliser gas flow rate of 0.98 L/min at standard mode. For CCT mode, the highest signal for both elements was obtained at 0.98L /min, but the highest signal/blank ratio was at 1.1 L/min (Figures 3.6 and 3.7).

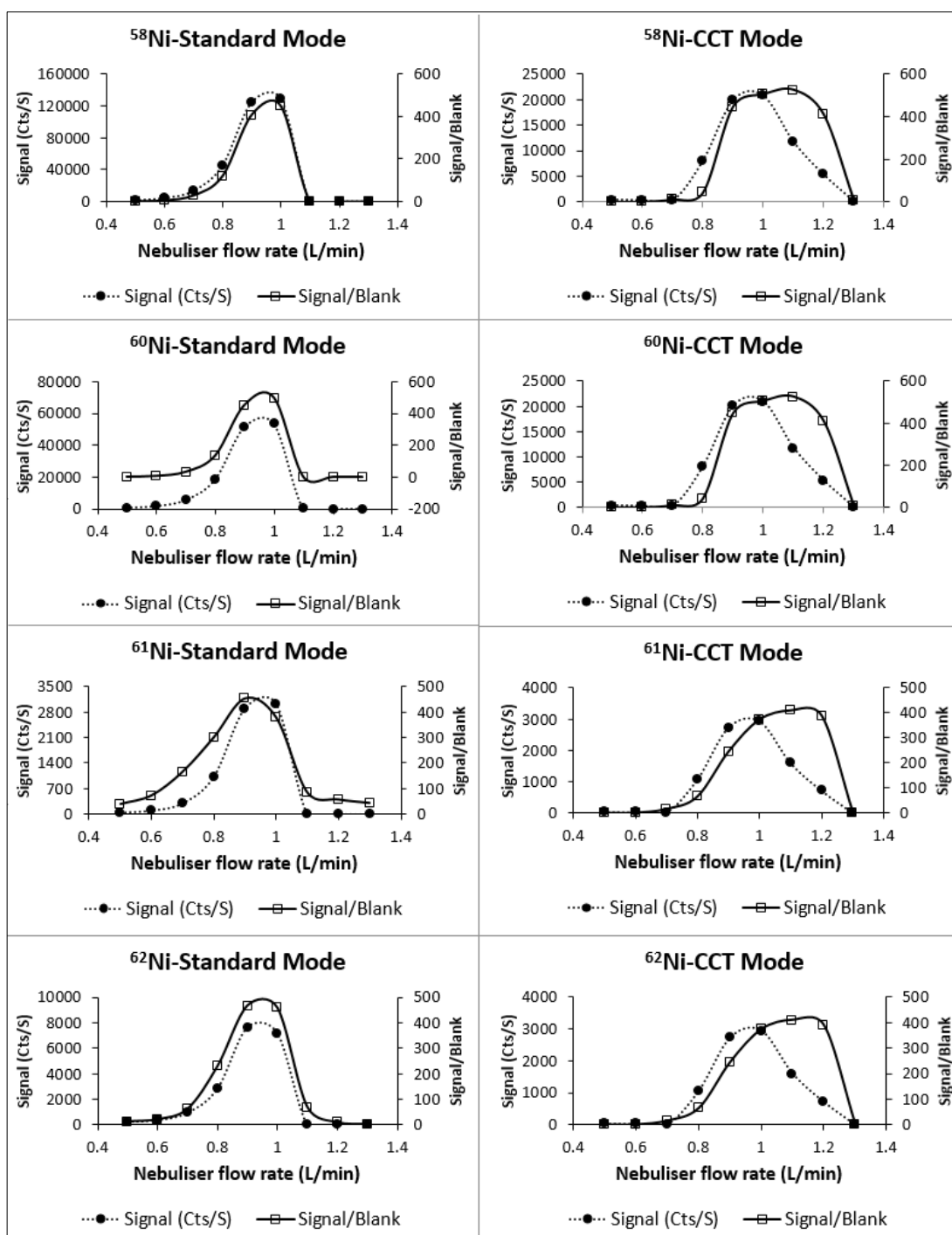


Figure 3.6 The signal and signal/blank ratios for nickel (30 ng/mL) using ICP-MS standard and CCT modes at different nebuliser gas flow rates (L/min)

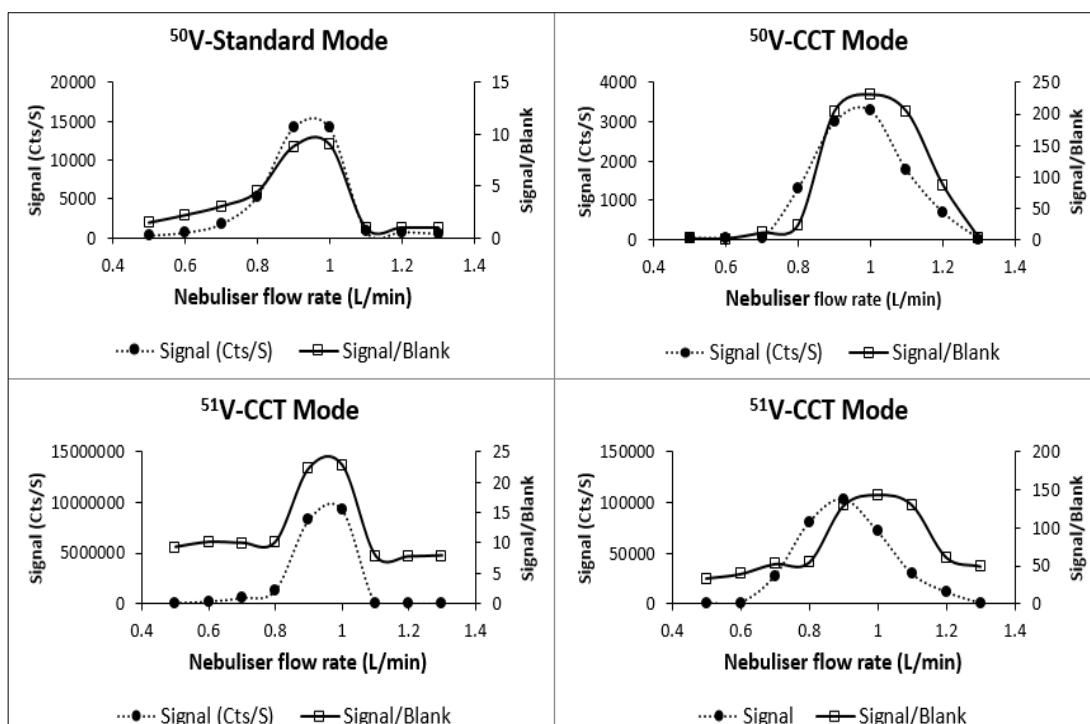


Figure 3.7 The signal and signal/blank ratios for vanadium (30 ng/mL) using ICP-MS standard and CCT modes at different nebuliser gas flow rates (L/min)

The nebuliser gas flow rate was adjusted to 0.98 L/min for both standard and CCT modes, because this rate gave the best sensitivity for most elements. The reduction in Ni and V sensitivity was approximately 5% in comparison with what was obtained at a flow rate of 1.1 L/min. However for Hg, the reduction in sensitivity is more significant (approximately 10%), but for the time efficiency and multi-element analysis this drop in sensitivity can be tolerated, because its PDE (30 µg/day) is much higher than the allowed 5 µg/day for Cd and Pb.

3.3.1.2 Optimisation of pump rate

As mentioned in Section 2.3.1.2, high pump speed leads to the formation of large droplets in the spray chamber which reduces the analytical sensitivity. This was also observed with ICP-MS-CCT as the standard signal for all elements dropped significantly at a pump rate of 50 rpm and more.

For As and Cd, the highest signal/blank ratio at standard mode was the highest at a pump speed of 40 rpm. However, using CCT mode, the highest signal/blank ratio was obtained at pump speed of 30 rpm, because at this speed the standard signal also improved significantly leading to an increase in the signal/blank ratio and thus higher sensitivity. See Figures 3.8 and 3.9.

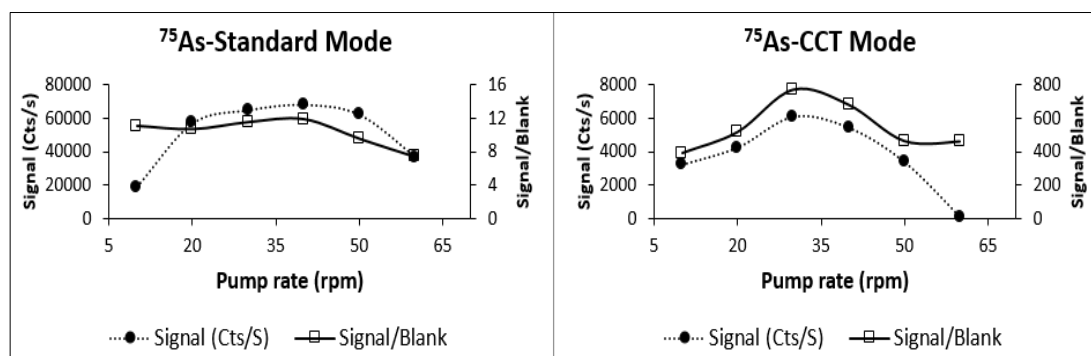


Figure 3.8 The signal and signal/blank ratios for arsenic (30 ng/mL) using ICP-MS standard and CCT modes at different pump rates (rpm)

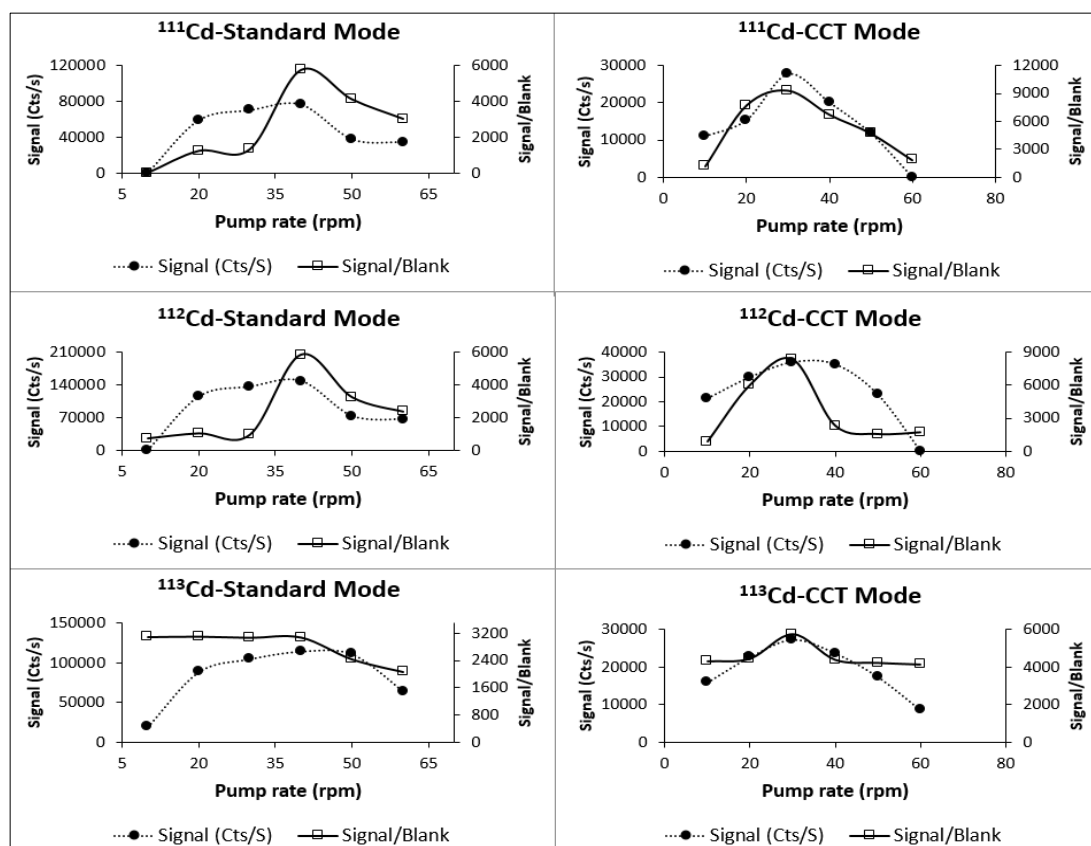


Figure 3.9 The signal and signal/blank ratios for cadmium (30 ng/mL) using ICP-MS standard and CCT modes at different pump rates (rpm)

Hg on the other hand showed a different behaviour towards changing the pump speed. Using ICP-MS-standard mode the highest standard signal and highest signal/blank ratio was obtained at a pump speed of 50 rpm (Figure 3.10). Using CCT, the standard signal increased gradually with increasing the pump rate until a speed of 50 rpm was reached. After that, the signal dropped significantly due to the formation of larger droplets. The signal/blank ratio was the highest using CCT at a pump rate of 20 rpm, which suggests that at this speed, the blank signal was the lowest and thus the best sensitivity for Hg was at a pump rate of 20 rpm.

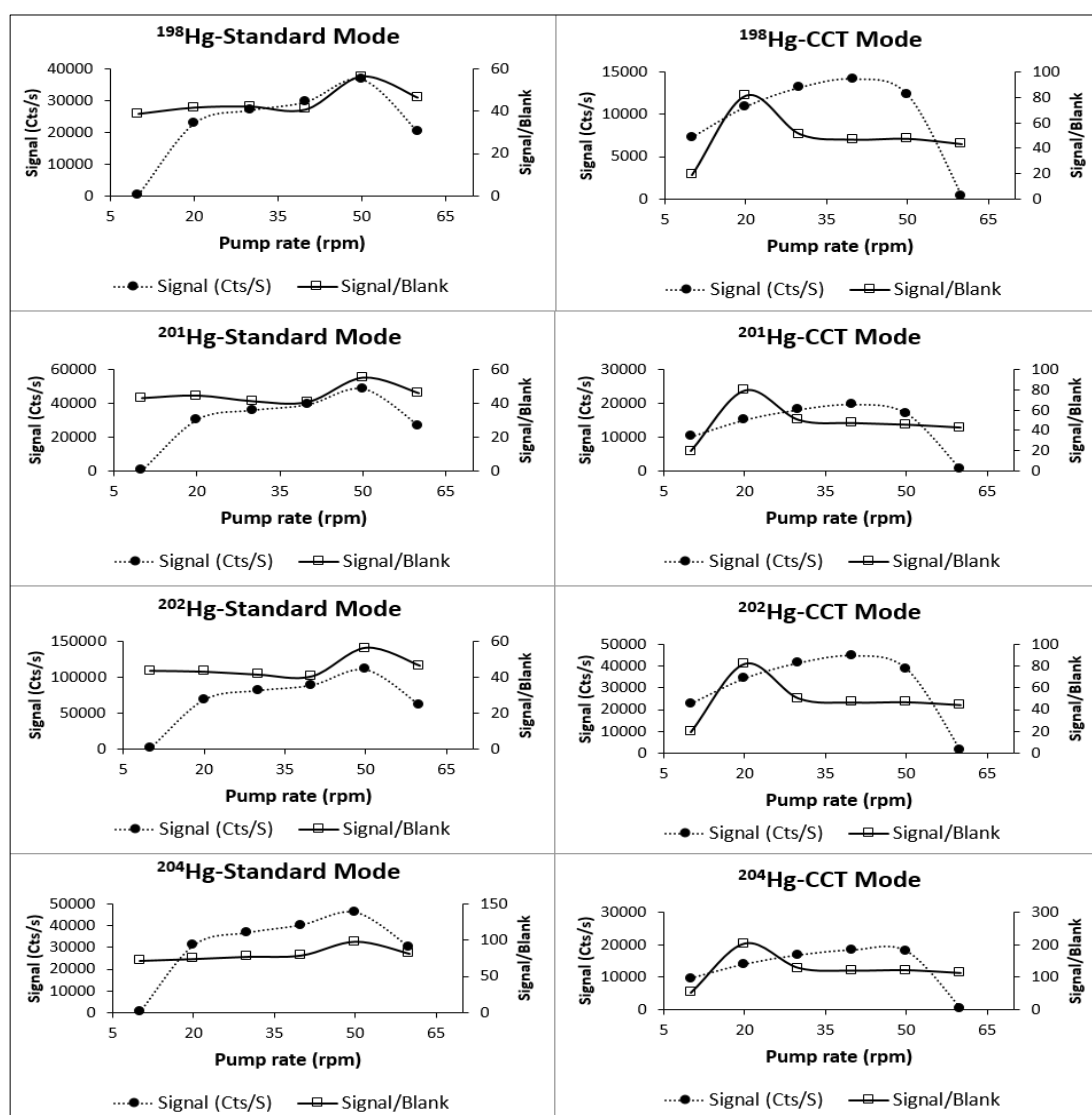


Figure 3.10 The signal and signal/blank ratios for mercury (30 ng/mL) using ICP-MS standard and CCT modes at different pump rates (rpm)

In the case of Pb (Figure 3.11), again, the standard signal using both modes increased with increasing the pump rate up to 50 rpm and then it dropped. However, the signal/blank ratio reached a maximum at a pump rate of 40 rpm on standard mode and 30 rpm on CCT mode then minimal changed occurred at higher rates. This can be explained as similar changes occurred to the blank causing the ratio to remain unchanged.

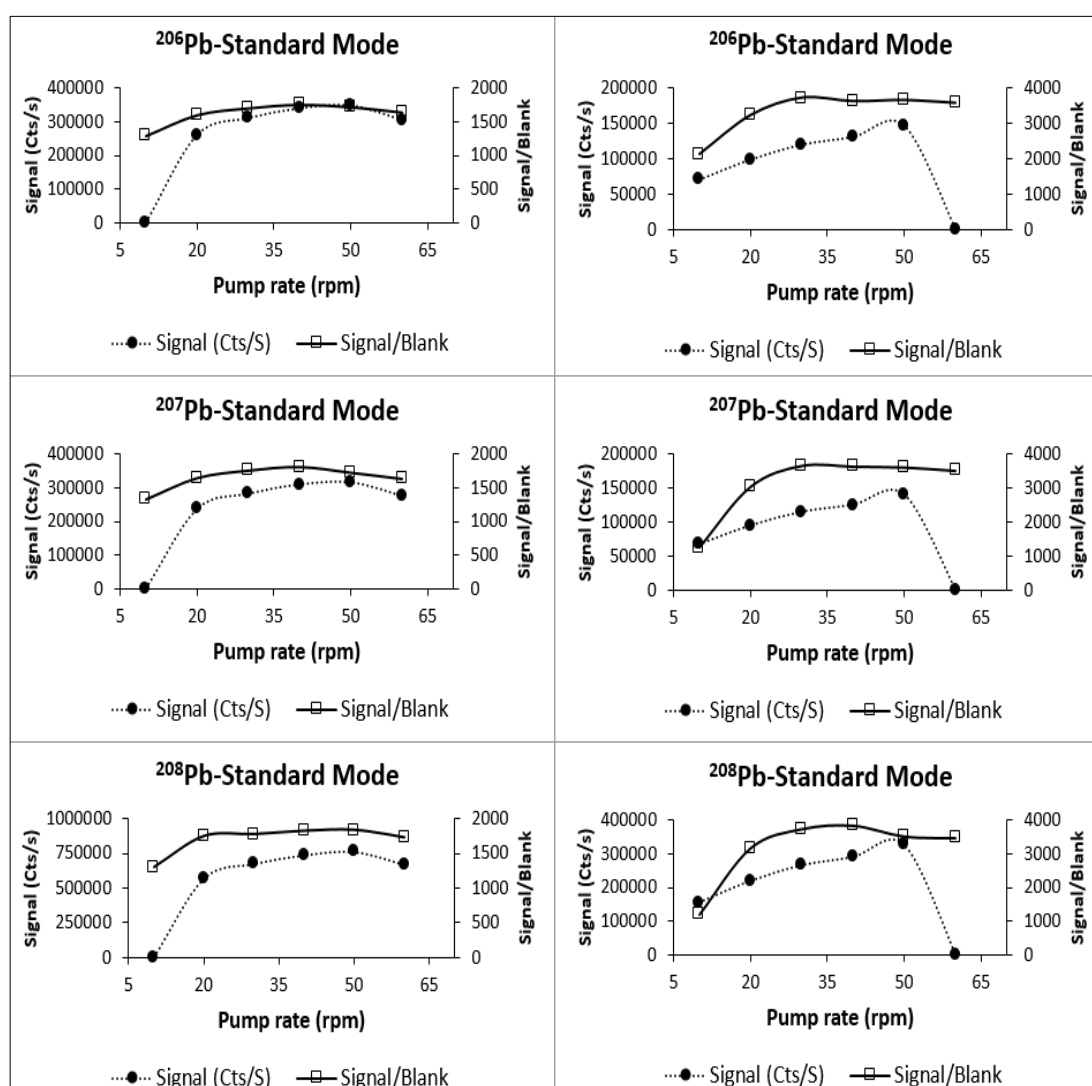


Figure 3.11 The signal and signal/blank ratios for lead (30 ng/mL) using ICP-MS standard and CCT modes at different pump rates (rpm)

The standard signal for Co and Ni showed a behaviour similar to Pb on both modes. In case the of the signal/blank ratio, using standard mode, the highest ratio was obtained on a pump rate of 40 rpm and then with increasing the pump rate to 60 rpm, both the signal and the signal/blank ratio dropped. Using CCT mode, the highest signal/blank ratio was obtained at a pump rate of 30 rpm. At higher pump rates, the signal/blank ratio decreased slightly for both elements (Figures 3.12 and 3.13).

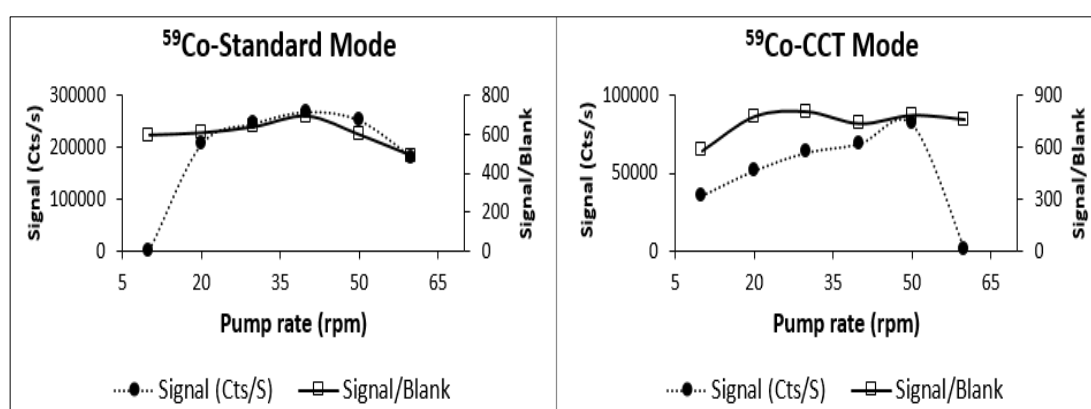


Figure 3.12 The signal and signal/blank ratios for cobalt (30 ng/mL) using ICP-MS standard and CCT modes at different pump rates (rpm)

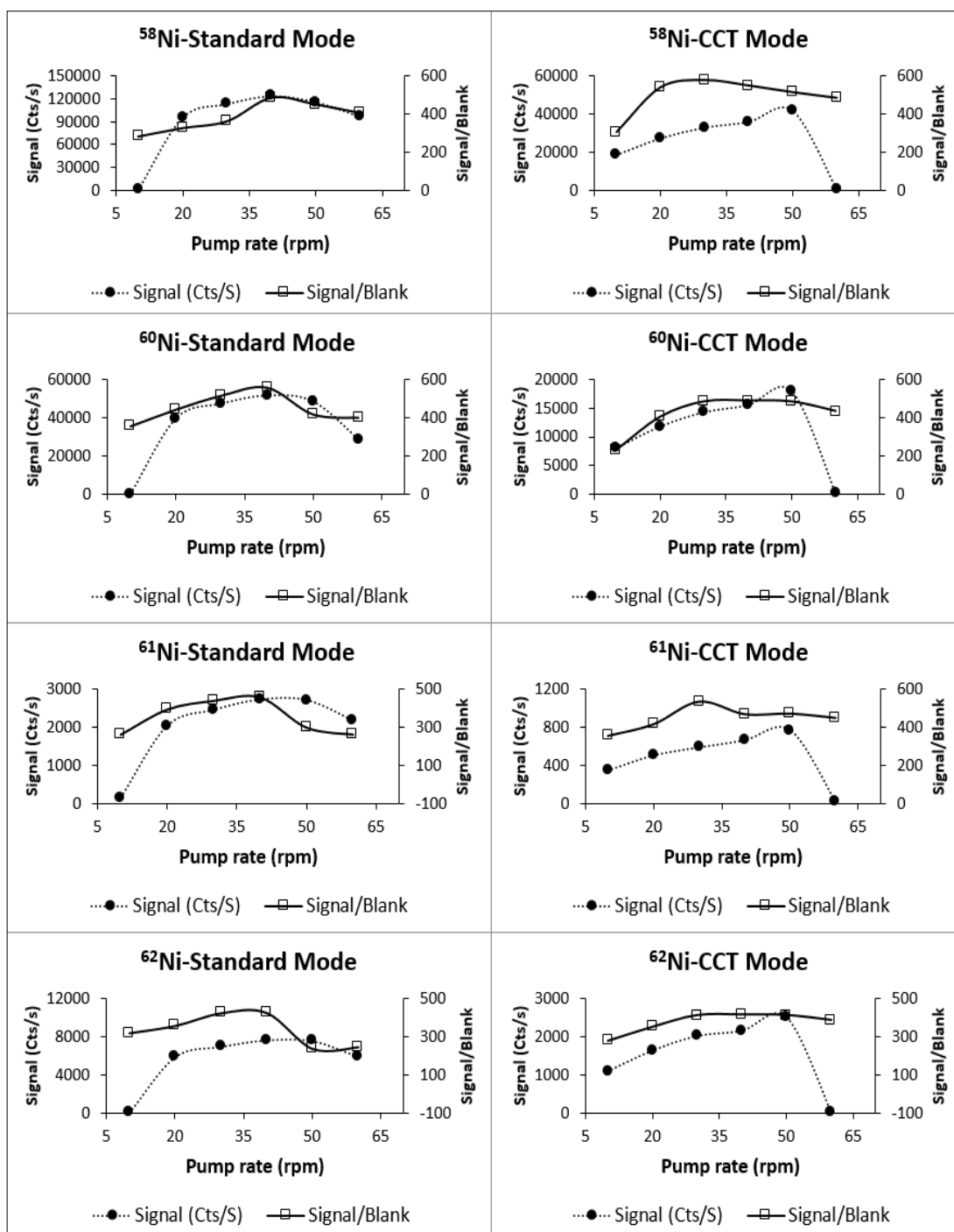


Figure 3.13 The signal and signal/blank ratios for nickel (30 ng/mL) using ICP-MS standard and CCT modes at different pump rates (rpm)

Finally, both the standard signal for V and the signal/blank using ICP-MS-standard mode increased with increasing the pump rate up to 40 rpm and then reached a plateau. Using CCT mode a behaviour similar to Ni was observed giving the highest signal/blank ratio at 40 rpm (Figure 3.14).

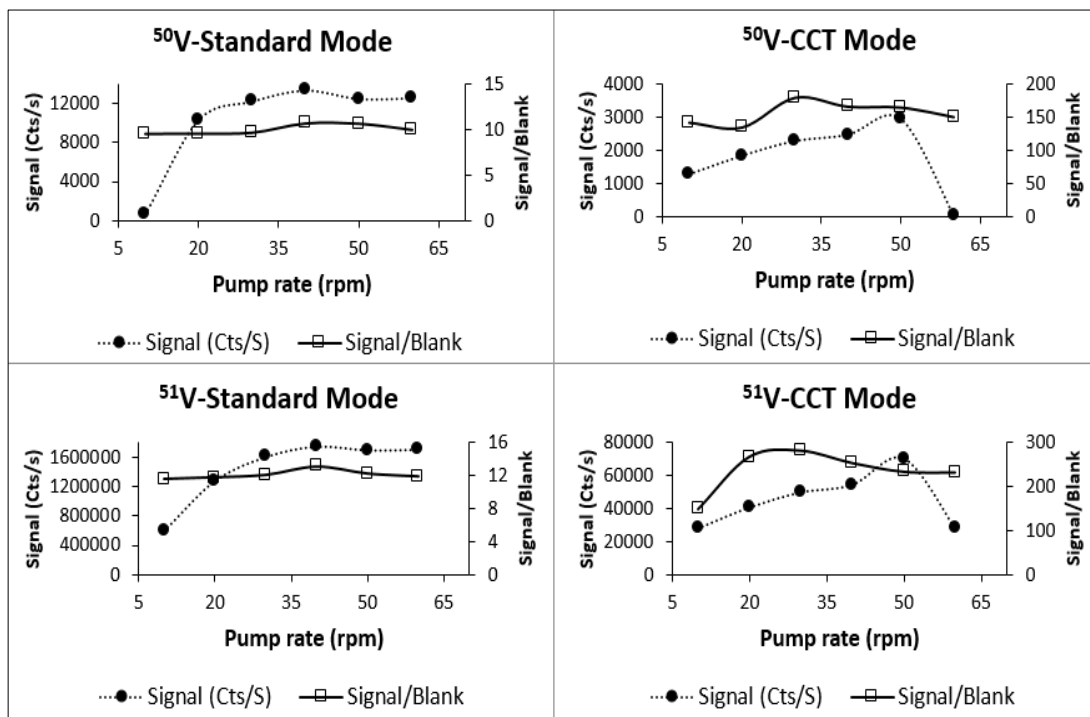


Figure 3.14 The signal and signal/blank ratios for vanadium (30 ng/mL) using ICP-MS standard and CCT modes at different pump rates (rpm)

The pump rate was adjusted to 40 rpm using standard mode and 30 rpm using CCT mode. These pump speeds gave the best sensitivity for all element except for Hg. The loss in Hg sensitivity is accepted (approximately 20%) for the sake of faster multi-element analysis and its relatively higher PDE (30 µg/day).

3.3.1.3 Optimisation of auxiliary gas flow rate

The auxiliary gas flow rate is used to change the position of the base of the plasma relative to the tube and the injector. Using ICP-MS-standard mode, the standard signal for all elements except As increased gradually with increasing the auxiliary gas flow rate. The signal/blank ratio reached a maximum at a flow rate of 0.9 L/min for ^{111}Cd , ^{112}Cd , ^{207}Pb and ^{208}Pb , while the remaining elements at their tested m/z ratio showed little or no change when the auxiliary gas flow rate was changed (Figures 3.15-3.21).

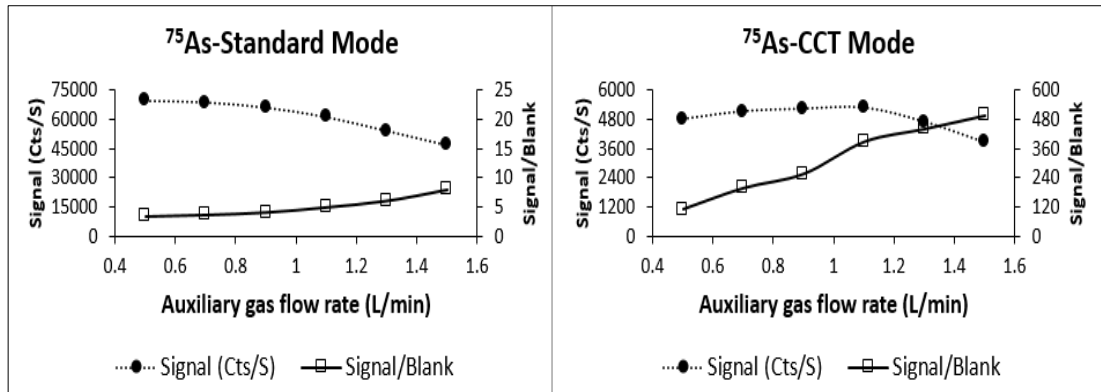


Figure 3.15 The signal and signal/blank ratios for arsenic (30 ng/mL) using ICP-MS standard and CCT modes at different auxiliary gas flow rates (L/min)

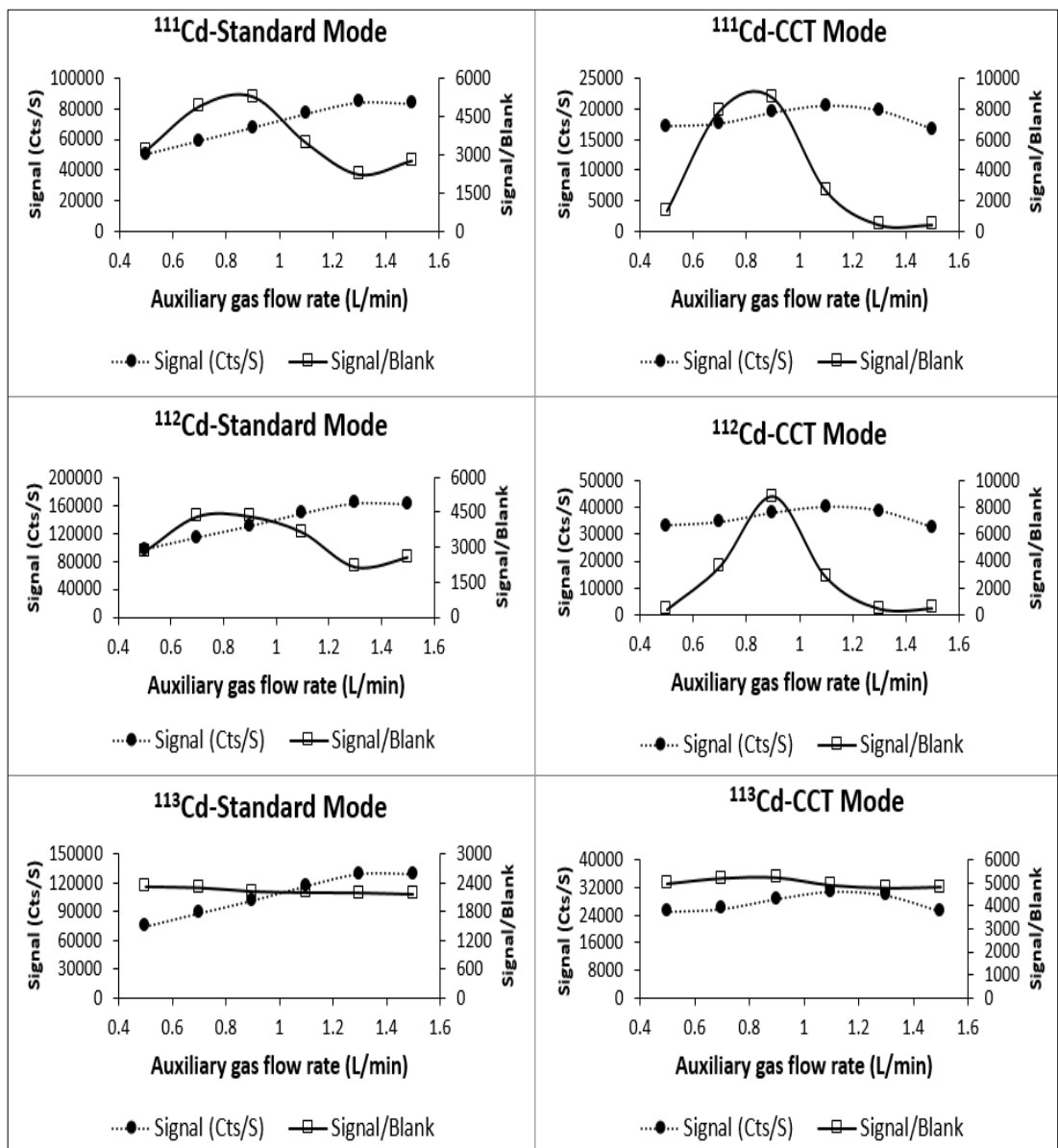


Figure 3.16 The signal and signal/blank ratios for cadmium (30 ng/mL) using ICP-MS standard and CCT modes at different auxiliary gas flow rates (L/min)

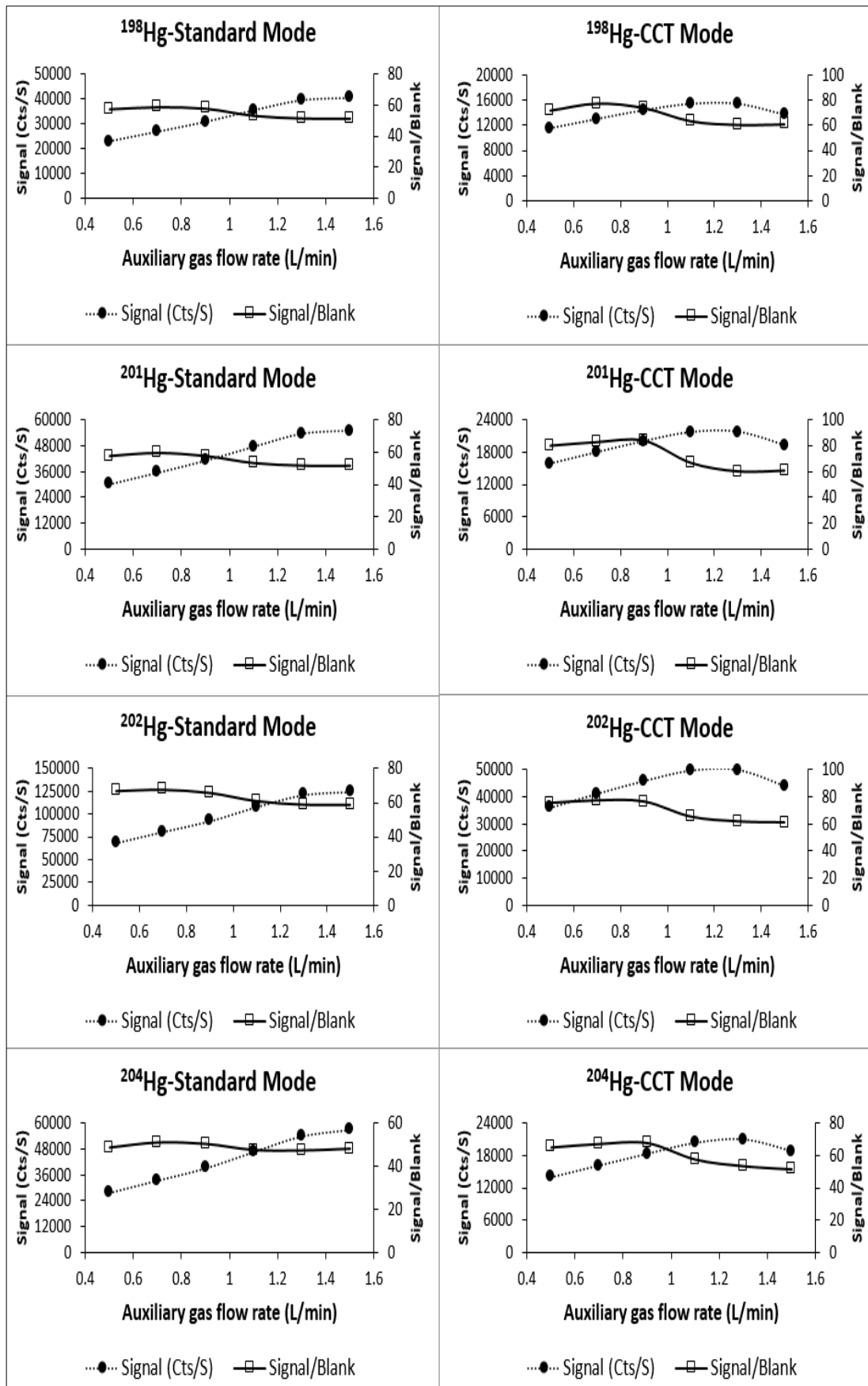


Figure 3.17 The signal and signal/blank ratios for cadmium (30 ng/mL) using ICP-MS standard and CCT modes at different auxiliary gas flow rates (L/min)

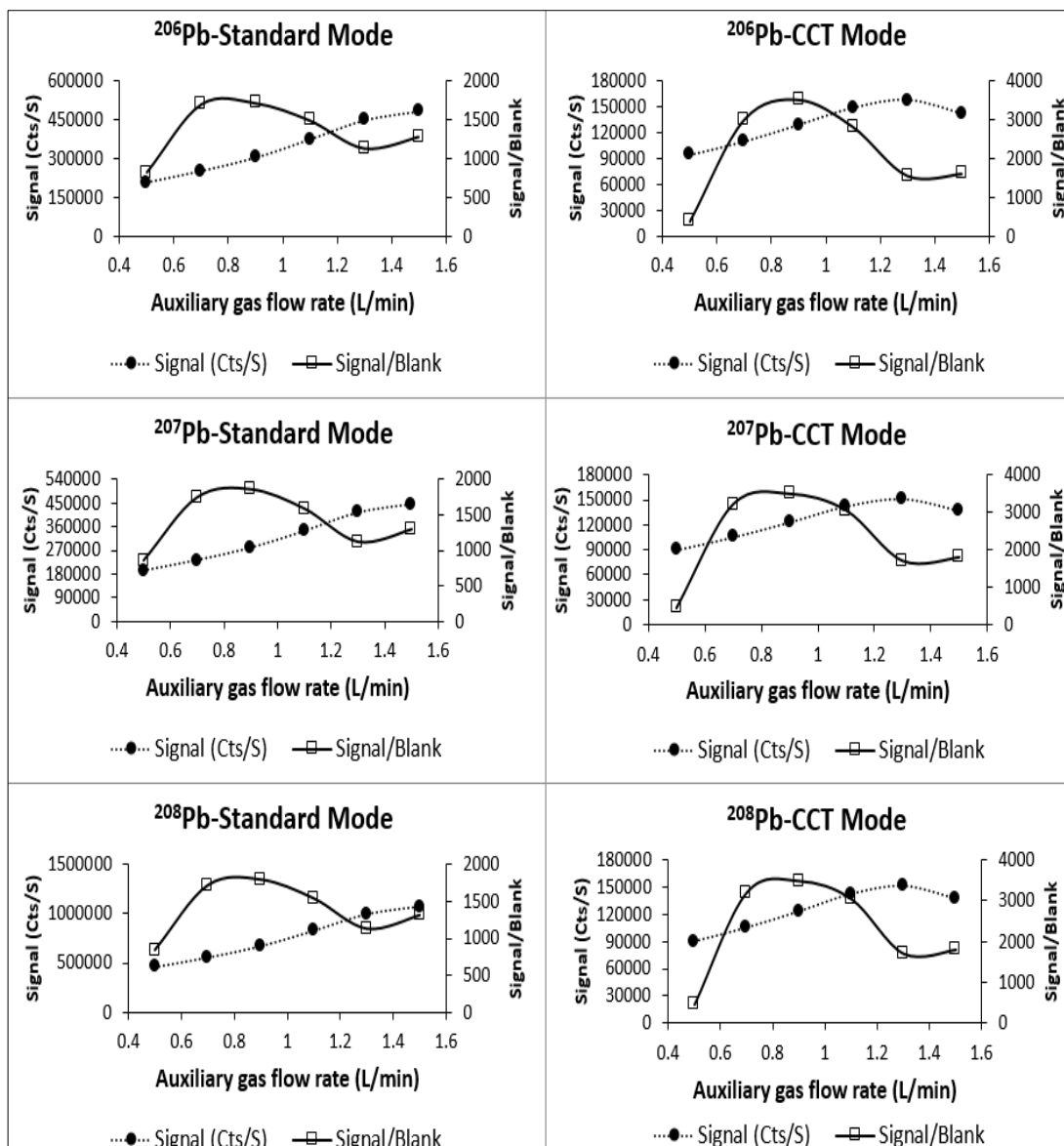


Figure 3.18 The signal and signal/blank ratios for lead (30 ng/mL) using ICP-MS standard and CCT modes at different auxiliary gas flow rates (L/min)

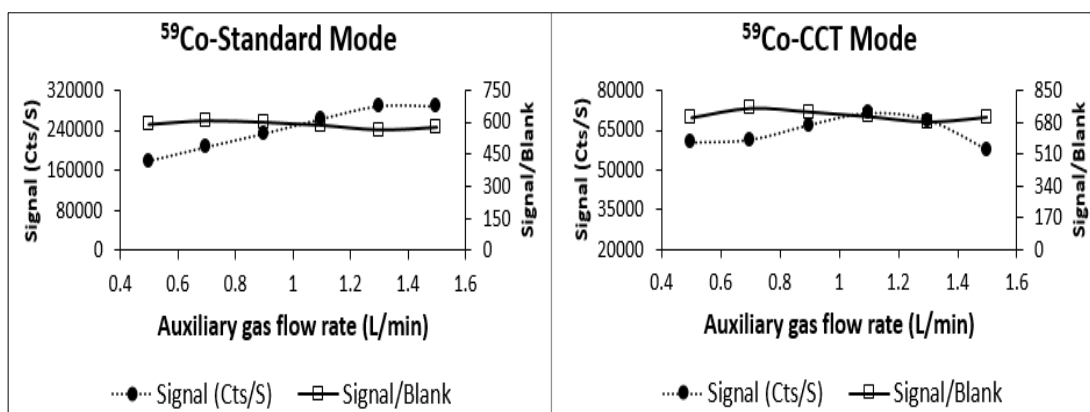


Figure 3.19 The signal and signal/blank ratios for cobalt (30 ng/mL) using ICP-MS standard and CCT modes at different auxiliary gas flow rates (L/min)

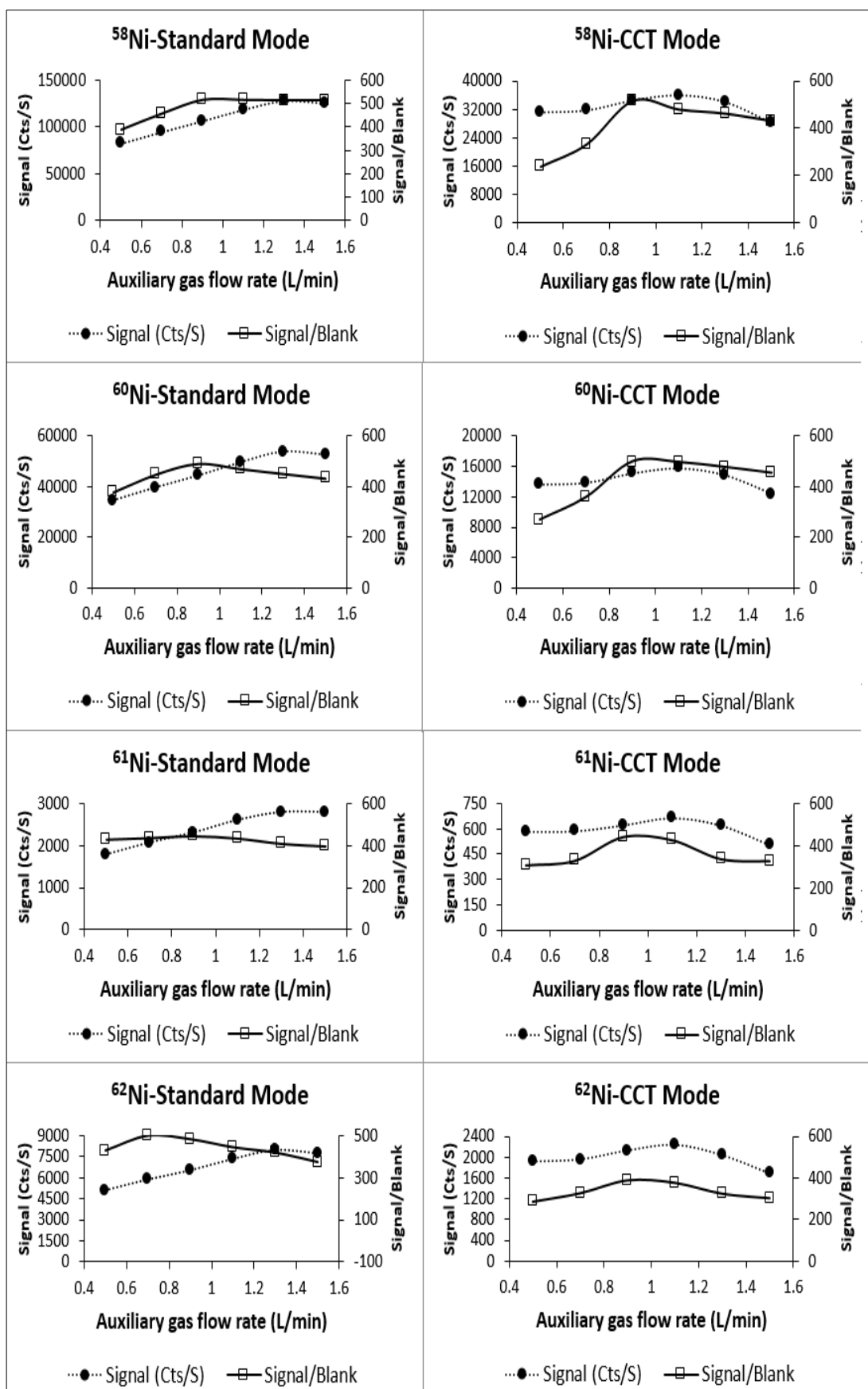


Figure 3.20 The signal and signal/blank ratios for nickel (30 ng/mL) using ICP-MS standard and CCT modes at different auxiliary gas flow rates (L/min)

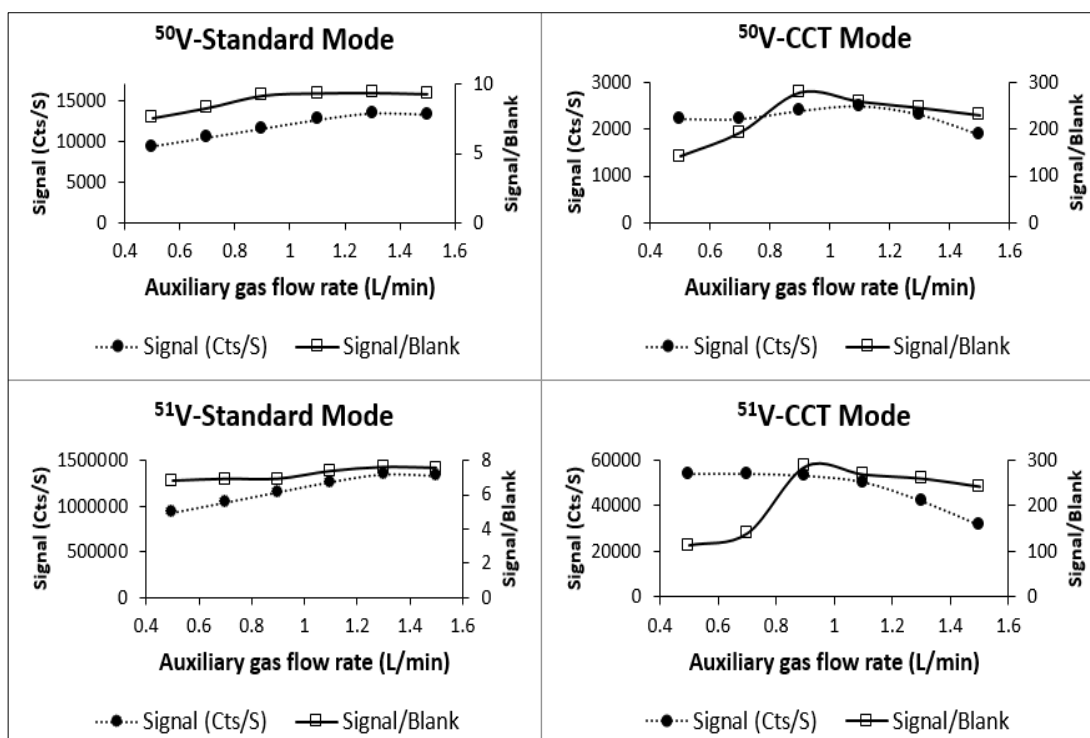


Figure 3.21 The signal and signal/blank ratios for vanadium (30 ng/mL) using ICP-MS standard and CCT modes at different auxiliary gas flow rates (L/min)

When using ICP-MS-CCT the standard signal for all elements, with exception of As, dropped when increasing the rate for more than 1.2-1.3 L/min, while the signal/blank ratio was improved at an auxiliary gas flow rate of 0.9 L/min. The sensitivity towards ^{113}Cd and ^{59}Co was not significantly changed with changing the auxiliary gas flow rates (Figures 3.15-3.21).

On the other hand, As sensitivity was improved with increasing the auxiliary gas flow rate using both standard and CCT modes (Figure 3.15).

The auxiliary gas flow rate was adjusted to 0.9 L/min for both standard and CCT modes.

3.3.1.4 Optimisation of coolant gas flow rate

The coolant gas flow is one of the conditions that has minimum effect on the analytical sensitivity. The standard signal for As improved slightly with increasing the

coolant gas flow rate from 10 to 12 L/min and then reached a plateau, when operating the ICP-MS using standard mode. Using CCT mode, the standard signal started to drop gradually when the coolant gas flow rate was increased to 16 L/min and more. The signal/blank ratio remained almost constant over the tested range using standard mode, but dropped slightly when the rate was increased to 16 L/min using CCT mode due to the drop in the standard signal (Figure 3.22).

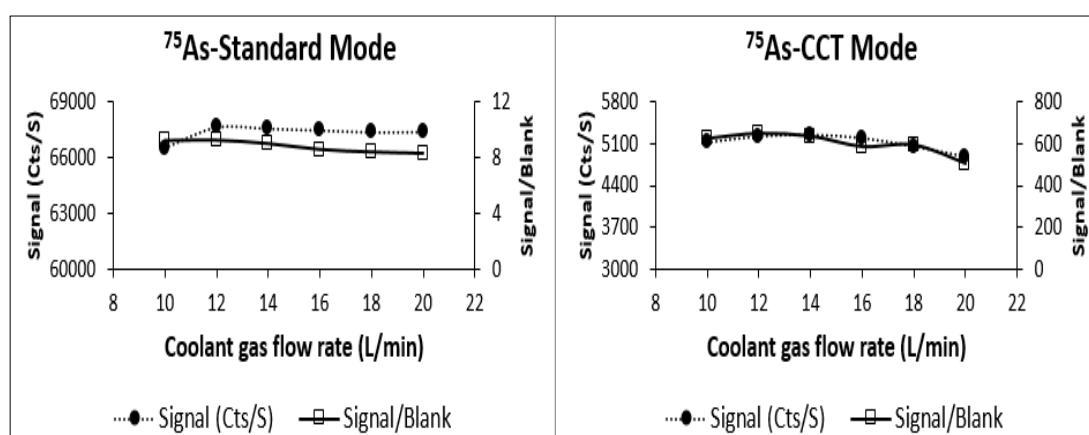


Figure 3.22 The signal and signal/blank ratios for arsenic (30 ng/mL) using ICP-MS standard and CCT modes at different coolant gas flow rates (L/min)

The standard signal for Cd dropped slightly with increasing the coolant gas flow rate using both modes, and the signal/blank ratio dropped severely at a coolant gas flow rate of 20 L/min when the instrument was operated on standard mode. Although the signal dropped at the same rate, this sharp decrease in the signal/blank ratio is due to the significant increase in the blank signal. The signal/blank ratio using CCT mode increased slightly when the coolant gas flow rate was increased up to 14 L/min, then it decreased. ¹¹³Cd is an exception as the signal/blank ratio remained almost constant and was not affected with changing the coolant gas flow rate (Figure 3.23).

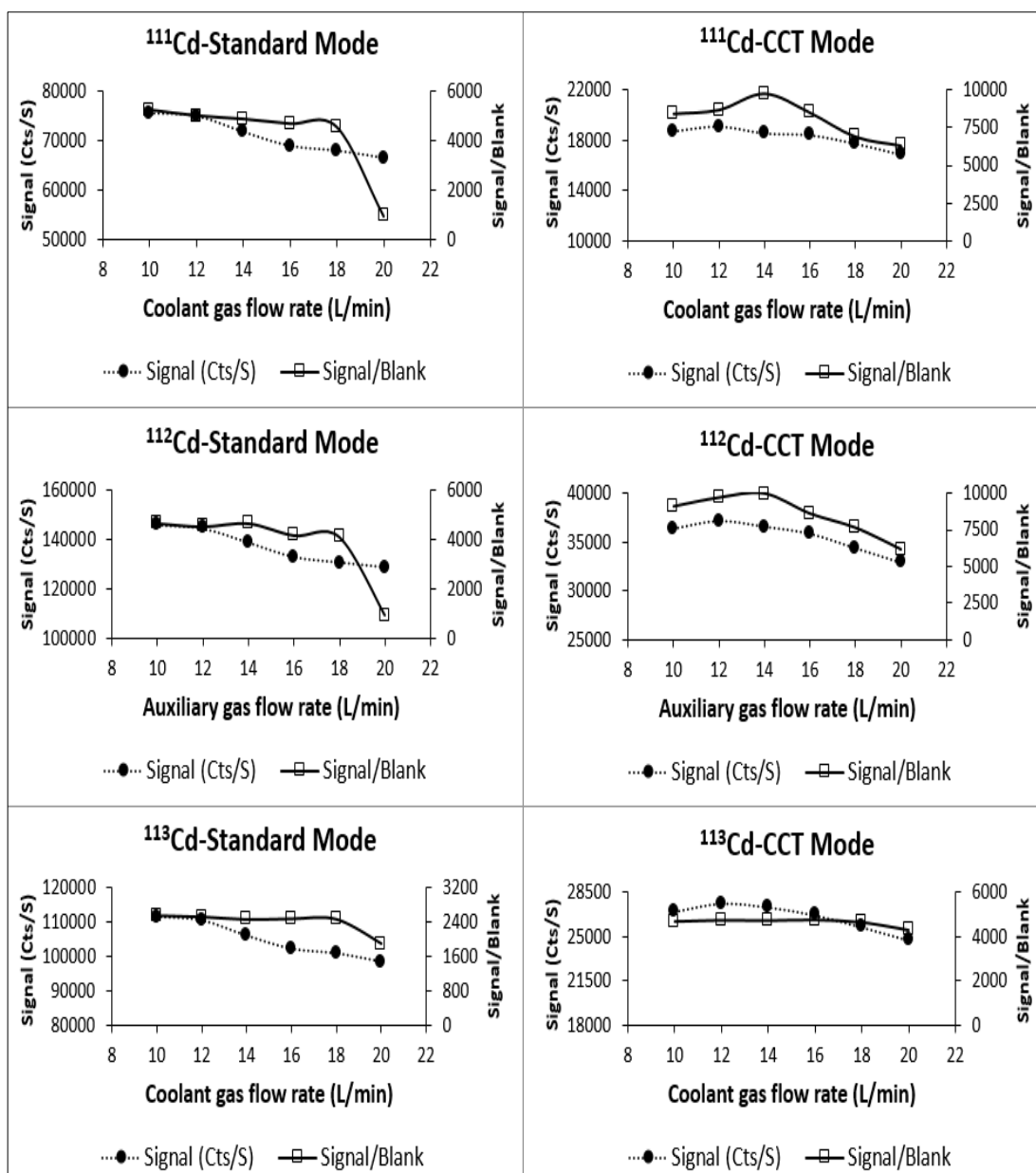


Figure 3.23 The signal and signal/blank ratios for cadmium (30 ng/mL) using ICP-MS standard and CCT modes at different coolant gas flow rates (L/min)

The standard signal for Hg behaved similarly to Cd on both modes, however, the signal/blank ratio gradually increased with increasing the coolant gas flow rate on both modes. This is due to the significant drop in the blank signal at higher rates causing the signal/blank ratio to increase regardless of the drop in the standard signal (Figure 3.24).

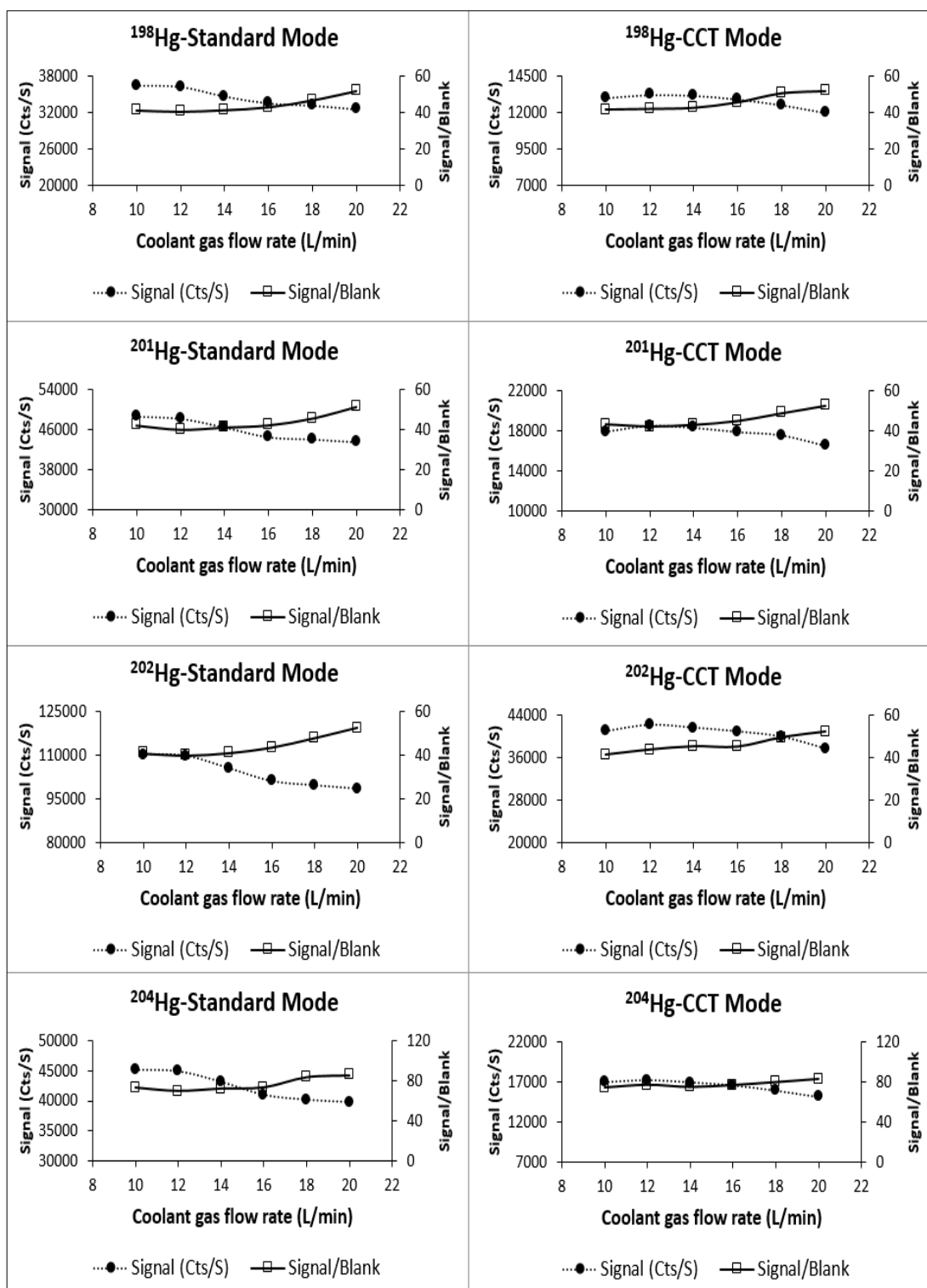


Figure 3.24 The signal and signal/blank ratios for mercury (30 ng/mL) using ICP-MS standard and CCT modes at different coolant gas flow rates (L/min)

The standard signal and signal/blank ratio for Pb using ICP-MS-standard mode behaviour was similar to Cd (Figure 3.23). The standard signal gradually decreased

with increasing the coolant gas flow rate and the signal/blank ratio was minimum on a rate of 20 L/min due to the increase in the blank signal. Using CCT mode the standard signal behaved similarly, but the signal/blank ratio changed slightly and gave the highest ratio at 14 L/min (Figure 3.25).

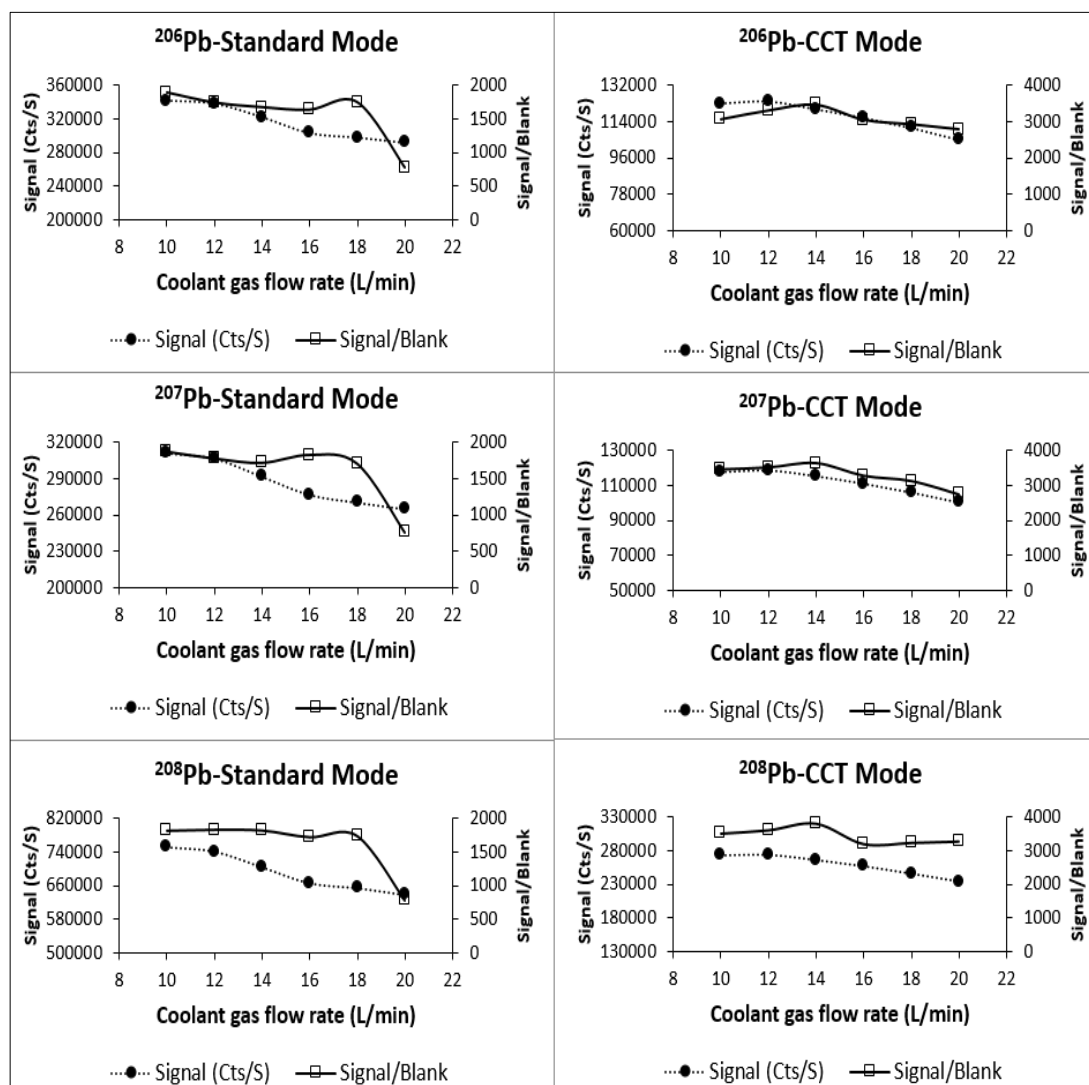


Figure 3.25 The signal and signal/blank ratios for lead (30 ng/mL) using ICP-MS standard and CCT modes at different coolant gas flow rates (L/min)

Class 2A elements; Co and Ni were affected similarly to Class 1 elements. The best signal/blank ratio and highest sensitivity was achieved at a coolant gas flow rate of 14 L/min. On the other hand, V sensitivity was not significantly affected with changing the rate using ICP-MS-CCT (Figures 3.26-3.28).

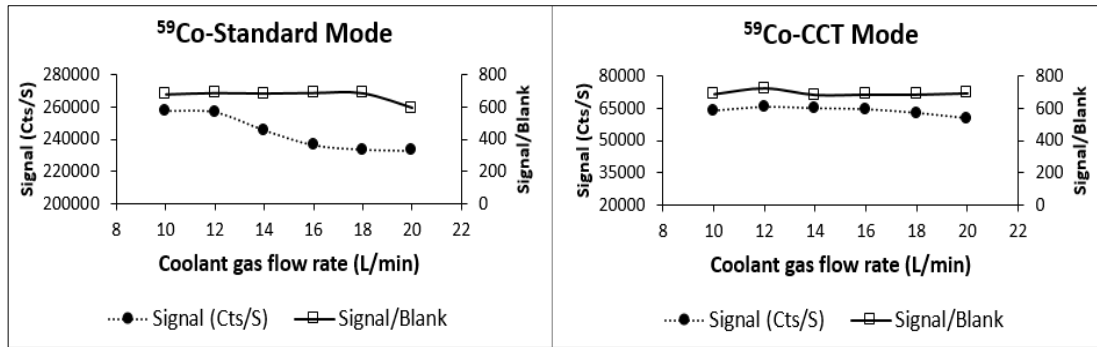


Figure 3.26 The signal and signal/blank ratios for cobalt (30 ng/mL) using ICP-MS standard and CCT modes at different coolant gas flow rates (L/min)

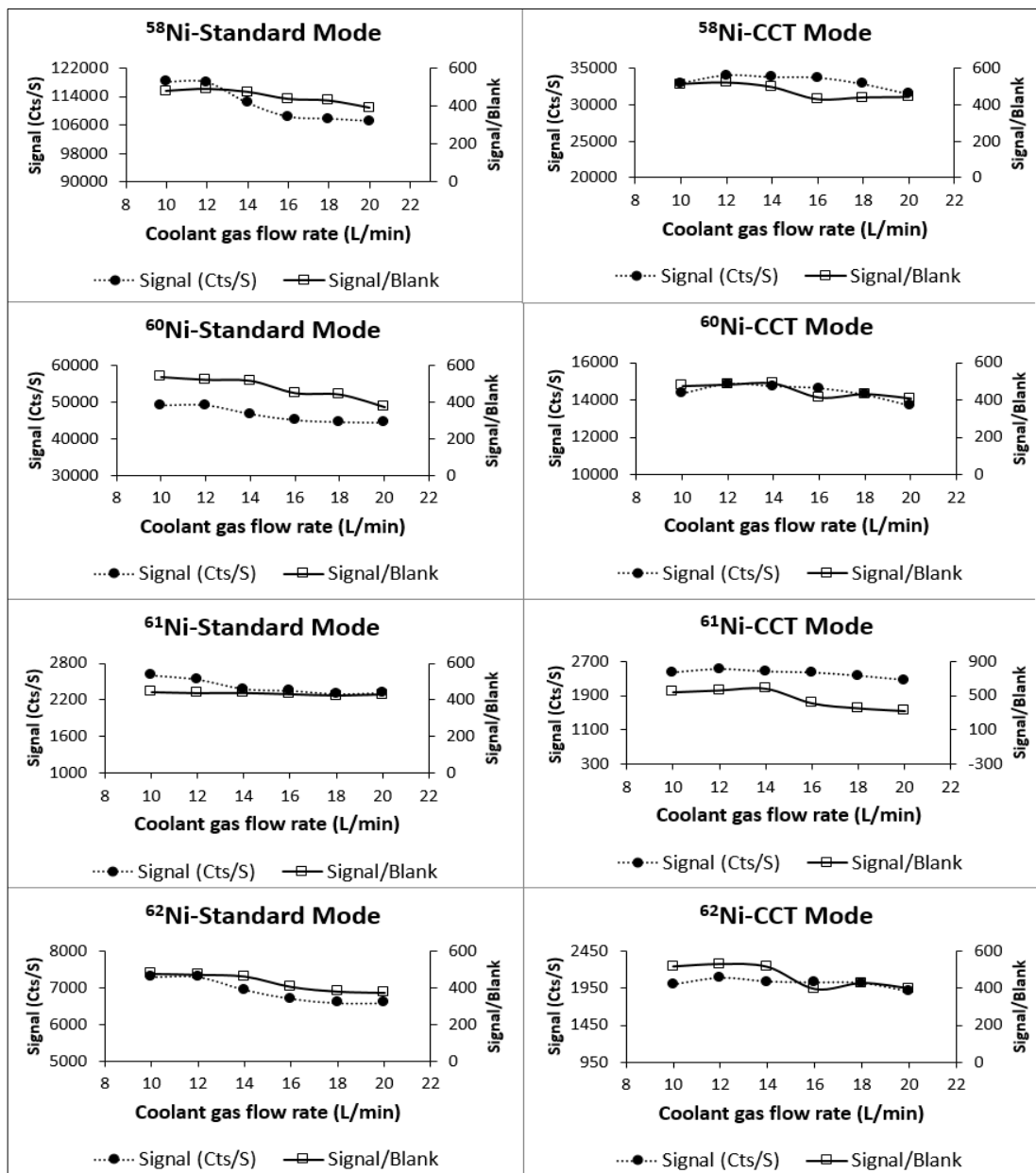


Figure 3.27 The signal and signal/blank ratios for nickel (30 ng/mL) using ICP-MS standard and CCT modes at different coolant gas flow rates (L/min)

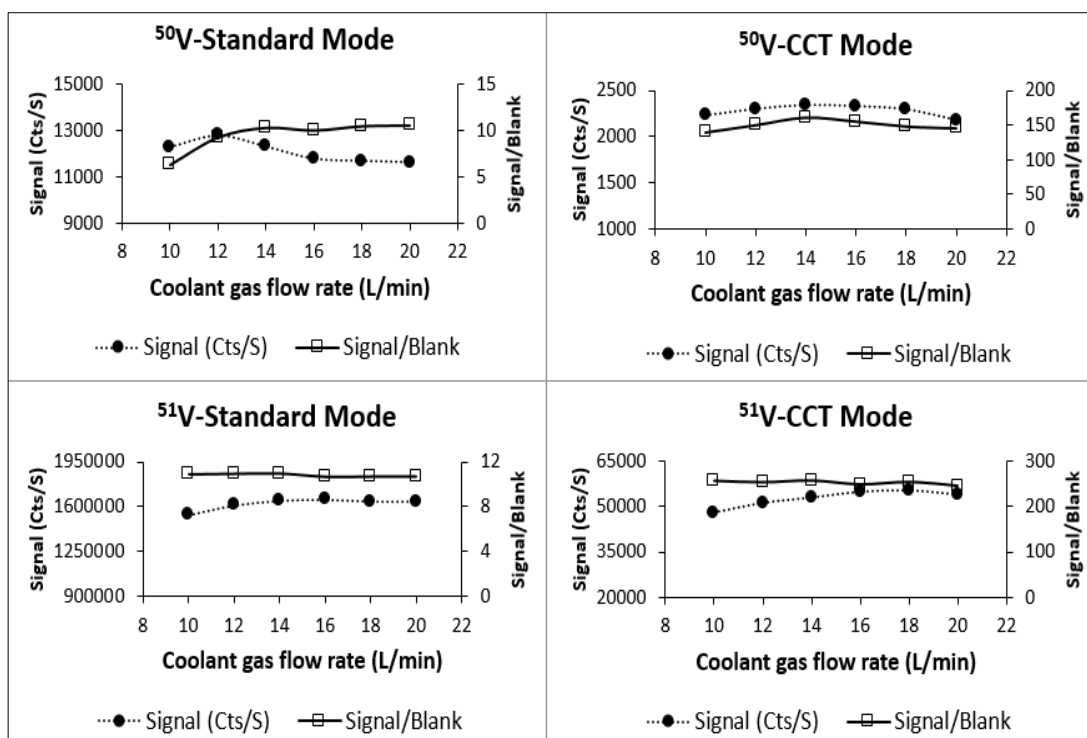


Figure 3.28 The signal and signal/blank ratios for vanadium (30 ng/mL) using ICP-MS standard and CCT modes at different coolant gas flow rates (L/min)

From the coolant gas flow rate optimisation results, the rate was adjusted to 14 L/min for both standard and CCT modes.

3.3.1.5 Optimisation of RF power

With ICP-MS-CCT, the plasma was extinguished at an RF power of 800 W. As a result, the signal/blank ratio for all elements using CCT mode were calculated over RF power range between 900 to 1500 W.

The highest signal/blank ratio for both Class 1 and Class 2A elements was obtained at an RF power of 900 W using both modes except for Hg, where the highest signal/blank ratio using standard mode was at 800 W.

Figures 3.29-3.35 represent the obtained signals and signal/blank ratios using different RF powers over a range of 800/900-1500 W.

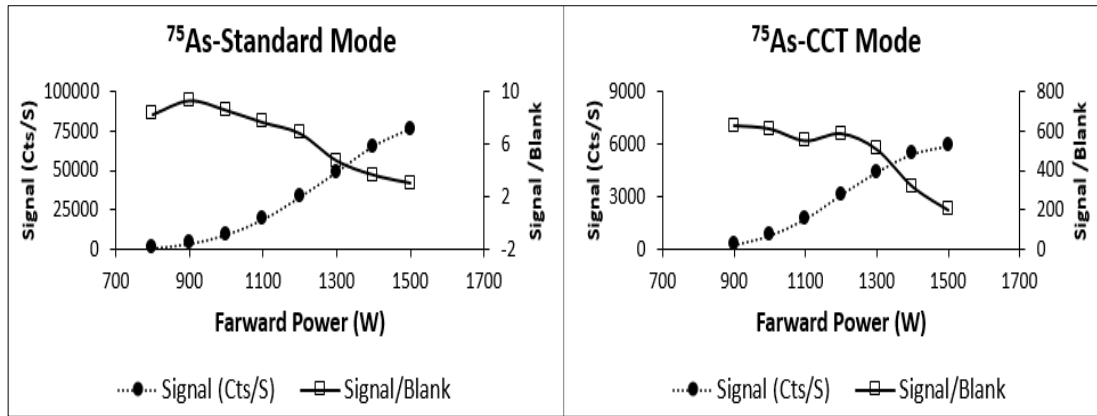


Figure 3.29 The signal and signal/blank ratios for arsenic (30 ng/mL) using ICP-MS standard and CCT modes at different RF powers (W)

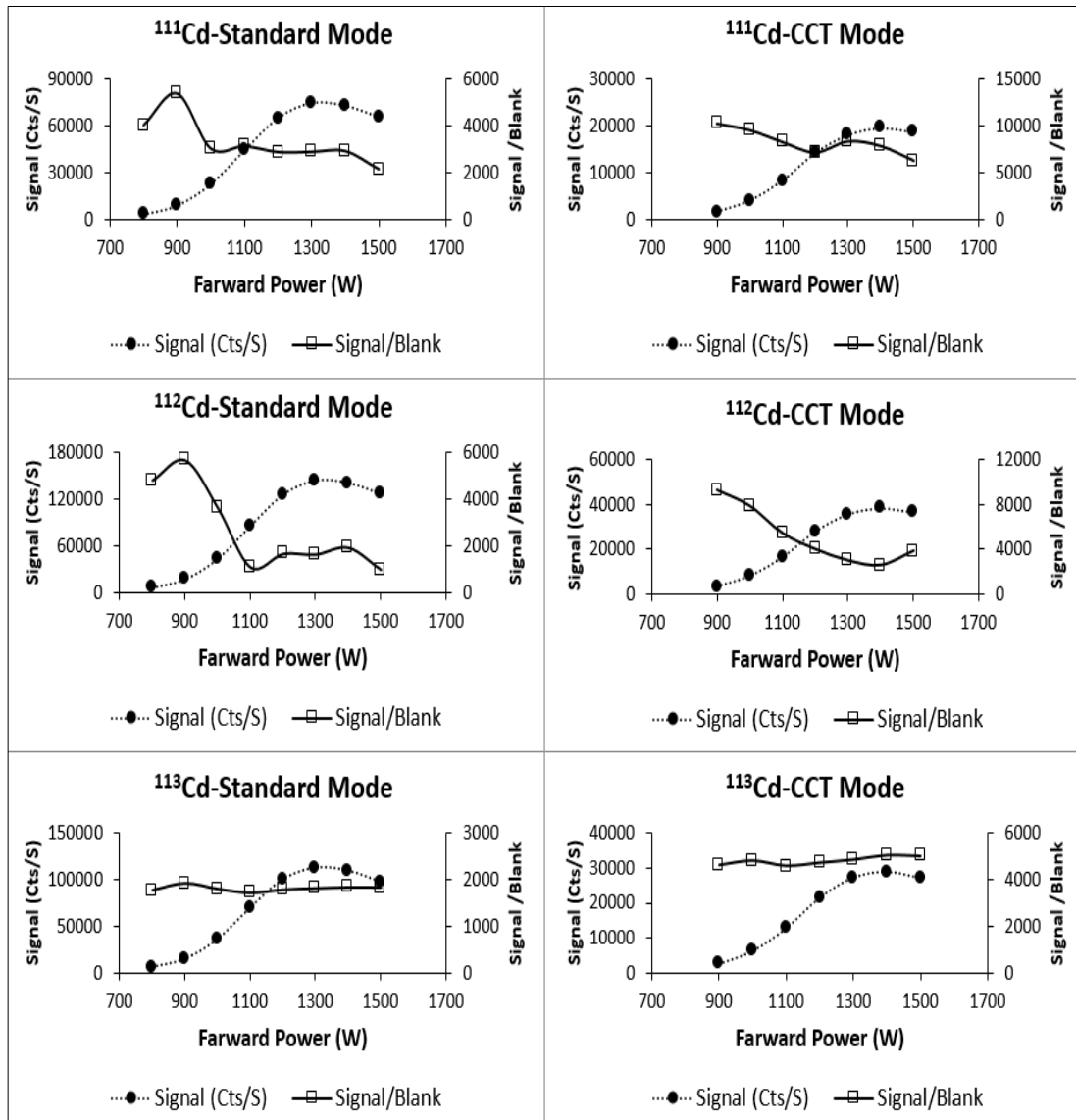


Figure 3.30 The signal and signal/blank ratios for cadmium (30 ng/mL) using ICP-MS standard and CCT modes at different RF powers (W)

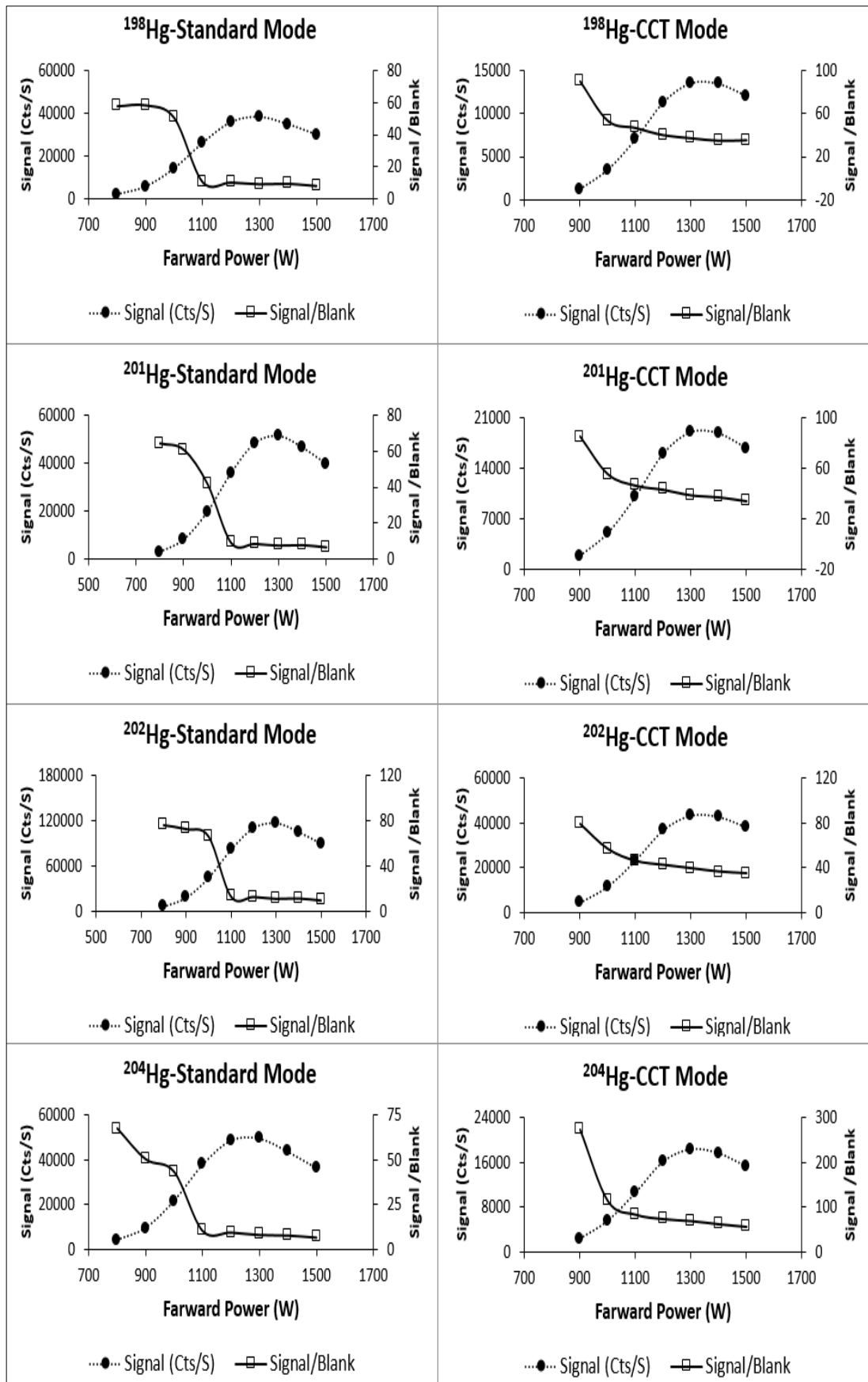


Figure 3.31 The signal and signal/blank ratios for mercury (30 ng/mL) using ICP-MS standard and CCT modes at different RF powers (W)

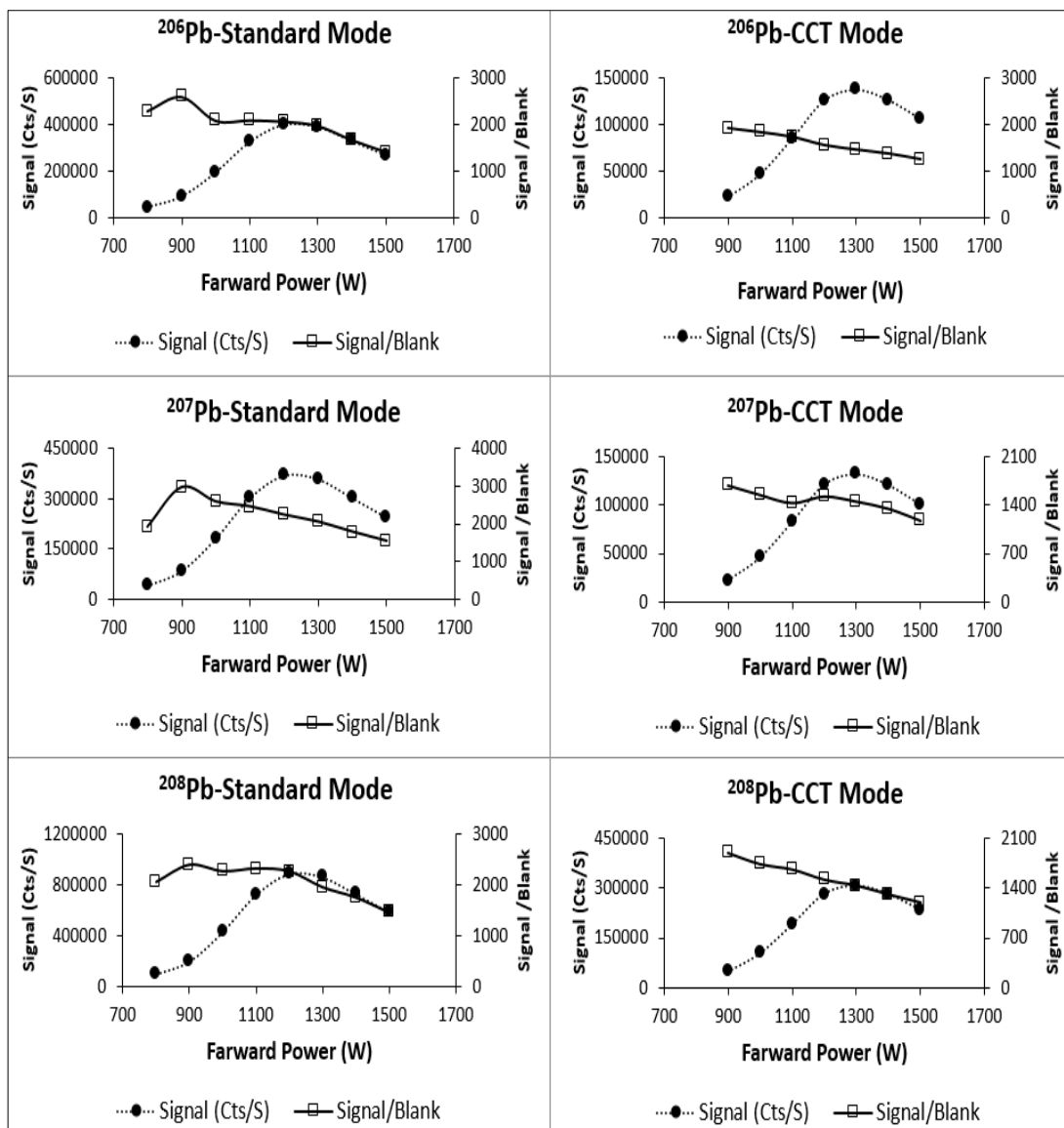


Figure 3.32 The signal and signal/blank ratios for lead (30 ng/mL) using ICP-MS standard and CCT modes at different RF powers (W)

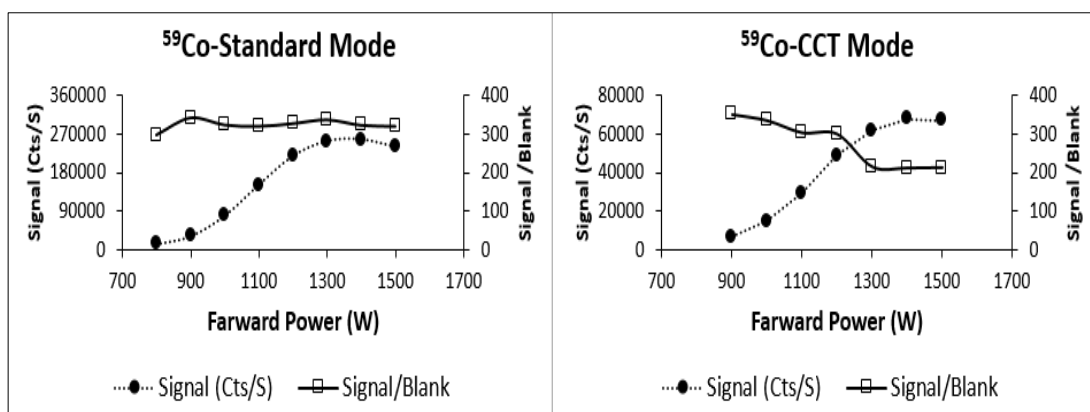


Figure 3.33 The signal and signal/blank ratios for cobalt (30 ng/mL) using ICP-MS standard and CCT modes at different RF powers (W)

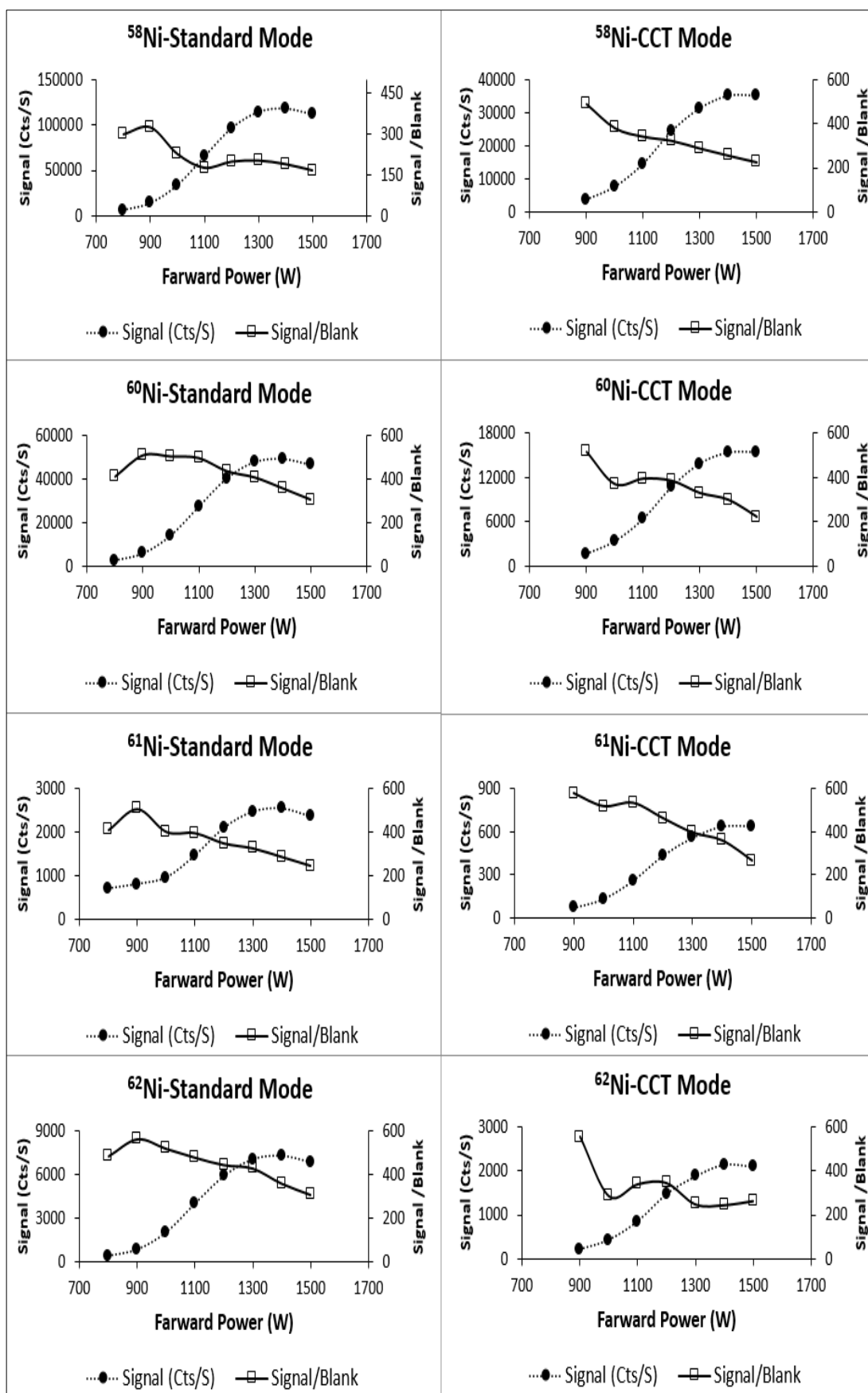


Figure 3.34 The signal and signal/blank ratios for nickel (30 ng/mL) using ICP-MS standard and CCT modes at different RF powers (W)

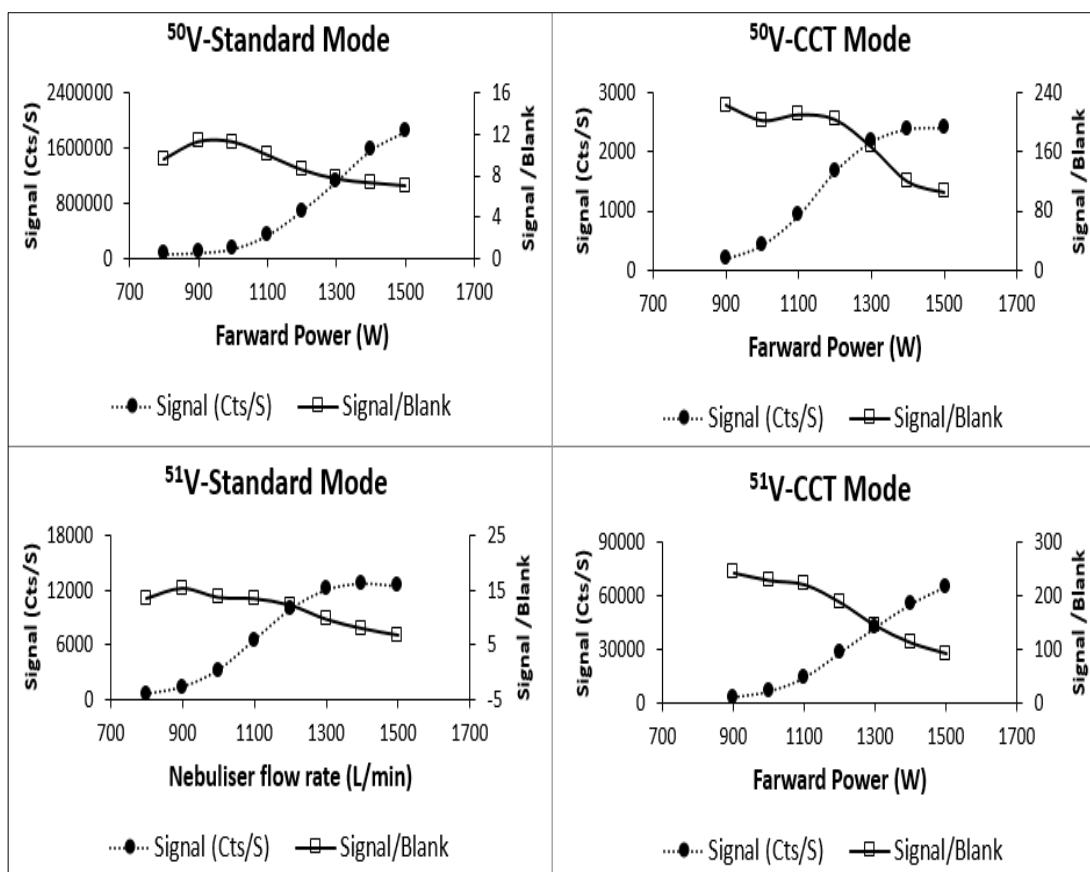


Figure 3.35 The signal and signal/blank ratios for vanadium (30 ng/mL) using ICP-MS standard and CCT modes at different RF powers (W)

Due to plasma stability issues at low RF powers, similar to those encountered in ICP-OES, the LoD and LoQ were assessed at different RF powers like in the case of ICP-OES (Section 2.3.1.5). The selected powers were 900 W, 1000 W, 1100 W, 1200 W, 1300 W, 1400 W and 1500 W.

Tables 3.6 and 3.7 illustrate the obtained LoD and LoQ at different RF powers.

Table 3.6 Class 1 and Class 2A LoDs and LoQs (ng/mL) calculated using ICP-MS-standard mode at different RF powers

Standard Mode	900 W	1100 W	1300 W	1400 W	1500 W	
⁷⁵ As	LoD	0.567	0.811	0.762	0.702	1.588
	LoQ	1.712	2.441	2.212	2.110	2.769
¹¹¹ Cd	LoD	0.187	0.152	0.045	0.037	0.026
	LoQ	0.586	0.443	0.098	0.091	0.075
¹¹² Cd	LoD	0.151	0.014	0.028	0.027	0.023
	LoQ	0.453	0.416	0.086	0.083	0.069
¹¹³ Cd	LoD	0.153	0.013	0.033	0.032	0.028
	LoQ	0.461	0.401	0.099	0.096	0.084
¹⁹⁸ Hg	LoD	0.917	0.763	0.619	0.583	0.562
	LoQ	2.759	2.289	1.877	1.795	1.724
²⁰¹ Hg	LoD	0.594	0.557	0.625	0.612	0.581
	LoQ	1.788	1.677	1.883	1.841	1.747
²⁰² Hg	LoD	0.615	0.688	0.643	0.599	0.604
	LoQ	1.873	1.991	1.865	1.832	1.753
²⁰⁴ Hg	LoD	0.145	0.661	0.321	0.303	0.562
	LoQ	0.437	1.996	0.966	0.915	1.693
²⁰⁶ Pb	LoD	0.349	0.136	0.061	0.066	0.100
	LoQ	1.051	0.409	0.184	0.199	0.301
²⁰⁷ Pb	LoD	0.347	0.135	0.061	0.065	0.078
	LoQ	1.043	0.407	0.183	0.197	0.231
²⁰⁸ Pb	LoD	0.316	0.132	0.059	0.065	0.083
	LoQ	0.927	0.409	0.185	0.198	0.248
⁵⁹ Co	LoD	0.264	0.242	0.136	0.108	0.096
	LoQ	0.804	0.722	0.417	0.332	0.296
⁵⁸ Ni	LoD	0.891	0.525	0.261	0.198	0.204
	LoQ	2.673	1.602	0.789	0.595	0.612
⁶⁰ Ni	LoD	0.237	0.206	0.147	0.136	0.129
	LoQ	0.712	0.627	0.445	0.415	0.397
⁶¹ Ni	LoD	0.211	0.187	0.135	0.191	0.201
	LoQ	0.622	0.581	0.394	0.591	0.623
⁶² Ni	LoD	0.271	0.315	0.153	0.145	0.196
	LoQ	0.828	0.955	0.461	0.437	0.588
⁵⁰ V	LoD	1.368	2.097	1.019	0.657	0.727
	LoQ	4.284	0.699	0.348	0.245	0.243
⁵¹ V	LoD	20.879	4.786	6.865	6.331	7.691
	LoQ	64.732	14.811	21.809	19.065	23.843

Table 3.7 Class 1 and Class 2A LoDs and LoQs (ng/mL) calculated using ICP-MS-CCT mode at different RF powers

CCT Mode		900 W	1100 W	1300 W	1400 W	1500 W
⁷⁵ As	LoD	0.209	0.030	0.064	0.048	0.060
	LoQ	0.622	0.095	0.191	0.149	0.181
¹¹¹ Cd	LoD	0.060	0.023	0.013	0.012	0.013
	LoQ	0.189	0.069	0.031	0.037	0.038
¹¹² Cd	LoD	0.067	0.028	0.013	0.007	0.008
	LoQ	0.199	0.063	0.041	0.022	0.023
¹¹³ Cd	LoD	0.063	0.021	0.011	0.013	0.014
	LoQ	0.191	0.062	0.032	0.039	0.041
¹⁹⁸ Hg	LoD	0.497	0.587	0.479	0.574	0.719
	LoQ	1.796	0.761	1.435	1.723	2.165
²⁰¹ Hg	LoD	0.512	0.496	0.480	0.567	0.972
	LoQ	1.241	1.487	1.441	1.705	2.021
²⁰² Hg	LoD	0.431	0.481	0.482	0.585	0.961
	LoQ	1.234	1.484	1.432	1.701	2.043
²⁰⁴ Hg	LoD	0.166	0.118	0.113	0.341	0.375
	LoQ	0.501	0.364	0.343	1.028	1.129
²⁰⁶ Pb	LoD	0.113	0.024	0.017	0.015	0.021
	LoQ	0.339	0.073	0.052	0.045	0.062
²⁰⁷ Pb	LoD	0.111	0.0233	0.017	0.014	0.021
	LoQ	0.336	0.0710	0.050	0.043	0.061
²⁰⁸ Pb	LoD	0.110	0.027	0.017	0.014	0.021
	LoQ	0.327	0.069	0.049	0.041	0.059
⁵⁹ Co	LoD	0.460	0.211	0.301	0.091	0.116
	LoQ	1.378	0.641	0.918	0.299	0.354
⁵⁸ Ni	LoD	0.327	0.171	0.151	0.077	0.095
	LoQ	0.981	0.515	0.481	0.232	0.287
⁶⁰ Ni	LoD	0.074	0.123	0.134	0.089	0.107
	LoQ	0.226	0.374	0.408	0.268	0.314
⁶¹ Ni	LoD	0.079	0.125	0.156	0.078	0.098
	LoQ	0.235	0.369	0.461	0.212	0.291
⁶² Ni	LoD	0.109	0.074	0.169	0.130	0.140
	LoQ	0.331	0.222	0.609	0.391	0.421
⁵⁰ V	LoD	1.195	0.139	0.128	0.007	0.010
	LoQ	3.625	0.417	0.040	0.201	0.032
⁵¹ V	LoD	6.980	0.589	0.741	0.159	0.191
	LoQ	20.859	1.791	2.223	0.485	0.581

RF of 1400 W was chosen as the optimum power for the simultaneous determination of the Class 1 and Class 2A elements, although Hg with CCT gave lower LoD and LoQ

at lower powers, but for the sake of time efficiency, it was determined to analyse Hg with the rest of the elements at 1400 W.

3.3.1.6 Optimisation of helium gas flow rate for operating CCT

From the previously demonstrated optimisation results, CCT mode improved the analytical sensitivity for most elements, which is consistent with previous findings that CCT reduces interferences (185, 187, 189). For example, ^{75}As LoQ was reduced from 2.110 to 0.149 ng/mL and ^{51}V LoQ dropped from 19.065 to 0.485 ng/mL when CCT mode was activated (Tables 3.4 and 3.5). This is expected as CCT has the ability to reduce polyatomic interferences as described in Section 1.6.4.1. As a result, all the samples were analysed using ICP-MS-CCT. $\text{He}_{(\text{g})}$ flow rate was optimised to get a suitable flow rate that will eliminate interferences without significantly reducing Class 1 and Class 2A elements sensitivity. Only helium was tested as a possible cell gas.

To optimise the $\text{He}_{(\text{g})}$ flow rate with samples containing different components, *NIST 3280 Multivitamin/Multielement tablets* were digested and analysed in triplicates using CCT mode with different $\text{He}_{(\text{g})}$ flow rates. This is in order to have a background noise similar to what can possibly be obtained with real samples. Percentage recoveries and RSDs were taken into consideration when determining the optimum $\text{He}_{(\text{g})}$ flow rate which is 3.5 L/min as shown in Table 3.8.

Table 3.8 NIST 3280 Multivitamin/Multielement tablets elemental recoveries (mean and RSD, (n=3)) using different helium gas flow rates with ICP-MS-CCT.

	He _(g) Flow Rate									
	2.5 L/min		3.0 L/min		3.5 L/min		4.0 L/min		4.5 L/min	
	%Rec*	RSD	%Rec	RSD	%Rec	RSD	%Rec	RSD	%Rec	RSD
As	41.67	22.37	44.08	20.01	104.1	4.52	105.2	17.92	95.21	15.6
Cd	68.65	1.16	86.36	0.63	95.63	2.44	104.8	6.08	105.1	23
Hg	N/A	N/A	N/A	N/A	N/A	N/A	N/A	N/A	N/A	N/A
Pb	101.5	1.58	102.8	2.55	97.84	2.7	97.97	5.11	97.04	2.97
Co	97.63	22.13	105.1	23.54	99.23	0.5	102.0	2.62	102.4	7.15
Ni	50.96	8.28	60.89	7.42	99.76	3.65	96.40	2.02	95.28	6.61
V	97.93	9.22	98.06	9.56	100.3	8.7	96.33	2.75	102.3	3.35

*%Recovery

Higher rates gave recoveries for the elements of interest in the range of 95-105%, but to minimise He_(g) consumption, 3.5 L/min was set as the optimum flow rate.

3.3.1.7 Selection of suitable internal standards and analytical atomic mass units

The atomic masses chosen for analysis as well as the internal standards used were selected based on the recovery results obtained using *NIST 3280* multivitamin/multielement tablets. As discussed in Section 1.4, *NIST 3280* tablets are composed of a formulation containing vitamin and carotenoid gelatine beadlets, a mineral pre-mix, and a binder, all compressed into tablets and film coated. The tablets contain minerals like Ca, Na, Mo, Fe and Sn that can cause significant interferences with the Class 1 and Class 2A elements.

Table 3.9 show the % recoveries and RSDs obtained using the optimised ICP-MS-CCT mode for all the elements of interest in *NIST 3280* using different internal standards.

Table 3.9 NIST 3280 elements' isotopes recoveries and RSDs using different internal standards

Element	⁴⁵ Sc		⁸⁹ Y		¹⁰³ Rh		¹¹⁵ In		¹⁵⁹ Tb	
	%Rec	RSD	%Rec	RSD	%Rec	RSD	%Rec	RSD	%Rec	RSD
⁷⁵ As	95.62	1.40	81.81	5.88	95.27	2.43	100.5	3.41	94.75	3.64
¹¹¹ Cd	95.62	5.19	85.91	5.19	95.11	2.58	105.9	0.46	97.23	1.68
¹¹² Cd	233.3	10.6	138.4	7.85	208.1	4.19	508.7	3.83	391.73	17.41
¹¹³ Cd	66.05	5.83	60.99	8.36	68.78	4.88	77.55	10.37	72.73	13.60
²⁰⁶ Pb	83.66	7.83	88.82	9.31	89.06	3.62	87.88	4.27	88.27	2.72
²⁰⁷ Pb	87.51	8.01	87.34	9.74	81.44	4.28	79.28	4.89	87.06	1.71
²⁰⁸ Pb	94.92	6.22	89.12	5.37	95.63	3.04	90.11	4.50	98.88	1.09
⁵⁹ Co	95.60	6.71	89.05	5.53	95.53	1.00	100.5	1.01	95.44	5.04
⁵⁸ Ni	743.0	11.5	447.9	9.34	811.0	13.6	940.6	4.33	645.68	13.40
⁶⁰ Ni	98.28	1.11	82.93	8.32	95.99	2.06	88.07	4.08	95.49	12.70
⁶¹ Ni	98.99	4.58	77.78	9.87	187.0	14.8	161.6	2.91	122.78	14.10
⁶² Ni	70.09	1.30	53.77	8.97	67.74	12.1	88.12	4.79	63.024	13.30
⁵⁰ V	1202	10.1	289.5	10.71	2244	9.00	2681.2	3.56	1826.9	21.60
⁵¹ V	95.47	0.27	86.19	2.18	100.40	2.82	105.14	3.56	94.88	0.87

The following atomic masses were selected for samples analysis: As (75 amu), Cd (111 amu), Pb (208 amu), Co (59 amu), Ni (60 amu) and V (51 amu). The isotopes with the highest abundance were used, except for Cd and Ni. ¹¹⁴Cd is the most abundant isotopes followed by ¹¹²Cd. However, both suffer from interferences that lead to false high concentrations. For example, ¹¹⁴Sn, ⁹⁷Mo¹⁶O¹H and ⁹⁸Mo¹⁶O interferes with ¹¹⁴Cd, while ¹¹²Sn, ⁴⁰Ca¹⁶O₂, ⁹⁵Mo¹⁶O¹H and ⁹⁶Mo¹⁶O⁺ interferes with ¹¹²Cd. In the case of Ni, ⁵⁸Ni suffers from interferences with ²³Na³⁵Cl⁺, ⁴⁰Ca¹⁸O⁺, ⁴⁰Ca¹⁷O¹H⁺, ⁴²Ca¹⁶O⁺, ²⁹Si₂⁺ and ²³Na³⁵Cl⁺(183, 184).

Although CCT can efficiently eliminate most of the polyatomic interferences, elements with similar m/z ratio remain capable of causing severe interferences(187, 295).

Regarding the internal standard, when ^{89}Y was used as an internal standard to compensate for matrix effect it gave lower concentrations than the certified values. Corrections using ^{45}Sc gave $\text{RSD} > 5\%$ with ^{208}Pb and ^{59}Co . On the other hand, ^{115}In produced recoveries $< 95\%$ for ^{208}Pb and ^{60}Ni . In case of using ^{159}Tb , the ^{208}Pb RDS was more than 10%. As a result, ^{103}Rh was selected as the internal standard to correct for the method's accuracy and improve the precision for Class 1 and Class 2A elements.

Because Hg is not included in *NIST 3280*, TAC-formulas that were described in Section 2.3.1.4.2 were used to test the method efficiency in analysing Hg. Table 3.10 represents the obtained results.

Table 3.10 Concentrations of Hg in TAC-formulas and RSDs using different internal standards, n=3

Formula-1 (30 %PDE) , Hg Concentration($\mu\text{g/g}$): Theoretical=6.48, ICP-OES=3.92, RSD=5.14%

Element	^{45}Sc		^{89}Y		^{103}Rh		^{115}In		^{159}Tb	
	($\mu\text{g/g}$)	RSD	($\mu\text{g/g}$)	RSD	($\mu\text{g/g}$)	RSD	($\mu\text{g/g}$)	RSD	($\mu\text{g/g}$)	RSD
^{198}Hg	4.01	10.86	1.81	9.48	3.04	8.94	4.58	5.59	3.39	6.09
^{201}Hg	4.02	10.94	1.82	9.67	3.99	8.86	4.58	5.84	3.39	6.18
^{202}Hg	4.02	10.81	1.83	9.61	3.83	8.51	4.58	5.89	3.39	6.25
^{204}Hg	3.81	11.82	1.65	10.29	2.69	8.91	4.33	6.84	3.16	6.99

Formula-2 (100 %PDE), Hg Concentration($\mu\text{g/g}$): Theoretical=19.45, ICP-OES=18.89, RSD=5.34%

Element	^{45}Sc		^{89}Y		^{103}Rh		^{115}In		^{159}Tb	
	($\mu\text{g/g}$)	RSD								
^{198}Hg	19.11	5.72	15.15	5.75	18.87	5.14	19.53	5.31	18.62	5.03
^{201}Hg	19.14	5.29	15.21	5.31	18.85	5.4	19.52	5.32	18.69	5.63
^{202}Hg	19.13	5.62	15.25	5.32	18.97	5.16	19.53	5.55	18.69	5.88
^{204}Hg	13.67	6.17	10.87	6.06	13.47	5.18	11.87	5.05	12.26	5.39

Table 3.10, continuedFormula-3 (300 %PDE), Hg Concentration($\mu\text{g/g}$): Theoretical=48.61, ICP-OES=51.09, RSD=7.84%

Element	⁴⁵ Sc		⁸⁹ Y		¹⁰³ Rh		¹¹⁵ In		¹⁵⁹ Tb	
	($\mu\text{g/g}$)	RSD	($\mu\text{g/g}$)	RSD	($\mu\text{g/g}$)	RSD	($\mu\text{g/g}$)	RSD	($\mu\text{g/g}$)	RSD
¹⁹⁸ Hg	53.16	9.31	45.31	9.23	49.98	8.87	52.49	8.74	49.75	8.66
²⁰¹ Hg	53.09	9.09	45.50	9.05	49.93	8.69	52.85	8.94	49.87	8.47
²⁰² Hg	53.07	9.06	45.51	9.03	50.15	8.42	52.86	8.55	49.88	8.57
²⁰⁴ Hg	45.99	10.15	32.03	10.13	40.92	9.01	46.52	9.99	38.03	8.97

Comparing the results obtained using ICP-MS-CCT with those obtained using ICP-OES, it is noticed that the choice of internal standard is important. Correction using ⁴⁵Sc, ¹¹⁵In gave higher results in comparison with the concentration obtained using ICP-OES, while ⁸⁹Y gave lower results. ¹⁰³Rh was also selected to correct for Hg and the atomic mass selected is 202 m/z.

3.3.2 Method validation and analytical figures of merit

3.3.2.1 Limits of detection and limits of quantification

LoD and LoQ were calculated for Class 1 and Class 2A elements at the selected m/z using the optimised ICP-MS conditions as described in Section 2.3.1.5.

The results are summarised in Table 3.11

Table 3.11 ICP-MS limits of detection and Limits of quantification for Class 1 and Class 2A elements

Element	Blanks	σ	Slope	Intercept	Av.+3 σ	Av.+10 σ	LoD ng/mL	LoQ ng/mL
	Av.*							
⁷⁵ As	28.00	5.67	390.98	26.17	45.03	84.77	0.048	0.149
¹¹¹ Cd	35.80	5.57	1585.50	33.05	52.52	91.54	0.012	0.037
²⁰² Hg	1212.53	883.42	5537.84	652.11	3862.76	10046.72	0.585	1.701
²⁰⁸ Pb	164.56	56.59	14477.39	137.28	334.39	730.56	0.014	0.041
⁵⁹ Co	84.85	73.62	2483.40	78.64	305.70	821.03	0.091	0.299
⁶⁰ Ni	47.75	107.48	4645.89	6.49	370.18	1122.52	0.078	0.240
⁵¹ V	7476.31	898.55	19355.67	7081.94	10171.97	16461.84	0.159	0.485

*Av. = Average

3.3.2.2 Linearity and Range

Eight concentration points were assayed in triplicate and showed good linearity in the tested range, with a correlation coefficient (R^2) value of above 0.995. The linear regression equation and its R^2 , for each of the calibration curves are summarised in Table 3.12.

Table 3.12 Linearity data for Class 1 and Class 2A elements using ICP-MS-CCT

Element	Range (ng/ml)	Calibration equation	R^2 Value
^{75}As	1-1000	$y = 185.73x + 26.169$	0.9999
^{111}Cd	1-1000	$y = 810.76x + 12.742$	0.9998
^{202}Hg	1-1000	$y = 1975.1x + 625.11$	0.9999
^{208}Pb	1-1000	$y = 14477x + 137.28$	0.9998
^{59}Co	1-1000	$y = 2483.4x + 78.639$	0.9999
^{60}Ni	1-1000	$y = 540.57x + 6.4974$	0.9998
^{51}V	1-1000	$y = 1269.8x + 708.19$	0.9997

3.3.2.3 Accuracy and precision

The accuracy and precision were evaluated using *NIST 3280*, where % recoveries between 95-105% indicate the method's accuracy and RSD less than 5% indicate the method's precision. The microwave assisted acid digestion procedure was revalidated as another instrument with larger vessels were used. In addition, the ICP-MS-CCT method sensitivity allows the quantification of Class 1 elements *using NIST 3280* except for Hg, which was validated using TAC-formulas. The results are displayed in Tables 3.13 and 3.14.

Table 3.13 Accuracy and repeatability results of the optimised ICP-MS-CCT method obtained using NIST 3280 expressed as % recoveries and RSDs respectively, n=3

Element	NIST 3280 certificate		Spike addition	
	% Recovery	RSD	Spiked Recovery	RSD
⁷⁵ As	100.86	3.40	97.34	0.47
¹¹¹ Cd	104.59	0.46	104.73	0.09
²⁰² Hg	N/A	N/A	97.94	1.23
²⁰⁸ Pb	102.54	2.90	98.21	0.15
⁵⁹ Co	100.52	1.01	95.20	0.23
⁶⁰ Ni	97.06	3.75	101.13	0.32
⁵¹ V	97.29	4.57	96.10	0.82

Table 3.14 Analysis results of three TAC formulas containing different levels of Class 1 and Class 2A, n=3

Element	Formula-1 (30%PED)	ICP-OES		ICP-MS-CCT	
	Theoretical(µg/g)	(µg/g)	RSD	(µg/g)	RSD
As	6.65	3.83	2.74	3.31	0.99
Cd	1.58	1.36	3.09	1.34	5.81
Hg	6.48	3.92	5.34	3.83	8.51
Pb	2.27	2.28	5.44	2.16	2.85
Co	8.68	7.96	5.51	8.92	3.58
Ni	6.58	5.79	4.53	5.52	2.31
V	22.25	19.64	3.64	20.49	3.22

Element	Formula-2 (100%PED)	ICP-OES		ICP-MS-CCT	
	Theoretical(µg/g)	(µg/g)	RSD	(µg/g)	RSD
As	19.8	15.17	4.61	16.61	7.4
Cd	5.26	4.94	3.75	4.78	0.38
Hg	19.45	18.89	5.14	18.96	5.16
Pb	6.67	6.41	3.94	5.95	3.72
Co	22.08	19.61	5.01	19.35	0.92
Ni	10.55	10.24	6.24	10.45	2.59
V	22.7	18.28	3.31	17.22	8.91

Element	Formula-3 (300%PED)	ICP-OES		ICP-MS-CCT	
	Theoretical(µg/g)	(µg/g)	RSD	(µg/g)	RSD
As	49.2	45.55	3.42	42.64	5.25
Cd	15.76	12.63	2.15	12.11	6.99
Hg	48.61	51.09	7.84	50.14	8.42
Pb	17.35	14.59	3.47	13.09	5.72
Co	50.12	37.67	7.76	37.18	6.36
Ni	16.75	13.43	5.94	12.59	6.69
V	0.9	< 0.000159	-	< 0.000159	-

3.3.3 Revalidation of the microwave assisted acid digestion procedure

The first step was to measure a blank of 8 ml reverse aqua regia subjected to the exact same procedure as *NIST 3280*. The elements concentrations were below LoDs as illustrated in Table 3.15, which was similar to the findings using ICP-OES.

Table 3.15 Obtained concentrations using the developed and optimised ICP-MS-CCT method for reverse aqua regia following microwave digestion, *n=3*

Element	Concentration (ng/mL)	%RSD
⁷⁵ As	<LoD (4.80X10 ⁻⁵)	1.89
¹¹¹ Cd	<LoD (1.20X10 ⁻⁵)	0.99
²⁰² Hg	<LoD (5.85X10 ⁻⁵)	2.50
²⁰⁸ Pb	0.001	2.30
⁵⁹ Co	0.001	0.42
⁶⁰ Ni	0.004	1.00
⁵¹ V	<LoD (1.59X10 ⁻⁵)	6.08

The next step was to compare the efficiency of the acid ratio 9 HNO₃: 1 HCl in extracting Class 1 elements with that of reverse aqua regia, since with ICP-MS all the elements of interest are in concentrations higher than LoQs even after dilution prior to analysis, except for Hg which is not part of *NIST 3280* formulation. From the results represented in Table 3.16, reverse aqua regia was more efficient in extracting Ni and As, so it is the digestion medium chosen to prepare pharmaceutical samples for analyses.

Table 3.16 Percentage recoveries for *NIST 3280* using 9 HNO₃: 1 HCl and reverse aqua regia for digestion, *n*=3

Stage 1: Ramp Time= 5 min, Temperature= 120°C, Hold time= 5 min

Stage 2: Ramp Time= 5 min, Temperature= 180°C, Hold time= 5 min

Stage 3: Ramp Time= 5 min, Temperature= 210°C, Hold time= 5 min

Element	9 HNO ₃ : 1 HCl		Reverse aqua regia	
	% Recovery	RSD	% Recovery	RSD
⁷⁵ As	93.61	6.03	100.86	3.40
¹¹¹ Cd	99.02	5.79	104.59	0.46
²⁰² Hg	N/A	N/A	N/A	N/A
²⁰⁸ Pb	101.14	8.27	102.54	2.90
⁵⁹ Co	99.83	5.46	100.52	1.01
⁶⁰ Ni	75.51	1.53	97.06	3.75
⁵¹ V	100.53	0.98	97.29	4.57

The final step to test the effect of temperature on extraction efficiency of As, Cd and Pd from *NIST 3280* tablets. Spiked samples were also analysed, and the recoveries obtained were compared with those calculated based on the certified elements concentrations in *NIST 3280*. As illustrated in Table 3.17 the results confirm the conclusions reached using ICP-OES which are depending on spike recoveries solely to measure the accuracy of the digestion-analysis methods is insufficient and a solid reference material is required for proper evaluation and validation of the methods. Furthermore, reaching a maximum temperature of 210°C was found to be necessary to ensure adequate extraction of Classes 1 and 2A elements consistently. Lower temperature, i.e. 200°C gave good extraction results, but occasionally, the extraction for some elements may fall below 95% or gave RSD >5%, so 210°C was selected as the for the final stage of digestion.

Table 3.17 NIST 3280 percentage recoveries using different temperatures for the microwave assisted acid digestion methods, $n=3$

Method 1				
Stage 1: Ramp Time= 5 min, Temperature= 50°C, Hold time= 5 min				
Stage 2: Ramp Time= 5 min, Temperature= 110°C, Hold time= 5 min				
Stage 3: Ramp Time= 5 min, Temperature= 140°C, Hold time= 5 min				
NIST 3280 certificate			Spike addition	
Element	% Recovery	RSD	Spiked Recovery	RSD
⁷⁵ As	10.57	89.76	99.51	0.72
¹¹¹ Cd	50.54	11.82	98.69	0.87
²⁰² Hg	N/A	N/A	100.83	2.45
²⁰⁸ Pb	89.26	2.35	100.32	1.55
⁵⁹ Co	51.80	7.07	100.20	0.47
⁶⁰ Ni	60.53	26.59	95.45	1.44
⁵¹ V	64.66	6.18	103.72	0.40
Method 2				
Stage 1: Ramp Time= 5 min, Temperature= 70°C, Hold time= 5 min				
Stage 2: Ramp Time= 5 min, Temperature= 130°C, Hold time= 5 min				
Stage 3: Ramp Time= 5 min, Temperature= 160°C, Hold time= 5 min				
NIST 3280 certificate			Spike addition	
Element	% Recovery	RSD	Spiked Recovery	RSD
⁷⁵ As	84.26	5.96	99.04	3.22
¹¹¹ Cd	93.45	5.88	104.70	2.10
²⁰² Hg	N/A	N/A	99.12	15.79
²⁰⁸ Pb	96.63	1.74	100.08	3.25
⁵⁹ Co	68.60	1.06	100.23	2.45
⁶⁰ Ni	65.13	1.16	96.67	9.72
⁵¹ V	62.93	1.08	95.36	3.05
Method 3				
Stage 1: Ramp Time= 5 min, Temperature= 90°C, Hold time= 5 min				
Stage 2: Ramp Time= 5 min, Temperature= 150°C, Hold time= 5 min				
Stage 3: Ramp Time= 5 min, Temperature= 180°C, Hold time= 5 min				
NIST 3280 certificate			Spike addition	
Element	% Recovery	RSD	Spiked Recovery	RSD
⁷⁵ As	102.59	32.89	103.64	0.64
¹¹¹ Cd	95.97	9.44	98.02	0.58
²⁰² Hg	N/A	N/A	97.21	3.19
²⁰⁸ Pb	97.82	3.21	99.47	0.79
⁵⁹ Co	60.31	3.27	95.06	0.86
⁶⁰ Ni	58.98	3.75	99.67	1.25
⁵¹ V	74.40	4.32	100.38	5.01

Table 3.17, continued

Method 4				
Stage 1: Ramp Time= 5 min, Temperature= 110°C, Hold time= 5 min				
Stage 2: Ramp Time= 5 min, Temperature= 170°C, Hold time= 5 min				
Stage 3: Ramp Time= 5 min, Temperature= 200°C, Hold time= 5 min				
Element	NIST 3280 certificate		Spike addition	
	% Recovery	RSD	Spiked Recovery	RSD
⁷⁵ As	98.43	4.94	95.00	0.16
¹¹¹ Cd	99.78	0.81	98.97	0.56
²⁰² Hg	N/A	N/A	104.94	1.89
²⁰⁸ Pb	97.27	4.13	99.22	0.91
⁵⁹ Co	96.25	7.65	99.58	0.45
⁶⁰ Ni	95.48	6.13	98.96	1.42
⁵¹ V	104.99	1.65	97.22	0.93
Method 5				
Stage 1: Ramp Time= 5 min, Temperature= 120°C, Hold time= 5 min				
Stage 2: Ramp Time= 5 min, Temperature= 180°C, Hold time= 5 min				
Stage 3: Ramp Time= 5 min, Temperature= 210°C, Hold time= 5 min				
Element	NIST 3280 certificate		Spike addition	
	% Recovery	RSD	Spiked Recovery	RSD
⁷⁵ As	100.86	3.40	97.34	0.47
¹¹¹ Cd	104.59	0.46	104.73	0.09
²⁰² Hg	N/A	N/A	97.94	1.23
²⁰⁸ Pb	102.54	2.90	98.21	0.15
⁵⁹ Co	100.52	1.01	95.20	0.23
⁶⁰ Ni	97.06	3.75	101.13	0.32
⁵¹ V	97.29	4.57	96.10	0.82

3.4 Analysis of pharmaceutical samples

The twelve products analysed with ICP-OES were reanalysed using ICP-MS and the products came in good agreement as illustrated in Table 3.18 and Table 3.19.

Table 3.18 Elemental impurities ($\mu\text{g}/\text{day}$) in analgesic tablets analysed using ICP-MS-CCT mode (mean \pm σ , $n=3$)

Products*	Elements	ICH Q3D oral PDEs ($\mu\text{g}/\text{day}$)	Concentration ($\mu\text{g}/\text{day}$)	Spiked Recovery	RSD
Paracetamol-value health	^{75}As	15	<LoD (4.80×10^{-5})	99.25	4.57
	^{111}Cd	5	0.48 ± 0.075	95.42	3.05
	^{202}Hg	30	<LoD (5.85×10^{-4})	96.74	2.87
	^{208}Pb	5	1.91 ± 0.002	98.88	4.09
	^{59}Co	50	0.98 ± 0.048	96.78	2.15
	^{60}Ni	200	51.01 ± 0.12	98.63	3.57
	^{51}V	100	<LoD (1.59×10^{-4})	99.57	3.57
Hedex Extra	^{75}As	15	<LoD (4.80×10^{-5})	95.98	4.15
	^{111}Cd	5	0.56 ± 0.086	102.56	3.64
	^{202}Hg	30	<LoD (5.85×10^{-4})	97.84	5.01
	^{208}Pb	5	3.87 ± 0.023	100.56	2.98
	^{59}Co	50	2.65 ± 0.910	103.48	5.14
	^{60}Ni	200	10.54 ± 0.59	101.59	3.58
	^{51}V	100	<LoD (1.59×10^{-4})	98.65	3.45
Anadin Extra	^{75}As	15	<LoD (4.80×10^{-5})	97.84	4.25
	^{111}Cd	5	0.39 ± 0.008	98.88	4.68
	^{202}Hg	30	<LoD (5.85×10^{-4})	96.57	3.57
	^{208}Pb	5	3.44 ± 0.047	95.89	1.98
	^{59}Co	50	1.87 ± 0.013	100.94	2.58
	^{60}Ni	200	<LoD (7.80×10^{-5})	99.99	2.76
	^{51}V	100	<LoD (1.59×10^{-4})	100.59	1.59
Paracetamol Bell's Healthcare	^{75}As	15	<LoD (4.80×10^{-5})	102.65	2.35
	^{111}Cd	5	0.68 ± 0.006	100.25	1.65
	^{202}Hg	30	<LoD (5.85×10^{-4})	95.78	4.05
	^{208}Pb	5	4.17 ± 0.041	103.54	2.08
	^{59}Co	50	<LoD (9.10×10^{-5})	98.57	3.64
	^{60}Ni	200	<LoD (7.80×10^{-5})	98.51	3.05
	^{51}V	100	<LoD (1.59×10^{-4})	97.99	2.35

*The remaining two products have all elements levels <LoD.

Table 3.19 Elemental impurities ($\mu\text{g}/\text{day}$) in cold and cough remedies analysed using ICP-MS-CCT mode (mean \pm σ , $n=3$)

Products	Elements	ICH Q3D oral PDEs ($\mu\text{g}/\text{day}$)	Concentration ($\mu\text{g}/\text{day}$)	Spiked Recovery	RSD
Tixylix	^{75}As	15	<LoD (4.80×10^{-5})	95.25	5.03
	^{111}Cd	5	5.96 ± 0.022	95.33	4.07
	^{202}Hg	30	<LoD (5.85×10^{-4})	97.73	3.07
	^{208}Pb	5	20.93 ± 0.035	95.89	4.09
	^{59}Co	50	13.13 ± 0.048	96.44	1.15
	^{60}Ni	200	10.01 ± 0.10	96.31	2.45
	^{51}V	100	<LoD (1.59×10^{-4})	98.26	4.10
Calpol SixPlus	^{75}As	15	<LoD (4.80×10^{-5})	96.86	5.06
	^{111}Cd	5	<LoD (1.20×10^{-5})	101.4	4.51
	^{202}Hg	30	18.10 ± 0.057	98.57	3.21
	^{208}Pb	5	50.97 ± 0.033	100.41	3.98
	^{59}Co	50	14.45 ± 0.048	103.48	5.14
	^{60}Ni	200	<LoD (7.80×10^{-5})	102.48	4.41
	^{51}V	100	<LoD (1.59×10^{-4})	97.93	2.89
Nelsons Sootha	^{75}As	15	<LoD (4.80×10^{-5})	99.53	3.27
	^{111}Cd	5	1.45 ± 0.050	103.85	4.79
	^{202}Hg	30	<LoD (5.85×10^{-4})	101.54	4.27
	^{208}Pb	5	10.33 ± 0.067	99.13	4.98
	^{59}Co	50	3.58 ± 0.052	105.06	1.85
	^{60}Ni	200	2.73 ± 0.083	101.56	1.22
	^{51}V	100	<LoD (1.59×10^{-4})	103.26	4.17
Calcough	^{75}As	15	<LoD (4.80×10^{-5})	99.61	3.55
	^{111}Cd	5	7.57 ± 0.051	96.73	2.95
	^{202}Hg	30	8.20 ± 0.028	95.53	5.06
	^{208}Pb	5	19.02 ± 0.055	96.87	4.61
	^{59}Co	50	4.63 ± 0.048	97.89	4.18
	^{60}Ni	200	15.69 ± 0.12	95.53	3.57
	^{51}V	100	<LoD (1.59×10^{-4})	99.26	1.19
Lemsip	^{75}As	15	<LoD (4.80×10^{-5})	96.16	4.43
	^{111}Cd	5	8.49 ± 0.25	96.86	2.17
	^{202}Hg	30	<LoD (5.85×10^{-4})	95.48	5.31
	^{208}Pb	5	21.47 ± 0.16	95.96	4.81

Products	Elements	ICH Q3D oral PDEs (µg/day)	Concentration (µg/day)	Spiked Recovery	RSD
Lemsip, continued	⁵⁹ Co	50	10.87 ± 0.13	99.73	3.29
	⁶⁰ Ni	200	13.67 ± 0.18	95.93	3.33
	⁵¹ V	100	<LoD (1.59X10 ⁻⁴)	96.26	2.68
Superdrug bronchial Balsam	⁷⁵ As	15	<LoD (4.80X10 ⁻⁵)	97.23	4.84
	¹¹¹ Cd	5	10.14 ± 0.079	95.86	2.62
	²⁰² Hg	30	<LoD (5.85X10 ⁻⁴)	95.81	1.59
	²⁰⁸ Pb	5	35.89 ± 0.022	98.46	5.8
	⁵⁹ Co	50	42.29 ± 0.068	96.65	4.48
	⁶⁰ Ni	200	21.86 ± 0.015	95.48	5.19
	⁵¹ V	100	<LoD (1.59X10 ⁻⁴)	95.33	2.85

The results obtained from analysis cold and flu powders as well as antacids are illustrated in Table 3.20 and Table 3.21.

Table 3.20 Elemental impurities (µg/day) in cold and flu powders analysed using ICP-MS-CCT mode (mean ± σ, n=3)

Products	Elements	ICH Q3D oral PDEs (µg/day)	Concentration (µg/day)	Spiked Recovery	RSD
Value Health- with vitamin C	⁷⁵ As	15	<LoD (4.80X10 ⁻⁵)	95.40	0.15
	¹¹¹ Cd	5	<LoD (1.20X10 ⁻⁵)	95.81	0.43
	²⁰² Hg	30	<LoD (5.85X10 ⁻⁴)	96.14	1.79
	²⁰⁸ Pb	5	0.43 ± 0.012	102.11	2.04
	⁵⁹ Co	50	0.54 ± 0.023	100.85	0.42
	⁶⁰ Ni	200	<LoD (7.80X10 ⁻⁵)	99.38	0.12
	⁵¹ V	100	<LoD (1.59X10 ⁻⁴)	103.29	1.16
Boots-with vitamin C	⁷⁵ As	15	<LoD (4.80X10 ⁻⁵)	96.59	0.66
	¹¹¹ Cd	5	<LoD (1.20X10 ⁻⁵)	97.66	0.47
	²⁰² Hg	30	<LoD (5.85X10 ⁻⁴)	96.26	1.01
	²⁰⁸ Pb	5	0.50 ± 0.030	104.81	0.46
	⁵⁹ Co	50	<LoD (9.10X10 ⁻⁵)	96.95	0.27
	⁶⁰ Ni	200	5.83 ± 0.078	98.57	0.48
	⁵¹ V	100	<LoD (1.59X10 ⁻⁴)	100.41	0.36

Products	Elements	ICH Q3D oral PDEs (µg/day)	Concentration (µg/day)	Spiked Recovery	RSD
Beechams Honey and Lemon	⁷⁵ As	15	<LoD (4.80X10 ⁻⁵)	98.16	1.89
	¹¹¹ Cd	5	<LoD (1.20X10 ⁻⁵)	100.5	1.88
	²⁰² Hg	30	5.30 ±0.069	97.15	2.49
	²⁰⁸ Pb	5	<LoD (1.40X10 ⁻⁵)	99.63	1.69
	⁵⁹ Co	50	<LoD (9.10X10 ⁻⁵)	105.19	0.8
	⁶⁰ Ni	200	<LoD (7.80X10 ⁻⁵)	101.64	1.36
	⁵¹ V	100	<LoD (1.59X10 ⁻⁴)	100.33	1.28
Beechams Blackcurrant	⁷⁵ As	15	<LoD (4.80X10 ⁻⁵)	96.47	0.86
	¹¹¹ Cd	5	<LoD (1.20X10 ⁻⁵)	102.45	0.87
	²⁰² Hg	30	4.29 ±0.108	95.69	0.73
	²⁰⁸ Pb	5	<LoD (1.40X10 ⁻⁵)	103.92	1.18
	⁵⁹ Co	50	<LoD (9.10X10 ⁻⁵)	104.42	1.11
	⁶⁰ Ni	200	0.81 ±0.098	95.63	1.04
	⁵¹ V	100	<LoD (1.59X10 ⁻⁴)	96.75	1.34
Lemsip- Breath Easy	⁷⁵ As	15	<LoD (4.80X10 ⁻⁵)	95.12	0.58
	¹¹¹ Cd	5	<LoD (1.20X10 ⁻⁵)	95.00	0.42
	²⁰² Hg	30	5.12 ±0.10	101.79	1.18
	²⁰⁸ Pb	5	2.77 ±0.028	102.44	0.93
	⁵⁹ Co	50	0.63 ±0.013	97.22	0.35
	⁶⁰ Ni	200	<LoD (7.80X10 ⁻⁵)	97.69	0.36
	⁵¹ V	100	14.6 ±0.41	98.21	1.03
Lemsip Max-Lemon	⁷⁵ As	15	<LoD (4.80X10 ⁻⁵)	103.23	0.78
	¹¹¹ Cd	5	<LoD (1.20X10 ⁻⁵)	103.45	1.04
	²⁰² Hg	30	5.04 ±0.87	103.98	2.98
	²⁰⁸ Pb	5	3.17 ±0.042	100.15	3.45
	⁵⁹ Co	50	<LoD (9.10X10 ⁻⁵)	101.22	0.67
	⁶⁰ Ni	200	<LoD (7.80X10 ⁻⁵)	104.23	0.73
	⁵¹ V	100	10.02	95.64	3.76

Table 3.21 Elemental impurities ($\mu\text{g/day}$) in antacids analysed using ICP-MS-CCT mode (mean $\pm \sigma$, $n=3$)

Products	Elements	ICH Q3D oral PDEs ($\mu\text{g/day}$)	Concentration ($\mu\text{g/day}$)	Spiked Recovery	RSD
Gaviscon suspension	⁷⁵ As	15	<LoD (4.80×10^{-5})	96.86	2.15
	¹¹¹ Cd	5	<LoD (1.20×10^{-5})	97.59	3.53
	²⁰² Hg	30	<LoQ (1.70×10^{-3})	95.48	4.09
	²⁰⁸ Pb	5	7.98 ± 0.22	96.58	2.75
	⁵⁹ Co	50	1.95 ± 0.06	99.81	1.69
	⁶⁰ Ni	200	6.71 ± 0.14	100.58	1.89
	⁵¹ V	100	<LoD (1.59×10^{-4})	97.62	2.84
Gaviscon chewable tablets	⁷⁵ As	15	0.82 ± 0.011	97.15	3.51
	¹¹¹ Cd	5	0.75 ± 0.036	98.69	1.58
	²⁰² Hg	30	<LoQ (1.70×10^{-3})	100.59	3.51
	²⁰⁸ Pb	5	0.48 ± 0.021	101.98	3.06
	⁵⁹ Co	50	0.83 ± 0.070	96.54	3.51
	⁶⁰ Ni	200	7.96 ± 0.210	98.75	2.94
	⁵¹ V	100	<LoD (1.59×10^{-4})	100.2	4.15
Rennie Extra	⁷⁵ As	15	0.79 ± 0.025	100.26	2.84
	¹¹¹ Cd	5	3.40 ± 0.130	97.59	3.13
	²⁰² Hg	30	<LoQ (1.70×10^{-3})	99.84	4.15
	²⁰⁸ Pb	5	1.73 ± 0.081	100.98	2.06
	⁵⁹ Co	50	0.99 ± 0.041	97.85	2.48
	⁶⁰ Ni	200	19.58 ± 0.26	97.53	2.90
	⁵¹ V	100	<LoD (1.59×10^{-4})	96.54	2.15
Superdrug	⁷⁵ As	15	8.53 ± 0.091	99.56	3.56
	¹¹¹ Cd	5	1.75 ± 0.180	102.35	2.45
	²⁰² Hg	30	<LoD (5.85×10^{-4})	98.56	3.56
	²⁰⁸ Pb	5	7.83 ± 0.56	96.53	1.59
	⁵⁹ Co	50	3.65 ± 0.24	103.58	4.98
	⁶⁰ Ni	200	12.68 ± 0.78	95.83	3.45
	⁵¹ V	100	15.03 ± 1.66	98.48	2.48
Rennie	⁷⁵ As	15	0.62 ± 0.05	100.98	1.48
	¹¹¹ Cd	5	1.88 ± 0.45	96.48	3.87
	²⁰² Hg	30	<LoD (5.85×10^{-4})	97.86	1.59
	²⁰⁸ Pb	5	0.74 ± 0.03	98.64	2.48
	⁵⁹ Co	50	1.86 ± 0.21	102.65	3.48
	⁶⁰ Ni	200	25.43 ± 0.39	96.56	1.45
	⁵¹ V	100	2.69 ± 0.15	98.63	1.89

Products	Elements	ICH Q3D oral PDEs ($\mu\text{g}/\text{day}$)	Concentration ($\mu\text{g}/\text{day}$)	Spiked Recovery	RSD
Bisodol	^{75}As	15	2.70 ± 0.11	97.53	2.15
	^{111}Cd	5	0.73 ± 0.09	98.87	1.85
	^{202}Hg	30	<LoQ (1.70×10^{-3})	103.45	3.68
	^{208}Pb	5	5.75 ± 0.56	99.99	2.35
	^{59}Co	50	1.82 ± 0.24	96.84	3.08
	^{60}Ni	200	38.08 ± 0.96	97.12	2.56
	^{51}V	100	8.788 ± 0.19	102.34	2.05

The final findings regarding the analysed pharmaceutical samples are that the analgesic tablets include Cd, Pd, Co and Ni, but all in acceptable concentrations below the PDEs. However, four out of the six cold and cough remedies will provide a daily concentration of Cd exceeding the regulations PDE of $5 \mu\text{g}/\text{day}$ and all of them provide Pd in concentrations more than the allowed $5 \mu\text{g}/\text{day}$. They also contain Hg, Co and Ni within the allowed PDEs. On the contrary, the cold and flu powders have Hg, Pb, Co, Ni and V in them but in concentrations that do not exceed the PDEs.

Regarding the antacids, all Class 1 and Class 2A elements were quantified and three products contain Pd in concentrations that will provide levels higher than the allowed PDE of $5 \mu\text{g}/\text{day}$ if the maximum daily dose is consumed.

Furthermore, even for the elements that were quantified in levels not exceeding their PDEs, in some products their concentrations in the maximum daily dose will provide about half the allowed PDE or more, like for example, Co in Superdrug bronchial Balsam and Pb in Lemsip cold and flu powders.

3.4 Conclusion

The developed ICP-MS method was successfully validated with *NIST 3280*. Excellent recoveries between 95-105% with good repeatability expressed as RSD of less than 5% for all elements were obtained with minimal interferences. Those limits met the regulations requirements.

The calculated LODs and LOQs were below the targeted limits, which also support the method suitability for EI determination.

The results obtained from the analysed pharmaceutical products show the need for validated methods to meet the new guidelines requirements and produce pharmaceutical products with minimum hazardous elements for human consumption. This is needed to avoid the toxic effects of elements like Pb for example, which was found in nine of the tested products in concentrations exceeding the allowed PDE of 5 µg/day and the exposure to it may cause gastrointestinal problems, anaemia, high blood pressure and sometimes even kidney dysfunction(6, 7).

Chapter 4

Speciation of Arsenic in Antacids

Using Reversed Phase HPLC-ICP-

MS

4. Speciation of Arsenic in Antacids Using Reversed Phase HPLC-ICP-MS

4.1 Introduction

To assess the 'risk factor' that is discussed within the regulation, speciation is suggested in cases where individual species may present an increased risk(10). A literature review of the area shows no published work on pharmaceutical products and speciation of metals as impurities, except for the speciation of arsenic in one injectable medication used for the treatment of visceral leishmaniasis(202).

The following work seeks to assess the species present in antacids since it is already known that As is present as demonstrated by the data provided in Section 3.4 and no information is available on the species present. These products are known to use sodium alginate to form a protective barrier for the stomach. The alginate maybe be seaweed derived, which is well known to contain As(206, 216, 296). As these papers clearly indicate the presence of the most toxic form As^{III} , it is essential to assess the species present in antacids to assess the risk and to see if the As is present in the most toxic form or not.

Several coupled separation and detection techniques have been used for arsenic speciation in numerous samples. ICP is one the most effective sources for elemental analysis and it is easy to couple with chromatographic techniques such HPLC. HPLC/ICP-OES is used in some studies for speciation. However, due to the higher sensitivity and wider linear dynamic range of ICP-MS; HPLC/ICP-MS is more commonly used and becomes favoured for this purpose due to the fact that the level

of elements in samples, whether they were environmental, pharmaceutical or medical is usually low(221, 297).

Other detection techniques(298) were also used for arsenic speciation, including coupled amperometric and ultraviolet detection(224), hydride generation atomic absorption spectrometry and hydride generation atomic fluorescence spectrometry(217, 232, 299).

The chemical nature of arsenic compounds introduces another challenge to arsenic speciation analysis, because the compounds differ in functional groups, molecular sizes and pKa values. For example, in neutral solutions arsenic will primarily exist as oxyanionic acid. The pKa's of the different species will be as follows: As^{III} [H₃AsO₃] pKa's= 9.3, 12.1 and 13.4, As^V [H₃AsO₄] pKa's=2.3, 6.9 and 11.5, MMA pKa's=3.6 and 8.2, DMA pKa's= 6.2, AsB pKa=2.2 as zwitter ion, AsC pKa=unknown as cation and the other arsenosugars as anions(299-301).

Accordingly, many chromatographic systems can be used to separate the species such as different types of ion chromatography methods and that include anion exchange, cation exchange, ion exclusion and ion pair chromatography(215). Reverse phase chromatography(302) was also used as well as combination of two or more techniques to achieve complete separation of the various compound(221, 241, 300).

Numerous samples were analysed for arsenic species throughout the years whether to comply with regulatory guidelines or to help assessing toxicity. Common environmental samples include air, water, soil and sediments(206, 220, 301, 303-305). Food related samples are also popular such as food supplements(306, 307),

juice(257, 308), rice(223, 226, 228, 256, 302), leafy vegetables(246, 247), poultry(255), seaweed, algae(33, 240, 309) and fish(219, 241). In addition to biologicals(4) like human hair, nails(225) and urine(53, 310).

In this work, a method to speciate four arsenic compounds; As^{III}, As^V, MMA and DMA in pharmaceutical antacid products using ion-pair reversed phase HPLC with ICP-MS for detection was developed and validated as pharmaceutical samples of this type do not appear in the published literature.

The analysed antacids can be classified to two major groups; the first is the antacids containing alginic acid or its derivatives. Alginic acid is refined from brown algae and it has cosmetic uses as well as pharmaceutical uses. Pharmaceutical grade alginate can be used in the manufacturing of gels, membranes, microspheres, dressings for wound healing and for controlling drug release. It is also used to create a foam barrier for coating the stomach and reducing oesophageal irritation in antacids(311, 312). The second group is antacids not containing alginates or any of its derivatives.

The antacids were grouped like that because algae and their derivatives are known to contain different arsenic species. In 1999, a study that measured the content of mineral arsenic in ten edible algae from different sources; France, Spain, Japan, Iceland, Australia, China and Hong Kong using bi-dimensional size-exclusion anion exchange HPLC with dual ICP-MS and electrospray MS/MS detection was published. The levels ranged from 1.9 to 62 µg/g(240). Another study conducted in 2009(33) showed that the seagrass *Posidonia oceanica* from the Mediterranean coast contains quantifiable concentrations of As^V, MMA, DMA, AsB and arsenoglycerol sugar. The species with the highest concentration was As^V = 0.366±0.008 µg/g. In the same study,

the brown algae *Durvillaea antarctica* and *Lessonia nigrescens* from the Chilean coast were also analysed. As^{III}, As^V, DMA and other arsenosugars were quantified in *Durvillaea antarctica* with As^{III} being the inorganic species with the highest concentration that is $0.304 \pm 0.090 \mu\text{g/g}$. For *Lessonia nigrescens*, the species with the highest concentration was As^{III} = $105 \pm 8 \mu\text{g/g}$. The only other species that was quantified was As^V. In this mentioned study anion and cation exchange HPLC-ICPMS were used for analysis(33).

In this work, arsenic was speciated in antacids using ion-pair reversed-phase chromatography, a technique where an ion-pairing agent is used to help retain ionic analytes and separate them.

4.2 Experimental

4.2.1 Reagents and Materials

See Sections 2.2.1 and 3.2.1.

Standard solutions of the following chemicals were prepared in water: sodium meta arsenite (As^{III}) (Sigma-Aldrich, USA), sodium arsenate (As^V) dibasic heptahydrate (Sigma-Aldrich, India), monosodium acid methane arsonate (MMA) sesquihydrate (Supelco, USA) and cacodylic acid (DMA) (Sigma-Aldrich, Israel). Aqueous stock solutions of the arsenic species were prepared at a concentration of 1 mg/L as As and stored in the dark at 4°C. Multispecies calibration standard solutions in water and 0.3 M phosphoric acid were freshly prepared from the stock solutions to get concentrations ranging from 1 to 50 ng/mL in addition to a blank.

Two mobile phases were tested based on previous studies(53, 217, 223, 302, 313) that performed As species separation using reversed phase chromatography. The

first mobile phase (mobile phase-1) consisted of 10mM sodium 1-butanedisulfonate (Sigma-Aldrich, Switzerland), 4mM malonic acid (Sigma-Aldrich, Japan), 4mM tetramethyl ammonium hydroxide pentahydrate (Sigma-Aldrich, USA), 5mM potassium dihydrogen orthophosphate (KH_2PO_4) (Fisher scientific, UK) and 0.05% acetonitrile (HPLC grade, Sigma-Aldrich, Israel). The second mobile phase (mobile phase-2) consisted of 10mM tetrabutylammonium (TBA) phosphate monobasic (Sigma-Aldrich, USA), 1mM malonic acid, 20mM potassium dihydrogen orthophosphate and 2% methanol (HPLC grade, Sigma-Aldrich, UK). The pH was adjusted using HCl and potassium hydroxide (Sigma-Aldrich, USA). The mobile phase was filtered through a 0.45 μm nylon membrane filter (Whatman, USA) and degassed before use.

4.2.2 Samples

Three antacid products that contain alginate derivatives and three antacids without alginates were acquired from local retailers in the Liverpool area. For more details, see Section 3.2.2.

4.2.3 Instrumentation

See Sections 2.2.3 and 3.2.3.

For liquid chromatographic separation a Thermo 4000 series HPLC pump, consisted of an injector fitted with a 100 μl PEEK injection loop and equipped with a Spectra autosampler (Thermo Fisher Scientific, USA) were used. The exit of the HPLC column was directly connected to the nebulizer of the ICP-MS with polyetheretherketone (PEEK) tubing (HPLC-ICP-MS). For reversed phase chromatography, a Phenomenex Kinetex C_{18} column (100X4.60 mm, 5 μm particles) was tested and a Phenomenex

Gemini C₁₈ column (250X4.60 mm, 4 µm particles) was used for optimum separation. Data was collected using Thermo-Plasma Lab Software.

The pH of the mobile phase was measured using pH 211 microprocessor pH meter (Hanna Instruments, UK). A benchtop centrifuge (Hettich, Germany) was used for the extracted samples prepared for arsenic speciation to separate the liquid from the solid residue.

4.2.4 HPLC analytical figures of merit and validation

The HPLC developed method was validated according to ICH Q2B guidelines(267).

4.2.4.1 Linearity and range

Linearity was studied in the range of 1 to 50 ng/mL using six standards with concentrations covering the specified range assayed in triplicate. The correlation coefficient (R^2), y-intercept and slope of the regression line were calculated.

4.2.4.2 Accuracy

Accuracy was assessed using nine determinations over three concentration levels (1, 10 and 50 ng/mL) covering the specified range and was assayed in triplicate. The percent recoveries of the four species were calculated for the three concentrations. The samples were mass balanced using the ICP-MS data.

4.2.4.3 Precision

Repeatability was assessed using the same procedure for the determination of the accuracy described in Section 4.2.4.2. For intermediate precision, the procedure was repeated for three consecutive days. The standard deviation and relative standard deviation were calculated for each type of the investigated precision.

4.2.5.4 Limits of detection (LoDs) and limits of quantification (LoQs)

With HPLC-ICP-MS, the signals generated are transient thus needed to be read using chromatography software incorporated into the transient signal components of the ICP-MS X Series. In each case, the peak area was used as the signal. Limits of detection (LoD) and Limits of quantification (LoQ) were calculated as described in Miller and Miller(268).

4.2.5 Sample preparation

4.2.4.1 Sample preparation for total determination of arsenic content

See Sections 2.2.4 and 3.2.4.

4.2.4.2 Optimisation of sample preparation for arsenic speciation

Arsenic was extracted using different temperatures and media describe in previous studies(216, 256, 306, 307). Ground solid samples (0.5g) were accurately weighed and extracted with 10 mL of the extraction medium. Water(223) and 0.3 M H_3PO_4 (306) were used as extraction medium. The tested methods include using SPD-80 microwave-assisted extraction procedure at a maximum temperature of 80°C (216, 256) and 95°C(306) for 30 minutes. Another method was to increase the temperature gradually starting from 55°C for 10 minutes, 75°C for 10 minutes and finally 95°C for 30 minutes(307), one hour and two hours. The samples were then centrifuged at 3600 rpm for 20 min, then the supernatant was filtered using 0.45 μ m PTFE membrane filter and assayed. In all subsequent work, H_3PO_4 was used as the extraction medium.

Arsenic was extracted from three samples from each product. In addition, three spiked samples (with 10 ng/mL of each species) were also prepared and the assay of all samples was performed in triplicate.

4.3 Results and discussion

A mixture of As^{III}, As^V, MMA and DMA with a concentration of 1 ng/mL was used to test the separation efficiency of the two selected mobile phases adjusted at different pH values using two different reversed phase columns. The columns were conditioned as the following:

Sequential elution of: 1) 100% methanol for 2 hrs, 2) 50% methanol for 2hrs, 3) 10% methanol for 2 hrs and finally, 4) the mobile phase for 3 hrs at a flow rate of 0.75 mL/min(302).

4.3.1 Testing the separation efficiency of mobile phase-1

Mobile phase-1 that consisted of 10mM sodium 1-butanefulfonate, 4mM malonic acid 4mM tetramethyl ammonium hydroxide pentahydrate 5mM KH₂PO₄ and 0.05% acetonitrile was tested as it had been reported that it could separate the four selected arsenic species in about 5 minutes isocratically(223, 254, 302). Gradient elution can cause baseline drift and thus extra time is required to reach equilibrium causing delay and increasing the total time needed for the analysis. In addition, this suggested method does not require a combination of two or more chromatographic techniques(223, 302) such as those that use of both anionic and cationic exchange chromatography for the same samples(33, 237). However, using similar mobile phase with two different columns was found to be inefficient in separating the four species, as the resolution between the peaks was poor as illustrated in Figure 4.1 and 4.2.

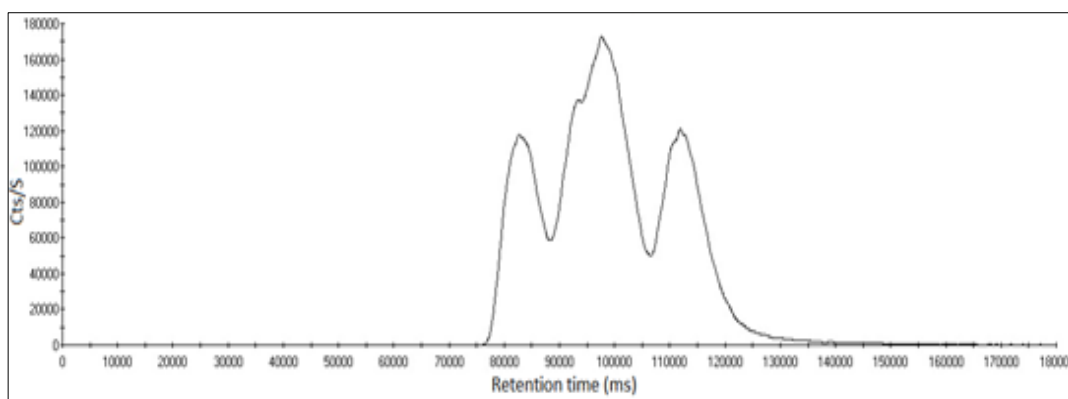


Figure 4.1 Obtained chromatogram for a mixture of As^V , As^{III} , MMA and DMA using mobile phase-1 pH =2.7 with Kinetex C_{18} column

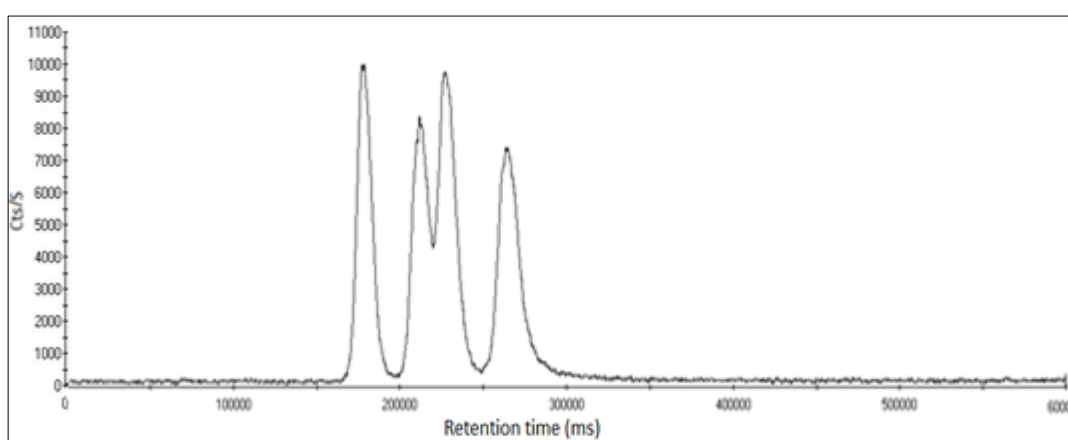


Figure 4.2 Obtained chromatogram for a mixture of As^V , As^{III} , MMA and DMA using mobile phase-1 at pH =2.7 with Gemini C_{18} column

Table 4.1 summarises the tested chromatographic conditions using mobile phase-1

Table 4.1 Tested chromatographic conditions using mobile phase-1

Mobile phase	10 mmol/L sodium 1-butanefulfonate, 4 mmol/L malonic acid, 4 mmol/L tetramethylammonium hydroxide, 5 mmol/L KH_2PO_4 and 0.05% acetonitrile
pH	2, 2.7*, 3, 4 and 4.5
Flow rate	0.75 ml/min
Columns	1. Phenomenex Kinetex C_{18} column (100X4.60 mm, 5 μm particles) 2. Phenomenex Gemini C_{18} column (250X4.60 mm, 4 μm particles)
Column temperature	Ambient
Injection volume	20 μL

*pH=2.7 is the pH recommended by the researches from which this mobile phase was adopted(302)

4.3.1.2 Optimisation of mobile phase-1

4.3.1.2.1 Effect of pH

The degree of arsenic species ionisation at different pH depends on their pKa.

Table 4.2 illustrates the structure and pKa of As^{III}, As^V, MMA and DMA.

Table 4.2 The structure and pKa of As^{III}, As^V, MMA and DMA

Abb.*	Name	Structure	pKa
As ^{III}	Arsenite (arsenous acid)	$\begin{array}{c} \text{OH} \\ \\ \text{As} \\ / \quad \backslash \\ \text{HO} \quad \text{OH} \end{array}$	9.3, 12.1, 13.4
As ^V	Arsenate (arsenic acid)	$\begin{array}{c} \text{O} \\ \\ \text{HO} - \text{As} - \text{OH} \\ \\ \text{OH} \end{array}$	2.3, 6.9, 11.5
MMA	Monomethylarsonic acid	$\begin{array}{c} \text{O} \\ \\ \text{---As---OH} \\ \\ \text{OH} \end{array}$	3.6, 8.2
DMA	Dimethylarsinic acid	$\begin{array}{c} \text{O} \\ \\ \text{---As---OH} \\ \\ \text{---} \end{array}$	6.2

*Abbreviation

As^{III} has a pKa value greater than 9, so at pH < 7 it will be present predominantly in the undissociated form as H₃AsO₃[°]. As^V will be mainly present as H₂AsO₄⁻ at pH between 3 and 7, and as HAsO₃²⁻ at pH >7(314).

In case of the methylated species, MMA will be present in both dissociated (CH₃AsO(OH)O⁻) and undissociated ,(CH₃AsO(OH)₂) forms at pH between 3 and 4 at higher pH the degree of ionisation of MMA will increase. DMA will be present in both

dissociated ((CH₃)₂As(O)O⁻) and undissociated (CH₃)₂As(O)OH) forms at pH between 6 and 7(314). Figure 4.3 show the ionisation process of As^{III}, As^V, MMA and DMA at different pH values.

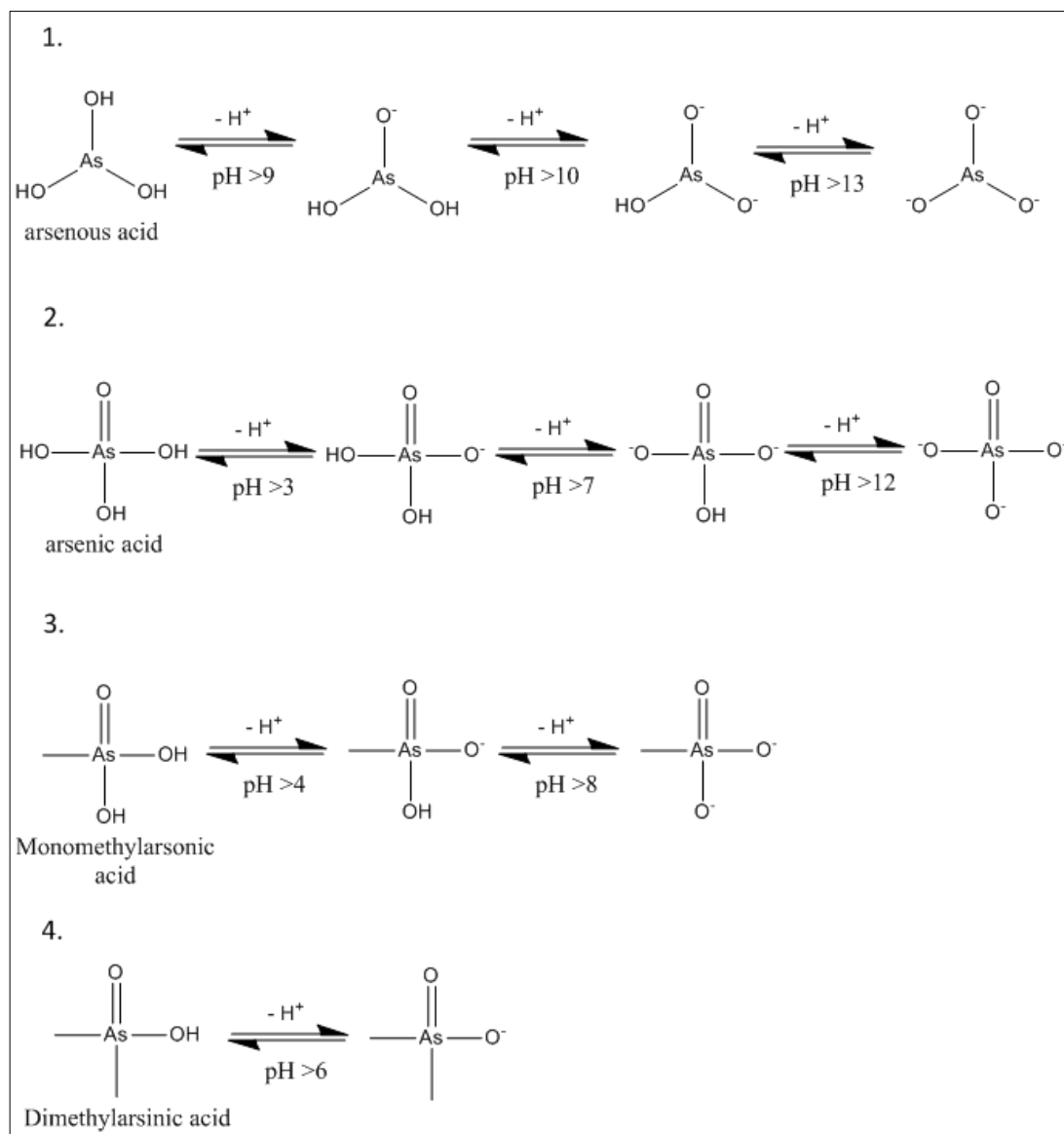


Figure 4.3 Ionisation of 1. As^{III}, 2. As^V, 3. MMA and 4. DMA at different pH

The degree of the species ionisation affects its interaction with the ion-pairing agent in the mobile phase and thus its retention time. The ionic end of ion-pairing agent interacts with the ionised arsenic species and its hydrophobic component interacts with the reversed-phase column.

In mobile phase-1, more than one ion pairing agent were added. Firstly, sodium 1-butanesulfonate was added to form ion pairs with cationic analytes, because in the study from which this mobile phase was adopted(302), tetramethylarsonium and arsenocholine were included. Figure 4.4 is a general illustration of the interaction between the positively charged arsenic species and 1-butanesulfonate.

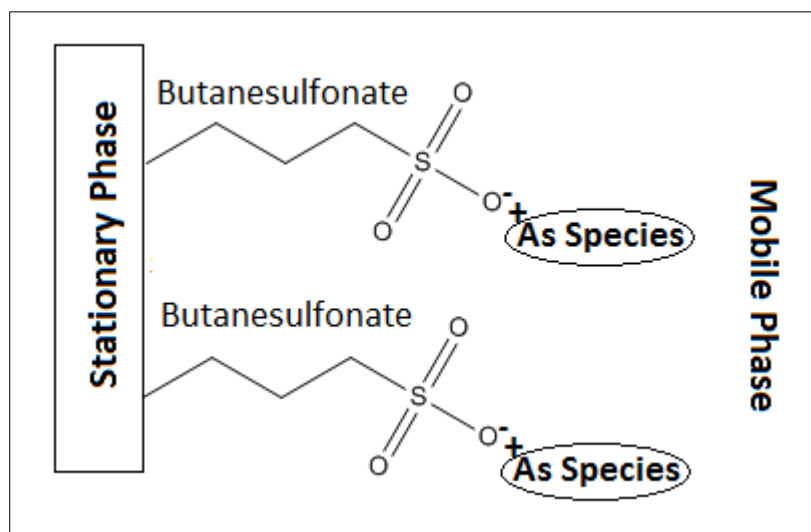


Figure 4.4 A general illustration of the interaction between the positively charged arsenic species and butanesulfonate as an ion pairing agent used with reversed phase chromatography

Secondly, tetramethylammonium hydroxide was added as ion-pairing agent to interact with anionic analytes. Figure 4.5 is a general illustration of the interaction between negatively charged arsenic species and tetramethylammonium ion.

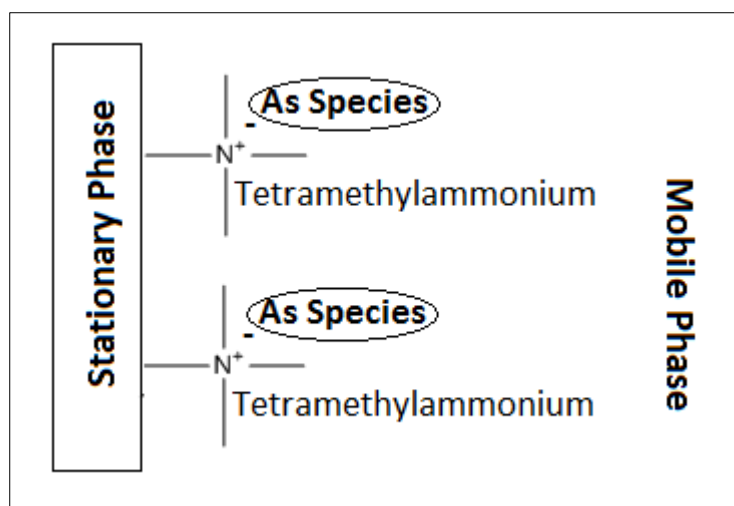


Figure 4.5 A general illustration of the interaction between the negatively charged arsenic species and tetramethylammonium as an ion pairing agent used with reversed phase chromatography

Higher ionisation of the analyte facilitates its interaction with the ion-pairing agent and thus its interaction with the stationary phase, which becomes governed by the hydrophobic interaction between the ion-pairing agent hydrophobic component and the relatively non-polar stationary phase.

pH 2.7 was recommended in the referenced paper(302) and to investigate the effect of pH on the separation of the four selected arsenic species, pH values of 2, 2.7, 3, 4 and 4.5 were tested.

Higher pH was reported to shorten the retention time of MMA and DMA with this mobile phase(302), so the effect of pH was investigated in values not exceeding 5.

Phenomenex Kinetex C_{18} column was assessed first with mobile phase-1 at different pH values in an attempted to separate the four arsenic species in the shortest possible time. The obtained chromatograms are represented in Figure 4.6.

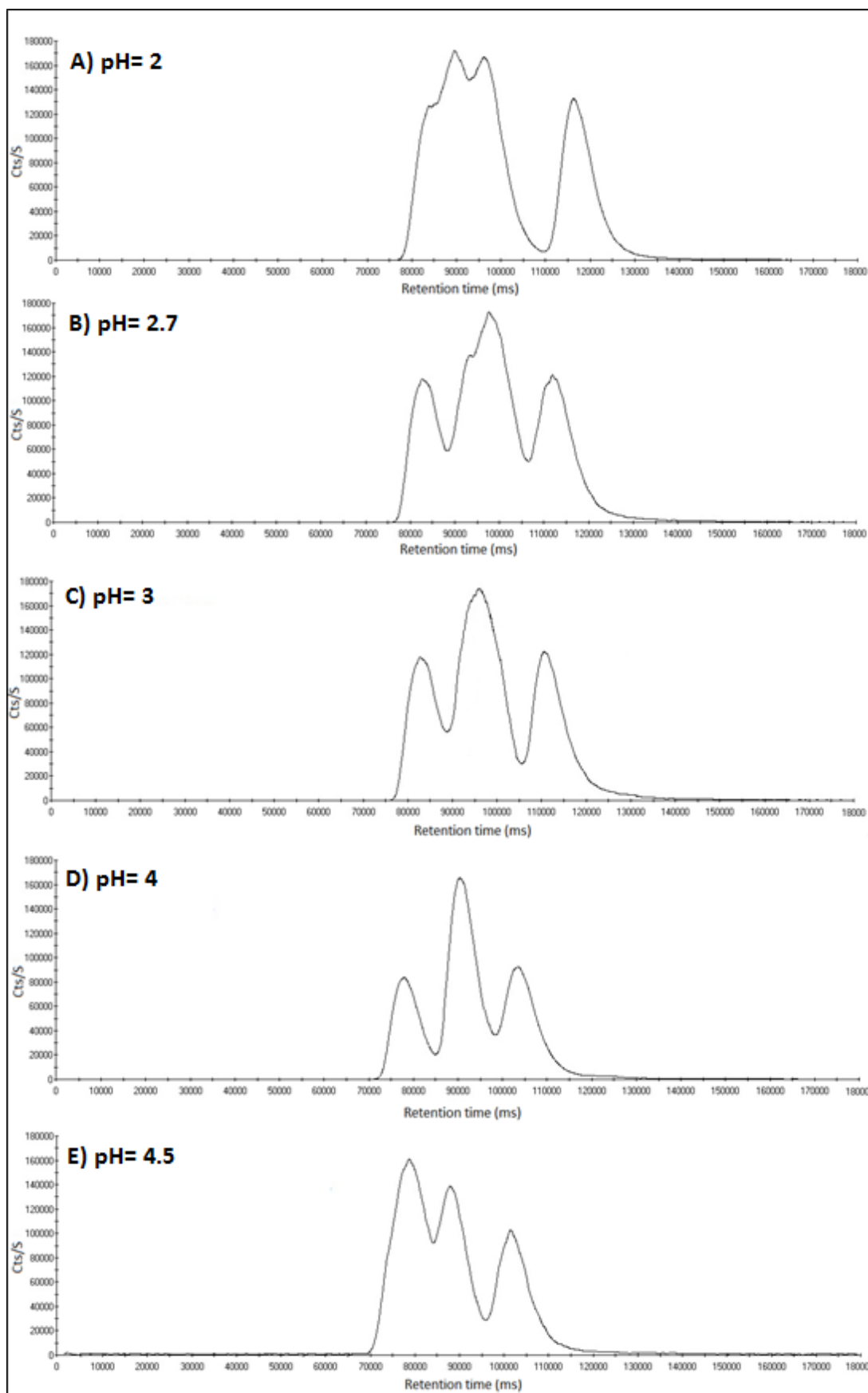


Figure 4.6 Chromatograms obtained using mobile phase-1 with Kinetex C₁₈ column at pH A)2, B)2.7, C)3, D)4 and E)4.5 respectively

To know the order of the species elution, a standard for each species was injected separately as well as a mixture of the four species. The result is illustrated in Figure

4.7.

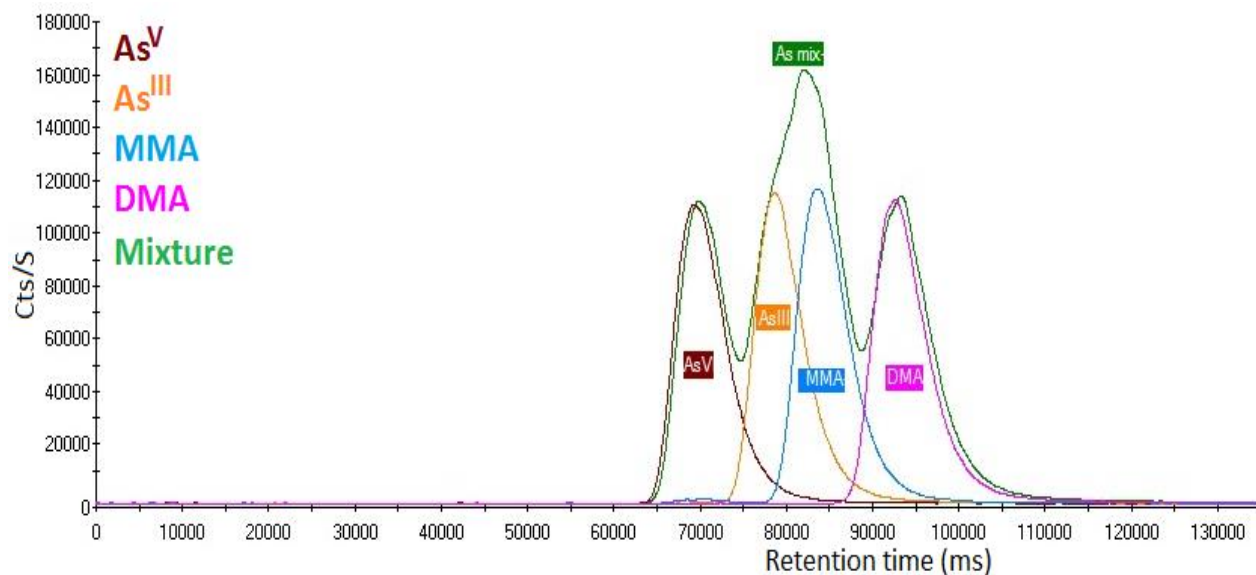


Figure 4.7 Order of elution of As^V, As^{III}, MMA and DMA using mobile phase-1 at pH=3 with with Kinetex C₁₈ column

As^V was the first species to elute followed by As^{III}, MMA and finally DMA. The elution order is similar to that obtained by Narukawa's et al(302). As^{III} and MMA peaks overlapped as illustrated in Figure 4.7. It was stated in the referenced work that As^{III} and MMA were very close to each other and overlapped after the analysis of multiple samples especially those containing high concentrations of sugars or proteins(302).

From the obtained chromatograms (Figure 4.6), using mobile phase-1 with Phenomenex Kinetex C₁₈ column did not separate the four arsenic species. This might be due to the need of more theoretical plates to achieve better separation, so Phenomenex Gemini C₁₈ column was used with the same mobile phase adjusted at different pH values to evaluate the separation efficiency of the method. Figure 4.8 represents the obtained chromatograms using mobile phase-1 adjusted to different pH values with Phenomenex Gemini C₁₈ column.

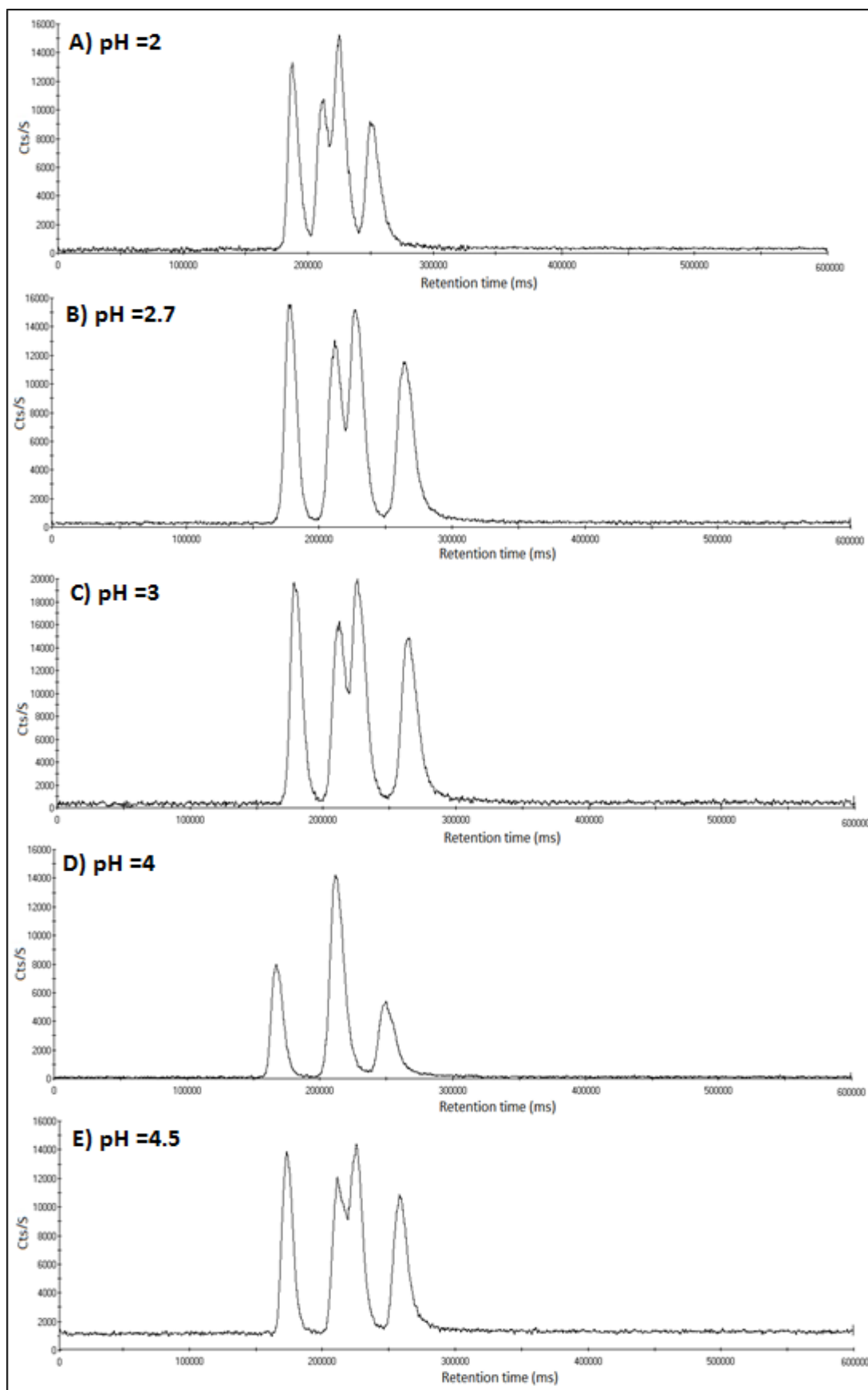


Figure 4.8 Chromatograms obtained using mobile phase-1 with Gemini C₁₈ column at pH A)2, B)2.7, C)3, D)4 and E)4.5 respectively

Even with the Phenomenex Gemini C₁₈ column, the arsenic species did not completely separate, as As^{III} and MMA peaks overlapped. In addition, changing the mobile phases' pH changed the retention times of As^V MMA and DMA with both columns, but without improving the separation. This can be explained due the reduced hydrophobic characters of the tested cationic ion pairing agent; tetramethylammonium hydroxide leading to the co-elution of As^{III} and MMA. Similar observations regarding the ion-pairing agent hydrophobic characteristics were noted by Afton et al(250). Afton et al(250) investigated tetraethyl ammonium perchlorate as an ion-pairing agent for the separation of Se and As in a method applied to river water, plant extract and urine matrices.

As a result, TBA which is an ion-pairing agent with more hydrophobic characteristics was used. Mobile phase-2 was adopted from the work of Do et al(53) and Hakala and Pyy(313).

4.3.2 Testing the separation efficiency of mobile phase-2

Mobile phase-2 consisted of 10mM TBA, 1mM malonic acid, 20mM potassium dihydrogen orthophosphate and 2% methanol. Although malonic acid was not included in the studies from which this mobile phase was adopted(53, 313), it was kept in the mixture because it was reported to act as a buffering agent that can improve arsenic species separation(203, 254, 302). The pH reported to be suitable for this mobile phase containing TBA was ranging between 6 and 7(53, 313), so this mobile phase was tried at pH=6.

Phenomenex Kinetex C₁₈ column and Phenomenex Gemini C₁₈ column were tested in a similar way to mobile phase-1. The results are illustrated in Figure 4.9.

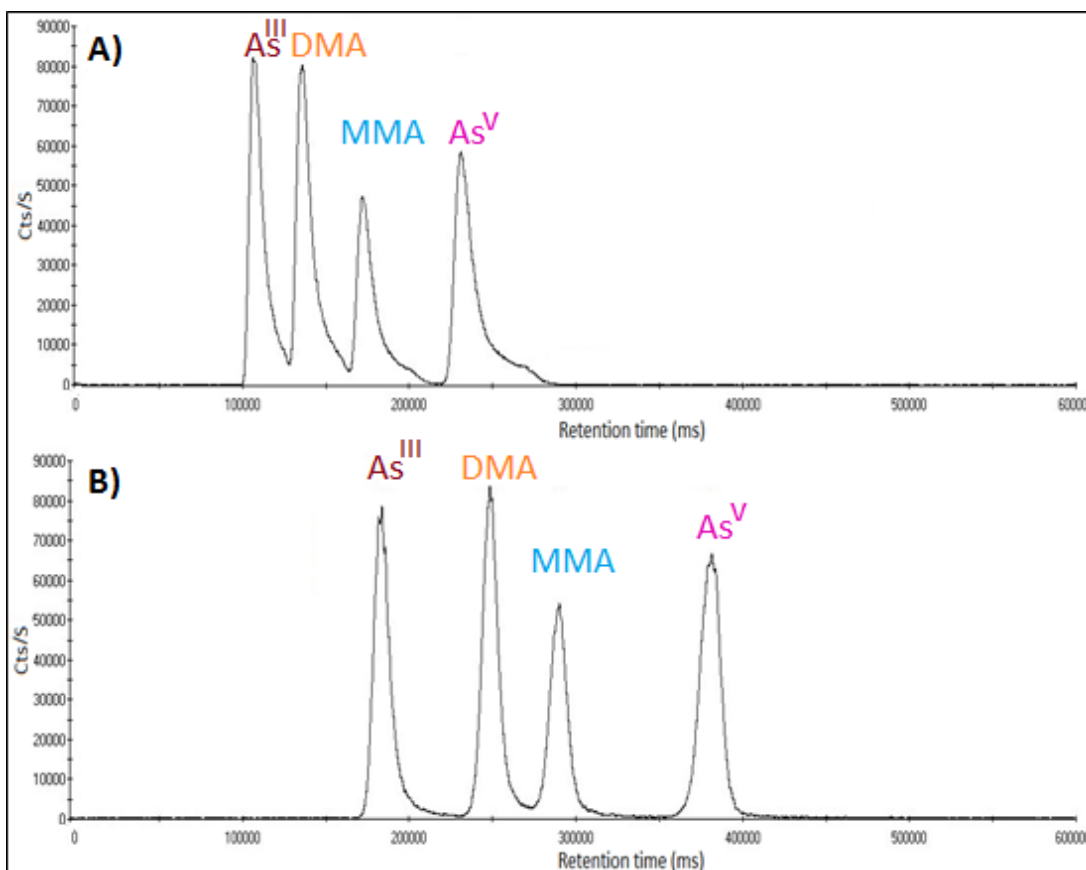


Figure 4.9 Chromatograms obtained using mobile phase-2 at pH=6 with A) Phenomenex Kinetex C₁₈ column and B) Phenomenex Gemini C₁₈ column

From Figure 4.9 mobile phase-2 was able to separate the four arsenic species of interest. The peaks resolution was calculated based on the following equation:

$$R_s = \frac{1.18(t_{r1} + t_{r2})}{W_{0.5,1} + W_{0.5,2}} \dots \text{Equation 4.1 (315)}$$

Where R_s is the resolution, t_r is the peak retention time ($t_{r1} < t_{r2}$) and $W_{0.5}$ is the full width at half the peak's maximum height. It is calculated for each two adjacent peaks.

A resolution ≥ 1.5 is considered acceptable(315).

Table 4.3 illustrates the resolution of the four arsenic species using Phenomenex Kinetex C₁₈ column and Phenomenex Gemini C₁₈ column.

Table 4.3 The resolution of the four arsenic species using mobile phase-2 with Phenomenex Kinetex C₁₈ column and Phenomenex Gemini C₁₈ column

	Phenomenex Kinetex C ₁₈	Phenomenex Gemini C ₁₈
As ^{III} - DMA	1.45	2.43
DMA - MMA	1.49	1.49
MMA - As ^V	1.82	2.79

As illustrated in Figure 4.9 and Table 4.3, the resolution enhanced using Phenomenex Gemini C₁₈ column and so it was used for the rest of experiments. However, the resolution for DMA and MMA is almost 1.5, so further experiments were carried out to improve the method's separation efficiency.

Table 4.4 summarises the tested chromatographic conditions using mobile phase-2.

Table 4.4 Tested chromatographic conditions using mobile phase-2

Mobile phase	10 mmol/L TBA, 1 mmol/L malonic acid, 20 mmol/L KH ₂ PO ₄ and 2% methanol
pH	3, 4, 5, 6 and 7
Flow rate	1 ml/min
Columns	(1) Phenomenex Kinetex C ₁₈ column (100X4.60 mm, 5 μm particles) (2) Phenomenex Gemini C ₁₈ column (250X4.60 mm, 4 μm particles)
Column temperature	Ambient
Injection volume	20 μL

4.3.2.2 Optimisation of mobile phase-2

4.3.2.2.1 Effect of pH

The effect of different pH values was investigated, because as mentioned before in Section 4.3.1.2.1, different pH can change the ionisation state of the species according to its pK_a value and thus its ability to form ion-pair with TBA. Figure 4.10 is a general illustration of the interaction between the negatively charged arsenic species and TBA.

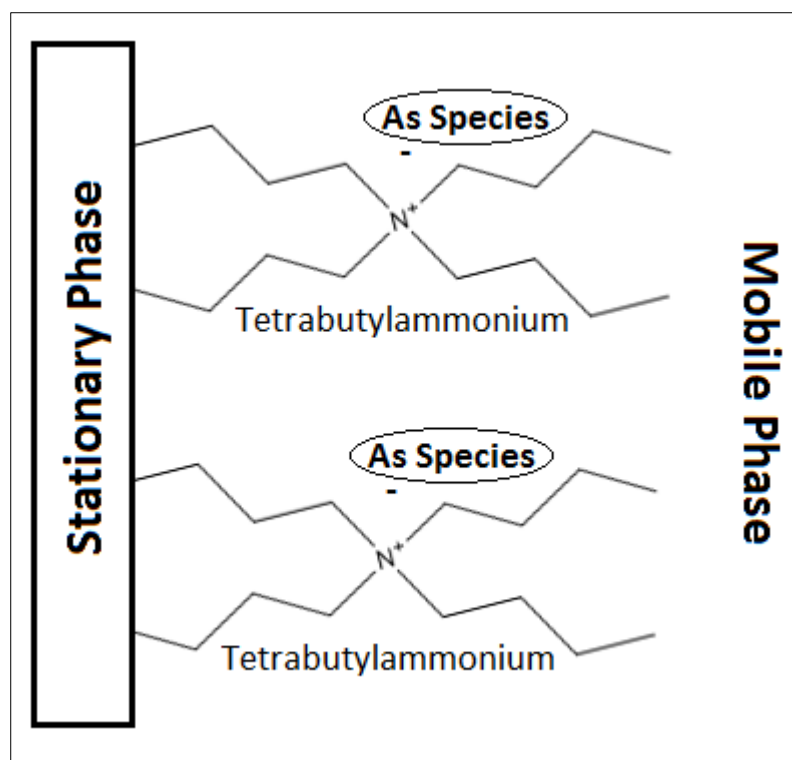


Figure 4.10 a general illustration of the interaction between the negatively charged arsenic species and TBA

To investigate the effect of mobile phase-2 pH on the separation of the four selected arsenic species, pH values of 3, 4, 5, 6 and 7 tested using Phenomenex Gemini C₁₈ column. The result is illustrated in Figure 4.11.

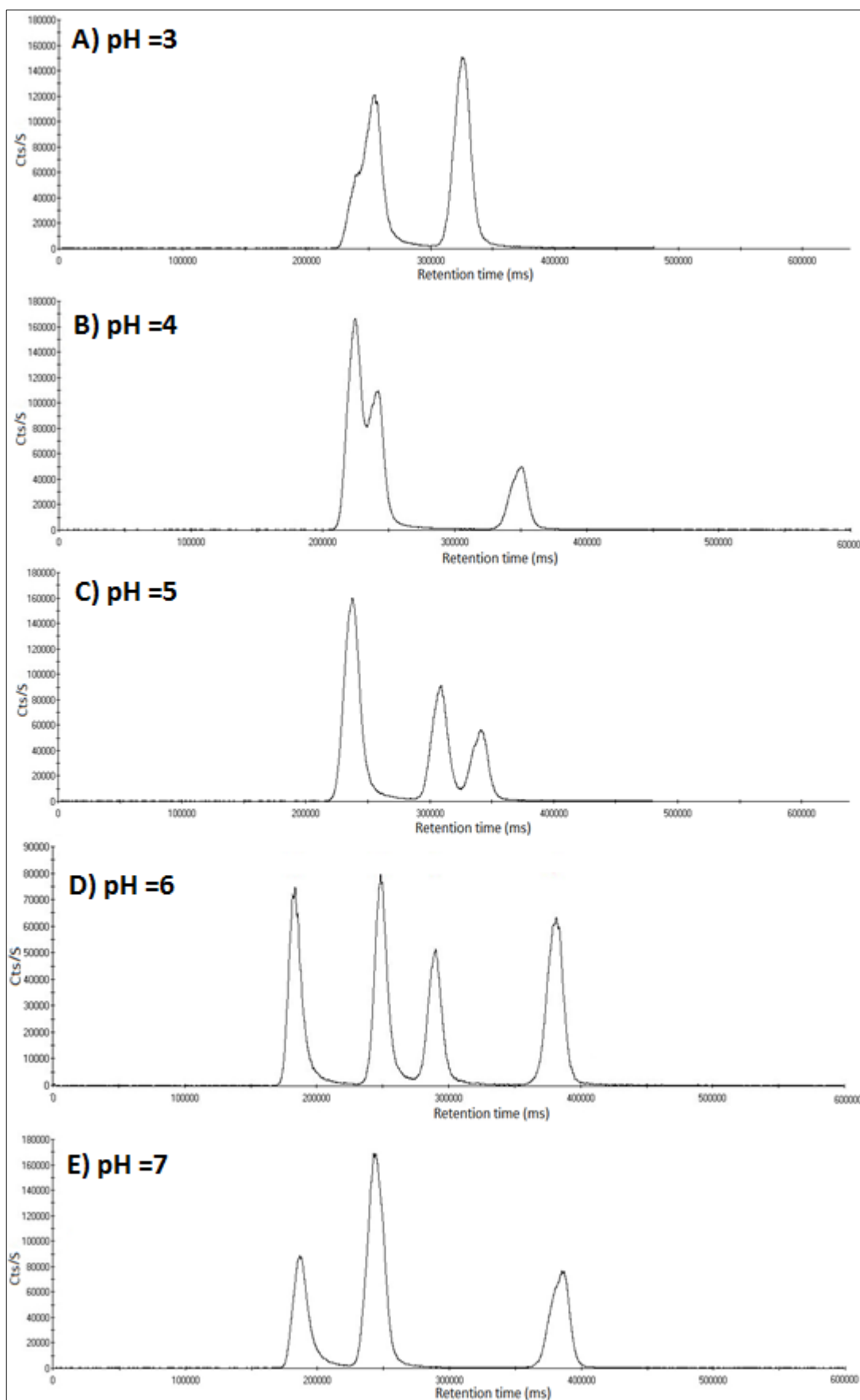


Figure 4.11 Chromatograms using mobile phase-2 with Phenomenex Gemini C₁₈ column at pH A)3, B)4, C)5, D)6 and E)7 respectively.

From the obtained chromatograms, the pH plays an important role in the species separation (see Figure 4.3). At $\text{pH} < 4$, As^{III} and DMA will be present dominantly in their unionised form and thus cannot ion-pair with TBA, so both will co-elute early. As^{V} and partially MMA will become ionised forming an ion-pair with TBA. The resulting neutral complexes will elute according to their hydrophobic interaction with the C_{18} column. At $\text{pH} = 6$, As^{III} still cannot form an ion-pair with TBA, because it will remain unionised, but the rest of the species will be ionised and will form an ion-pair with TBA. However, at $\text{pH} = 7$ MMA and DMA will have similar interaction with the column and thus their peaks overlapped, because at this pH both species will almost completely be ionised thus form an ion-pair with TBA to the same extent and due to their structural similarity their hydrophobic interaction with the C_{18} stationary phase is very similar. Do et al(53) used the same mobile phase at pH 7 to speciate As in urine samples, but in this work, this pH gave poor resolution. The difference in the samples' pH may have accounted for the resolution change. It can also be noticed in the referenced work that MMA and DMA peaks are close to each other(53).

From the obtained pH optimisation results, pH 6 was chosen as the optimum value, and this pH is consistent with a previous work that used a similar mobile phase to separate As species in urine(313). In that study the mobile phase lacked an organic component like methanol or acetonitrile and the early-eluting As^{III} and DMA peaks were close to each other(313). Mobile phases containing TBA as ion-pairing agents and used with reversed phase chromatography were applied to urine samples and water(53, 313), but never applied to pharmaceutical samples.

4.3.2.2.2 Composition of mobile phase-2

The effect of the concentration of the ion-pairing agent itself was studied by comparing the obtained chromatograms when different concentrations of TBA were used in the mobile phase.

TBA concentrations ranging from 0 to 20 mmol/L were investigated. The results are illustrated in Figure 4.12.

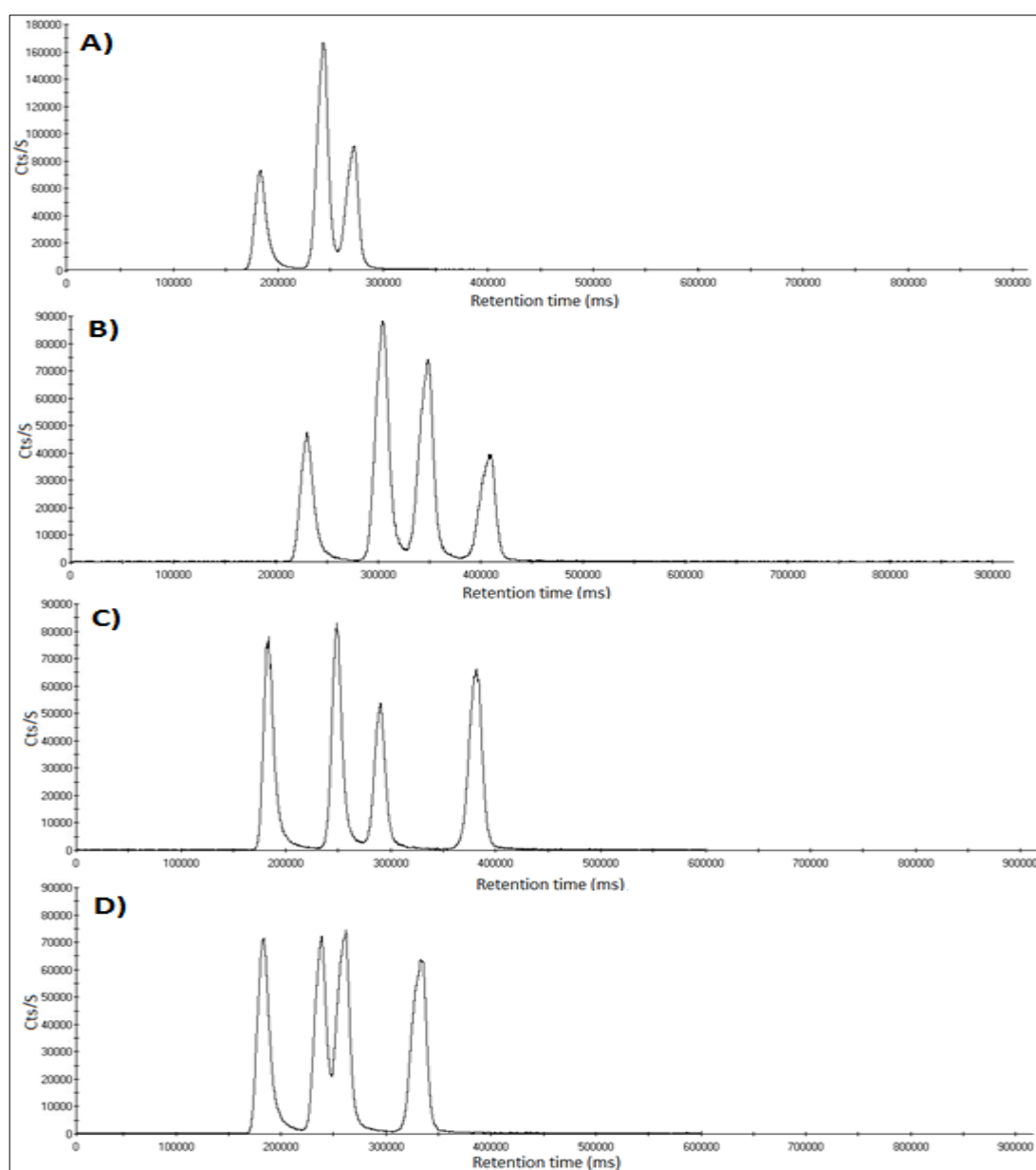


Figure 4.12 Chromatogram obtained using Phenomenex Gemini C₁₈ column + mobile phase-2 containing A) 0 mmol/L TBA, B) 5 mmol/L TBA, C) 10 mmol/L TBA and D) 20 mmol/L TBA

Removing TBA completely caused DMA and MMA peaks to merge and As^V to elute early. Because ion-pairs with hydrophobic tails are not formed to be retained by the stationary phase. As^{III} was not affected as expected.

Reducing the concentration of TBA from 10 mmol/L to 5 mmol/L separated the four species but decreased the resolution between MMA and As^V. On the other hand, increasing TBA concentration to 20 mmol/L made DMA and MMA peaks to overlap.

As a result, TBA concentration of 10 mmol/L was maintained with the rest of the experiments.

The effect of each of the components on the separation efficiency was tested by removing one component each time and studying the produced chromatogram. The first component removed was the buffering agent KH₂PO₄ and that led to delayed elution of the four peaks to more than 10 minutes as seen in Figure 4.13.

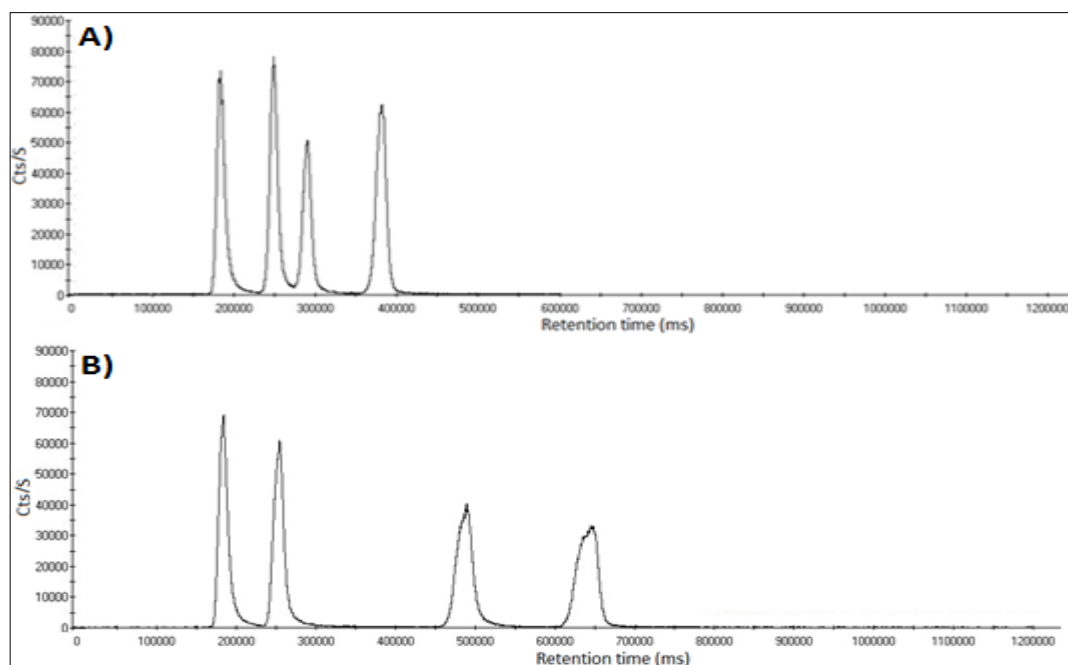


Figure 4.13 Chromatogram obtained using Phenomenex Gemini C₁₈ column column + mobile phase-2 at pH=6. A) 10 mmol/L TBA, 1 mmol/L malonic acid, 20 mmol/L KH₂PO₄ and 2% methanol, B) 10 mmol/L TBA, 1 mmol/L malonic acid and 2% methanol

KH_2PO_4 concentration modifies the ionic force of the mobile phase. MMA and As^{V} elution was delayed with removing KH_2PO_4 , while As^{III} and DMA peaks retention times were not changed (Figure 4.13). As^{III} is present mainly as unionised species at $\text{pH}=6$, so its retention time is not affected and it is eluting first because it lacks the ability to form ion-pair with TBA. Because the run time increased with the removal of the buffering agent, it was kept in further experiments.

The next component removed was malonic acid. The obtained chromatogram is represented in Figure 4.14.

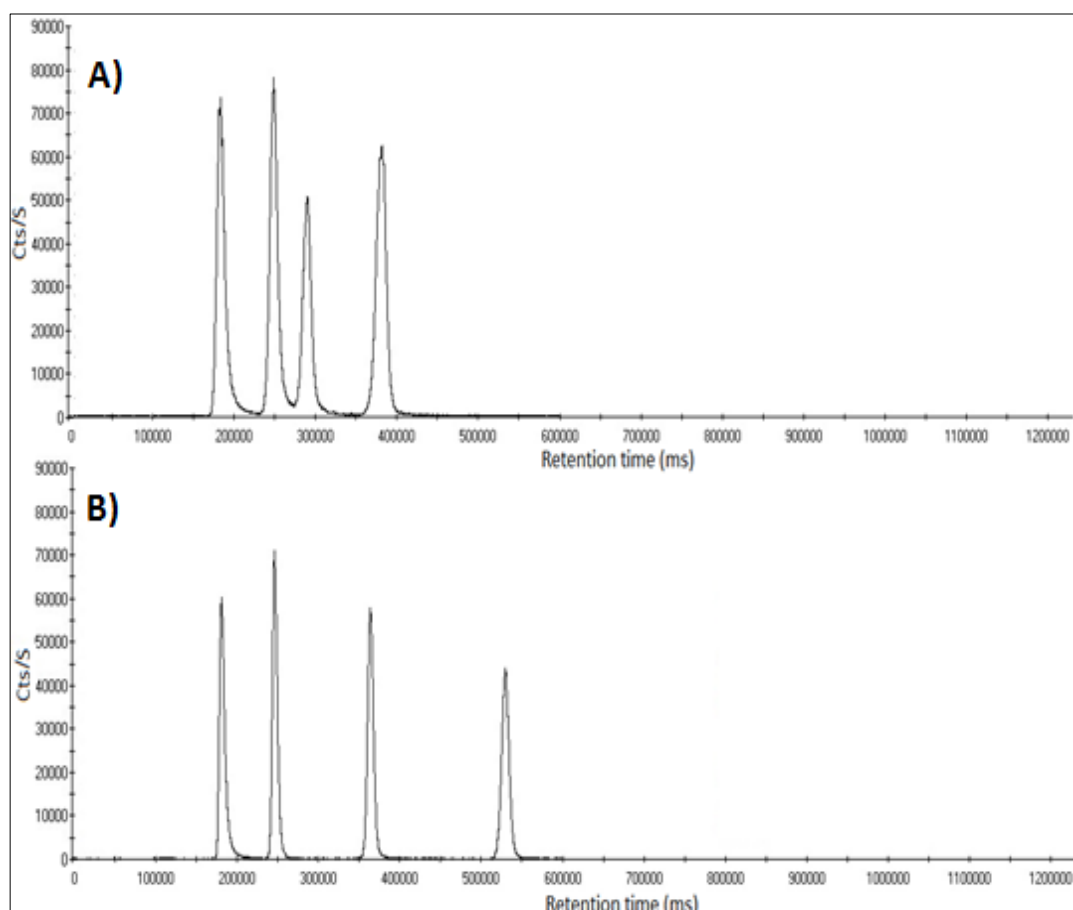


Figure 4.14 Chromatograms obtained using Phenomenex Gemini C_{18} column + mobile phase-2 at $\text{pH}=6$. A) 10 mmol/L TBA, 1 mmol/L malonic acid, 20 mmol/L KH_2PO_4 and 2% methanol, B) 10 mmol/L TBA, 20 mmol/L KH_2PO_4 and 2% methanol

Malonic acid changes the ionic force of the eluent. Removing it from the mobile phase improved the resolution particularly for DMA-MMA. See Table 4.5.

Table 4.5 The resolution of the four arsenic species using Phenomenex Gemini C₁₈ column and mobile phase-2 with and without malonic acid at pH=6

	With malonic acid	Without malonic acid
As ^{III} - DMA	2.43	6.40
DMA - MMA	1.49	11.31
MMA - As ^V	2.77	14.69

Although the total run time increased from 7 minutes to 10 minutes when malonic acid was removed from the mobile phase, the significant improvement in the resolution of DMA and MMA peaks lead to the removal of malonic acid from the mobile phase used with the rest of the experiments. The improvement in peaks resolution can be explained due the fact that malonic acid has a pKa of 2.83 and 5.69, so at pH=6 it will be ionised as illustrated in Figure 4.15.

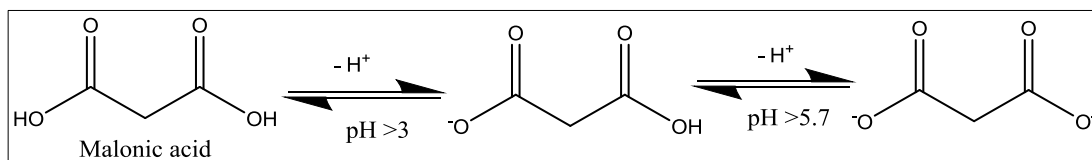


Figure 4.15 Ionisation of malonic acid at different pH

Malonate ions can compete with the negatively charged arsenic species for TBA leading to a decrease in their formation of ion pairs and thus decrease their partitioning with the stationary phase causing a reduction in their retention time.

Finally, a mobile phase that consists only of 10 mmol/L TBA and 2% methanol was tried and it was noticed that As^V was severely affected where its elution was completed after 15 minutes and the resolution of DMA – MMA was reduced, see Figure 4.16.

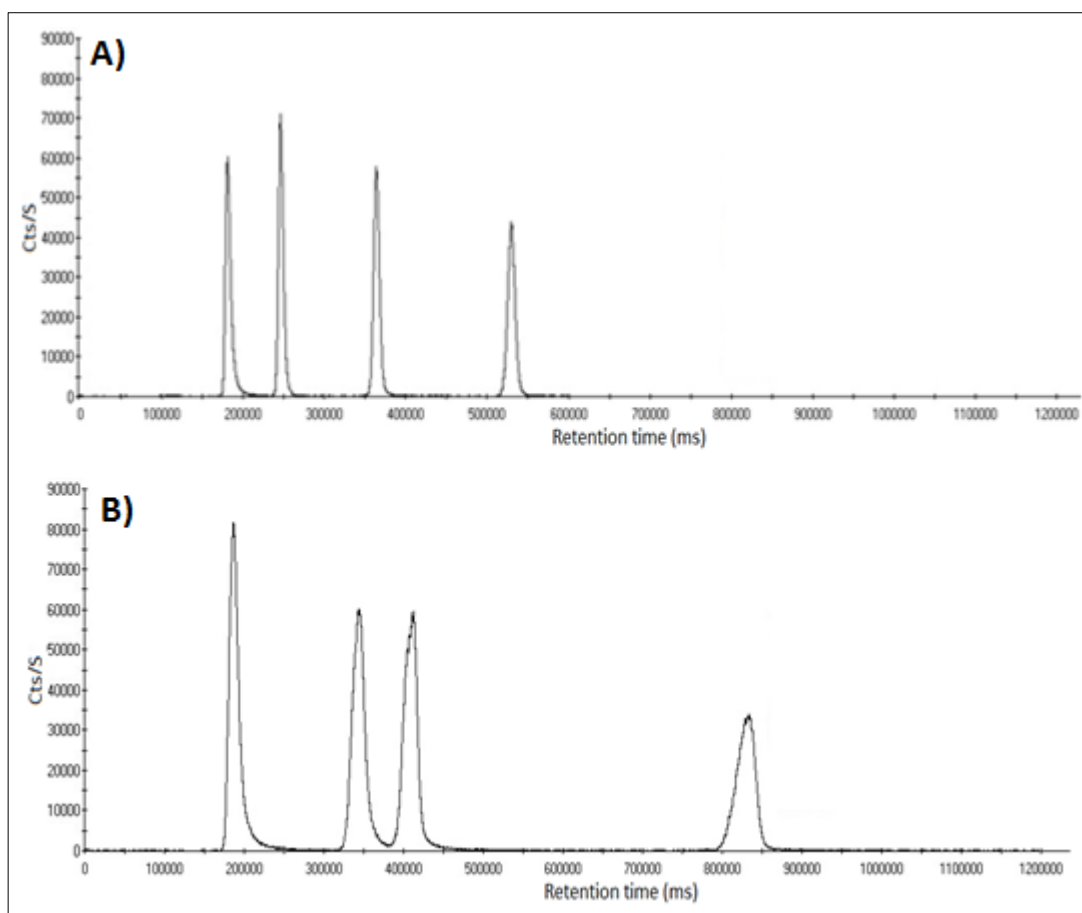


Figure 4.16 Chromatogram obtained using Phenomenex Gemini C₁₈ column + mobile phase-2 at pH=6. A) 10 mmol/L TBA, 20 mmol/L KH₂PO₄ and 2% methanol, B) 10 mmol/L TBA and 2% methanol

These observed changes can be explained as a result of changing the mobile phase's ionic force which has an influence mainly on As^V in addition to the methylated species. Similar effects on the species ion-pair reversed phase separation were observed when changing the ionic strength by increasing or decreasing the concentration of TBA itself and/or the addition of disodium phosphate Na₂HPO₄ and H₃PO₄(53).

2% Methanol was added in all cases to enhance the elution power especially towards As^V. Previous study (53) showed that without an organic solvent As^V will need more than 25 minutes to elute which is not practical for routine analysis(53). A methanol concentration of more than 2% cannot be used in order not to hinder the detection

ability of ICP-MS by affecting the plasma stability. It would require the addition of oxygen ashing to remove the excess solvent. As^{III} was least affected by all the mobile phase changes as a result of it being unionised at $\text{pH} < 10$ and thus not interacting at all with TBA.

From the discussed experiments the mobile phase that was used for this work consisted of 10 mmol/L TBA, 20 mmol/L KH_2PO_4 and 2% methanol at $\text{pH} = 6$. The retention times for As^{III} is 3.19 min., MMA is 4.19 min., DMA is 6.15 min., and As^{V} is 8.91 min., accordingly, the total run time less than 10 minutes which is reasonable, see Figure 4.17.

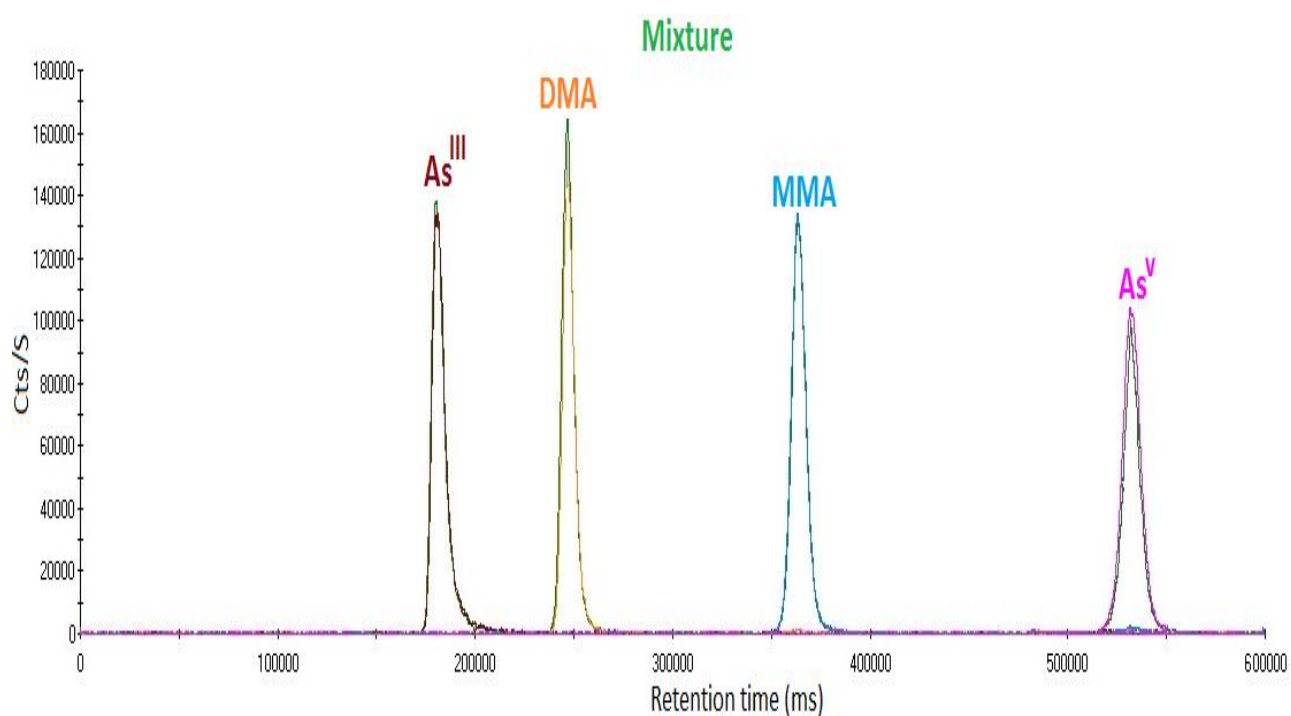


Figure 4.17 Illustration of As-species elution order; obtained by injecting a standard of each species separately as well as a mixture of the four selected As-species

4.3.3 HPLC method validation

4.3.2.1 Linearity and range

Linearity in the range of 1 to 50 ng/mL for all four species gave R² value of more than 0.995. The results are summarised in Table 4.6.

Table 4.6 Linearity results for the developed HPLC-ICP-MS method

Species	Exact range (ng/mL)	Linear regression line equation: Y= bX + a where b is the slope and a is the intercept	R ²
As ^{III}	1.015-50.758	y= 892119x + 3883.5	0.9998
DMA	1.026-51.291	y= 858110x + 1828.8	0.9996
MMA	0.912-45.579	y= 863210x + 47742	0.9997
As ^V	1.000-50.013	y= 869141x + 45364	0.9984

4.3.2.2 Accuracy and precision

Calibration and test standards were freshly prepared and analysed on three consecutive days. The four species' recoveries were always between 95-102% and the RSDs were always less than 5%. Detailed results are presented in Table 4.7.

Table 4.7 Accuracy and Precision results, n=3

	Day 1		Day 2		Day 3			
	Conc.*	% Rec.**	Conc.	% Rec.	Conc.	% Rec.		
As^{III}, Theoretical Concentration= 1.02 ng/mL								
1	0.99	99.38	1	0.99	99.38	1	0.97	96.51
2	0.98	97.75	2	0.97	97.02	2	0.99	98.61
3	0.96	96.01	3	0.97	96.73	3	0.97	96.54
σ	0.02		σ	0.01		σ	0.02	
RSD	1.73		RSD	1.24		RSD	1.24	

Table 4.7, continued

Day 1			Day 2			Day 3		
As^{III}, Theoretical Concentration= 10.2 ng/mL								
	Conc.	% Rec.		Conc.	% Rec.		Conc.	% Rec.
1	9.61	95.17	1	9.99	98.99	1	10.28	101.79
2	10.09	99.88	2	9.94	98.47	2	9.96	98.67
3	9.99	98.91	3	9.71	96.21	3	9.81	97.18
σ	0.25		σ	0.15		σ	0.24	
RSD	2.54		RSD	1.50		RSD	2.37	
As^{III}, Theoretical Concentration= 50.76 ng/mL								
	Conc.	% Rec.		Conc.	% Rec.		Conc.	% Rec.
1	49.18	96.90	1	49.68	97.90	1	51.64	101.76
2	48.27	95.10	2	49.01	96.58	2	50.61	99.72
3	49.91	98.34	3	51.00	100.49	3	49.97	98.47
σ	0.83		σ	1.01		σ	0.84	
RSD	1.68		RSD	2.02		RSD	1.66	
DMA, Theoretical Concentration= 1.03 ng/mL								
	Conc.	% Rec.		Conc.	% Rec.		Conc.	% Rec.
1	1.01	101.07	1	0.98	97.53	1	0.95	95.23
2	0.95	95.09	2	0.97	97.27	2	0.98	97.93
3	0.95	95.36	3	0.99	99.38	3	0.99	98.72
σ	0.25		σ	0.01		σ	0.02	
RSD	2.53		RSD	1.17		RSD	1.88	
DMA, Theoretical Concentration= 10.26 ng/mL								
	Conc.	% Rec.		Conc.	% Rec.		Conc.	% Rec.
1	10.30	100.99	1	9.61	94.25	1	10.14	99.45
2	9.78	95.92	2	9.88	96.91	2	10.06	98.59
3	10.15	99.46	3	10.16	99.66	3	9.89	96.97
σ	0.034		σ	0.8		σ	0.13	
RSD	1.17		RSD	2.79		RSD	1.28	

Table 4.7, continued

Day 1			Day 2			Day 3		
DMA, Theoretical Concentration= 51.29 ng/mL								
	Conc.	% Rec.		Conc.	% Rec.		Conc.	% Rec.
1	52.69	102.73	1	49.67	96.85	1	51.73	100.86
2	50.26	97.99	2	48.87	95.27	2	49.80	97.11
3	49.53	96.57	3	50.27	98.00	3	50.17	97.81
σ	1.66		σ	0.70		σ	1.02	
RSD	3.26		RSD	1.42		RSD	2.03	
MMA, Theoretical Concentration= 0.91 ng/mL								
	Conc.	% Rec.		Conc.	% Rec.		Conc.	% Rec.
1	0.85	95.34	1	0.91	101.08	1	0.89	99.86
2	0.87	97.68	2	0.86	95.26	2	0.85	95.28
3	0.86	95.44	3	0.88	98.61	3	0.86	95.53
σ	0.01		σ	0.03		σ	0.02	
RSD	1.37		RSD	2.97		RSD	2.65	
MMA, Theoretical Concentration= 9.12 ng/mL								
	Conc.	% Rec.		Conc.	% Rec.		Conc.	% Rec.
1	8.91	97.93	1	9.19	101.03	1	9.24	101.61
2	9.05	99.45	2	9.41	103.41	2	9.11	100.06
3	9.36	102.88	3	9.06	99.59	3	9.04	99.33
σ	0.23		σ	0.18		σ	0.11	
RSD	2.53		RSD	1.90		RSD	1.16	
MMA, Theoretical Concentration= 45.56 ng/mL								
	Conc.	% Rec.		Conc.	% Rec.		Conc.	% Rec.
1	44.93	98.58	1	44.45	97.51	1	46.00	100.92
2	44.78	98.25	2	43.66	95.80	2	44.80	98.30
3	43.49	95.42	3	45.61	100.06	3	44.912	98.53
σ	0.79		σ	0.98		σ	0.66	
RSD	1.78		RSD	2.19		RSD	1.46	

Table 4.7, continued

Day 1		Day 2		Day 3				
As^V, Theoretical Concentration= 1.00 ng/mL								
	Conc.	% Rec.		Conc.	% Rec.		Conc.	% Rec.
1	0.96	96.77	1	0.95	95.16	1	0.95	95.77
2	0.94	94.33	2	0.97	97.21	2	0.96	95.95
3	0.99	99.32	3	0.96	96.01	3	0.99	99.78
σ	0.03		σ	0.010		σ	0.02	
RSD	2.58		RSD	1.07		RSD	2.33	
As^V, Theoretical Concentration= 10.00 ng/mL								
	Conc.	% Rec.		Conc.	% Rec.		Conc.	% Rec.
1	10.25	97.93	1	10.20	101.99	1	10.39	103.90
2	10.08	99.45	2	9.82	98.21	2	9.98	99.81
3	10.35	102.88	3	9.82	98.19	3	10.21	102.15
σ	0.14		σ	0.22		σ	0.21	
RSD	2.53		RSD	2.20		RSD	2.01	
As^V, Theoretical Concentration= 50.01 ng/mL								
	Conc.	% Rec.		Conc.	% Rec.		Conc.	% Rec.
1	50.80	101.37	1	48.30	96.37	1	49.08	97.93
2	49.52	98.80	2	50.09	99.95	2	50.00	99.76
3	50.46	100.67	3	49.22	98.21	3	48.28	96.32
σ	0.67		σ	0.89		σ	0.86	
RSD	1.32		RSD	1.82		RSD	1.75	

*Concentration, **% Recovery

4.3.2.3 Limits of detection (LoDs) and limits of quantification (LoQs)

The calculated limit of detection and limit of quantification were as follows: As^{III} (0.0954- 0.279 ng/mL), DMA (0.118- 0.339 ng/mL), MMA (0.122- 0.353 ng/mL) and As^V (0.118- 0.362 ng/mL) respectively.

4.3.4 Samples preparation and analysis

4.3.4.1 Determination of total arsenic concentration in six antacid products

Before working on optimising the extraction procedure, total arsenic level in six commercially available antacid products was analysed by digesting 0.5g of the samples in 8 mL of reverse aqua regia followed by filtering and diluting the samples before analysing them using ICP-MS-CCT mode as described in Section 3.2.7. The results are summarised in Table 4.8.

Table 4.8 Total arsenic concentration $\pm \sigma$ (ng/g) in commercially available antacids, $n=3$

Antacid*	Total As Concentration	Daily Exposure in maximum dose (ng/day)
1. Gaviscon suspension	<LoD (0.048)	N/A
2. Gaviscon chewable tablets	38.25 \pm 0.54	819.53 \pm 11.59
3. Rennie Extra	27.99 \pm 0.90	786.92 \pm 25.42
4. Superdrug	452.17 \pm 4.85	8527.45 \pm 91.49
5. Rennie	47.28 \pm 3.85	615.11 \pm 50.10
6. Bisodol	372.43 \pm 15.18	2702.07 \pm 110.16

*Antacids 1-3 contain alginates, while antacids 4-5 do not contain any

As explained in experimental section 4.2.4.2, more than one temperature and extraction medium were used. Although in some research diluted acids such as nitric acid, hydrochloric acid, sulfuric acid and formic acid(223, 302, 307) were used as extraction media. Other studies(302, 306) suggested the use of diluted phosphoric acid instead, because it gives good extraction recoveries and sharp peaks when HPLC is used for separation(302, 306). For this reason 0.3 M phosphoric acid was chosen in this work in addition to water(216, 256, 316), which is widely used in previous published work. The concentration of phosphoric acid used (0.3 M) was based on the work of Wolle et al(306). Different concentration ranging from 0.1–0.5 M were tried

by Wolle et al(306) and 0.3 M was found to be the optimum concentration. 0.3 M phosphoric acid was also used for arsenic speciation in plants by Bohari et al(204).

The use of organic solvents such as methanol, acetonitrile, acetone and chloroform(244, 248, 258, 317, 318) as extraction medium for sample preparation was avoided due to the need of complete evaporation of the organic phase before analysing using ICP-MS as the detector. This evaporation phase is used to avoid plasma temperature suppression effects.

4.3.4.2 Investigating the arsenic microwave assisted extraction efficiency of water and 0.3 M phosphoric acid.

All the samples were freshly prepared and analysed within the same day.

Water was used to extract arsenic from the antacids using microwave assisted extraction at 80°C for 30 minutes, but the extracted levels for all species were below the LoDs. The obtained chromatogram is illustrated in Figure 4.18.

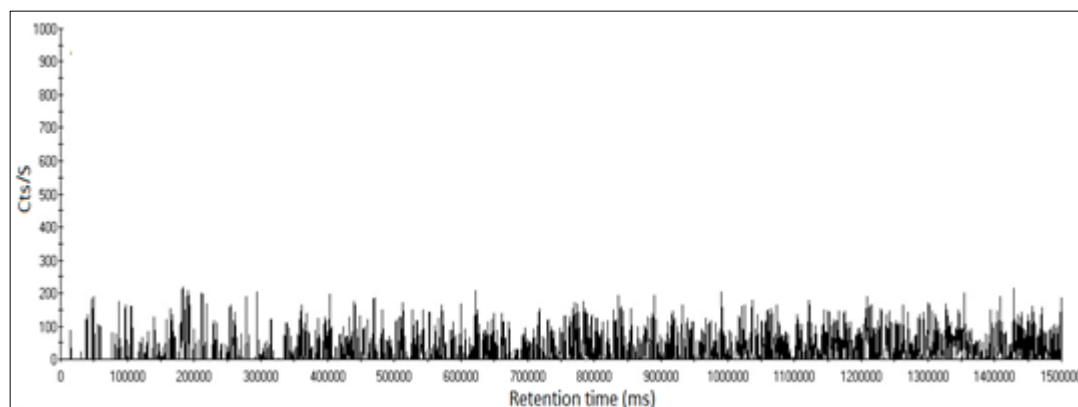


Figure 4.18 Obtained chromatogram for Gaviscon chewable tablets using microwave assisted extraction with water for 30 minutes at 80°C

In an attempt to enhance the extraction, the temperature was increased to 95°C, but still the levels did not exceed the LOQs. The obtained chromatogram is illustrated in Figure 4.19.

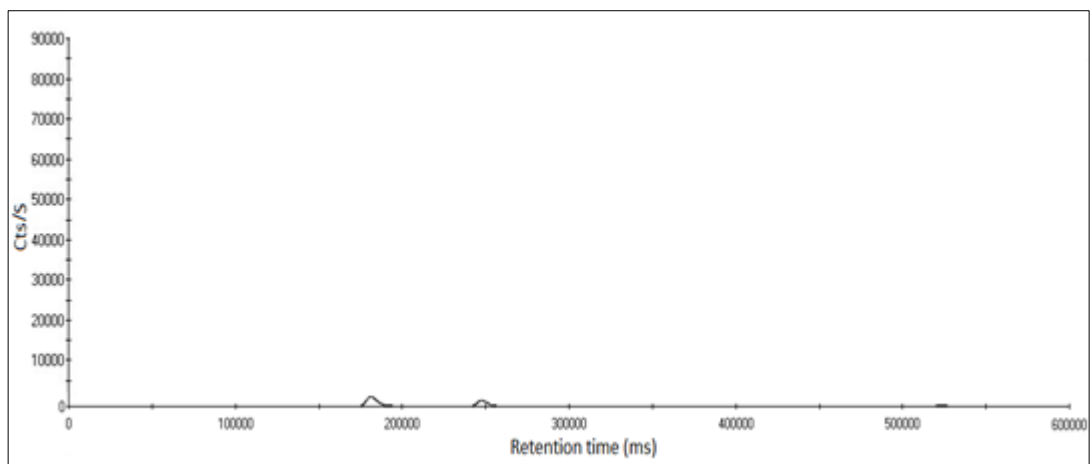


Figure 4.19 Obtained chromatogram for Gaviscon chewable tablets using microwave assisted extraction with water for 30 minutes at 95°C

The next step was using 0.3M phosphoric acid instead of water with the microwave for 30 minutes at 95°C as well. The extraction improved but still the concentrations are at borderline with the LoQs, see Figure 4.20.

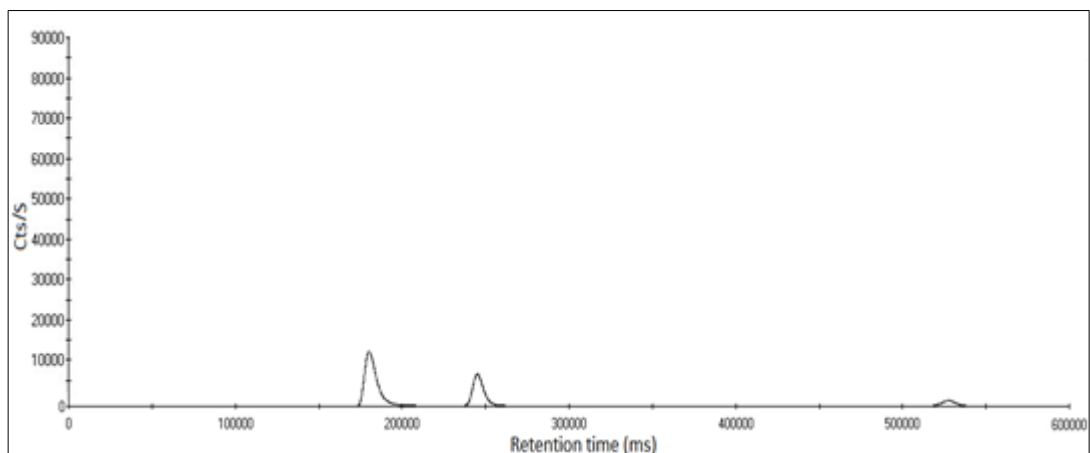


Figure 4.20 Obtained chromatogram for Gaviscon chewable tablets using microwave assisted extraction with H₃PO₄ for 30 minutes at 95°C

4.3.4.3 Optimisation of the microwave assisted extraction procedure using 0.3 M H₃PO₄

To improve arsenic extraction from antacids, gradual increase of temperature was attempted starting from 55 °C for 10 minutes, 75°C for 10 minutes and finally 95°C

for 30 minutes as suggested by Jackson et al(307). This method lead to significant improvement in the extraction efficiency as the levels of the extracted arsenic was about 75% of the total. The method was applied to antacids containing alginates and because the total As concentration for Gaviscon suspension was below LoD, arsenic was extracted from Gaviscon chewable tablets and Rennie Extra only. The results are displayed in Table 4.9.

Table 4.9 Concentration of arsenic species $\pm \sigma$ (ng/g) using microwave assisted extraction with 0.3M H₃PO₄ at 55°C for 10 minutes, 75°C for 10 minutes and 95°C for 30 minutes, $n=3$

	Gaviscon chewable tablets		Rennie Extra	
	Concentration	Spiked Recovery	Concentration	Spiked Recovery
As ^{III}	16.24 \pm 0.66	101.5%	12.40 \pm 0.61	95.4%
DMA	8.29 \pm 0.33	95.6%	8.72 \pm 0.34	96.4%
MMA	<LoD (0.048)	97.7%	<LoD (0.048)	102.9%
As ^V	7.18 \pm 0.33	100.7%	<LoQ (0.149)	103.6%
Total As	38.25 \pm 0.54		27.99 \pm 0.90	
%Extracted	83.10%		75.47%	

The final attempt to optimise the extraction procedure was to increase the hold time at 95°C for one hour instead of 30 minutes. This increased the recoveries to more than 95% for both the products without affecting the species stability and thus was considered the optimum procedure. The results are displayed in Table 4.10.

Table 4.10 Concentration of arsenic species $\pm \sigma$ (ng/g) in antacids containing alginate using microwave assisted extraction with 0.3 M H₃PO₄ at 55°C for 10 minutes, 75°C for 10 minutes and 95°C for 60 minutes, $n=3$

	Gaviscon chewable tablets		Rennie Extra	
	Concentration	Spiked Recovery	Concentration	Spiked Recovery
As ^{III}	17.61 \pm 0.64	99.6	12.91 \pm 0.27	96.5
DMA	11.62 \pm 0.32	104.2	9.74 \pm 0.14	95.2
MMA	<LoD (0.048)	97.7	<LoD (0.048)	95.0
As ^V	8.51 \pm 0.29	99.6	4.62 \pm 0.08	102.9
Total Extracted	37.74		27.26	
Total As	38.25 \pm 0.54		27.99 \pm 0.90	
%Extracted	98.67%		97.42%	

To make sure that H₃PO₄, microwave temperature and extraction time were not affecting the species stability, spiked samples that had undergone the whole procedure were analysed and spiked recoveries were calculated giving 95% or higher which suggests that the species were stable using these extraction conditions. The results are displayed in Table 4.11.

Table 4.11 % Recovery of spiked samples prepared in water and H₃PO₄ subjected to the microwave extraction procedure; 55°C for 10 minutes, 75°C for 10 minutes and 95°C for 60 minutes, n=3

	Spiked As species in water		Spiked As species H ₃ PO ₄	
	% Recovery	RSD	% Recovery	RSD
As ^{III}	101.80	1.32	100.90	1.30
DMA	99.00	1.66	100.70	1.52
MMA	101.17	2.12	102.63	2.37
As ^V	95.40	1.29	99.87	1.99

Increasing the hold time at 95°C to greater than 60 minutes resulted in all the As^{III} being converted to As^V even when the medium was water, which suggest that the microwave power itself in the presence of weak acids can alter the species if the samples are exposed to microwaves for a time exceeding 80 minutes. The same procedure of exposing a standard in water and another one in H₃PO₄ for microwaves using the optimised extraction method was performed. The results clearly demonstrates that 0.3 M H₃PO₄ will not oxidise As^{III} to As^V. Figure 4.21 demonstrates the interconversion of As^{III} to As^V when using the microwave for more than 80 minutes regardless of the presence or absence of an oxidising acid like H₃PO₄.

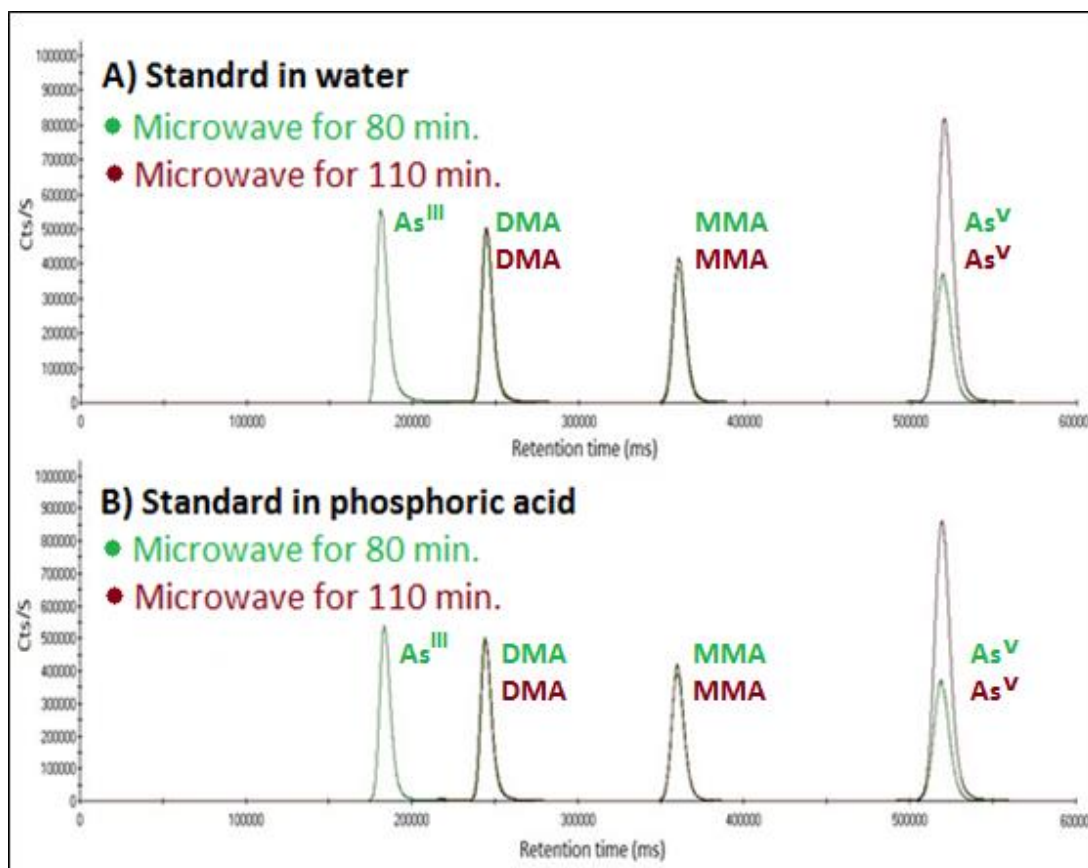


Figure 4.21 The interconversion of As^{III} to As^V after exposing a standard in water and H_3PO_4 to microwaves for more than 80 minutes

4.4.4. Speciation of arsenic in antacids

The optimised microwave assisted extraction procedure using 0.3 M H_3PO_4 at 55°C for 10 minutes, 75°C for 10 minutes and 95°C for 60 minutes, was used to extract As from 5 antacid products that had a quantifiable level of total arsenic as displayed in Table 4.8

The results for Gaviscon chewable tablets and Rennie Extra antacids containing alginate were displayed in Table 4.10.

Gaviscon suspension has similar ingredients to Gaviscon chewable tablets, but it is formulated as a suspension and thus contains large quantity of water. In an attempt to concentrate the arsenic in it, the liquid formula was dried in an oven at 80°C, and

three samples containing 0.5g of the dried mass were analysed to measure the total arsenic content and another three samples were used to extract the arsenic species.

The results are displayed in Table 4.12.

Table 4.12 Arsenic content in the dried mass obtained from Gaviscon suspension

	Total Concentration (ng/g)	RSD	Spiked Recovery
⁷⁵ As	59.49	4.35	96.54
Extracted species	Concentration (ng/g)	RSD	Spiked Recovery
As ^{III}	22.87	4.761	98.06
DMA	17.41	3.884	98.59
MMA	<LoD (0.048)	-	97.71
As ^V	15.89	3.789	103.68
Total Extracted	56.18		
%Extracted	94.44%		

The speciation results for antacid products that do not contain alginates are displayed in Table 4.13.

Table 4.13 Concentration of arsenic species $\pm \sigma$ (ng/g) in antacids without alginates using microwave assisted extraction with 0.3 M H₃PO₄ at 55°C for 10 minutes, 75°C for 10 minutes and 95°C for 1 hours, n=3

	Superdrug		Rennie		Bisodol	
	Conc.*	Spiked Rec.**	Conc.	Spiked Rec.	Conc.	Spiked Rec.
As ^{III}	265.50±4.73	95.9	24.98±0.82	99.9	207.81±6.24	96.3
DMA	<LoD (0.048)	98.5	<LoD (0.048)	95.4	<LoD (0.048)	102.7
MMA	<LoD (0.048)	104.7	<LoD (0.048)	100.9	<LoD (0.048)	104.5
As ^V	172.50±5.81	102.7	20.40±0.69	103.3	164.21±6.22	103.3
Total Extracted	438.00		45.38		372.02	
Total As	452.17±4.85		47.28±3.85		372.43±15.18	
%Extracted	96.87%		95.98%		99.89%	

*Concentration

**Recovery

An example of the obtained chromatograms for a product containing alginate and another one without is presented in Figure 4.22.

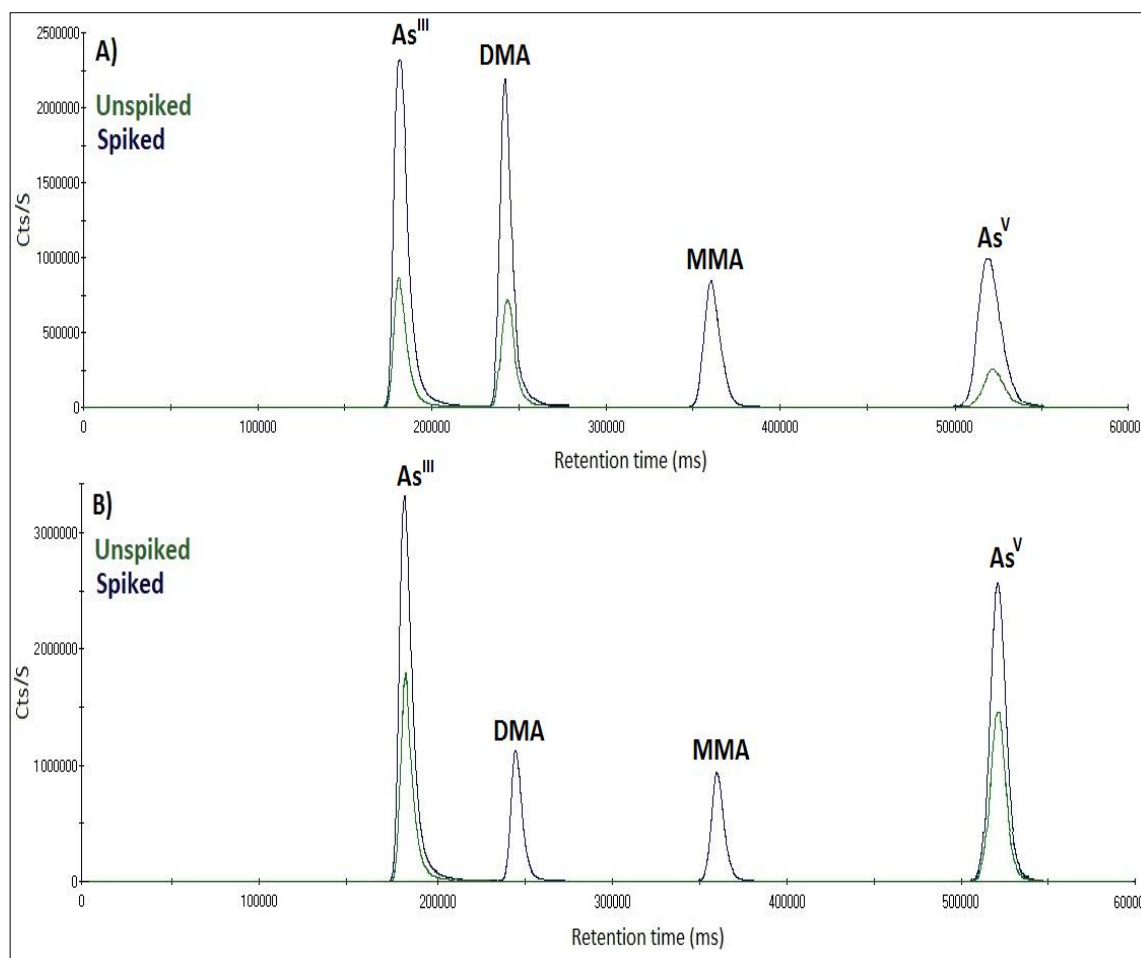


Figure 4.22 Obtained chromatograms for Rennie Extra with alginate & Rennie without alginate using microwave assisted extraction with 0.3 M H₃PO₄ at 55°C for 10 minutes, 75°C for 10 minutes and 95°C for 60 minutes

From the speciation results, it was found that all the products contain As^{III} and As^V, and the products that contain alginate derivatives also contain DMA (product 1, 2 and 3). Alginate is usually obtained from brown algae, including species of *Durvillaea*, *Laminaria*, *Lessonia*, *Ascophyllum*, *Ecklonia*, *Macrocystis* and *Sargassum*. However, *Sargassum* is only used when nothing else is available of the other species(312, 319, 320). Previous studies where some of these species were analysed found them to contain As^{III}, As^V and DMA(33, 321, 322). For example, *Durvillaea antarctica* was found to contain 0.304 mg/Kg of As^{III}, 0.114 mg/Kg of As^V and 0.103 mg/Kg of DMA. In addition, *Lessonia nigrescens* was found to contain 105 mg/Kg of As^{III} and 18.5

mg/Kg of As^V(33). *Laminaria* species were found to contain inorganic As species in concentrations ranging from 0.12 to 8.32 mg/Kg(323) and *Sargassum* was found to contain 62.3% of its total arsenic content in the form of As^V(324).

In addition, these antacid products contain weak bases to neutralise excess stomach acid such as calcium carbonate, magnesium carbonate and sodium bicarbonate. When some pharmaceutical excipients(31) were analysed for trace metals, arsenic was found in the following: sodium alginate in a concentration of 420 ng/g, calcium carbonate in a concentration of 10 ng/g and magnesium carbonate in a concentration of 130 ng/g. Sodium bicarbonate was not included in that study and no information was available regarding the presence or absence of arsenic as EI in it(31). These excipients, other than sodium alginate are also contributing to the arsenic concentration found in the analysed antacids as it is clear that products 4, 5 and 6 were also found to have arsenic in them in the form of As^{III} and As^V although they do not have alginate derivatives within their ingredients.

It also noted that the dosage form of the pharmaceutical product contributes to the total amount of EI that patients can be exposed to on daily basis when consuming the product. An example is Gaviscon. The suspension formula contains considerable amount of water that diluted other solid ingredients, which led to the reduction of total arsenic concentration.

Since As^{III} is the most toxic species, its percentage was calculated with regards to the total arsenic concentration in each product. The results are displayed in Table 4.14.

Table 4.14 Percentage of As^{III} in the analysed antacid products

Antacid*	% of As^{III}
Gaviscon chewable tablets	46.03
Rennie Extra	46.10
Superdrug	58.71
Rennie	52.83
Bisodol	55.79

* Gaviscon suspension was excluded because As required a pre-concentration step in order to increase its concentration above the LoQ

4.4 Conclusion

Arsenic speciation in pharmaceutical products has not been published in the literature previously. This optimised HPLC-ICP-MS method proved to be capable of analysing and speciating arsenic in antacids. Although in the selected antacids, the levels do not exceed the maximum allowed daily dose (15 µg/mL) according to ICH-Q3D guidelines, the fact that the species with the highest concentration is As^{III} raises questions regarding how much these products can be considered safe for human consumption. This should also alert manufacturers and regulators to control the quality and safety of their products. Keeping in mind that many people suffering from indigestion or gastrointestinal acid reflux can take these products on an almost daily bases for a considerable period although it is not recommended(325). This will expose them to a regular intake of As^{III} even though the level is below the regulated limit.

Chapter 5

General Conclusion and Future

Work

5.1 General Conclusion

With the new guidelines recently coming into effect, the need for new methods to determine elemental impurities in pharmaceuticals was highly emphasised in this work. Twenty-four commercially available pharmaceutical products were analysed using optimised and validated ICP-OES and ICP-MS equipped with collision reaction cell methods for the simultaneous analysis of arsenic, cadmium, mercury, lead, cobalt, nickel and vanadium. With four products found to contain cadmium in concentration exceeding the allowed PDE of 5 µg/day and nine products exceed the lead PDE of 5 µg/day, the need for new regulations is urgently required to ensure the safety of pharmaceutical products to consumers.

It was found that not just some products exceed the allowed PDE, but also in some cases, the level of the elements present is 30% or more of the regulation's PDE, like cobalt in Superdrug bronchial Balsam and lead in Lemsip cold and flu powders. According to the guidelines, this requires establishment of controls to ensure that the elemental impurities level does not exceed the PDE in the pharmaceutical products in which elements are in levels exceeding 30% of their PDEs.

This work also highlights the fact that even products without active pharmaceutical ingredients may contain significant amount of elemental impurities, which emphasises the reality that one of the major sources for pharmaceutical impurities is the excipients used for the formulation of pharmaceutical products.

The developed ICP-OES, ICP-MS and microwave assisted acid digestion for pharmaceutical products methods were successfully validated using the only commercially available standard reference material *NIST 3280*

Multivitamin/Multielement tablets as well as from supporting results obtained using TAC tablets that are still under development.

The methods showed excellent recoveries between 95-105% with good repeatability expressed as RSD of less than 5% for all elements. Those limits met the regulations requirements. In addition, these methods are specific, as for ICP-OES any spectra with major interferences were excluded and only those with minimal interferences were chosen for analysis. In case of using ICP-MS, collision reaction cell with helium gas was used to minimise polyatomic interferences and any isotopes suffering from major interferences were excluded from analysis. LoDs and LoQs were below the target limits, which supports the suitability of the ICP-OES and ICP-MS for elemental impurities determination.

Additionally, the need of a suitable solid reference material was brought to attention for proper validation of the analytical methods required of analysing pharmaceuticals for the purpose of determining elemental impurities, because relying on methods like spiked recoveries only may give a false indication about the efficiency and validity of the chosen analytical method.

Regarding arsenic speciation, the optimised reversed phase HPLC-ICP-MS method was successful in analysing four arsenic species, As^{III}, As^V, MMA and DMA and also questions the safety of pharmaceutical products that contain high level of toxic species like As^{III}.

5.2 Future work

The optimised digestion method proved to be efficient in extracting Class 1 and Class 2A elements, but changes of the acid ratio, acid volume used, hold time duration and/or temperature may be required for elements from different classes particularly 2B which have not been investigated extensively but maybe present due to intentional addition. A solid reference material that include these elements in representative concentration will be needed to ensure the digestion method efficiency.

Regarding speciation, very limited work on pharmaceutical products has been published in this area. However, it is essential; to know what species are present from elements like arsenic, which was speciated in this work, mercury and chromium for example, where Cr^{VI} is known to be toxic and carcinogenic unlike Cr^{III}(326, 327). This will provide better understanding of the toxicity of trace metals present in pharmaceutical products.

Speciation analysis requires considerable work to optimise a method that is able to differentiate species of the same element with similar properties. The extraction method also needs considerable amount of optimisation and may differ according to the nature of the samples to be analysed. The need of suitable reference materials containing various species of elements is also required for proper optimisation and validation of the developed speciation methods. Speciation analysis for pharmaceutical products is expected to gain greater interest in the upcoming years with the new regulation implemented and with the increasing attention to the safety of pharmaceutical products offered to consumers.

References

References

1. Lewen N, Mathew S, Schenkenberger M, Raglione T. A rapid ICP-MS screen for heavy metals in pharmaceutical compounds. *J Pharm Biomed Anal.* 2004;35(4):739-52.
2. Liu J, Shi JZ, Yu LM, Goyer RA, Waalkes MP. Mercury in traditional medicines: is cinnabar toxicologically similar to common mercurials? *Exp Biol Med (Maywood).* 2008;233(7):810-7.
3. Parascandola J. *King of poisons: a history of arsenic.* Washington, DC: Potomac Books, Inc; 2012.
4. Maher WA, Ellwood MJ, Krikowa F, Raber G, Foster S. Measurement of arsenic species in environmental, biological fluids and food samples by HPLC-ICPMS and HPLC-HG-AFS. *J Anal At Spectrom.* 2015;30(10):2129-83.
5. Hughes MF, Beck BD, Chen Y, Lewis AS, Thomas DJ. Arsenic exposure and toxicology: a historical perspective. *Toxicol Sci.* 2011;123(2):305-32.
6. Pearce JM. Burton's line in lead poisoning. *Eur Neurol.* 2007;57(2):118-9.
7. Bustamante ND, Macias-Konstantopoulos WL. Retained lumbar bullet: a case report of chronic lead toxicity and review of the literature. *J Emerg Med.* 2016;51(1):45-9.
8. <232> Elemental Impurities-Limits: USP; Available from: <http://www.usp.org/sites/default/files/usp/document/our-work/chemical-medicines/key-issues/c232-usp-39.pdf>[Accessed 16/10/2017].
9. <233> Elemental Impurities-Procedures: USP; Available from: <https://hmc.usp.org/sites/default/files/documents/HMC/GCs-Pdfs/c233.pdf>[Accessed 16/10/2017].
10. ICHQ3D. Guideline for Elemental Impurities: International Conference on Harmonisation of Technical Requirements for Registration of Pharmaceuticals for Human Use; Available from: http://www.ich.org/fileadmin/Public_Web_Site/ICH_Products/Guidelines/Quality/Q3D/Q3D_Step2b.pdf [Accessed 16/10/2017].
11. Blake K. Harmonization of the USP, EP and JP heavy metals testing procedures. *Pharmaceutol Forum.* 1995;21(6):1632-7.
12. Wang T, Wu J, Hartman R, Jia X, Egan RS. A multi-element ICP-MS survey method as an alternative to the heavy metals limit test for pharmaceutical materials. *J Pharm Biomed Anal* 2000;23(5):867-90.
13. Nageswara Rao R, Talluri MV. An overview of recent applications of inductively coupled plasma-mass spectrometry (ICP-MS) in determination of inorganic impurities in drugs and pharmaceuticals. *J Pharm Biomed Anal.* 2007;43(1):1-13.
14. Abernethy DR, Destefano AJ, Cecil TL, Zaidi K, Williams RL. USP Metal Impurities Advisory Panel. Metal Impurities in food and drugs. *Pharmaceutical Research.* 2010;27(5):750-5.
15. Teasdale A, Chéry CC, Cook G, Glennon J, Lee CW, Harris L, et al. Implementation of ICH Q3D elemental impurities guideline: challenges and opportunities. *Pharm Technol* 2015;39(3):36-89.
16. Barin JS, Mello PA, Mesko MF, Duarte FA, Flores EM. Determination of elemental impurities in pharmaceutical products and related matrices by ICP-based methods: a review. *Anal Bioanal Chem.* 2016;408(17):4547-66.
17. Murty ASRK, Kulshresta UC, Rao TN, M.V.N.K. T. Determination of heavy metals in selected drug substances by inductively coupled plasma-mass spectrometry. *Indian J Chem Technol* 2005;12(2):229-31.
18. Muller AL, Oliveira JS, Mello PA, Muller EI, Flores EM. Study and determination of elemental impurities by ICP-MS in active pharmaceutical ingredients using single reaction chamber digestion in compliance with USP requirements. *Talanta.* 2015;136:161-9.

19. Lasztity A, Kelko-Levai A, Varga I, Zih-Perenyi K, Bertalan E. Development of atomic spectrometric methods for trace metal analysis of pharmaceuticals. *Microchem J.* 2002;73(1):59-63.
20. Heveling J. Heterogeneous catalytic chemistry by example of industrial applications. *J Chem Educ* 2012;89(12):1530-6.
21. Arhancet JP, Davis ME, Merola JS, Hanson BE. Hydroformylation by supported aqueous-phase catalysis: a new class of heterogeneous catalysts. *Nature.* 1989;339(6224):454-5.
22. Baleizao C, Garcia H. Chiral salen complexes: an overview to recoverable and reusable homogeneous and heterogeneous catalysts. *Chem Rev.* 2006;106(9):3987-4043.
23. Margu E, Queralt I, Hidalgo M. Determination of platinum group metal catalyst residues in active pharmaceutical ingredients by means of total reflection X-ray spectrometry. *Spectrochim Acta, Part B.* 2013;86:50-4.
24. Resano M, Flrez MdR, Queralt I, Margu E. Determination of palladium, platinum and rhodium in used automobile catalysts and active pharmaceutical ingredients using high-resolution continuum source graphite furnace atomic absorption spectrometry and direct solid sample analysis. *Spectrochim Acta, Part B* 2015;105:38-46.
25. ICHQ3C(R6). Impurities: guideline for residual solvents 2016; Available from: http://www.ich.org/fileadmin/Public_Web_Site/ICH_Products/Guidelines/Quality/Q3C/Step4/Q3C_R5_Step4.pdf [Accessed 01/12/2017].
26. Baldrick P. Pharmaceutical excipient development: the need for preclinical guidance. *Regul Toxicol Pharmacol.* 2000;32(2):210-8.
27. Pifferi G, Restani P. The safety of pharmaceutical excipients. *Il Farmaco.* 2003;58(8):541-50.
28. Kemsley J. Eyes on excipients. *Chem Eng News.* 2014;92.5:9-11.
29. Schoneker D. Elemental impurities-excipients realities and challenges: International Pharmaceutical Excipients Council of the Americas; 1 May 2013; Available from: [http://ipeamericas.org/sites/default/files/EF13May1HallA2DaveSchoneker\(IPEC\).pdf](http://ipeamericas.org/sites/default/files/EF13May1HallA2DaveSchoneker(IPEC).pdf) [Accessed 04/12/2017].
30. Apte S. Elemental impurity limits in excipients. *J Excipients and Food Chem* 2013;4(1):1-3.
31. Li G, Schoneker D, Ulman KL, Sturm JJ, Thackery LM, Kauffman JF. Elemental impurities in pharmaceutical excipients. *J Pharm Sci.* 2015;104(12):4197-206.
32. FDA. Water for pharmaceutical use: United States Department of Health and Human Services [updated 03/23/2015]; Available from: <https://www.fda.gov/ICECI/Inspections/InspectionGuides/InspectionTechnicalGuides/ucm072925.htm> [Accessed 19/12/2017].
33. Ruiz Chanco MJ, Lpez Snchez JF, Rubio R. Occurrence of arsenic species in the seagrass *Posidonia oceanica* and in the marine algae *Lessonia nigrescens* and *Durvillaea antarctica*. *J Appl Phycol* 2009;22(4):465-72.
34. Handbook of isolation and characterization of impurities in pharmaceuticals: Academic press; 2003.
35. Krause KP, O. K, Mder K, Gust R, Mller RH. Heavy metal contamination of nanosuspensions produced by high-pressure homogenisation. *Int J Pharm* 2000;196(2):169-72.
36. Tyler G. ICP MS or ICP AES and AAS? A comparison. *Spectrosc Eur.* 7:14.
37. Singh A, Sharma PK, Malviya R. Eco friendly pharmaceutical packaging material. *World Sci Appl J.* 2011;14(11):1703-16.
38. FDA. Guidance for industry, container closure systems for packaging human drugs and biologics May 1999; Available from: <https://www.fda.gov/downloads/drugs/guidances/ucm070551.pdf> [Accessed 05/12/2015].

39. Jenke DR, Stults CL, Paskiet DM, Ball DJ, Nagao LM. Materials in manufacturing and packaging systems as sources of elemental impurities in packaged drug products: a literature review. *PDA J Pharm Sci Technol*. 2015;69(1):1-48.
40. Fliszar KA, Walker D, Allain L. Profiling of metal ions leached from pharmaceutical packaging materials. *PDA J Pharm Sci Technol* 2006 60(6):337-42.
41. Bee JS, Nelson SA, Freund E, Carpenter JF, Randolph TW. Precipitation of a monoclonal antibody by soluble tungsten. *J Pharm Sci*. 2009;98(9):3290-301.
42. <231> Heavy Metals: USP; Available from: http://www.pharmacopeia.cn/v29240/usp29nf24s0_c231.html [Accessed 18/10/2017].
43. Wang T, Wu J, Jia X, Bu X, Santos I, Egan RS. An atomic spectroscopic method as an alternative to both USP heavy metals <231> and USP residue on ignition <281>. *USP Pharmacopeial Forum*. 2003;29(4):1328- 36.
44. Schenkenberger M, Lewen N. Inductively coupled plasma–optical emission spectroscopy as an alternative to the heavy metals test. *USP Pharmacopeial Forum*. 2004;30(6):2271.
45. Stoving C, Jensen H, Gammelgaard B, Sturup S. Development and validation of an ICP-OES method for quantitation of elemental impurities in tablets according to coming US pharmacopeia chapters. *J Pharm Biomed Anal*. 2013;84:209-14.
46. Nam KH, Isensee R, Infantino G, Putyera K, Wang X. Microwave induced combustion for ICP MS a generic approach to trace elemental analyses of pharmaceutical products. *Spectroscopy*. 2011;26(4).
47. Zachariadis GA, Kapsimali DC. Development of a rapid multi-element method of analysis of antitussive syrups by inductively coupled plasma atomic emission spectrometry and direct sample introduction. *J Pharm Biomed Anal*. 2006;41(4):1212-9.
48. Meermann B, Sperling M. Hyphenated techniques as tools for speciation analysis of metal-based pharmaceuticals: developments and applications. *Anal Bioanal Chem*. 2012;403(6):1501-22.
49. USP Heavy Metals Testing Methodologies Workshop. United States 26-27 August 2008. Summary Institute of Medicine (IOM) of the National Academy of Sciences; Available from: <http://www.usp.org/sites/default/files/usp/document/our-work/chemical-medicines/key-issues/2008-MetalsWorkshopSummary.pdf> [Accessed 17/10/2017].
50. Van Hoecke K, Catry C, Vanhaecke F. Optimization of sample preparation and a quadrupole ICP-MS measurement protocol for the determination of elemental impurities in pharmaceutical substances in compliance with USP guidelines. *J Anal At Spectrom* 2012;27(11):1909.
51. *Pharmacopeial Forum* 42(2) [Mar.–Apr. 2016]: USP; Available from: http://www.uspnf.com/sites/default/files/usp_pdf/EN/USPNF/usp-nf-commentary/pf_422_ira_commentary.pdf [Accessed 17/10/2017].
52. Gorby MS. Arsenic poisoning. *West J Med*. 1988;149(3):308-15.
53. Do B, Alet P, Pradeau D, Poupon J, Guillely–Gaillot M, Guyon F. On line reversed phase liquid chromatography hydride generation emission spectrometry speciation of arsenic in urine. *J Chromatogr B Biomed*. 2000;740(2):179-86.
54. Ratnaik RN. Acute and chronic arsenic toxicity. *Postgrad Med J*. 2003;79(933):391-6.
55. B’Hymer C, Caruso JA. Arsenic and its speciation analysis using high-performance liquid chromatography and inductively coupled plasma mass spectrometry. *J Chromatogr A*. 2004;1045(1-2):1-13.
56. Exposure to arsenic: a major public health concern World Health Organization; 2010; Available from: <http://www.who.int/ipcs/features/arsenic.pdf> [Accessed 02/10/2017].
57. Waalkes MP. Cadmium carcinogenesis in review. *J Inorg Biochem*. 2000;79(1):241-4.

58. Johri N, Jacquillet G, Unwin R. Heavy metal poisoning: the effects of cadmium on the kidney. *Biomaterials*. 2010;23(5):783-92.
59. Bernard A. Cadmium & its adverse effects on human health. *Indian J Med Res*. 2008;128(4):557-64.
60. Duruibe JO, Ogwuegbu MO, Ekwurugwu JN. Heavy metal pollution and human biotoxic effects. *Int J Phys Sci*. 2007;2(5):112-8.
61. Flick DF, Kraybill HF, DImitroff JM. Toxic effects of cadmium: a review. *Environ Res* 1971;4(2):71-85.
62. Graeme KA, Pollack CV. Heavy metal toxicity, part I: arsenic and mercury. *J Emerg Med*. 1998;16(1):45-56.
63. Bernhoft RA. Mercury toxicity and treatment: a review of the literature. *J Environ Public Health*. 2012;2012:460508.
64. Houston MC. Role of mercury toxicity in hypertension, cardiovascular disease, and stroke. *J Clin Hypertens (Greenwich)*. 2011;13(8):621-7.
65. Gidlow DA. Lead toxicity. *Occup Med (Lond)*. 2015;65(5):348-56.
66. Needleman H. Lead poisoning. *Annu Rev Med*. 2004;55:209-22.
67. Graeme KA, Pollack CV. Heavy metal toxicity, part II: lead and metal fume fever. *J Emerg Med*. 1998;16(2):171-7.
68. Vallee BL, Ulmer DD. Biochemical effects of mercury, cadmium, and lead. *Annu Rev Biochem*. 1972;41(1):91-128.
69. Hildebrand MP. Lead toxicity in a newborn. *J Pediatr Health Care*. 2011;25(5):328-31.
70. WHO. International lead poisoning prevention awareness campaign, Week of action 22-28 October 2017: The World Health Organization; Available from: http://www.who.int/ipcs/lead_campaign/QandA_lead_2017_en.pdf [Accessed 29/12/2017].
71. Inorganic and organic lead compounds. IARC monographs on the evaluation of carcinogenic risks to humans. Vol. 87. Lyon, France, 2006.: International Agency for the Research on Cancer (IARC); Available from: <https://monographs.iarc.fr/ENG/Monographs/vol87/mono87.pdf> [Accessed 20/10/2017].
72. Smith KS, Huyck HL. An overview of the abundance, relative mobility, bioavailability, and human toxicity of metals. *The environmental geochemistry of mineral deposits*. 1999;6:29-70.
73. Barceloux DG, Barceloux D. Cobalt. *Journal of Toxicology: Clinical Toxicology*. 1999;37(2):201-16.
74. Schirrmacher UO. Case of cobalt poisoning. *Br Med J*. 1967;1(5539):544-5.
75. Alexander CS. Cobalt-beer cardiomyopathy: a clinical and pathologic study of twenty-eight cases. *Am J Med*. 1972;53(4):395-417.
76. Lahaye D, Demedts M, Van den Oever R, Roosels D. Lung diseases among diamond polishers due to cobalt? *Lancet*. 1984;323(8369):156-7.
77. Oldenburg M, Wegner R, Baur X. Severe cobalt intoxication due to prosthesis wear in repeated total hip arthroplasty. *J Arthroplasty*. 2009;24(5):825 e15-20.
78. Machado C, Appelbe A, Wood R. Arthroprosthetic cobaltism and cardiomyopathy. *Heart Lung Circ*. 2012;21(11):759-60.
79. Steens W, von Foerster G, Katzer A. Severe cobalt poisoning with loss of sight after ceramic-metal pairing in a hip--a case report. *Acta Orthop*. 2006;77(5):830-2.
80. Simonsen LO, Harbak H, Bennekou P. Cobalt metabolism and toxicology--a brief update. *Sci Total Environ*. 2012;432:210-5.
81. Apostoli P, Catalani S, Zaghini A, Mariotti A, Poliani PL, Vielmi V, et al. High doses of cobalt induce optic and auditory neuropathy. *Exp Toxicol Pathol*. 2013;65(6):719-27.
82. Leysens L, Vinck B, Van Der Straeten C, Wuyts F, Maes L. Cobalt toxicity in humans--A review of the potential sources and systemic health effects. *Toxicology*. 2017;387:43-56.

83. Shi Z. Nickel carbonyl: toxicity and human health. *Science of the total environment. Sci Total Environ.* 1994;148(2-3):293-8.
84. Kincaid JF, Stanley EL, Beckworth CH, Sunderman FW. Nickel poisoning. III. Procedures for detection, prevention, and treatment of nickel carbonyl exposure including a method for the determination of nickel in biologic materials. *Am J Clin Pathol.* 1956;26(2):107-9.
85. Cempel M, Nikel G. Nickel: A Review of Its Sources and Environmental Toxicology. *Pol J Environ Stud.* 2006;15(3):375-82.
86. Zdrojewicz Z, Popowicz E, Winiarski J. Nickel-role in human organism and toxic effects. *Pol Merkur Lekarski.* 2016;41(242):115-8.
87. Chervona Y, Arita A, Costa M. Carcinogenic metals and the epigenome: understanding the effect of nickel, arsenic, and chromium. *Metallomics.* 2012;4(7):619-27.
88. Das KK, Das SN, Dhundasi SA. Nickel, its adverse health effects & oxidative stress. *Indian J Med Res.* 2008;128(4):412.
89. Barceloux DG, Barceloux D. Vanadium. *J Toxicol Clin Toxicol.* 1999;37(2):265-78.
90. Chapter 6.12. Vanadium. *Air Quality Guidelines - Second Edition Copenhagen, Denmark: World Health Organization-Regional Office for Europe; 2000; Available from: http://www.euro.who.int/_data/assets/pdf_file/0016/123082/AQG2ndEd_6_12vanadium.PDF [Accessed 18/12/2017].*
91. Bunk DM. Reference materials and reference measurement procedures: an overview from a national metrology institute. *Clin Biochem Rev.* 2007;28(4):131-7.
92. SRM Definitions U.S.: The National Institute of Standards and Technology; Available from: <https://www.nist.gov/srm/srm-definitions> [Accessed 28/12/2017].
93. Certificate of Analysis: Standard Reference Material 3280 Multivitamin/Multielement Tablets U.S.: National Institute of Standards & Technology; 2016 [Available from: <https://www-s.nist.gov/srmors/certificates/3280.pdf> [Accessed 11/02/2016].
94. Wasilewska M, Goessler W, Zischka M, Maichin B, Knapp G. Efficiency of oxidation in wet digestion procedures and influence from the residual organic carbon content on selected techniques for determination of trace elements. *J Anal At Spectrom.* 2002;17(9):1121-5.
95. Abu-Samra A, Morris JS, Koirtyohann SR. Wet ashing of some biological samples in a microwave oven. *Anal Chem.* 1975;47(8):1475-7.
96. Elemental Impurities - Procedures<233>: USP; Available from: <https://hmc.usp.org/sites/default/files/documents/HMC/GCs-Pdfs/c233.pdf> [Accessed 06/09/2016].
97. Barin JS, Tischer B, Picoloto RS, Antes FG, da Silva FEB, Paula FR, et al. Determination of toxic elements in tricyclic active pharmaceutical ingredients by ICP-MS: a critical study of digestion methods. *J Anal At Spectrom* 2014;29(2).
98. Matusiewicz H. Systems for microwave-assisted wet digestion. Microwave-assisted sample preparation for trace element analysis 2014. p. 77-98.
99. Muller ALH, Muller EI, Barin JS, Flores EMM. Microwave-assisted digestion using diluted acids for toxic element determination in medicinal plants by ICP-MS in compliance with United States pharmacopeia requirements. *Anal Methods.* 2015;7(12):5218-25.
100. Flores ÉMM, Barin JS, Mesko MF, Knapp G. Sample preparation techniques based on combustion reactions in closed vessels — A brief overview and recent applications. *Spectrochim Acta, Part B* 2007;62(9):1051-64.
101. Link DD, Kingston HMS. Use of microwave-assisted evaporation for the complete recovery of volatile species of inorganic trace analytes. *Anal Chem.* 2000;72 2908-13
102. Barbosa Jr F, Palmer CD, Krug FJ, Parsons PJ. Determination of total mercury in whole blood by flow injection cold vapor atomic absorption spectrometry with room temperature digestion using tetramethylammonium hydroxide. *J Anal At Spectrom.* 2004;19(8).

103. Nóbrega JA, Santos MC, de Sousa RA, Cadore S, Barnes RM, Tatro M. Sample preparation in alkaline media. *Spectrochim Acta, Part B* 2006;61(5):465-95.
104. J.M. Osepchuk JM. A history of microwave-heating applications. *IEEE Trans Microw Theory Tech.* 1984;32:1200-24.
105. Federal communications commission- Microwave; Available from: <https://www.fcc.gov/wireless/bureau-divisions/broadband-division/microwave> [Accessed 18/10/2017].
106. Sattel S. Electromagnetic waves and how they work [Internet]: Eagle Academy - Autodesk Inc.; Available from: <https://www.autodesk.com/products/eagle/blog/electromagnetic-wireless-electronic-basics/> [Accessed 18/10/2017].
107. Sun J, Wang W, Yue Q. Review on microwave-matter interaction fundamentals and efficient microwave-associated heating strategies. *Materials* 2016;9(4).
108. Venkatesh MS, Raghavan GSV. An overview of microwave processing and dielectric properties of agri-food materials. *Biosyst Eng.* 2004;88(1):1-18.
109. Kubrakova IV, Toropchenova ES. Microwave heating for enhancing efficiency of analytical operations (Review). *Inorg Mater* 2008;44(14):1509-19.
110. Staff NRC. Microwave processing of materials. Washington, D.C: National Academy Press; 1994.
111. Mello PA, Brian JS, Guarnieri RA. Microwave heating. In: Flores EMM, editor. Microwave-assisted sample preparation for trace element determination. 1 ed: Newnes; 2014. p. 416.
112. Flores EM e. Microwave-assisted sample preparation for trace element determination: Newnes; 2014 May 3.
113. Gregory AP, Clarke RN. A review of RF and microwave techniques for dielectric measurements on polar liquids. *IEEE Trans Microw Theory Tech.* 2006;13(4):727-43.
114. Mingos DMP, Baghurst DR. Tilden Lecture. Applications of microwave dielectric heating effects to synthetic problems in chemistry. *Chem Soc Rev.* 1991;20(1):1-47.
115. Stuerge D. Microwave-material interactions and dielectric properties, key ingredients for mastery of chemical microwave processes. *Microwaves in organic synthesis.* Weinheim, Germany: Wiley-VCH Verlag GmbH & Co. KGaA; 2006.
116. Kingston HM, Jassie LBI. Introduction to microwave sample preparation: theory and practice. Washington: American Chemical Society; 1988.
117. Matusiewicz H. Systems for microwave-assisted wet digestion. In: Flores EMM, editor. Microwave-assisted sample preparation for trace element determination. 1 ed: Newnes; 2014. p. 416.
118. Nüchter M, Müller U, Ondruschka B, Tied A, Lautenschläger W. Microwave-Assisted Chemical Reactions. *Chemical Engineering & Technology.* 2003;26(12):1207-16.
119. Schön U, Messinger J, Eichner S, Kirschning A. Comparison of monomode and multimode microwave equipment in Suzuki–Miyaura reactions—en route to high throughput parallel synthesis under microwave conditions. *Tetrahedron Lett* 2008;49(20):3204-7.
120. Stalling DL, inventor; OI Corp, assignee. High pressure relief for microwave digestion vessel assembly. United States patent 5,948,307 1999.
121. Microwave digestion system: Multiwave GO: Anton Paar GmbH, 2017; Available from: <https://www.anton-paar.com/uk-en/products/details/microwave-digestion-system-multiwave-go/> [Accessed 20/10/2017].
122. Levine KE, Ross GT, Fernando RA, Blake JC, Sparacino CM, Pellizzari ED. Trace element content of senna study material and selected senna-based dietary supplements as determined by inductively coupled plasma-optical emission spectrometry and inductively coupled plasma-mass spectrometry. *Commun Soil Sci Plant Anal.* 2004;35(5-6):835-51.

123. Huang J, Hu X, Zhang J, Li K, Yan Y, Xu X. The application of inductively coupled plasma mass spectrometry in pharmaceutical and biomedical analysis. *J Pharm Biomed Anal.* 2006;40(2):227-34.
124. Krejčova A, Kahoun D, Cernohorsky T, Pouzar M. Determination of macro and trace element in multivitamins preparations by inductively coupled plasma optical emission spectrometry with slurry sample introduction. *Food Chem* 2006;98(1):171-8.
125. Zachariadis GA, Michos CE. Development of a slurry introduction method for multi-element analysis of antibiotics by inductively coupled plasma atomic emission spectrometry using various types of spray chamber and nebulizer configurations. *J Pharm Biomed Anal.* 2007;43(3):951-8.
126. Venzago C, Popp M, Kovac J, Kunkel A. Pharmacopeial requirements for elemental impurities: a novel approach to the trace determination of osmium by oxidative pressure vessel sample digestion and measurement using inductively coupled plasma mass spectrometry (ICP-MS) after complexation and stabilisation. *J Anal At Spectrom* 2013;28(7):1125.
127. Kaczala S, Costa AB, Posselt EL, Barin JS, Flores EMM, Dressler VL. Element determination in pharmaceuticals using direct solid analysis-electrothermal vaporization inductively coupled plasma optical emission spectrometry. *J Braz Chem Soc.* 2015.
128. Wei X-S, Wu Y-W, Han L-J. Determination of lead and cadmium in water and pharmaceutical products by inductively coupled plasma optical emission spectrometry with preconcentration by thiourea immobilized silica. *Anal Lett* 2015;48(6):996-1008.
129. Chen FF. *Introduction to plasma physics: Springer Science & Business Media; 2012 Dec 6.*
130. Goldston RJ, Rutherford PH. *Introduction to Plasma Physics: CRC Press; 1995 Nov 1.*
131. Tonks L, Langmuir I. A general theory of the plasma of an arc. *Phys Rev* 1929;34(6):876.
132. Piel A. *Plasma physics: an introduction to laboratory, space, and fusion plasmas: Springer; 2017 Sep 7.*
133. Montaser A, McLean JA, Liu H, Mermet JM. *An introduction to ICP spectrometries for elemental analysis 1992.*
134. Boss CB, Fredeen KJ. *Concepts, instrumentation and techniques in inductively coupled plasma optical emission spectrometry. Norwalk: Perkin Elmer; 1999.*
135. Miles D. *The application of inductively coupled plasmas to the analysis of natural waters and acidic deposition: Institute of Terrestrial Ecology; 1987.*
136. Fassel VA. Quantitative elemental analyses by plasma emission spectroscopy. *Science.* 1978;202(4364):183-91.
137. Dickinson GW, Fassel VA. Emission spectrometric detection of the elements at the nanogram per milliliter level using induction-coupled plasma excitation Ames Lab, Iowa. 1969 Jan 1.
138. Greenfield S, McGeachin HM, Smith PB. Nebulization effects with acid solutions in ICP spectrometry. *Anal Chim Acta* 1976 84(1):67-78.
139. Koirtyohann SR, Jones JS, Jester CP, Yates DA. Use of spatial emission profiles and a nomenclature system as aids in interpreting matrix effects in the low-power argon inductively coupled plasma. *Spectrochim Acta, Part B* 1981;36(1):49-59.
140. Niu H, Houk RS. Fundamental aspects of ion extraction in inductively coupled plasma mass spectrometry. *Spectrochim Acta, Part B* 1996;51(8):779-815.
141. Houk RS, Fassel VA, Flesch GD, Svec HJ, Gray AL, Taylor CE. Inductively coupled argon plasma as an ion source for mass spectrometric determination of trace elements. *Anal Chem.* 1980;52(14):2283.

142. Greenfield S, Jones IL, McGeachin HM, Smith PB. Automatic multi-sample simultaneous multi-element analysis with a HF plasma torch and direct reading spectrometer. *Anal Chim Acta* 1975;74(2):225-45.
143. Maessen FJ, Balke J, De Boer JL. Preservation of accuracy and precision in the analytical practice of low power ICP-AES. *Spectrochim Acta, Part B* 1982;37(6):517-26.
144. Falk K, Emons H. Speciation of arsenic compounds by ion-exchange HPLC-ICP-MS with different nebulizers. *J Anal At Spectrom.* 2000;15(6):643-9.
145. Thomas R. *Practical guide to ICP-MS.* USA: Marcel Dekker, Inc.; 2004.
146. Bouyssiere B, Ordóñez YN, Lienemann C-P, Schaumlöffel D, Łobiński R. Determination of mercury in organic solvents and gas condensates by μ flow-injection — inductively coupled plasma mass spectrometry using a modified total consumption micronebulizer fitted with single pass spray chamber. *Spectrochim Acta, Part B* 2006;61(9):1063-8.
147. Baker SA, Miller-Ihli NJ. Comparison of a cross-flow and microconcentric nebulizer for chemical speciation measurements using CZE-ICP-MS. *Appl Spectrosc* 1999 53(4):471-8.
148. Gaines P. Sample introduction for ICP-MS and ICP-OES. *Spectroscopy.* 2005;20(1).
149. Todolí J-L, Mermet J-M. Influence of the spray chamber design for vapor-based liquid sample introduction at room temperature in ICP-AES. *J Anal At Spectrom.* 2002;17(3):211-8.
150. Mermet JM. Revisitation of the matrix effects in inductively coupled plasma atomic emission spectrometry: the key role of the spray chamber. *J Anal At Spectrom* 1998;13(5):419-22.
151. Warra AA, Jimoh WLO. Overview of an inductively coupled plasam (ICP) system. *Int J Chem Res.* 2011;3(2):41-8.
152. Bohr N. Atomic structure. *Nature* 1921;107(2682):104.
153. Nicholson JW. The constitution of atoms and molecules. *Nature.* 1914;93(2324):268-9.
154. Bohr N. On the constitution of atoms and molecules. *Philos Mag.* 1913;26(6):1-25.
155. Bray I, Fursa DV, Kadyrov AS, Stelbovics AT, Kheifets AS, Mukhamedzhanov AM. Electron- and photon-impact atomic ionisation. *Phys Rep.* 2012;520(3):135-74.
156. Lichte FE, Koirtjohann SR. Induction coupled plasma emission from a different angle. *Federation of Analytical Chemistry and Spectroscopy Societies.* 1976;2:192.
157. Demers DR. Evaluation of the axially viewed (end-on) inductively coupled argon plasma source for atomic emission spectroscopy. *Appl Spectrosc* 1979;33(6):584-91.
158. Lajunen LHJ, Perämäki P. *Spectrochemical analysis by atomic absorption and emission.* 2 ed. Cambridge Royal society of chemistry; 2004.
159. Hopkinson GR, Goodman TM, Prince SR. *A guide to the use and calibration of detector array equipment:* SPIE Press; 2004.
160. Lepla KC, Horlick G. Photodiode array systems for inductively coupled plasma-atomic emission spectrometry. *Appl Spectrosc* 1989;43(7):1187-95.
161. Lutz G. *Semiconductor radiation detectors.* Berlin: Springer; 1999 1999 Oct.
162. Dearnaley G. Solid-state radiation detectors. *Contemp Phys.* 1967 8(6):607-26.
163. Barnard TW, Crockett MI, Ivaldi JC, Lundberg PL, Yates DA, Levine PA, et al. Solid-state detector for ICP-OES. *Anal Chem.* 1993;65(9):1231-9.
164. The Thermo Scientific iCAP 7000 Plus Series ICP-OES Unique Charge Injection Device (CID) Detector: Thermo Scientific, 2016; Available from: <https://tools.thermofisher.com/content/sfs/brochures/TN-43335-ICP-OES-CID-Detector-iCAP-7000-Plus-Series-TN43335-EN.pdf> [Accessed 22/12/2017].
165. Ghazi AA, Atta MA, Qamar S. Spectral interference and line selection for trace element analysis in a multi-component matrix using inductively coupled plasma atomic emission spectroscopy. *J Chem Soc Pak.* 2005;27(1):49-58.

166. Olesik JW. Elemental analysis using ICP-OES and ICP/MS. *Anal Chem.* 1991;63(1):12A-21A.
167. Twyman RM. Interferences and background correction. *Atomic emission spectrometry*: Elsevier Ltd; 2005.
168. Gaines P. ICP Operations Guide. A guide for using ICP-OES and ICP-MS. *Inorganic Ventures.* 2011:4-8.
169. Moore GL. Introduction to inductively coupled plasma atomic emission spectrometry: Elsevier; 2012 2012 Dec 2.
170. Todolí JL, Gras L, Hernandis V, Mora J. Elemental matrix effects in ICP-AES. *J Anal At Spectrom.* 2002;17(2):142-69.
171. Batsala M, Chandu B, Sakala B, Nama S, Domatoti S. Inductively coupled plasma mass spectrometry (ICP-MS). *Int J Res Pharm Chem.* 2012;2(3):671-80.
172. Montaser A. *Inductively coupled plasma mass spectrometry*: John Wiley & Sons; 1998 1998 Apr 22.
173. Hill SJ. *Inductively coupled plasma spectrometry and its applications*: John Wiley & Sons; 2008
174. Begley IS, Sharp BL. Characterisation and correction of instrumental bias in inductively coupled plasma quadrupole mass spectrometry for accurate measurement of lead isotope ratios. *J Anal At Spectrom* 1997;12(4):395-402.
175. Date AR, Gray AL. Plasma source mass spectrometry using an inductively coupled plasma and a high resolution quadrupole mass filter. *Analyst.* 1981;106(1269):1255-67.
176. Houk RS. Mass spectrometry of inductively coupled plasmas. *Anal Chem.* 1986 58(1):97A-105A.
177. Rehkämper M, Schönbacher M, Stirling CH. Multiple collector ICP-MS: introduction to instrumentation, measurement techniques and analytical capabilities. *Geostand Geoanalytical Res.* 2001;25(1):23-40.
178. Cottingham KL. Product review: ICPMS: It's elemental.
179. Thomas R. A beginner's guide to ICP-MS. *Spectroscopy.* 2001;16(4):38-42.
180. Kent AJR. In-situ analysis of Pb isotope ratios using laser ablation MC-ICP-MS: Controls on precision and accuracy and comparison between Faraday cup and ion counting systems. *J Anal At Spectrom.* 2008;23(7).
181. Lum T-S, Sze-Yin Leung K. Strategies to overcome spectral interference in ICP-MS detection. *J Anal At Spectrom.* 2016;31(5):1078-88.
182. Moens LJ, Vanhaecke FF, Bandura DR, Baranov VI, Tanner SD. Elimination of isobaric interferences in ICP-MS, using ion-molecule reaction chemistry: Rb/Sr age determination of magmatic rocks, a case study. *J Anal At Spectrom.* 2001;16(9):991-4.
183. May TW, Wiedmeyer RH. A table of polyatomic interferences in ICP-MS. *At Spectrosc* 1998;19:150-5.
184. Date AR, Cheung YY, Stuart M. The influence of polyatomic ion interferences in analysis by inductively coupled plasma source mass spectrometry (ICP-MS). *Spectrochim Acta, Part B* 1987;42(1-2):3-20.
185. Jackson B, Liba A, Nelson J. Advantages of reaction cell ICP-MS on doubly charged interferences for arsenic and selenium analysis in foods. *J Anal At Spectrom.* 2014;2015.
186. Gray AL, Williams JG. Communication. Oxide and doubly charged ion response of a commercial inductively coupled plasma mass spectrometry instrument. *J Anal At Spectrom* 1987;2(1):81-2.
187. Neubauer K, Völlkopf U. The benefits of a dynamic reaction cell to remove carbon- and chloride-based spectral interferences by ICP-MS. *At Spectrosc* 1999;20:64-8.
188. Bandura DR, Baranov VI, Tanner SD. Reaction chemistry and collisional processes in multipole devices for resolving isobaric interferences in ICP-MS. *Fresenius J Anal Chem.* 2001;370(5):454-70.

189. Simpson LA, Thomsen M, Alloway BJ, Parker A. A dynamic reaction cell (DRC) solution to oxide-based interferences in inductively coupled plasma mass spectrometry (ICP-MS) analysis of the noble metals. *J Anal At Spectrom* 2001;16(12):1375-80.
190. Tanner SD, Baranov VI. Theory, design, and operation of a dynamic reaction cell for ICP-MS. *At Spectrosc* 1999;20(45-52).
191. Brenner IJ, editor An overview of magnetic sector inductively coupled ICP and GD-MS. 12th ISMAS Symposium cum Workshop on Mass Spectrometry; 2007; Cidade de Goa, Dona Paula, Goa.
192. Brenner IJ. Inductively coupled plasma mass spectrometry applications. In: Lindon JC, Tranter GE, Koppenaal DW, editors. *Encyclopedia of Spectroscopy and Spectrometry*. Third ed: Academic Press; 2016. p. 229-35.
193. Barling J, Weis D. Influence of non-spectral matrix effects on the accuracy of Pb isotope ratio measurement by MC-ICP-MS: implications for the external normalization method of instrumental mass bias correction. *J Anal At Spectrom*. 2008;23(7).
194. Tanner SD. Space charge in ICP-MS: calculation and implications. *Spectrochim Acta, Part B*. 1992;47(6):809-23.
195. Gillson GR, Douglas DJ, Fulford JE, Halligan KW, Tanner SD. Nonspectroscopic interelement interferences in inductively coupled plasma mass spectrometry. *Anal Chem*. 1988;60(14):1472-4.
196. Vanhaecke F, Vanhoe H, Dams R, Vandecasteele C. The use of internal standards in ICP-MS. *Talanta*. 1992;39(7):737-42.
197. Das AK, Chakraborty R, Cervera ML, de la Guardia M. Metal speciation in solid matrices. *Talanta*. 1995;42(8):1007-30.
198. Matusiewicz H, Ślachciński M. Development of a new hybrid technique for inorganic arsenic speciation analysis by microchip capillary electrophoresis coupled with hydride generation microwave induced plasma spectrometry. *Microchemical Journal*. 2012;102:61-7.
199. Kitagawa F, Shiomi K, Otsuka K. Analysis of arsenic compounds by capillary electrophoresis using indirect UV and mass spectrometric detections. *Electrophoresis*. 2006;27(11):2233-9.
200. Schramel O, Michalke B, Kettrup A. Application of capillary electrophoresis-electrospray ionisation mass spectrometry to arsenic speciation. *J Anal At Spectrom*. 1999;14(9):1339-42.
201. Butcher DJ. Atomic fluorescence spectrometry: A review of advances in instrumentation and novel applications. *Applied Spectroscopy Reviews*. 2016;51(5):397-416.
202. Moraes DP, Svoboda M, Matoušek T, Flores EMM, Dědina J. Selective generation of substituted arsines-cryotrapping-atomic absorption spectrometry for arsenic speciation analysis in N-methylglucamine antimonate. *Journal of Analytical Atomic Spectrometry*. 2012;27(10).
203. Le X, Ma M. Short-column liquid chromatography with hydride generation atomic fluorescence detection for the speciation of arsenic. *Anal Chem*. 1998;70(9):1926-33.
204. Bohari Y, Lobos G, Pinochet H, Pannier F, Astruc A, Potin-Gautier M. Speciation of arsenic in plants by HPLC-HG-AFS: extraction optimisation on CRM materials and application to cultivated samples. *Journal of Environmental Monitoring*. 2002;4(4).
205. Nearing MM, Koch I, Reimer KJ. Complementary arsenic speciation methods: A review. *Spectrochimica Acta Part B: Atomic Spectroscopy*. 2014;99:150-62.
206. Clough R, Harrington CF, Hill SJ, Madrid Y, Tyson JF. Atomic spectrometry update: review of advances in elemental speciation. *Journal of Analytical Atomic Spectrometry*. 2017;32(7):1239-82.

207. Lewen N. The use of atomic spectroscopy in the pharmaceutical industry for the determination of trace elements in pharmaceuticals. *J Pharm Biomed Anal.* 2011;55(4):653-61.
208. Narin I, Kars A, Soylak M. A novel solid phase extraction procedure on Amberlite XAD-1180 for speciation of Cr(III), Cr(VI) and total chromium in environmental and pharmaceutical samples. *J Hazard Mater.* 2008;150(2):453-8.
209. Gallignani M, Ayala C, Brunetto M, Burguera M, Burguera J. Flow analysis–hydride generation–Fourier transform infrared spectrometric determination of antimony in pharmaceuticals. *Talanta.* 2003;59(5):923-34.
210. Wang W, Chen Z, Davey DE, Naidu R. Extraction of selenium species in pharmaceutical tablets using enzymatic and chemical methods. *Microchimica Acta.* 2008;165(1-2):167-72.
211. Seby F, Gleyzes C, Grosso O, Plau B, Donard OF. Speciation of antimony in injectable drugs used for leishmaniasis treatment (Glucantime(R)) by HPLC-ICP-MS and DPP. *Anal Bioanal Chem.* 2012;404(10):2939-48.
212. Cabral LM, Juliano VN, Dias LR, Dornelas CB, Rodrigues CR, Villardi M, et al. Speciation of antimony (III) and antimony (V) using hydride generation for meglumine antimoniate pharmaceutical formulations quality control. *Memorias Do Instituto Oswaldo Cruz.* 2008;103(2):130-7.
213. Lukaszczyk L, Zyrnicki W. Speciation analysis of Sb(III) and Sb(V) in antileishmaniotic drug using Dowex 1 x 4 resin from hydrochloric acid solution. *J Pharm Biomed Anal.* 2010;52(5):747-51.
214. Goenaga-Infante H, Sturgeon R, Turner J, Hearn R, Sargent M, Maxwell P, et al. Total selenium and selenomethionine in pharmaceutical yeast tablets: assessment of the state of the art of measurement capabilities through international intercomparison CCQM-P86. *Anal Bioanal Chem.* 2008;390(2):629-42.
215. Ammann AA. Arsenic speciation analysis by ion chromatography - A critical review of principles and applications. *Am J Analyt Chem* 2011;02(01):27-45.
216. Avula B, Wang YH, Khan IA. Arsenic speciation and fucoxanthin analysis from seaweed dietary supplements using LC-MS. *J AOAC Int.* 2015;98(2):321-9.
217. Anawar HM. Arsenic speciation in environmental samples by hydride generation and electrothermal atomic absorption spectrometry. *Talanta.* 2012;88:30-42.
218. Chen R, Smith BW, Winefordner JD, Tu MS, Kertulis G, Ma LQ. Arsenic speciation in Chinese brake fern by ion-pair high-performance liquid chromatography–inductively coupled plasma mass spectrometry. *Anal Chim Acta.* 2004;504(2):199-207.
219. Dufailly V, Noël L, Frémy J-M, Beauchemin D, Guérin T. Optimisation by experimental design of an IEC/ICP-MS speciation method for arsenic in seafood following microwave assisted extraction. *J Anal At Spectrom* 2007;22(9).
220. Rahman MM, Chen Z, Naidu R. Extraction of arsenic species in soils using microwave-assisted extraction detected by ion chromatography coupled to inductively coupled plasma mass spectrometry. *Environ Geochem Health.* 2009;31 Suppl 1:93-102.
221. Gong Z, Lu X, Ma M, Watt C, Le XC. Arsenic speciation analysis. *Talanta.* 2002;58:77-96.
222. Sadee B, Foulkes ME, Hill SJ. Coupled techniques for arsenic speciation in food and drinking water: a review. *Journal of Analytical Atomic Spectrometry.* 2015;30(1):102-18.
223. Narukawa T, Suzuki T, Inagaki K, Hioki A. Extraction techniques for arsenic species in rice flour and their speciation by HPLC-ICP-MS. *Talanta.* 2014;130:213-20.
224. Boucher P, Accominotti M, Vallon JJ. Arsenic speciation by ion pair reversed phase liquid chromatography with coupled amperometric and ultraviolet detection. *J Chromatogr Sci.* 1996;34(5):226-9.

225. Mandal BK, Ogra Y, Suzuki KT. Speciation of arsenic in human nail and hair from arsenic-affected area by HPLC-inductively coupled argon plasma mass spectrometry. *Toxicology and Applied Pharmacology*. 2003;189(2):73-83.
226. Geng A, Wang X, Wu L, Wang F, Chen Y, Yang H, et al. Arsenic accumulation and speciation in rice grown in arsenic acid-elevated paddy soil. *Ecotoxicol Environ Saf*. 2017;137:172-8.
227. Hsu KC, Sun CC, Huang YL. Arsenic speciation in biomedical sciences: recent advances and applications. *Kaohsiung J Med Sci*. 2011;27(9):382-9.
228. Narukawa T, Chiba K, Sinaviwat S, Feldmann J. A rapid monitoring method for inorganic arsenic in rice flour using reversed phase-high performance liquid chromatography-inductively coupled plasma mass spectrometry. *J Chromatogr A*. 2017;1479:129-36.
229. Aitio A, Cantor KP, Attfield MD, Demers PA, Fowler BA, Grandjean P, et al. IARC Monographs-Arsenic, metals, fibres, and dusts: A review of human carcinogens. International Agency for Research on Cancer. 2012;Volume 100 C:1-469.
230. Jain CK, Ali I. Arsenic occurrence toxicity and speciation techniques. *Water Res* 2000;34(17):4304-12.
231. team TACSmaec. Arsenic and cancer risk. American Cancer Society. 2014.
232. Pizarro I, Gómez M, Cámara C, Palacios MA. Arsenic speciation in environmental and biological samples. *Analytica Chimica Acta*. 2003;495(1-2):85-98.
233. Radke B, Jewell L, Namieśnik J. Analysis of arsenic species in environmental samples. *Crit Rev Anal Chem*. 2012;42(2):162-83.
234. Ahmed MF. An overview of arsenic removal technologies in Bangladesh and India. Proceedings of BUET-UNU international workshop on technologies for arsenic removal from drinking water, Dhaka 2001:5-7.
235. Ono FB, Tappero R, Sparks D, Guilherme LR. Investigation of arsenic species in tailings and windblown dust from a gold mining area. *Environ Sci Pollut Res*. 2016;23(1):683-74.
236. Francesconi KA, Edmonds JS. Arsenic and marine organisms. In: Sykes AG, editor. *Advances in Inorganic Chemistry*. 44: Academic Press; 1996. p. 147-89.
237. Maher WA, Duncan E, Dilly G, Foster S, Krikowa F, Lombi E, et al. Arsenic concentrations and species in three hydrothermal vent worms, *Ridgeia piscesae*, *Paralvinella sulficola* and *Paralvinella palmiformis*. *Deep Sea Res, Part I*. 2016;116(41-48).
238. Krishnakumar PK, Qurban MA, Stiboller M, Nachman KE, Joydas TV, Manikandan KP, et al. Arsenic and arsenic species in shellfish and finfish from the western Arabian Gulf and consumer health risk assessment. *Sci Total Environ*. 2016;566:1235-44.
239. Arroyo-Abad U, Pfeifer M, Mothes S, Stärk HJ, Piechotta C, Mattusch J, et al. Determination of moderately polar arsenolipids and mercury speciation in freshwater fish of the River Elbe (Saxony, Germany). *Environ Pollut*. 2016;208:458-66.
240. McSheehy S, Szpunar J. Speciation of arsenic in edible algae by bi-dimensional size-exclusion anion exchange HPLC with dual ICP-MS and electrospray MS/MS detection. *J Anal At Spectrom* 2000;15(1):79-87.
241. Sloth JJ, Larsen EH, Julshamn K. Determination of organoarsenic species in marine samples using gradient elution cation exchange HPLC-ICP-MS. *Journal of Analytical Atomic Spectrometry*. 2003;18(5):452-9.
242. Amayo KO, Petursdottir A, Newcombe C, Gunnlaugsdottir H, Raab A, Krupp EM, et al. Identification and quantification of arsenolipids using reversed-phase HPLC coupled simultaneously to high-resolution ICPMS and high-resolution electrospray MS without species-specific standards. *Anal Chem*. 2011;83(9):3589-95.
243. Whaley-Martin KJ, Koch I, Reimer KJ. Arsenic species extraction of biological marine samples (*Periwinkles*, *Littorina littorea*) from a highly contaminated site. *Talanta*. 2012;88:187-92.

244. Kirby J, Maher W. Measurement of water-soluble arsenic species in freeze-dried marine animal tissues by microwave-assisted extraction and HPLC-ICP-MS. *J Anal At Spectrom* 2002;17(8):838-43.
245. Foster S, Maher W, Krikowa F, Apte S. A microwave-assisted sequential extraction of water and dilute acid soluble arsenic species from marine plant and animal tissues. *Talanta*. 2007;71(2):537-49.
246. Sadee BA, Foulkes ME, Hill SJ. A study of arsenic speciation in soil, irrigation water and plant tissue: A case study of the broad bean plant, *Vicia faba*. *Food Chem*. 2016;210:362-70.
247. Ma L, Yang Z, Kong Q, Wang L. Extraction and determination of arsenic species in leafy vegetables: Method development and application. *Food Chem*. 2017;217:524-30.
248. Schmidt AC, Reisser W, Mattusch J, Peter Popp P, Wennrich R. Evaluation of extraction procedures for the ion chromatographic determination of arsenic species in plant materials. *J Chromatogr A*. 2000;889(1-2):83-91.
249. Yathavakilla SK, Fricke M, Creed PA, Heitkemper DT, Shockey NV, Schwegel C, et al. Arsenic speciation and identification of monomethylarsonous acid and monomethylthioarsonic acid in a complex matrix. *Anal Chem*. 2008;80(3):775-82.
250. Afton S, Kubachka K, Catron B, Caruso JA. Simultaneous characterization of selenium and arsenic analytes via ion-pairing reversed phase chromatography with inductively coupled plasma and electrospray ionization ion trap mass spectrometry for detection applications to river water, plant extract and urine matrices. *J Chromatogr A*. 2008;1208(1-2):156-63.
251. Vela NP, Heitkemper DT, Stewart KR. Arsenic extraction and speciation in carrots using accelerated solvent extraction, liquid chromatography and plasma mass spectrometry. *The Analyst*. 2001;126(7):1011-7.
252. Sadee BA, Foulkes ME, Hill SJ. An evaluation of extraction techniques for arsenic in staple diets (fish and rice) utilising both classical and enzymatic extraction methods. *Food Addit Contam Part A Chem Anal Control Expo Risk Assess*. 2016;33(3):433-41.
253. Kubachka KM, Shockey NV, Hanley TA, Conklin SD, Heitkemper DT. Elemental analysis manual: Section 4.11: Arsenic speciation in rice and rice products using high performance liquid chromatography-inductively coupled plasma- mass spectrometric determination. FDA. 2012;Version 1.1.
254. Narukawa T, Suzuki T, Inagaki K, Hioki A. Extraction techniques for arsenic species in rice flour and their speciation by HPLC-ICP-MS. *Talanta*. 2014;130(213-220).
255. Jackson BP, Bertsch PM. Determination of Arsenic Speciation in Poultry Wates by IC-ICP-MS. *Environ Sci Technol* 2001;35(24):4868-73.
256. Narukawa T, Inagaki K, Kuroiwa T, Chiba K. The extraction and speciation of arsenic in rice flour by HPLC-ICP-MS. *Talanta*. 2008;77(1):427-32.
257. Wang Z, Nadeau L, Sparling M, Forsyth D. Determination of arsenic species in fruit juice and fruit drink products using ion pair chromatography coupled to inductively coupled plasma mass spectrometry. *Food Anal Methods*. 2014;8(1):173-9.
258. Caruso JA, B'Hymer C, Heitkemper DT. An evaluation of extraction techniques for arsenic species from freeze-dried apple samples. *Analyst*. 2001;126(2):136-40.
259. Marcinkowska M, Baralkiewicz D. Multielemental speciation analysis by advanced hyphenated technique - HPLC/ICP-MS: a review. *Talanta*. 2016;161:177-204.
260. Schöppenthau J, Dunemann L. Hyphenated HPLC/ICP-MS and HPLC/ICP-OES techniques for the characterization of metal and non-metal species. *Fresenius' J Anal Chem*. 1994;349(794-799).
261. Choudhary F, Iqbal Z, Khan T, Ashraf MU. Trace metals analysis in selected pharmaceutical multimineral formulations. *Pak J Pharm Sci* 2005;18(2):40-3.

262. Kauffman JF, Westenberger BJ, Robertson JD, Guthrie J, Jacobs A, Cummins SK. Lead in pharmaceutical products and dietary supplements. *Regul Toxicol Pharmacol*. 2007;48(2):128-34.
263. Orisakwe OE, Nduka JK. Lead and cadmium levels of commonly administered pediatric syrups in Nigeria: a public health concern? *Sci Total Environ*. 2009;407(23):5993-6.
264. Arantes de Carvalho GG, Nunes LC, Florêncio de Souza P, Krug FJ, Alegre TC, Santos Jr D. Evaluation of laser induced breakdown spectrometry for the determination of macro and micronutrients in pharmaceutical tablets. *J Anal At Spectrom* 2010;25(6):803.
265. Wollein U, Bauer B, Habernegg R, Schramek N. Potential metal impurities in active pharmaceutical substances and finished medicinal products - A market surveillance study. *Eur J Pharm Sci*. 2015;77:100-5.
266. Tyler G, S. JY. ICP-OES, ICP-MS and AAS Techniques Compared. ICP Optical Emission Spectroscopy Technical Note. 1995;5.
267. ICHQ2B. Validation of analytical procedures: methodology 1996; Available from: <https://www.fda.gov/downloads/drugs/guidances/ucm073384.pdf> [Accessed 03/10/2017].
268. Miller JC, Miller JN. *Statistics for analytical chemistry*. 6 ed. England: Pearson Education Limited; 2010.
269. Forrester MB. Work-related health emergency cases due to hydrofluoric acid exposures reported to Texas poison centers. *Int J Occup Med Environ Health*. 2012;25(4):456-62.
270. Ozcan M, Allahbeickaraghi A, Dundar M. Possible hazardous effects of hydrofluoric acid and recommendations for treatment approach: a review. *Clin Oral Investig*. 2012;16(1):15-23.
271. Pappas R. Sample preparation problem solving for inductively coupled plasma-mass spectrometry with liquid introduction systems I. Solubility, chelation, and memory effects. *Spectroscopy*. 2012;27(5):20-31.
272. Allibone J, Fatemian E, Walker P. Determination of mercury in potable water by ICP-MS using gold as a stabilising agent. *J Anal At Spectrom* 1999;14:235-9.
273. Nardi EP, Evangelista FS, Tormen L, Saint´Pierre TD, Curtius AJ, Souza SSd, et al. The use of inductively coupled plasma mass spectrometry (ICP-MS) for the determination of toxic and essential elements in different types of food samples. *Food Chemistry*. 2009;112(3):727-32.
274. Siaka M, Owens CM, Birch GF. Evaluation of some digestion methods for the determination of heavy metals in sediment samples by Flame-AAS. *Anal Lett* 1998;31(4):703-18.
275. Dunmin WS, Dunyi L. Precise Re-Os dating of molybdenite using Carius tube, NTIMS and ICPMS. In: A P, editor. *Mineral Deposits at the Beginning of the 21st Century*: CRC Press; 2001. p. 405-7.
276. Mierzwa J, Sun YC, Chung YT, Yang MH. Comparative determination of Ba, Cu, Fe, Pb and Zn in tea leaves by slurry sampling electrothermal atomic absorption and liquid sampling inductively coupled plasma atomic emission spectrometry. *Talanta*. 1998;47(5):1263-70.
277. Mangum SJ. Microwave digestion- EPA method 3052 on the Multiwave 3000 USA: PerkinElmer, Inc., 2009; Available from: https://www.perkinelmer.com/lab-solutions/resources/docs/APP_MicrowaveDigestionMultiwave.pdf [Accessed 15/11/2017].
278. Optimizing analytical performance in ICP-OES applications. Application note: GBC Scientific; Available from: http://www.gbcscientific.com/appnotes/icp_oes_app_note_002.pdf [Accessed 1/07/2015].
279. Pan C, Zhu G, Browner RF. Role of auxiliary gas flow in organic sample introduction with inductively coupled plasma atomic emission spectrometry. *J Anal At Spectrom*. 1992;7(8):1231-7.

280. Uchida H, Ito T. Inductively coupled nitrogen plasma mass spectrometry assisted by adding argon to the outer gas. *J Anal At Spectrom.* 1995;10(10):843-8.
281. Uchida H. Effects of Central Argon Flow Rate on Characteristics of Inductively Coupled Plasma. *Spectrosc Lett.* 1981;14(10):665-74.
282. Kutseva NK, Kryuchkova SL, Pirogova SV, Naumova SV, Kryuchkov VA, Chamaev AV. Microwave sample preparation in the determination of metals in waste water. *J Anal Chem.* 2000;55(12):1142-7.
283. Sastre J, Sahuquillo A, Vidal M, Rauret G. Determination of Cd, Cu, Pb and Zn in environmental samples: microwave-assisted total digestion versus aqua regia and nitric acid extraction. *Anal Chim Acta.* 2002;462(1):59-72.
284. Wu S, Feng X, Wittmeier A. Microwave digestion of plant and grain reference materials in nitric acid or a mixture of nitric acid or a mixture of nitric acid and hydrogen peroxide for the determination of multi-elements by inductively coupled plasma mass spectrometry. *J Anal At Spectrom* 1997;12(8):797-806.
285. Baldwin S, Deaker M, Maher W. Low-volume microwave digestion of marine biological tissues for the measurement of trace elements. *Analyst.* 1994;119(8):1701-4.
286. Besecker KD, Rhoades JCB, Jones BT, Barnes KW. Closed-vessel nitric acid microwave digestion of polymers. *Appl Sci Res.* 1998 Mar 1;19(55-59).
287. Akinyele IO, Shokunbi OS. Comparative analysis of dry ashing and wet digestion methods for the determination of trace and heavy metals in food samples. *Food Chem.* 2015;173:682-4.
288. Hseu ZY. Evaluating heavy metal contents in nine composts using four digestion methods. *Bioresour Technol.* 2004;95(1):53-9.
289. Leopold K, Foulkes M, Worsfold P. Methods for the determination and speciation of mercury in natural waters--a review. *Anal Chim Acta.* 2010;663(2):127-38.
290. Sedcole JR, Lee J, Pritchard MW. Internal standard selection in the presence of matrix interactions in an inductively coupled argon plasma optimised for simultaneous multielement analysis by atomic emission spectrometry. *Spectrochim Acta, Part B* 1986;41(3):227-35.
291. Grotti M, Magi E, Leardi R. Selection of internal standards in inductively coupled plasma atomic emission spectrometry by principal component analysis. *Journal of Analytical Atomic Spectrometry.* 2003;18(3):274-81.
292. Fischer L, Zipfel B, Koellensperger G, Kovac J, Bilz S, Kunkel A, et al. Flow injection combined with ICP-MS for accurate high throughput analysis of elemental impurities in pharmaceutical products according to USP <232>/<233>. *J Pharm Biomed Anal.* 2014;95:121-9.
293. Rudovica V, Viksna A, Actins A. Application of LA-ICP-MS as a rapid tool for analysis of elemental impurities in active pharmaceutical ingredients. *J Pharm Biomed Anal.* 2014;91:119-22.
294. K.J R, P.D T. Table of isotopic masses and natural abundances. *Pure Appl Chem.*71:1593-607.
295. Pick D, Leiterer M, Einax JW. Reduction of polyatomic interferences in biological material using dynamic reaction cell ICP-MS. *Microchemical Journal.* 2010;95(2):315-9.
296. Hsieh YJ, Jiang SJ. Application of HPLC-ICP-MS and HPLC-ESI-MS procedures for arsenic speciation in seaweeds. *J Agric Food Chem.* 2012;60(9):2083-9.
297. Shibata Y, Morita M. Speciation of arsenic by reversed-phase high performance liquid chromatography-inductively coupled plasma mass spectrometry. *Anal Sci.* 1989;5(1):107-9.
298. Chen ML, Ma LY, Chen XW. New procedures for arsenic speciation: a review. *Talanta.* 2014;125:78-86.

299. Le XC, Ma M. Speciation of arsenic compounds by using ion-pair chromatography with atomic spectrometry and mass spectrometry detection. *J Chromatogr A*. 1997;764(1):55-64.
300. Larsen EH, Hansen SH. Separation of arsenic species by ion-pair and ion exchange high performance liquid chromatography. *Microchim Acta*. 1992;109(1):47-51.
301. Fendorf S, Nico PS, Kocar BD, Masue Y, Tufano KJ. Arsenic chemistry in soils and sediments. *Dev Soil Sci*. 2010;34:357-78.
302. Narukawa T, Matsumoto E, Nishimura T, Hioki A. Reversed phase column HPLC-ICP-MS conditions for arsenic speciation analysis of rice flour. *Anal Sci* 2015;31(6):521-7.
303. Rahman MS, Clark MW, Yee LH, Comarmond MJ, Payne TE, Kappen P, et al. Arsenic solid-phase speciation and reversible binding in long-term contaminated soils. *Chemosphere*. 2017;168:1324-36.
304. Leermakers M, Baeyens W, De Gieter M, Smedts B, Meert C, De Bisschop HC, et al. Toxic arsenic compounds in environmental samples: Speciation and validation. *TrAC Trends in Analytical Chemistry*. 2006;25(1):1-10.
305. Komorowicz I, Baralkiewicz D. Arsenic and its speciation in water samples by high performance liquid chromatography inductively coupled plasma mass spectrometry--last decade review. *Talanta*. 2011;84(2):247-61.
306. Wolle MM, Rahman GM, Kingston HM, Pamuku M. Speciation analysis of arsenic in prenatal and children's dietary supplements using microwave-enhanced extraction and ion chromatography-inductively coupled plasma mass spectrometry. *Anal Chim Acta*. 2014;818:23-31.
307. Jackson BP, Taylor VF, Punshon T, Cottingham KL. Arsenic concentration and speciation in infant formulas and first foods. *Pure Appl Chem*. 2012;84(2):215-23.
308. Ernstberger H, Neubauer K, Shelton CT. Accurate and Rapid Determination of Arsenic Speciation in Apple Juice PerkinElmer application note. 2015.
309. Rubio R, Ruiz-Chancho MJ, López-Sánchez JF, Rubio R, López-Sánchez JF. Sample pre-treatment and extraction methods that are crucial to arsenic speciation in algae and aquatic plants. *TrAC, Trends Anal Chem* 2010;29(1):53-69.
310. Chen LW, Lu X, Le XC. Complementary chromatography separation combined with hydride generation-inductively coupled plasma mass spectrometry for arsenic speciation in human urine. *Anal Chim Acta*. 2010;675(1):71-5.
311. Draget KI, Skjåk-Bræk G, Smidsrød O. Alginate based new materials. *Int J Biol Macromol*. 1997;21(1):47-55.
312. Laurienzo P. Marine polysaccharides in pharmaceutical applications: an overview. *Mar Drugs*. 2010;8(9):2435-65.
313. Hakala E, Lauri Pyy P. Selective determination of toxicologically important arsenic species in urine by high-performance liquid chromatography-hydride generation atomic absorption spectrometry. *J Anal At Spectrom*. 1992;7:191-6.
314. Yu C, Cai Q, Guo Z-X, Yang Z, Khoo SB. Inductively coupled plasma mass spectrometry study of the retention behavior of arsenic species on various solid phase extraction cartridges and its application in arsenic speciation. *Spectrochimica Acta Part B: Atomic Spectroscopy*. 2003;58(7):1335-49.
315. Snyder LR, Kirkland JJ, Glajch JL. *Practical HPLC method development*. 2 ed. United States: John Wiley & Sons, INC.; 1997.
316. Francesconia K, Visoottivisethb P, Sridokchanb W, Goessler W. Arsenic species in an arsenic hyperaccumulating fern, *Pityrogramma alomelanos*: a potential phytoremediator of arsenic-contaminated soils. *Sci Total Environ*. 2002;284(1-3):27-35.
317. Branch s, Ebdont L, Peter O'Neill P. Determination of arsenic species in fish by directly coupled high-performance liquid chromatography-inductively coupled plasma mass spectrometry. *J Anal At Spectrom* 1994;9:33-7.

318. Beauchemin D, Siu KWM, McLaren JW, Berman SS. Determination of arsenic species by high-performance liquid chromatography-inductively coupled plasma mass spectrometry. *J Anal At Spectrom.* 1989;4:285-9.
319. Skaugrud Ø, Hagen A, Borgersen B, Dornish M. Biomedical and pharmaceutical applications of alginate and chitosan. *Biotechnol Genet Eng Rev.* 1999;16(1):23-40.
320. Szekalska M, Puciłowska A, Szymańska E, Ciosek P, Winnicka K. Alginate: current uses and future perspectives in pharmaceutical and biomedical applications. *Int J Polym Sci* 2016;2016:1-17.
321. Dembitsky VM, Rezanka T. Natural occurrence of arseno compounds in plants, lichens, fungi, algal species, and microorganisms. *Plant Science.* 2003;165(6):1177-92.
322. Morita M, Shibata Y. Chemical form of arsenic in marine macroalgae. *J Organomet Chem.* 1990;4(3):181-90.
323. Taylor VF, Jackson BP. Concentrations and speciation of arsenic in New England seaweed species harvested for food and agriculture. *Chemosphere.* 2016;163:6-13.
324. Tukai R, Maher WA, McNaught IJ, Ellwood MJ, M. C. Occurrence and chemical form of arsenic in marine macroalgae from the east coast of Australia. *Marine Freshwater Res.* 2002;53(6):971-80.
325. Antacids National Health Service (NHS), UK.; 2016 [updated 14/11/2016]; Available from: <http://www.nhs.uk/conditions/antacid-medicines/Pages/Definition.aspx> [Accessed 13/10/2017].
326. Costa M. Toxicity and carcinogenicity of Cr (VI) in animal models and humans. *Crit Rev Toxicol.* 1997;27(5):431-42.
327. Dayan AD, Paine AJ. Mechanisms of chromium toxicity, carcinogenicity and allergenicity: review of the literature from 1985 to 2000. *Hum Exp Toxicol.* 2001;20(9):439-51.

Meetings, Conferences and Publications

Meetings

Poster Presentation

Thiab S, Riby P, Wainwright M. (20th June 2016). Determination of Trace Metals in Pharmaceuticals using ICP-OES. LJMU, The Faculty of Science Post Graduate Research Seminar and Poster Day, Liverpool, UK.

Oral Presentation

Thiab S, Riby P, Wainwright M, Roberts M, Nelms, S. (15-16th June 2016). Trace Metals in Pharmaceuticals using ICP-OES – Headaches and Other Issues. ICP-OES and ICP-MS User Meeting - Thermo Fisher Scientific, Cheshire, UK.

Conferences

Oral Presentation

Thiab S, Riby P, Wainwright M. (5th- 9th March 2017). The Development of Analytical Procedures for Analysis of Trace Metals in Pharmaceutical Formulations. Pittcon Conference and Expo, Chicago, Illinois, USA.

Poster Presentation

Thiab S, Riby P, Wainwright M. (4th- 6th July 2016). The Development of Analytical Procedures for Analysis and Speciation of Trace Metals in Pharmaceutical Formulations. Biennial National Atomic Spectroscopy Symposium, Liverpool, UK.

Conference proceeding

Thiab S, Riby P, Wainwright M. The development of analytical procedures using ICP-OES and ICP-MS for the analysis of trace metals in pharmaceutical formulations. B J Pharm. 2017; 2(2), S2-4. Proceedings of the 8th APS international PharmSci. Short listed to Geoffery Philips Analytical Science Award.

Upcoming Conference

Thiab S, Riby P, Wainwright M. (February/March 2018) The speciation of arsenic in antacid formulations as part of Q3D regulations. Pittcon Conference and Expo. Orlando, Florida, USA.

Publication

In preparation:

Thiab S, Riby P, Wainwright M. Development of an ICP-OES method as an alternative to ICP-MS for the ICH Q3D regulations for elemental impurities in pharmaceutical products.

Thiab S, Riby P, Wainwright M. The Development and validation of an ICP-MS method for the determination of elemental impurities in pharmaceutical products according to USP232/233 and ICH-Q3D guidelines.

Thiab S, Riby P, Wainwright M. Speciation of arsenic using reversed phase HPLC-ICP-MS in antacids.

Funding

2015-2017 Applied Science Private University (ASU) - Amman, Jordan £ 54,000